PARTITIONED TIME DISCRETIZATION FOR ATMOSPHERE-OCEAN INTERACTION

by

Jeffrey M. Connors

B.S. Engr. in Engineering Physics,

University of Pittsburgh, 2003

Submitted to the Graduate Faculty of

the Department of Mathematics in partial fulfillment

of the requirements for the degree of

Doctor of Philosophy

University of Pittsburgh

2010

UNIVERSITY OF PITTSBURGH

DEPARTMENT OF MATHEMATICS

This dissertation was presented

by

Jeffrey M. Connors

It was defended on

April 27, 2010

and approved by

William J. Layton, Ph. D., Professor of Mathematics

Ivan Yotov, Ph. D., Professor of Mathematics

Catalin Trenchea, Ph. D., Asst. Professor of Mathematics

Noel J. Walkington, Ph. D., Professor of Mathematics

Dissertation Director: William J. Layton, Ph. D., Professor of Mathematics

PARTITIONED TIME DISCRETIZATION FOR ATMOSPHERE-OCEAN INTERACTION

Jeffrey M. Connors, PhD

University of Pittsburgh, 2010

Numerical algorithms are proposed, analyzed and tested for improved efficiency and reliability of the dynamic core of climate codes. The commonly used rigid lid hypothesis is assumed, which allows instantaneous response of the interface to changes in mass. Additionally, moisture transport is ignored, resulting in a static interface. A central algorithmic feature is the numerical decoupling of the atmosphere and ocean calculations by a semi-implicit treatment of the interface data, i.e. partitioned time stepping. Algorithms are developed for simplified continuum models retaining the key mathematical structure of the atmosphere-ocean equations.

The work begins by studying linear parameterization of momentum flux in terms of wind shear, coupling the equations. Partitioned variants of backward-Euler are developed allowing large time steps. Higher order accuracy is achieved by deferred correction. Adaptations are developed for nonlinear coupling. Most notably an application of geometric averaging is used to retain unconditional stability. This algorithm is extended to allow different size time steps for the subcalculations. Full numerical analyses are performed and computational experiments are provided.

Next, heat convection is added including a nonlinear parameterization of heat flux in terms of wind shear and temperature. A partitioned algorithm is developed for the atmosphere and ocean coupled velocity-temperature system that retains unconditional stability. Furthermore, uncertainty quantification is performed in this case due to the importance of reliably calculating heat transport phenomena in climate modeling. Noise is introduced in

two coupling parameters with an important role in stability. Numerical tests investigate the variance in temperature, velocity and average surface temperature.

Partitioned methods are highly efficient for linearly coupled 2 fluid problems. Extensions of these methods for nonlinear coupling where the interface data is processed properly before passing yield highly efficient algorithms. One reason is due to their strong stability properties. Convergence also holds under time step restrictions not dependent on mesh size. It is observed that two-way coupling (requiring knowledge of both atmosphere and ocean velocities on the interface) generates less uncertainty in the calculation of average surface temperature compared to one-way models (only requiring knowledge of the wind velocity).

TABLE OF CONTENTS

LIST OF TABLES

LIST OF FIGURES

PREFACE

Naturally I admit a huge feeling of gratitude to my advisor Dr. William Layton. His contributions to my successful tenure as a graduate student and Ph.D. candidate extend beyond availability for discussions, teaching technical skills (both in mathematics and writing) and aiding me in understanding the deep concepts of fluid dynamics and turbulence modeling. He has done an excellent job of teaching me the many additional tools needed to build a career. Also, perhaps most importantly, he has encouraged me at every turn and pushed me to succeed until I was surprised to find what I could accomplish, demonstrating patience the whole way.

I have been fortunate to be able to take a number of fundamental courses in numerical mathematics with Dr. Ivan Yotov, who treats his role as a teacher seriously and does a thorough job. My research has benefited as a result and I am grateful he is on my committee. I wish to thank my committee member Dr. Catalin Trenchea who taught me many useful mathematical tools and concepts in studying optimization and control theory. Also, I am thankful for Dr. Noel Walkington's participation on my committee. He has made a number of useful suggestions about my work and raised important questions for me to consider, which I appreciate.

I will also acknowledge some other key people from whom I have learned much, particularly in terms of computing skills. Dr. Jason Howell has been a highly supportive and helpful collaborator. I have learned a lot developing FreeFem++ code and numerical tests with him and had many useful scientific discussions. He has been particularly helpful in regards to material in Chapters 2, 5 and 6. Dr. Mike Sussman has taught me many critical computer skills. Additionally he has contributed to discussions of my work during numerous presentations, both formal and informal, and been available as a mentor on the side offering advice

and encouragement. Dr. Alex Labovschii helped me to develop the deferred correction theory for Chapter 3. Finally, Benjamin Ganis has helped immensely in the development of the material in Chapter 7 and has helped me further my computing skills.

Heartfelt thanks goes out to my wife's parents, Kathy and Brian McKain, who have supported me in every way during my graduate studies. Then to conclude, I want to express my gratitude toward my loving and supportive wife Kaitlin. I cannot sufficiently thank her, but I dedicate this work to her as she has dedicated herself to supporting my dreams.

1.0 INTRODUCTION: THE DYNAMIC CORE OF CLIMATE MODELS AND COMPUTATIONAL DIFFICULTIES

Broadly, a "climate model" includes the effects of a long list of relevant climate variables. This is not limited to velocity and pressure of the atmosphere and ocean, temperature, humidity, salinity and gaseous concentrations. Many climate models are built by taking the best code for simulating the atmosphere, the best code for the ocean, land processes and formation, ablation and motion of sea ice and coupling these subprocesses together by calculating and passing fluxes of quantities exchanged across their interfaces. It is also common to distinguish between model dynamical processes and other model physics.

The "dynamic core" of climate models refers typically to the numerical schemes for resolving large scale transport phenomena. This includes resolving the large eddies of fluid flow coupled to transport of (e.g.) heat, oxygen and carbon dioxide. In contrast, moisture processes (precipitation and evaportation), radiative and cloud processes, surface dynamics and turbulence are often treated as a separate component (in the sense of programming) of a climate model termed physical parameterizations. This work studies numerical algorithms with application toward the dynamic core of climate models.

The goal of climate models is to understand how environmental policy may influence the future climate. A current focus is the effect of carbon dioxide distributions and overall concentration on globally averaged surface temperature. It is widely believed now that computer codes to perform these calculations must take into account almost every conceivable component of the climate such as sea-ice, glaciers, land vegetation, rivers, oceans, the atmosphere, snow pack, land and ocean bottom topography and many other factors. The interactions between every component must be accounted for, including all physical variables such as fluid velocity, heat, salinity, humidity, gas concentrations requiring huge numbers of spatial

degrees of freedom. Resolving climate statistics requires long time calculations. Mainly this is because the deep ocean currents are slow but contain most of the carbon dioxide, and ocean mixing has a large effect on the climate over thousands of years. Thus a fundamental modeling problem exists of solving huge systems of equations over hundreds of thousands of time steps. Performing such demanding computations efficiently and reliably is considered to be one of the great challenges in scientific computing.

Much of the pioneering work originally leading to coupled climate models was performed in the 1950's - 1960's by a group of researchers seeking to use computer technology to perform atmospheric calculations over smaller time periods. These researchers designed a computer system at what became Princeton's Geophysical Fluid Dynamics Laboratory (GFDL) and also performed ocean calculations. At first atmosphere and ocean calculations were not coupled together. The first coupled atmosphere-ocean model was developed at the GFDL by Manabe and Bryan in the late 1960's, [50]. A number of such models now exist and these models have grown to include more refined physics. Some current full scale Global Circulation Models (GCMs) with coupled atmosphere-ocean components include:

- Community Climate Systems Model (CCSM) at the National Center for Atmospheric Research
- Geophysical Fluid Dynamics Laboratory Coupled Model version 2.x (GFDL CM2.x) at the National Oceanic and Atmospheric Administration
- MIT's Global Circulation Model (MITgcm)
- Hadley Centre Coupled Model, version 3 (HadCM3) at the Met Office Hadley Centre for Climate Change, UK
- Meteorological Research Institute Coupled Global Climate Model version 2.x (MRI-CGCM2.x) at MRI, Japan
- CGCM4/CanCM4 at the Canadian Center for Climate Modeling and Analysis, Canada
- ECHAM5/MPI-OM at the Max Planck Institute for Meteorology, Germany
- BCC-CM1 at the Beijing Climate Center, China
- BCCR-BCM2.0 at the Bejerknes Center for Climate Research, Norway
- CNRM-CM3 at the Centre National de Recherches Météorologiques, France
- CSIRO-MK3.0 at the Commonwealth Scientific and Research Organization, Australia

The CCSM model provides an example of how GCMs are structured. The code consists of four main components for land, sea-ice, atmosphere and the ocean which solve internally for their respective variables. The processes of each component are coupled to other components. This coupling is implemented by passing flux quantities such as momentum, heat and mass (water) to a separate "flux coupler" code which passes the data between components. The flux coupler manages tasks such as flux calculations due to regridding and separate time steps for the different components to ensure conservation of flux quantities. In this way the computations are parallelized for efficiency while maintaining physical fidelity. Decades have been spent in developing these components and in improving numerical methods used therein. This thesis considers only the atmosphere and ocean components.

A number of modeling ideas have been implemented in climate codes to improve the overall efficiency. In the case of atmosphere-ocean interaction, one such idea is the *rigid lid* hypothesis. Understanding this hypothesis requires an understanding of how heat, momentum and water (humidity and precipitation) flow between the atmosphere and ocean. It is well known that fluxes of these quantities are essentially constant across what are known as the Prandtl layers of the atmosphere and ocean. The Prandtl layers are of constant thickness, on the order of 1 kilometer in the atmosphere and 100 meters in the ocean. Relative to the horizontal scale of the interface, these layers are very thin. The goal of climate modeling is not to know (for example) the wind speed at a given point and time, but to establish trends in the climate, i.e. statistical measurements. This requires computations to conserve fluxed quantities, but not to resolve the details of thin boundary layers, saving computational expense. Thus in the rigid lid hypothesis the variable values at the interface are interpreted as the values these quantities would have near the edge of the Prandtl layers. Then coupling relationships are developed using flux relationships. This treates the "interface" between the atmosphere and ocean as responding instantly to mass changes and not admitting surface waves. Figure 1 provides a visual description where the z-direction is normal to the ocean surface (height).

The current work considers parameterizations for heat and momentum flux. Formulas and their derivations are presented in [47], part of a series of papers analyzing the full coupled

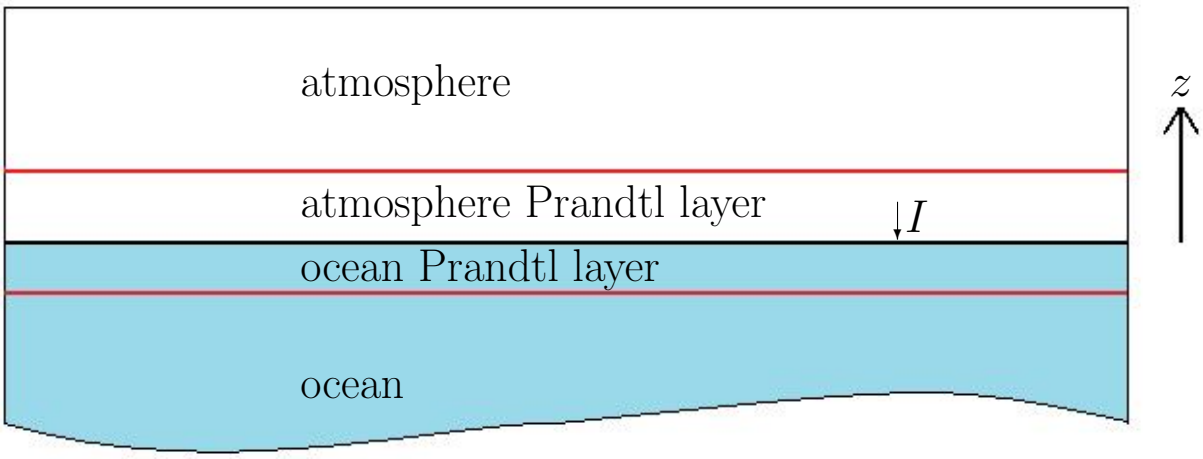

Figure 1: Prandtl layers in the atmosphere and ocean, coupled across an interface I.

atmosphere-ocean equations. At the interface these relationships take the form

$$\rho^a \nu^a \frac{\partial(u^a \cdot \tau)}{\partial z} = \rho^a C_I |u^a - u^s|^\alpha (u^a - u^o) \cdot \tau \tag{1.1}$$

$$\begin{aligned} c_p^s \rho^s \nu^s \frac{\partial T^s}{\partial z} &= C_{sol} - C_{ir}(T^s - T^a) \\ &- c_p^a \rho^a C_{conv} |u^s - u^a|^\alpha (T^s - T^a) + \rho^a L C_L (q - q_{ae}) \end{aligned} \tag{1.2}$$

where the superscript a denotes "atmosphere" and s denotes "sea". The left hand sides of (1.1) - (1.2) are momentum flux from the atmosphere and heat flux from the ocean, respectively. The right hand sides are their parameterizations in terms of velocity and temperature on the interface. Density is ρ^x, turbulent viscocity is ν^x, temperature is T^x, velocity u^x and c_p^x is heat capacity for $x = a, s$. Equation (1.1) holds for each vector τ tangent to the interface. The mixing ratio of water vapor in air is q with equilibrium value q_{ae}. The parameter α is typically 0 or 1. The parameters C_I, C_{sol}, C_{ir}, C_{conv} and C_L are all positive. The latent heat of vaporization of water is L. The size of these parameters controls the following effects:

- C_I : wind shear stress
- C_{sol} : solar radiation

- C_{ir} : longwave (infrared) radiation
- C_{conv} : convective heat transfer
- C_L : latent heat transfer

Relationships for momentum flux from the ocean and heat flux from the atmosphere follow by setting the sum of fluxes across the interface to zero. Since evaporation and precipitation are not studied in this work, we take $C_L = 0$.

The atmosphere and ocean subproblems are solved independently as components of the climate code and fluxes are passed so as to conserve important invariants between them as described above. Improved efficiency is obtained by allowing the atmosphere and ocean to use different spatial grids and time steps. This exploits the differences in the most important spatial and time scales for the atmosphere and ocean. In the atmosphere the dominant eddies are between 500-10,000 km over time scales up to 1 year, [52]. In [70] it is commented that typical atmospheric eddies are around 10^4 km over time periods around a day. In the ocean it is desirable to resolve eddies on the order of 10 - 10,000 km, [52], over time scales exceeding 1000 years [8, 28]. The majority of energy in oceanic flow occurs in the *mesoscale* regime around 100-300 km, [70]. The result is simulations requiring a finer spatial grid for the ocean and smaller time steps in the atmosphere.

Some climate calculations require a "spin-up" phase to first bring the system to equilibrium with fixed parameters and forcings to generate an appropriate initial state for the subsequent evolutionary test. Due to the $\approx$ 1000 year overturn for the deep ocean this requires a calculation sometimes exceeding 3000 years for spin-up followed by the evolution problem itself, possibly also in excess of 1000 years. In the spin-up phase it is desirable to take as large a time step as possible for the system. However, one of the major hurdles for climate codes is time step restrictions more severe than the fundamental restriction forced by the relevant wave speeds. Besides the need to perform long time calculations there is another consideration which translates to astronomical amounts of computational time: reliability.

One of the primary goals of climate modeling is to predict the effects of carbon dioxide distributions and concentrations on average temperatures. This is a major point of discussion at the Intergovernmental Panel on Climate Change, the key informational source internationally for environmental policy makers. Reliability of climate statistics is critical.

Numerous uncertainty quantification studies are being performed with GCMs to determine how well this data can be predicted. Typically, large ensembles of climate runs (often thousands) are used to determine uncertainty. Each ensemble element represents a different choice of parameters, initial conditions or other prescribed data. The need to determine model reliability compounds the problem of computation time for climate research. As a result, constant work is being done to increase climate code efficiency.

1.0.1 Chapter Description

This work begins in Chapter 2 with a study of a coupled system of heat equations with linear coupling (see (1.4) below) as a simplification avoiding the nonlinearity in the coupling and due to convection. Let the global domain Ω be the union of subdomains Ω_1 and Ω_2 and the interface $I = \partial\Omega_1 \cap \partial\Omega_2$. The problem is: *given* $\nu_i > 0, f_i : [0,T] \to H^1(\Omega_i), u_i(0) \in H^1(\Omega_i)$ *and* $\kappa \in \mathbb{R}$, *find (for* $i = 1, 2$*)* $u_i : \overline{\Omega}_i \times [0,T] \to \mathbb{R}$ *satisfying*

$$
\begin{aligned}
u_{i,t} - \nu_i \Delta u_i &= f_i, \quad \text{in } \Omega_i, && (1.3)\\
-\nu_i \nabla u_i \cdot \hat{n}_i &= \kappa(u_i - u_j), \quad \text{on } I,\ i,j = 1,2\,,\ i \neq j\,, && (1.4)\\
u_i(x,0) &= u_i^0(x), \quad \text{in } \Omega_i, && (1.5)\\
u_i &= g_i, \quad \text{on } \Gamma_i = \partial\Omega_i \setminus I. && (1.6)
\end{aligned}
$$

Finite elements are used for spatial discretization of all problems in this and later chapters. The key is development of novel partitioned time stepping techniques. Here, three time discretizations are introduced. One is a fully implicit (coupled) algorithm using backward-Euler. The next is a partitioned variation which treats the interface degrees of freedom for the (decoupled) subdomain equations implicitly. The third variation treats the global parts of the equations implicitly but uses an extrapolation of the interface degrees of freedom from the previous time level. It is proved that the second and third variations differ in that the former is stable for any size time step regardless of mesh size or choice of any other problem parameters. The latter algorithm requires that the time step size scale proportionally with the dissipation parameters and inversely with the square of the interface parameter in the coupling condition. Optimal order convergence rates are proved. The time accuracy is to

first order. Numerical tests are performed which demonstrate that precisely this behavior is observed in practice.

In Chapter 3 higher order accuracy in time is sought by deferred correction for the same problem (1.3) - (1.6). The deferred correction algorithm performs successive linear calculations beginning with a first-order in time numerical approximation from Chapter 2. It is proved that higher accuracy in time (order Δt^q) can be achieved by solving $q-1$ of these successive linear problems. A complete stability and convergence analysis is provided. Computations verify the higher convergence rate for the case $q=2$ and improved accuracy over the uncorrected solution.

A first step toward nonlinear coupling (1.8) is taken in Chapter 4. The system of ODEs resulting from spatial discretization of two Navier-Stokes equations with nonlinear coupling across a common interface is used as a model and reduced to the 2×2 ODE system

$$\begin{aligned} \frac{d\mathbf{x}}{dt} + A(\mathbf{x})\mathbf{x} + \kappa|x_1 - y_1|(x_1 - y_1)[\mathbf{1}\ ,\ \mathbf{0}]^T &= \mathbf{f}(t) \\ \frac{d\mathbf{y}}{dt} + B(\mathbf{y})\mathbf{y} + \kappa|x_1 - y_1|(y_1 - x_1)[\mathbf{1}\ ,\ \mathbf{0}]^T &= \mathbf{g}(t), \end{aligned} \tag{1.7}$$

where the matrices A and B can be decomposed into the sum of symmetric and skew-symmetric components representing diffusion and convection (linearized by extrapolation), respectively. Time stepping methods successful for this system have a good chance of extending to full discretizations for the nonlinearly coupled fluid equations. The purpose is to aid in development of numerical methods as the analysis of the ODE system reduces technical details. Indeed, two time stepping algorithms for the system are developed which are unconditionally stable and decoupled. One method employs an extrapolation of data used in the coupling terms featuring a novel usage of geometric averaging to retain stability. The other method is a modification of a more intuitive extension of ideas from Chapter 2 that retains stability (and optimal convergence) by adding numerical dissipation. A full numerical analysis for both methods is provided and numerical tests are performed. It is shown that while the methods are stable, asymptotic convergence rates require smaller time steps than would be expected from the case of linear coupling. The addition of numerical diffusion appears less promising than the geometric averaging technique and is not explored further in the subsequent chapters. A fully implicit and monolithically coupled algorithm

is used for comparison. The numerical decoupling of the equations is observed to introduce error comparing with the coupled algorithm.

The partitioned method of Chapter 4 using geometric averaging is adapted to the case of two incompressible Navier-Stokes fluids with nonlinear coupling in Chapter 5. The coupling conditions are

$$-\nu_i \hat{n}_i \cdot \nabla u_i \cdot \hat{\tau} = \kappa |u_i - u_j|(u_i - u_j) \cdot \hat{\tau}, \;\; i, j = 1, 2 \text{ and } i \neq j, \tag{1.8}$$

where $\hat{n}_i$ is the outward pointing unit normal vector on $\partial\Omega_i \cap I$ for $i = 1, 2$ and $\hat{\tau}$ any unit tangent vector on I. It is proved that the proposed numerical method is unconditionally stable. A time step restriction is required to guarantee optimal convergence rates with respect to the time step and mesh sizes. This restriction is of the form

$$\Delta t \leq C(\mathbf{u}, \mathbf{f})/D, \;\; D = \left\{ (1 + \kappa^4) \max\{\nu_1^{-3}, \nu_2^{-3}\} \right\},$$

where the generic constant $C(\mathbf{u}, \mathbf{f}) > 0$ depends only on the solution $\mathbf{u}$ and forcing $\mathbf{f}$, not on the mesh size, time step size or other problem parameters appearing in D. In fact, for small values of the interface parameter, the restriction is very similar to that of the NSE on a single domain using backward-Euler. Computational evidence is provided that the geometric averaging technique helps the stability of the method with nonlinear coupling versus a more direct extension of the techniques in Chapter 2. Convergence rates are studied numerically using two tests. In one a manufactured solution is used on two coupled rectangular domains. It is observed that an error plateau occurs, as in the tests of Chapter 4. By this it is meant that as the time step is decreased, the error decreases at a suboptimal rate and does not predictably improve until below some critical time step size. The computational expense of exploring the behavior at smaller time steps was deemed too prohibitive and this remains an open question. In the second test motivated by the work of Bresch and Koko [12], a reference solution was generated using a relatively fine mesh and small time steps with a fully implicit algorithm to eliminate errors due to numerical decoupling. Convergence rates for the partitioned algorithm were calculated from this reference solution. The errors in this case were more in line with the expected asymptotic behavior.

The work of Chapters 2 - 5 demonstrate the possible application of partitioned time stepping to decouple the atmosphere and ocean momentum equations and use large time steps. The partitioned method of Chapter 5 is adapted in Chapter 6 to allow different time step sizes for the two subdomain calculations. As described above this is absolutely necessary in atmosphere-ocean calculations due to the different spatial and time scales of the subproblems. Indeed, there is no restriction on the relative size of mesh elements used for the subdomains in the discretization proposed in Chapter 6. The unconditional stability of the adapted algorithm is proved, and convergence is shown with a time step restriction similar to that in Chapter 5 except depending further on the ratio of time step sizes, denoted by $m = \Delta s/\Delta t$ with Δt the time step size for the atmosphere and Δs the time step size for the ocean. The restriction is of the form

$$C\Delta t \left\{2 + \nu_1^{-1} + \nu_2^{-1}) + (\nu_1^{-3} + \nu_2^{-3})(1 + m^2 + m\kappa^4)\right\} < 1,$$

where the generic constant $C > 0$ depends only on the solution $\mathbf{u}$ and body forcing $\mathbf{f}$. The efficiency of this algorithm is demonstrated using a test with properties that mimic the relative dynamics of the atmosphere and ocean. Specifically, letting Ω_1 represent the atmosphere domain and Ω_2 the ocean domain, boundary conditions are imposed to generate a wind on Ω_1 with fast oscillations compared to Ω_2. However, the smaller kinetic viscocity in Ω_2 induces a thin boundary layer due to the wind shear, requiring a smaller mesh than in Ω_1. Using more time steps in Ω_1 than in Ω_2 for this test case a speed-up of about 13 is demonstrated. It is observed that the ratio of time steps may increased by a factor of 8 with a factor of 3.7 increase in relative error for velocity in the sense of $H^1(\Omega)$. Perhaps more importantly, the effect on a chosen statistical measurement, average velocity, is an order of magnitude smaller than the H^1-spatial error when increasing the time step size on Ω_2.

The extension of time stepping ideas to the case of natural convection is performed in Chapter 7. A system of equations for velocity, pressure and temperature is introduced based upon the equations analyzed by Lions, Temam and Wang [47, 48, 49]. Bouyancy forcing is implemented via the Boussinesq approximation. In this case the temperature coupling

conditions are given by

$$
\begin{aligned}
-\alpha_i \hat{n}_i \cdot \nabla T_i &= (-1)^{i+1} C_{sol} + C_{ir}(T_i - T_j) \\
&\quad + C_{conv}|u_i - u_j|(T_i - T_j),
\end{aligned} \tag{1.9}
$$

where C_{sol}, C_{ir} and C_{conv} have meaning as described above for the coupling condition (1.2), T_1 and T_2 are the temperatures and the values α_i are heat diffusion parameters on Ω_i, $i = 1, 2$. The velocity coupling conditions are precisely (1.8). This chapter also explores uncertainty quantification, focusing on noise in the nonlinear interface parameters C_{conv} and κ. These parameters are studied due to their role in stability. It is expected that in practice noise will occur in these parameters due to their being prescribed based upon empirical observations and recalculated time step by time step numerically by nonlinear relationships.

A partitioned scheme is introduced for the system of equations using the ideas of Chapter 5 to retain unconditional stability, which is subsequently proved. A coupled algorithm is also studied for comparison. A full numerical investigation of uncertainty is performed for a test problem with qualitative behavior similar to the large scale motions of the atmosphere and ocean. The forcing is implemented by simulated solar heating and radiative cooling in the upper atmosphere. As expected, large variances occur in the pointwise velocity and temperature fields over a sufficiently large time. The variances are observed to propagate away from the interface into the bulk fluid. It is not clear from pointwise data that the variance for the coupled code will be less than that of the uncoupled code. Average surface temperature and associated variance is calculated and compared. The effect of using a common simplification of the coupling conditions (1.1) - (1.2) on average surface temperature is also studied. It is found that variance in average temperature is smallest for the coupled algorithm and largest using the afforementioned simplification of the coupling conditions. The thesis in concluded in Chapter 8 with a discussion of the overall results and suggestions for future work.

2.0 TIME STEPPING FOR A PARABOLIC LINEARLY COUPLED PROBLEM

2.1 INTRODUCTION

There are many problems in which different physical models, different parameter regimes or different solution behaviors are coupled across interfaces. Such problems also arise when legacy codes, highly optimized for particular processes, are considered the benchmark for solving the individual subproblems. One approach to coupled problems is monolithic solution methods. In these the globally coupled problem is assembled at each time step and then solved by iterative methods (with uncoupling in preconditioning and residual calculations). With very large problems or when using legacy codes, partitioned time marching algorithms are preferred. In these the subdomain solvers are used as a black box; each time step involves passing information across the interface followed by solving the individual subproblems independently. Typical applications in which partitioned time stepping approach is highly desirable include atmosphere-ocean coupling and fluid-solid interaction problems, for example, see [12, 14, 16]. In Section 2.1.2, a motivating atmosphere–ocean coupling problem is described, and a simplified model that is the focus of this work is presented in Section 2.1.1.

2.1.1 A Model Problem

In this work, a simplified model of diffusion through two adjacent materials which are coupled across their shared and rigid interface I through a jump condition is considered. This problem captures some of the time-stepping difficulties of the ocean-atmosphere problem described in 2.1.2. The domain consists of two subdomains Ω_1 and Ω_2 coupled across an interface I

(example in Figure 2 below). The problem is: *given* $\nu_i > 0, f_i : [0,T] \to H^1(\Omega_i), u_i(0) \in H^1(\Omega_i)$ *and* $\kappa \in \mathbb{R}$, *find (for* $i = 1,2$*)* $u_i : \overline{\Omega}_i \times [0,T] \to \mathbb{R}$ *satisfying*

$$\begin{aligned} u_{i,t} - \nu_i \Delta u_i &= f_i, \quad \text{in } \Omega_i, && (2.1)\\ -\nu_i \nabla u_i \cdot \hat{n}_i &= \kappa(u_i - u_j), \quad \text{on } I,\ i,j = 1,2\,,\ i \neq j\,, && (2.2)\\ u_i(x,0) &= u_i^0(x), \quad \text{in } \Omega_i, && (2.3)\\ u_i &= g_i, \quad \text{on } \Gamma_i = \partial\Omega_i \setminus I. && (2.4) \end{aligned}$$

Let

$$X_i := \{v_i \in H^1(\Omega_i) : v_i = 0 \text{ on } \Gamma_i\}.$$

For $u_i \in X_i$ we denote $\mathbf{u} = (u_1, u_2)$ and $X := \{\mathbf{v} = (v_1, v_2) : v_i \in H^1(\Omega_i) : v_i = 0 \text{ on } \Gamma_i, i = 1,2\}$. A natural subdomain variational formulation for (2.1)-(2.4), obtained by multiplying (2.1) by v_i, integrating and applying the divergence theorem, is to find (for $i,j = 1,2, i \neq j$) $u_i : [0,T] \to X_i$ satisfying

$$(u_{i,t}, v_i)_{\Omega_i} + (\nu_i \nabla u_i, \nabla v_i)_{\Omega_i} + \int_I \kappa(u_i - u_j) v_i ds = (f_i, v_i)_{\Omega_i}, \text{ for all } v_i \in X_i. \quad (2.5)$$

The natural monolithic variational formulation for (2.1)-(2.4) is found by summing (2.5) over $i,j = 1,2$ and $i \neq j$ and is to find $\mathbf{u} : [0,T] \to X$ satisfying

$$(\mathbf{u}_t, \mathbf{v}) + (\nu \nabla \mathbf{u}, \nabla \mathbf{v}) + \int_I \kappa[\mathbf{u}][\mathbf{v}] ds = (f, \mathbf{v}), \forall v \in X, \quad (2.6)$$

where $[\cdot]$ denotes the jump of the indicated quantity across the interface I , $(\cdot,\cdot)$ is the $L^2(\Omega_1 \cup \Omega_2)$ inner product and $\nu = \nu_i$ and $f = f_i$ in Ω_i.

Comparing (2.6) and (2.5) we see that *the monolithic, globally coupled problem (2.6) has a monolithic, global energy that is exactly conserved, (in the appropriate sense),* (set $\mathbf{v} = \mathbf{u}$ in (2.6)). *The subdomain sub-problems* (2.5) *do not posses a subdomain energy which behaves similarly due to energy transfer back and forth across the interface* I.

Related domain decomposition methods have been developed for splitting a single heat equation across an interface selected for computational convenience. Dawson and Du [25] analyzed an overlapping method requiring a minimum subdomain overlap for a given mesh width. A weak formulation is defined on the overlapping strip, and the complementary

areas of the domain are discretized separately with a procedure to estimate the interface data. Blum, Lisky and Rannacher [9] study uncoupling strategies based on updating data on artificial boundaries of overlapping subdomains via an explicit formula, then solving the problem separately on each subdomain and defining the updated global approximation via an averaging process. Another approach is treating the interface data as a Lagrange multiplier. For an elliptic problem with similarities to (2.1)-(2.4), Burman and Hansbo [15] showed the addition of a penalty term on the interface in a mixed finite element Lagrangian formulation provides a stable, decoupled method with error control.

In this chapter, two first-order in time, non-overlapping uncoupling methods for (2.1)-(2.4) are presented: a partitioned method, and an implicit-explicit (IMEX) partitioned method. These two are compared to the standard monolithic, coupled implicit method. The main difference between the methods is the manner in which the interface term in (2.5) is advanced in time to give one step black box decoupling of the subdomain problems in Ω_1 and Ω_2.

2.1.2 A Motivating Problem: Atmosphere-Ocean Coupling

Models of atmosphere-ocean interactions often involve many physical processes across multiple space and time scales. An essential feature is the interaction of the flows across an interface I. Three-dimensional, highly optimized codes for each sub-problem's physics and complex physical models make it highly desirable to be able to solve alternately atmosphere and ocean sub-problems by passing information across I. To simplify the problem to that core difficulty, consider advancing the coupled flow of one fluid across I with fluid on the other side of I. Let, as a first step, the interface to be approximated by a rigid lid. Let Ω_1, Ω_2 be the two domains sharing the interface I as a segment of their boundary, as in Figure 2.

Let τ be any tangent vector on the interface I and n_i the outward unit normal vectors of Ω_i on I. This leads to the problem for the velocity u_i, pressure p_i and stress Π_i

$$u_{i,t} + u_i \cdot \nabla u_i - \nu_i \Delta u_i + \nabla p_i = f_i \, , \nabla \cdot u_i = 0 \ \text{ in } \Omega_i, \tag{2.7}$$

$$u_i \cdot n_i = 0 \text{ on } I \, ,$$

$$n_i \cdot \Pi_i \cdot \tau = \kappa |u_i - u_j| (u_i - u_j) \cdot \tau, i, j = 1, 2, i \neq j, \ \text{on } I \tag{2.8}$$

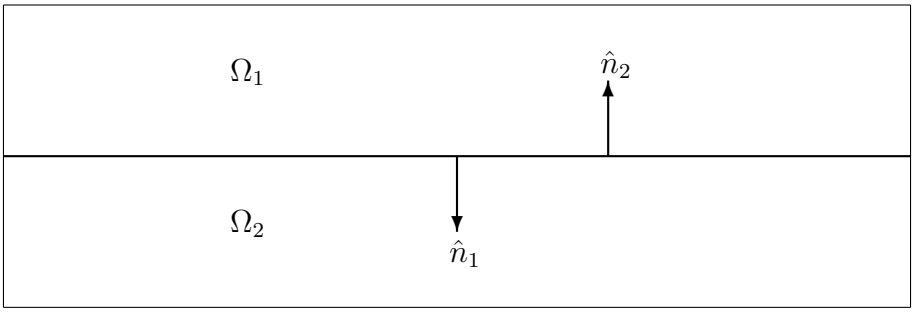

Figure 2: Example subdomains, coupled across an interface I.

with stress $\Pi_i \equiv \nu_i(\nabla u_i + (\nabla u_i)^{tr}) - p_i \mathrm{I}$ and suitable initial conditions and lateral boundary conditions on $\partial\Omega_i \backslash I$, $i = 1, 2$, and $\kappa \in \mathbb{R}$. The key difficulty, like (2.5),(2.6), is that, while the coupled, monolithic, kinetic energy is conserved, the kinetic energy in each subdomain can fluctuate due to energy transport back and forth across the interface I. Incorrect partitioning of the two subdomains can input nonphysical energy into the calculation.

One approach to such problems is to assemble the monolithic, coupled problem at each step. If the coupled problem is solved by preconditioned iterative methods, uncoupling can occur in the residual calculation and in the preconditioning step. See Bresch and Koko [12] for interesting results. Results are also available for decoupling the fluid-fluid problem using spectral methods, commonly employed in solving fluid problems with periodic boundary conditions (see [7, 46]). There are also problems where, e.g., highly optimized physical parameterizations of each subproblem are built into the subdomain codes. In such problems, the subdomain solvers are best viewed as black boxes when designing the timestepping methods, as the view studied herein.

The remainder of this work is organized as follows: in Section 2.2, notation and mathematical time-stepping algorithms are described: an IMEX method which partitions the problem by lagging all the interface terms and a partitioned method based on passing interface values across I at each timestep. Results regarding the stability and accuracy of the two partitioned algorithms are presented in Section 2.3. Convergence results for these methods are presented in Section 2.4. In Section 2.5, numerical experiments that support

the theoretical results and investigate computational issues are given.

2.2 NOTATION AND PRELIMINARIES

This section presents the two schemes for (2.1)-(2.4), and provides the necessary definitions and lemmas for their stability and convergence analysis. For $D \subset \Omega$, the Sobolev space $H^k(D) = W^{k,2}(D)$ is equipped with the usual norm $\|\cdot\|_{H^k(D)}$, and semi-norm $|\cdot|_{H^k(D)}$, for $1 \leq k < \infty$, e.g. Adams [1]. The L^2 norm is denoted by $\|\cdot\|_D$. For functions $v(x,t)$ defined for almost every $t \in (0,T)$ on a function space $V(D)$, we define the norms $(1 \leq p \leq \infty)$

$$\|v\|_{L^\infty(0,T;V)} = \operatorname*{ess\,sup}_{0<t<T} \|v(\cdot,t)\|_V \quad \text{and} \quad \|v\|_{L^p(0,T;V)} = \left(\int_0^T \|v\|_V^p dt\right)^{1/p}.$$

The dual space of the Banach space V is denoted V'.

Let the domain $\Omega \subset \mathbb{R}^d$ (typically $d = 2, 3$) have convex, polygonal subdomains Ω_i for $i = 1, 2$ with $\partial\Omega_1 \cap \partial\Omega_2 = \Omega_1 \cap \Omega_2 = I$. Let Γ_i denote the portion of $\partial\Omega_i$ that is not on I, i.e. $\Gamma_i = \partial\Omega_i \setminus I$. For $i = 1, 2$, let $X_i = \{v \in H^1(\Omega_i) : v|_{\Gamma_i} = g_i\}$, let $(\cdot,\cdot)_{\Omega_i}$ denote the standard L^2 inner product on Ω_i, and let $(\cdot,\cdot)_{X_i}$ denote the standard H^1 inner product on Ω_i. Define $X = X_1 \times X_2$ and $L^2(\Omega) = L^2(\Omega_1) \times L^2(\Omega_2)$ for $\mathbf{u}, \mathbf{v} \in X$ with $\mathbf{u} = [u_1, u_2]^T$ and $\mathbf{v} = [v_1, v_2]^T$, define the L^2 inner product

$$(\mathbf{u}, \mathbf{v}) = \sum_{i=1,2} \int_{\Omega_i} u_i v_i \, dx \,,$$

and H^1 inner product

$$(\mathbf{u}, \mathbf{v})_X = \sum_{i=1,2} \left(\int_{\Omega_i} u_i v_i \, dx + \int_{\Omega_i} \nabla u_i \cdot \nabla v_i \, dx \right),$$

and the induced norms $\|\mathbf{v}\| = (\mathbf{v}, \mathbf{v})^{1/2}$ and $\|\mathbf{v}\|_X = (\mathbf{v}, \mathbf{v})_X{}^{1/2}$, respectively. The case where $g_i = 0, i = 1, 2$ will be considered here, and can be easily extended to the case of nonhomogeneous Dirichlet conditions on $\partial\Omega_i \setminus I$.

Lemma 2.2.1. *$(X, \|\cdot\|_X)$ is a Hilbert space.*

Proof. The choice of boundary conditions for X_1 and X_2 will ensure $X_i \subset H^1(\Omega_i)$, $i = 1, 2$ are closed subspaces. Hence by the definitions of $(\cdot,\cdot)_X$ and $\|\cdot\|_X$, $(X, \|\cdot\|_X)$ is a Hilbert space. □

2.2.1 Discrete Formulation

Let $\mathcal{T}_i$ be a triangulation of Ω_i and $\mathcal{T}_h = \mathcal{T}_1 \cup \mathcal{T}_2$. Take $X_{i,h} \subset X_i$ to be conforming finite element spaces for $i = 1, 2$, and define $X_h = X_{1,h} \times X_{2,h} \subset X$. It follows that $X_h \subset X$ is a Hilbert space with corresponding inner product and induced norm. For $\mathbf{u} \in X$, define the operators $A, B : X \to (X)'$ via the Riesz Representation Theorem as

$$\big(A\mathbf{u}, \mathbf{v}\big) = \sum_{i=1,2} \nu_i \int_{\Omega_i} \nabla u_i : \nabla v_i \, dx, \quad \forall \mathbf{v} \in X \text{ and} \tag{2.9}$$

$$\big(B\mathbf{u}, \mathbf{v}\big) = \kappa \int_I [\mathbf{u}]\,[\mathbf{v}]\, ds, \ \forall \mathbf{v} \in X\,. \tag{2.10}$$

The discrete operators $A_h, B_h : X_h \to (X_h)' = X_h$ are defined analogously by restricting (2.9) and (2.10) to $\mathbf{v}_h \in X_h$. With this notation the coupled problem can be written

$$\frac{\partial \mathbf{u}}{\partial t} + A\mathbf{u} + B\mathbf{u} = \mathbf{f}, \ \mathbf{u}(x, 0) = \mathbf{u}_0. \tag{2.11}$$

For $t_k \in [0, T]$, $\mathbf{u}^k$ will denote the discrete approximation to $\mathbf{u}(t_k)$.

2.2.1.1 Fully Implicit Scheme We use the fully implicit coupled scheme as a point of comparison with the two partitioned ones we study. The monolithic, globally coupled Backward Euler in time, FEM in space method is as follows. Given $u_1^n \in X_1^h, u_2^n \in X_2^h$ solve globally (for $i, j = 1, 2, i \neq j$) for $u_1^{n+1} \in X_1^h, u_2^{n+1} \in X_2^h$ satisfying

$$\left(\frac{u_i^{n+1} - u_i^n}{\triangle t}, v_i\right)_{\Omega_i} + (\nu_i \nabla u_i^{n+1}, \nabla v_i)_{\Omega_i} + \int_I \kappa(u_i^{n+1} - u_j^{n+1}) v_i ds = (f_i^{n+1}, v_i)_{\Omega_i}, \ \forall v_i \in X_i^h. \tag{2.12}$$

This standard first-order implicit scheme can be written as follows.

Algorithm 2.2.1 (Implicit Scheme)**.** *Let* $\Delta t > 0$, $\mathbf{f} \in L^2(\Omega)$. *For each* $M \in \mathbb{N}, M \leq \frac{T}{\Delta t}$, *given* $\mathbf{u}^n \in X_h$, $n = 0, 1, 2, \cdots, M-1$, *find* $\mathbf{u}^{n+1} \in X_h$ *satisfying*

$$\frac{\mathbf{u}^{n+1} - \mathbf{u}^n}{\Delta t} + A_h \mathbf{u}^{n+1} + B_h \mathbf{u}^{n+1} = \mathbf{f}(t^{n+1}) \,. \tag{2.13}$$

The monolithic implicit scheme (2.13) is unconditionally stable. To see this, set $\mathbf{u} = (u_1, u_2), \nu = (\nu_1, \nu_2)$ in $\Omega = (\Omega_1, \Omega_2)$. If (2.12) is summed it is obvious that the true solution's energy is bounded (set $\mathbf{v} = \mathbf{u}$ below). Indeed, $\mathbf{u}$ satisfies:

$$\left(\frac{\mathbf{u}_i^{n+1} - \mathbf{u}_i^n}{\triangle t}, \mathbf{v} \right) + (\nu \nabla \mathbf{u}^{n+1}, \nabla \mathbf{v}) + \int_I \kappa [\mathbf{u}^{n+1}][\mathbf{v}] ds = (f, \mathbf{v}), \tag{2.14}$$

and setting $\mathbf{v} = \mathbf{u}^{n+1}$ one verifies stability of the monolithic method.

2.2.1.2 The Implicit-Explicit Partitioned Scheme

The calculations in (2.12), (2.13) and (2.14) uncouple into subdomain solves if the B_h term in (2.13) (the interface term) is lagged. This is equivalent to using an IMEX scheme in (2.11) and is a standard partitioned time stepping method. Passing u_j^n across I, this reads: given $u_1^n \in X_1^h, u_2^n \in X_2^h$ (passed across I as known data) solve on each subdomain (for $i, j = 1, 2, i \neq j$) for $u_1^{n+1} \in X_1^h, u_2^{n+1} \in X_2^h$

$$\left(\frac{u_i^{n+1} - u_i^n}{\triangle t}, v_i \right)_{\Omega_i} + (\nu_i \nabla u_i^{n+1}, \nabla v_i)_{\Omega_i} + \int_I \kappa (u_i^n - u_j^n) v_i ds = (f_i, v_i)_{\Omega_i}. \tag{2.15}$$

IMEX schemes have been commonly employed in a variety of applications, including incompressible fluid calculations, [2, 4, 39]. If the operators A_h and B_h defined above are simultaneously diagonalizable, one may rewrite the discrete equations using an eigenbasis common to A_h and B_h and derive a stability condition like

$$|1 - \Delta t \mu_j| \leq |1 + \Delta t \lambda_j|, \; j = 1, 2, \cdots, N,$$

where N is the dimension of X_h and A_h and B_h have eigenvalues $\{\lambda_j\}_{j=1}^N$ and $\{\mu_j\}_{j=1}^N$, respectively. Using the fact that the maximum eigenvalue of B_h is order h^{-1} when X_h satisfies an inverse inequality, stability is then guaranteed under a timestep restriction $\Delta t \leq C\, h$. In the present context, A_h and B_h are not assumed to commute, and thus eigenmode stability results are not applicable. Some stability results for this (simplest) IMEX method have been proven in [2, 39].

In fluid-structure interaction (FSI) problems the analogous time stepping method has been observed to exhibit exponential energy growth, [16]. Burman and Fernández [14] have shown for a simplified FSI problem that a penalty term added to the interface operator provides stabilization, and first-order accuracy in time can be recovered using defect correction. In Theorem 2.4.2 we show that the partitioned method (2.15) is unconditionally stable (in the discretization parameters) for the global problem (under a condition on the coupling coefficient κ and viscosities ν_i).

Algorithm 2.2.2 (First-order IMEX Scheme)**.** *Let* $\Delta t > 0$, $\mathbf{f} \in L^2(\Omega)$. *For each* $M \in \mathbb{N}, M \leq \frac{T}{\Delta t}$, *given* $\mathbf{u}^n \in X_h$, $n = 0, 1, 2, \cdots, M-1$, *find* $\mathbf{u}^{n+1} \in X_h$ *satisfying*

$$\frac{\mathbf{u}^{n+1} - \mathbf{u}^n}{\Delta t} + A_h \mathbf{u}^{n+1} + B_h \mathbf{u}^n = \mathbf{f}(t^{n+1}), \tag{2.16}$$

or, in variational form,

$$\left(\frac{\mathbf{u}^{n+1} - \mathbf{u}^n}{\Delta t}, \mathbf{v}\right) + \left(A_h \mathbf{u}^{n+1}, \mathbf{v}\right) + \left(B_h \mathbf{u}^n, \mathbf{v}\right) = \left(\mathbf{f}(t^{n+1}), \mathbf{v}\right), \ \forall \mathbf{v} \in X_h \,. \tag{2.17}$$

Adapting a stability result in Section 2.3, it shall be shown in Theorem 2.4.1 that this method is stable provided

$$\Delta t \leq C \, \min\{\nu_1, \nu_2\} \, \kappa^{-2}.$$

2.2.1.3 A Data-Passing Partitioned Scheme The second partitioned method we study decouples by solving the problems on Ω_i with interface data for $u_j, i \neq j$ coming from the previous time step. Requiring each linear solve to incorporate the interface operator sacrifices flexibility in implementation in exchange for a more accurate and stable scheme (Sections 3,4), while still admitting an easy parallelization. This method is: given $u_1^n \in X_1^h, u_2^n \in X_2^h$ solve on each subdomain (for $i, j = 1, 2, i \neq j$) for $u_1^{n+1} \in X_1^h, u_2^{n+1} \in X_2^h$

$$\left(\frac{u_i^{n+1} - u_i^n}{\triangle t}, v_i\right)_{\Omega_i} + (\nu_i \nabla u_i^{n+1}, \nabla v_i)_{\Omega_i} + \int_I \kappa(u_i^{n+1} - u_j^n) v_i ds = (f_i, v_i)_{\Omega_i}. \tag{2.18}$$

Summing (2.18) over $i = 1, 2$ gives an equivalent form to (2.18).

Algorithm 2.2.3 (Partitioned Scheme)**.** *Let $\Delta t > 0$, $\mathbf{f} \in L^2(\Omega)$. For each $M \in \mathbb{N}, M \leq \frac{T}{\Delta t}$, given $\mathbf{u}^n \in X_h$, $n = 0, 1, 2, \cdots, M-1$, find $\mathbf{u}^{n+1} \in X_h$ satisfying*

$$\begin{aligned}\left(\frac{u_i^{n+1} - u_i^n}{\Delta t}, v_i\right) + \nu_i \left(\nabla u_i^{n+1}, \nabla v_i\right) + \kappa \int_I (u_i^{n+1} - u_j^n) v_i \, ds \\ = \left(f_i(t^{n+1}), v_i\right), \ i \neq j, \ \forall v_i \in X_{i,h} \, .\end{aligned} \tag{2.19}$$

2.2.2 Analytical Tools

In this section results that will be utilized in the stability and convergence analysis are presented. It is necessary to work with norms induced by the operators A and B, and relate these norms back to $\|\cdot\|$ and $\|\cdot\|_X$. The next lemma serves to introduce useful norms for the numerical analysis and prove equivalence with the $\|\cdot\|_X$-norm.

Lemma 2.2.2. *Let $\mathbf{v} = (v_1, v_2) \in X$ and $\delta \geq 0$. Then*

$$\|\mathbf{v}\|_{A+\delta I} = \left\{ \sum_{i=1,2} \nu_i \int_{\Omega_i} |\nabla v_i|^2 \, dx + \delta \sum_{i=1,2} \int_{\Omega_i} |v_i|^2 \, dx \right\}^{1/2} \tag{2.20}$$

defines a norm on X. Furthermore, there exists $C = C(d, \Omega_1, \Omega_2) > 0$ such that if $\delta \in \mathbb{R}^+$ satisfies

$$\delta \geq C \, \kappa^2 \max\{\nu_1^{-1}, \nu_2^{-1}\}, \tag{2.21}$$

then it follows

$$\|\mathbf{v}\|_{A+\delta I-B} = \left\{ \sum_{i=1,2} \nu_i \int_{\Omega_i} |\nabla v_i|^2 \, dx + \delta \sum_{i=1,2} \int_{\Omega_i} |v_i|^2 \, dx - \kappa \int_I |v_1 - v_2|^2 \, ds \right\}^{1/2}$$

defines a norm on X. The above norms are equivalent to $\|\cdot\|_X$.

Proof. The first assertion follows from noting the Poincaré–Friedrichs inequality holds on X_1 and X_2 under the boundary conditions, and thus that the norm is derived from an inner product on X. Then equivalence to the norm $\|\cdot\|_X$ is clear. It can also be shown that $\|\mathbf{v}\|_{A+\delta I-B}$ is derived from an inner product by defining

$$(\mathbf{u},\mathbf{v})_{A+\delta I-B} = \sum_{i=1,2} \nu_i \int_{\Omega_i} \nabla u_i : \nabla v_i \, dx + \delta \sum_{i=1,2} \int_{\Omega_i} u_i \cdot v_i \, dx - \kappa \int_I (u_1 - u_2)(v_1 - v_2) \, ds \, .$$

Linearity and symmetry are clear. It remains to prove definiteness and equivalence to $\|\cdot\|_A$. Note that

$$\begin{aligned}
\kappa \int_I |v_1 - v_2|^2 \, ds &\leq \kappa \left\{ \|v_1\|^2_{L^2(I)} + 2\|v_1\|_{L^2(I)}\|v_2\|_{L^2(I)} + \|v_2\|^2_{L^2(I)} \right\} \\
&\leq 2\kappa \left\{ \|v_1\|^2_{L^2(I)} + \|v_2\|^2_{L^2(I)} \right\} \\
&= 2\kappa \left\{ \|v_1\|^2_{L^2(\partial\Omega_1)} + \|v_2\|^2_{L^2(\partial\Omega_2)} \right\} .
\end{aligned}$$

Application of the trace inequality [11] followed by Young's inequality yields

$$\begin{aligned}
&\kappa \int_I |v_1 - v_2|^2 \, ds \leq \kappa \, C(d,\Omega_1,\Omega_2) \left\{ \|v_1\|_{L^2(\Omega_1)} \|\nabla v_1\|_{L^2(\Omega_1)} + \|v_2\|_{L^2(\Omega_2)} \|\nabla v_2\|_{L^2(\Omega_2)} \right\} \\
&\leq \kappa \, C(d,\Omega_1,\Omega_2) \left\{ \frac{1}{2\gamma_1} \|v_1\|^2_{L^2(\Omega_1)} + \frac{\gamma_1}{2} \|\nabla v_1\|^2_{L^2(\Omega_1)} + \frac{1}{2\gamma_2} \|v_2\|^2_{L^2(\Omega_2)} + \frac{\gamma_2}{2} \|\nabla v_2\|^2_{L^2(\Omega_2)} \right\} .
\end{aligned}$$

Choose $\gamma_i = \dfrac{\nu_i}{\kappa \, C(d,\Omega_1,\Omega_2)}$ for $i = 1,2$ and $\delta = \dfrac{\kappa^2 \, C(d,\Omega_1,\Omega_2)^2}{2} \max\{\nu_1^{-1}, \nu_2^{-1}\}$. Then

$$\begin{aligned}
&\kappa \int_I |v_1 - v_2|^2 \, ds \leq \delta \|v_1\|^2_{L^2(\Omega_1)} + \frac{\nu_1}{2} \|\nabla v_1\|^2_{L^2(\Omega_1)} + \delta \|v_2\|^2_{L^2(\Omega_2)} + \frac{\nu_2}{2} \|\nabla v_2\|^2_{L^2(\Omega_2)} \\
&\quad \Rightarrow \frac{1}{2} \left\{ \nu_1 \|\nabla v_1\|^2_{L^2(\Omega_1)} + \nu_2 \|\nabla v_2\|^2_{L^2(\Omega_2)} \right\} \\
&\qquad \leq \sum_{i=1,2} \nu_i \int_{\Omega_i} |\nabla v_i|^2 \, dx + \delta \sum_{i=1,2} \int_{\Omega_i} |v_i|^2 \, dx - \kappa \int_I |v_1 - v_2|^2 \, ds \\
&\quad \Rightarrow \frac{1}{2} \|\mathbf{v}\|^2_A \leq \|\mathbf{v}\|^2_{A+\delta I-B} \, .
\end{aligned}$$

holds for this choice of $\delta > 0$. This proves $(\mathbf{u},\mathbf{u})_{A+\delta I-B} = 0 \Leftrightarrow \mathbf{u} = 0$ for any $\mathbf{u} \in X$, and hence $\|\cdot\|_{A+\delta I-B}$ is a norm on X. Last, to prove equivalence with $\|\cdot\|_A$, note that

$$\begin{aligned}
\|\mathbf{v}\|^2_{A+\delta I-B} \leq \|\mathbf{v}\|^2_{A+\delta I} &= \sum_{i=1,2} \left\{ \delta \|v_i\|^2_{L^2(\Omega_i)} + \nu_i \|\nabla v_i\|^2_{L^2(\Omega_i)} \right\} \\
&\leq \left\{ 1 + \delta \, \max \left\{ \frac{C^2_{PF}(\Omega_1)}{\nu_1}, \frac{C^2_{PF}(\Omega_2)}{\nu_2} \right\} \right\} \|\mathbf{v}\|^2_A \, .
\end{aligned}$$

holds by applying the Poincaré - Friedrichs inequality. □

The following discrete Gronwall lemma from [36] will also be utilized in the subsequent analysis.

Lemma 2.2.3. *Let k, M, and $a_\mu, b_\mu, c_\mu, \gamma_\mu$, for integers $\mu > 0$, be nonnegative numbers such that*

$$a_n + k\sum_{\mu=0}^{n} b_\mu \leq k\sum_{\mu=0}^{n} \gamma_\mu a_\mu + k\sum_{\mu=0}^{n} c_\mu + M \text{ for } n \geq 0. \tag{2.22}$$

Suppose that $k\gamma_\mu < 1$, for all μ, and set $\sigma_\mu \equiv (1 - k\gamma_\mu)^{-1}$. Then,

$$a_n + k\sum_{\mu=0}^{n} b_\mu \leq exp\left(k\sum_{\mu=0}^{n} \sigma_\mu\gamma_\mu\right)\left\{k\sum_{\mu=0}^{n} c_\mu + M\right\} \text{ for } n \geq 0. \tag{2.23}$$

2.3 STABILITY

Stability of the approximations in Algorithm 2.2.2 and Algorithm 2.2.3 is established here.

Lemma 2.3.1. *(IMEX Stability) Let $\mathbf{u}^{n+1} \in X^h$ satisfy (2.17) for each $n \leq \frac{T}{\Delta t} - 1$, and $0 < \Delta t < (2\delta + 1)^{-1}$ for δ satisfying (2.21). Then $\exists C_1, C_2 > 0$ independent of h, Δt such that $\mathbf{u}^{n+1}$ satisfies:*

$$\left\|\mathbf{u}^{n+1}\right\|^2 + \Delta t\sum_{k=0}^{n+1} \|\mathbf{u}^k\|_X^2 \leq C_1(\delta)e^{C_2(\delta)T}\left\{\|\mathbf{u}^0\|^2 + \Delta t\|\mathbf{u}^0\|_X^2 + \Delta t\sum_{k=0}^{n} \left\|\mathbf{f}(t^{k+1})\right\|^2\right\}.$$

Proof. Choose $\mathbf{v} = \mathbf{u}^{k+1}$ in (2.17). Then it follows:

$$\left(\frac{\mathbf{u}^{k+1} - \mathbf{u}^k}{\Delta t}, \mathbf{u}^{k+1}\right) + \left(A_h\mathbf{u}^{k+1}, \mathbf{u}^{k+1}\right) + \left(B_h\mathbf{u}^k, \mathbf{u}^{k+1}\right) = \left(\mathbf{f}(t^{k+1}), \mathbf{u}^{k+1}\right).$$

Add $\delta(\mathbf{u}^{k+1}, \mathbf{u}^{k+1})$ to both sides and apply (2.20). Then apply Young's inequality to bound below the term

$$\left(\frac{\mathbf{u}^{k+1} - \mathbf{u}^k}{\Delta t}, \mathbf{u}^{k+1}\right) \geq \frac{1}{2\Delta t}\left(\|\mathbf{u}^{k+1}\|^2 - \|\mathbf{u}^k\|^2\right),$$

resulting in

$$\frac{1}{2\Delta t}\left(\|\mathbf{u}^{k+1}\|^2 - \|\mathbf{u}^k\|^2\right) + \|\mathbf{u}^{k+1}\|_{A+\delta I}^2 + \left(B_h\mathbf{u}^k, \mathbf{u}^{k+1}\right) \leq \left(\mathbf{f}(t^{k+1}), \mathbf{u}^{k+1}\right) + \delta\|\mathbf{u}^{k+1}\|^2.$$

Now

$$\left(B_h\mathbf{u}^k, \mathbf{u}^{k+1}\right) \geq -\frac{1}{2}\left(B_h\mathbf{u}^{k+1}, \mathbf{u}^{k+1}\right) - \frac{1}{2}\left(B_h\mathbf{u}^k, \mathbf{u}^k\right).$$

Then split the term

$$\|\mathbf{u}^{k+1}\|^2_{A+\delta I} = \frac{1}{2}\|\mathbf{u}^{k+1}\|^2_{A+\delta I} + \frac{1}{2}\left(\|\mathbf{u}^{k+1}\|^2_{A+\delta I} - \|\mathbf{u}^k\|^2_{A+\delta I}\right) + \frac{1}{2}\|\mathbf{u}^k\|^2_{A+\delta I}.$$

These results imply the new estimate

$$\begin{aligned}\frac{1}{2\Delta t}\left(\|\mathbf{u}^{k+1}\|^2 - \|\mathbf{u}^k\|^2\right) + \frac{1}{2}\|\mathbf{u}^{k+1}\|^2_{A+\delta I-B} + \frac{1}{2}\left(\|\mathbf{u}^{k+1}\|^2_{A+\delta I} - \|\mathbf{u}^k\|^2_{A+\delta I}\right) + \frac{1}{2}\|\mathbf{u}^k\|^2_{A+\delta I-B}\\ \leq \left(\mathbf{f}(t^{k+1}), \mathbf{u}^{k+1}\right) + \delta\|\mathbf{u}^{k+1}\|^2.\end{aligned}$$

Apply Hölder's and Young's inequality on the RHS. Summing over $k = 0, 1, 2, \cdots, n$ yields

$$\begin{aligned}\frac{1}{2\Delta t}\left(\|\mathbf{u}^{n+1}\|^2 - \|\mathbf{u}^0\|^2\right) + \frac{1}{2}\left(\|\mathbf{u}^{n+1}\|^2_{A+\delta I} - \|\mathbf{u}^0\|^2_{A+\delta I}\right)&\\ + \frac{1}{2}\sum_{k=0}^{n}\left\{\|\mathbf{u}^{k+1}\|^2_{A+\delta I-B} + \|\mathbf{u}^k\|^2_{A+\delta I-B}\right\}&\\ \leq \frac{1}{2}\sum_{k=0}^{n}\|\mathbf{f}(t^{k+1})\|^2 + \frac{2\delta+1}{2}\sum_{k=0}^{n}\|\mathbf{u}^{k+1}\|^2.&\end{aligned}$$

Rearranging terms,

$$\begin{aligned}\|\mathbf{u}^{n+1}\|^2 + \Delta t\|\mathbf{u}^{n+1}\|^2_{A+\delta I} + \Delta t\sum_{k=0}^{n}\left\{\|\mathbf{u}^{k+1}\|^2_{A+\delta I-B} + \|\mathbf{u}^k\|^2_{A+\delta I-B}\right\}&\\ \leq \|\mathbf{u}^0\|^2 + \Delta t\|\mathbf{u}^0\|^2_{A+\delta I} + \Delta t\sum_{k=0}^{n}\|\mathbf{f}(t^{k+1})\|^2 + \Delta t(2\delta+1)\sum_{k=0}^{n}\|\mathbf{u}^{k+1}\|^2.&\end{aligned}$$

Taking $\gamma_n \equiv 2\delta + 1$ in Lemma 2.2.3, it follows that

$$\begin{aligned}\|\mathbf{u}^{n+1}\|^2 + \Delta t\|\mathbf{u}^{n+1}\|^2_{A+\delta I} + \Delta t\sum_{k=0}^{n}\left\{\|\mathbf{u}^{k+1}\|^2_{A+\delta I-B} + \|\mathbf{u}^k\|^2_{A+\delta I-B}\right\}&\\ \leq e^{C_2(\delta)T}\left\{\|\mathbf{u}^0\|^2 + \Delta t\|\mathbf{u}^0\|^2_{A+\delta I} + \Delta t\sum_{k=0}^{n}\|\mathbf{f}(t^{k+1})\|^2\right\},&\end{aligned}$$

where $C_2(\delta) = (2\delta+1)(1 - \Delta t(2\delta+1)^{-1})$. Applying Lemma 2.2.2 and simple inequalities determines $C_1(\delta)$, and the final result. □

Unlike the IMEX scheme, the data-passing partitioned algorithm is stable when κ is large compared to the dissipation constants ν_1, ν_2.

Lemma 2.3.2. *(Data-Passing Partitioned Stability) Let* $\mathbf{u}^{n+1} \in X^h$ *satisfy (2.19) for each* $n \in \left\{0, 1, \cdots, \frac{T}{\Delta t} - 1\right\}$. *Then* $\exists C > 0$ *independent of* h, Δt *such that* $\mathbf{u}^{n+1}$ *satisfies:*

$$\left\|\mathbf{u}^{n+1}\right\|^2 + \Delta t \left\|\mathbf{u}^{n+1}\right\|_I^2 + \Delta t \sum_{k=0}^{n+1} \|\mathbf{u}^k\|_X^2 \leq C \left\{ \|\mathbf{u}^0\|^2 + \Delta t \|\mathbf{u}^0\|_I^2 + \Delta t \sum_{k=0}^{n} \left\|\mathbf{f}(t^{k+1})\right\|^2 \right\}.$$

Proof. Choose $\mathbf{v} = \mathbf{u}^{k+1}$ in (2.19). Then it follows:

$$\left(\frac{u_i^{k+1} - u_i^k}{\Delta t}, u_i^{k+1}\right)_{\Omega_i} + \nu_i \|\nabla u_i^{k+1}\|_{\Omega_i}^2 + \kappa \int_I (u_i^{k+1} - u_j^k) u_i^{k+1}\, ds = \left(f_i(t^{k+1}), u_i^{k+1}\right)_{\Omega_i}, \ i \neq j.$$

Rearrange terms and bound the LHS below as in Lemma 2.3.1,

$$\begin{aligned}
\frac{1}{2\Delta t}\left(\|u_i^{k+1}\|_{\Omega_i}^2 - \|u_i^k\|_{\Omega_i}^2\right) + \nu_i \|\nabla u_i^{k+1}\|_{\Omega_i}^2 + \kappa \|u_i^{k+1}\|_I^2 & \\
= \left(f_i(t^{k+1}), u_i^{k+1}\right)_{\Omega_i} + \kappa \int_I u_j^k u_i^{k+1}\, ds & \\
\leq C_{PF}(\Omega_i) \|f_i(t^{k+1})\|_{\Omega_i} \|\nabla u_i^{k+1}\|_{\Omega_i} + \kappa \|u_j^k\|_I \|u_i^{k+1}\|_I. &
\end{aligned}$$

Young's inequality is applied next on the RHS. Summing over $i, j = 1, 2$, $i \neq j$ yields

$$\begin{aligned}
\frac{1}{2\Delta t}\left(\|\mathbf{u}^{k+1}\|^2 - \|\mathbf{u}^k\|^2\right) + \frac{1}{2}\|\mathbf{u}^{k+1}\|_A^2 + \frac{\kappa}{2}\left(\|\mathbf{u}^{k+1}\|_I^2 - \|\mathbf{u}^k\|_I^2\right) & \\
\leq C(\nu_1^{-1}, \nu_2^{-1}) \|f(t^{k+1})\|^2. &
\end{aligned}$$

Multiply through by $2\Delta t$ and sum over $k = 0, 1, \cdots, n$:

$$\begin{aligned}
\|\mathbf{u}^{n+1}\|^2 - \|\mathbf{u}^0\|^2 + \Delta t \sum_{k=0}^{n} \|\mathbf{u}^{k+1}\|_A^2 + \kappa \Delta t \left(\|\mathbf{u}^{n+1}\|_I^2 - \|\mathbf{u}^0\|_I^2\right) & \\
\leq C(\nu_1^{-1}, \nu_2^{-1}) \Delta t \sum_{k=0}^{n} \|f(t^{k+1})\|^2. &
\end{aligned}$$

Add the initial data to the right hand side. Then applying Lemma 2.2.2 and simple inequalities yields the final result.

□

2.4 CONVERGENCE

The necessary theoretical framework is in place to proceed to the convergence analysis for Algorithm 2.2.2 and Algorithm 2.2.3. Algorithm 2.2.1 is unconditionally stable and converges optimally in the same discrete energy norm of Theorem 2.4.1, the proof of which is straightforward.

Theorem 2.4.1. *(Convergence of the IMEX scheme) Let* $\mathbf{u}(t;x) \in X$ *for all* $t \in (0,T)$ *solve (2.1)–(2.4), such that* $\mathbf{u}_t \in L^2(0,T;X)$ *and* $\mathbf{u}_{tt} \in L^2(0,T;L^2(\Omega))$. *Then* $\exists C_1, C_2 > 0$ *independent of* h, Δt *such that for any* $n \in \{0,1,2,\cdots,M-1 = \frac{T}{\Delta t} - 1\}$ *and* $0 < \Delta t < (2+2\delta)^{-1}$ *with* δ *chosen according to (2.21), the solution* $\mathbf{u}^{n+1} \in X_h$ *of (2.17) satisfies:*

$$
\begin{aligned}
&\|\mathbf{u}(t^{n+1}) - \mathbf{u}^{n+1}\|^2 + \Delta t\|\mathbf{u}(t^{n+1}) - \mathbf{u}^{n+1}\|_X^2 + \frac{3\Delta t}{4}\sum_{k=0}^{n}\|\mathbf{u}(t^{k+1}) - \mathbf{u}^{k+1}\|_X^2 \\
&\qquad \le C_1(\delta)e^{C_2(\delta)T}\Big\{\|\mathbf{u}(0) - \mathbf{u}^0\|^2 + \Delta t\|\mathbf{u}(0) - \mathbf{u}^0\|_X^2 + \Delta t^2\|\mathbf{u}_t\|^2_{L^2(0,T;X)} \\
&\qquad + \Delta t^2\|\mathbf{u}_{tt}\|^2_{L^2(0,T;L^2(\Omega))} \\
&\qquad + \inf_{\mathbf{v}^0 \in X_h}\left\{\|\mathbf{u}(0) - \mathbf{v}^0\|^2 + \Delta t\|\mathbf{u}(0) - \mathbf{v}^0\|_X^2\right\} + \inf_{\mathbf{v} \in X_h}\|(\mathbf{u}(0) - \mathbf{v})_t\|^2 \\
&\qquad + T\max_{k=1,2,\cdots,n+1}\inf_{\mathbf{v}^k \in X_h}\|\mathbf{u}(t^k) - \mathbf{v}^k\|_X^2\Big\}.
\end{aligned}
$$

Proof. Restricting test functions to X_h, subtract (2.17) from (2.6) to get the error equation:

$$
\left(\mathbf{u}_t(t^{k+1}) - \frac{\mathbf{u}^{k+1} - \mathbf{u}^k}{\Delta t}, \mathbf{v}\right) + \left(A(\mathbf{u}(t^{k+1}) - \mathbf{u}^{k+1}), \mathbf{v}\right) + \left(B(\mathbf{u}(t^{k+1}) - \mathbf{u}^k), \mathbf{v}\right) = 0.
$$

Define $\mathbf{r}^{k+1} = \mathbf{u}_t(t^{k+1}) - \frac{\mathbf{u}(t^{k+1}) - \mathbf{u}(t^k)}{\Delta t}$ and rearrange terms.

$$
\begin{aligned}
\left(\mathbf{r}^{k+1}, \mathbf{v}\right) + \Big(\frac{\mathbf{u}(t^{k+1}) - \mathbf{u}^{k+1}}{\Delta t} - \frac{\mathbf{u}(t^k) - \mathbf{u}^k}{\Delta t}, \mathbf{v}\Big) + \left(A(\mathbf{u}(t^{k+1}) - \mathbf{u}^{k+1}), \mathbf{v}\right) \\
+ \left(B(\mathbf{u}(t^{k+1}) - \mathbf{u}^k), \mathbf{v}\right) = 0, \ \forall \mathbf{v} \in X_h.
\end{aligned} \tag{2.24}
$$

Define for each $k = 0, 1, 2, \cdots$ the functions $(\mathbf{u}(t^k) - \mathbf{v}^k) + (\mathbf{v}^k - \mathbf{u}^k) = \boldsymbol{\eta}^k + \boldsymbol{\phi}^k$, where $\mathbf{v}^k \in X_h$ is arbitrary. Then by adding and subtracting $\mathbf{v}^k$ where appropriate, (2.24) may be rewritten as

$$\begin{aligned} &\frac{1}{\Delta t}\left(\boldsymbol{\phi}^{k+1} - \boldsymbol{\phi}^k, \mathbf{v}\right) + \left(A\boldsymbol{\phi}^{k+1}, \mathbf{v}\right) + \left(B(\mathbf{u}(t^{k+1}) - \mathbf{u}^k), \mathbf{v}\right) \\ &\qquad = -\frac{1}{\Delta t}\left(\boldsymbol{\eta}^{k+1} - \boldsymbol{\eta}^k, \mathbf{v}\right) - \left(\mathbf{r}^{k+1}, \mathbf{v}\right) - \left(A\boldsymbol{\eta}^{k+1}, \mathbf{v}\right), \ \forall \mathbf{v} \in X_h. \end{aligned} \tag{2.25}$$

To treat the B-term, only first-order accuracy in time need be maintained, so adding and subtracting $B\mathbf{u}(t^k)$, it follows

$$B\mathbf{u}(t^{k+1}) - B\mathbf{u}^k = B(\mathbf{u}(t^{k+1}) - \mathbf{u}(t^k)) + B\boldsymbol{\eta}^k + B\boldsymbol{\phi}^k.$$

Hence by choosing $\mathbf{v} = \boldsymbol{\phi}^{k+1}$, (2.25) becomes

$$\begin{aligned} &\frac{1}{\Delta t}\left(\boldsymbol{\phi}^{k+1} - \boldsymbol{\phi}^k, \boldsymbol{\phi}^{k+1}\right) + \|\boldsymbol{\phi}^{k+1}\|_A^2 + \left(B\boldsymbol{\phi}^k, \boldsymbol{\phi}^{k+1}\right) \\ &\qquad = -\frac{1}{\Delta t}\left(\boldsymbol{\eta}^{k+1} - \boldsymbol{\eta}^k, \boldsymbol{\phi}^{k+1}\right) - \left(\mathbf{r}^{k+1}, \boldsymbol{\phi}^{k+1}\right) - \left(A\boldsymbol{\eta}^{k+1}, \boldsymbol{\phi}^{k+1}\right) \\ &\qquad - \left(B\boldsymbol{\eta}^k, \boldsymbol{\phi}^{k+1}\right) - \left(B(\mathbf{u}(t^{k+1}) - \mathbf{u}(t^k)), \boldsymbol{\phi}^{k+1}\right). \end{aligned}$$

The first term on the LHS is bounded below as in the proof of Lemma 2.3.1. Add $\delta\|\boldsymbol{\phi}^{k+1}\|^2$ to both sides, and apply $\|\boldsymbol{\phi}^{k+1}\|_A^2 + \delta\|\boldsymbol{\phi}^{k+1}\|^2 = \|\boldsymbol{\phi}^{k+1}\|_{A+\delta I}^2$. This results in a new bound

$$\begin{aligned} &\frac{1}{2\Delta t}\left(\|\boldsymbol{\phi}^{k+1}\|^2 - \|\boldsymbol{\phi}^k\|^2\right) + \|\boldsymbol{\phi}^{k+1}\|_{A+\delta I}^2 + \left(B\boldsymbol{\phi}^k, \boldsymbol{\phi}^{k+1}\right) \\ &\qquad \le -\frac{1}{\Delta t}\left(\boldsymbol{\eta}^{k+1} - \boldsymbol{\eta}^k, \boldsymbol{\phi}^{k+1}\right) - \left(\mathbf{r}^{k+1}, \boldsymbol{\phi}^{k+1}\right) - \left(A\boldsymbol{\eta}^{k+1}, \boldsymbol{\phi}^{k+1}\right) \\ &\qquad - \left(B\boldsymbol{\eta}^k, \boldsymbol{\phi}^{k+1}\right) - \left(B(\mathbf{u}(t^{k+1}) - \mathbf{u}(t^k)), \boldsymbol{\phi}^{k+1}\right) + \delta\|\boldsymbol{\phi}^{k+1}\|^2. \end{aligned} \tag{2.26}$$

The error terms involving the operator B must be absorbed into the $A + \delta I$ norms. First split $\|\boldsymbol{\phi}^{k+1}\|_{A+\delta I}^2 = \frac{1}{2}\|\boldsymbol{\phi}^{k+1}\|_{A+\delta I}^2 + \frac{1}{2}\left(\|\boldsymbol{\phi}^{k+1}\|_{A+\delta I}^2 - \|\boldsymbol{\phi}^k\|_{A+\delta I}^2\right) + \frac{1}{2}\|\boldsymbol{\phi}^k\|_{A+\delta I}^2$. Then bound

below $\left(B\boldsymbol{\phi}^k, \boldsymbol{\phi}^{k+1}\right) \geq -\frac{1}{2}\left(B\boldsymbol{\phi}^{k+1}, \boldsymbol{\phi}^{k+1}\right) - \frac{1}{2}\left(B\boldsymbol{\phi}^k, \boldsymbol{\phi}^k\right)$, so from (2.26) after multiplying through by 2 comes the bound

$$\begin{aligned}\frac{1}{\Delta t}\left(\|\boldsymbol{\phi}^{k+1}\|^2 - \|\boldsymbol{\phi}^k\|^2\right) + \|\boldsymbol{\phi}^{k+1}\|^2_{A+\delta I-B} + \|\boldsymbol{\phi}^k\|^2_{A+\delta I-B} \\ + \left(\|\boldsymbol{\phi}^{k+1}\|^2_{A+\delta I} - \|\boldsymbol{\phi}^k\|^2_{A+\delta I}\right) \leq -\frac{2}{\Delta t}\left(\boldsymbol{\eta}^{k+1} - \boldsymbol{\eta}^k, \boldsymbol{\phi}^{k+1}\right) \\ -2\left(\mathbf{r}^{k+1}, \boldsymbol{\phi}^{k+1}\right) - 2\left(A\boldsymbol{\eta}^{k+1}, \boldsymbol{\phi}^{k+1}\right) - 2\left(B\boldsymbol{\eta}^k, \boldsymbol{\phi}^{k+1}\right) \\ -2\big(B(\mathbf{u}(t^{k+1}) - \mathbf{u}(t^k)), \boldsymbol{\phi}^{k+1}\big) + 2\delta\|\boldsymbol{\phi}^{k+1}\|^2.\end{aligned} \tag{2.27}$$

The right hand side of (2.27) must be bounded in a suitable way. The first two terms require only Hölder's and Young's inequalities to bound as

$$-\frac{2}{\Delta t}\left(\boldsymbol{\eta}^{k+1} - \boldsymbol{\eta}^k, \boldsymbol{\phi}^{k+1}\right) - 2\left(\mathbf{r}^{k+1}, \boldsymbol{\phi}^{k+1}\right) \leq \left\|\frac{\boldsymbol{\eta}^{k+1} - \boldsymbol{\eta}^k}{\Delta t}\right\|^2 + \|\mathbf{r}^{k+1}\|^2 + 2\|\boldsymbol{\phi}^{k+1}\|^2 . \tag{2.28}$$

The remaining three terms in (2.27) require special treatment. Using (2.9), apply Hölder's inequality to derive the first of the necessary bounds.

$$\begin{aligned}-2\left(A\boldsymbol{\eta}^{k+1}, \boldsymbol{\phi}^{k+1}\right) &= -2\sum_{i=1,2}\left\{\nu_i \int_{\Omega_i} \nabla\boldsymbol{\eta}_i^{k+1} \cdot \nabla\boldsymbol{\phi}_{h,i}^{k+1}\, dx\right\} \\ &\leq \sum_{i=1,2}\nu_i \left\{\int_{\Omega_i} |\nabla\boldsymbol{\eta}_i^{k+1}|^2\, dx\right\}^{1/2}\left\{\int_{\Omega_i} |\nabla\boldsymbol{\phi}_{h,i}^{k+1}|^2\, dx\right\}^{1/2} \\ &\leq C(\nu_1,\nu_2)\|\boldsymbol{\eta}^{k+1}\|_X\|\boldsymbol{\phi}^{k+1}\|_X .\end{aligned}$$

Applying Lemma 2.2.2, note that $\|\boldsymbol{\phi}^{k+1}\|_X \leq C\,\|\boldsymbol{\phi}^{k+1}\|_{A+\delta I-B}$. Then use Young's inequality to get the bound

$$\begin{aligned}-2\left(A\boldsymbol{\eta}^{k+1}, \boldsymbol{\phi}^{k+1}\right) &\leq C\,\|\boldsymbol{\eta}^{k+1}\|_X\|\boldsymbol{\phi}^{k+1}\|_{A+\delta I-B} \\ &\leq C\,\|\boldsymbol{\eta}^{k+1}\|_X^2 + \frac{1}{12}\|\boldsymbol{\phi}^{k+1}\|^2_{A+\delta I-B} .\end{aligned} \tag{2.29}$$

The two remaining terms in (2.27) requiring bounds are treated in the same way. In general, for $\boldsymbol{\phi} = (\phi_1, \phi_2) \in X$ and $\boldsymbol{\psi} = (\psi_1, \psi_2) \in X_h$, bound the term $-2\left(B\boldsymbol{\phi}, \boldsymbol{\psi}\right)$ as follows. Note that, by (2.10),

$$-2\left(B\boldsymbol{\phi}, \boldsymbol{\psi}\right) = \kappa \int_I (\phi_1 - \phi_2)(\psi_1 - \psi_2)\, ds \leq \kappa \left\{\int_I |\phi_1 - \phi_2|^2\, ds\right\}^{1/2}\left\{\int_I |\psi_1 - \psi_2|^2\, ds\right\}^{1/2} .$$

From the proof of Lemma 2.2.2 it is clear these two last terms can be bounded above in the norm $\|\cdot\|_X$. Furthermore, Lemma 2.2.2 also implies

$$\begin{aligned} -2\,(B\boldsymbol{\phi},\boldsymbol{\psi}) &\le C(\kappa,\Omega_1,\Omega_2)\,\|\boldsymbol{\phi}\|_X\|\boldsymbol{\psi}\|_X \le C\,\|\boldsymbol{\phi}\|_X\|\boldsymbol{\psi}\|_{A+\delta I-B} \\ &\le C\,\|\boldsymbol{\phi}\|_X^2 + \frac{1}{12}\|\boldsymbol{\psi}\|_{A+\delta I-B}^2\,. \end{aligned} \tag{2.30}$$

Hence by taking $\boldsymbol{\psi}=\boldsymbol{\phi}^{k+1}$ and either $\boldsymbol{\phi}=\mathbf{u}(t^{k+1})-\mathbf{u}(t^k)$ or $\boldsymbol{\phi}=\boldsymbol{\eta}^k$ in (2.30) provides the needed bounds for (2.27). Combine results (2.28)–(2.30) to derive the new bound from (2.27) given by

$$\begin{aligned} &\frac{1}{\Delta t}\left(\|\boldsymbol{\phi}^{k+1}\|^2-\|\boldsymbol{\phi}^{k}\|^2\right)+\|\boldsymbol{\phi}^{k+1}\|_{A+\delta I-B}^2+\|\boldsymbol{\phi}^{k}\|_{A+\delta I-B}^2 \\ &\qquad+\left(\|\boldsymbol{\phi}^{k+1}\|_{A+\delta I}^2-\|\boldsymbol{\phi}^{k}\|_{A+\delta I}^2\right)\le\left\|\frac{\boldsymbol{\eta}^{k+1}-\boldsymbol{\eta}^k}{\Delta t}\right\|^2+\|\mathbf{r}^{k+1}\|^2 \\ &\qquad\qquad+2(1+\delta)\|\boldsymbol{\phi}^{k+1}\|^2+C\,\|\boldsymbol{\eta}^{k+1}\|_X^2+C\,\|\mathbf{u}(t^{k+1})-\mathbf{u}(t^k)\|_X^2 \\ &\qquad\qquad\qquad+C\,\|\boldsymbol{\eta}^{k}\|_X^2+\frac{3}{12}\|\boldsymbol{\phi}^{k+1}\|_{A+\delta I-B}^2. \end{aligned} \tag{2.31}$$

Now the last term on the RHS of (2.31) is subsumed. After multiplying through by Δt and summing over $k=0,1,2,\cdots,n$ it follows

$$\begin{aligned} &\|\boldsymbol{\phi}_h^{n+1}\|^2+\Delta t\|\boldsymbol{\phi}_h^{n+1}\|_{A+\delta I}^2+\frac{3\Delta t}{4}\sum_{k=0}^{n}\|\boldsymbol{\phi}^{k+1}\|_{A+\delta I-B}^2+\Delta t\sum_{k=0}^{n}\|\boldsymbol{\phi}^{k}\|_{A+\delta I-B}^2 \\ &\quad\le\|\boldsymbol{\phi}_h^{0}\|^2+\Delta t\|\boldsymbol{\phi}_h^{0}\|_{A+\delta I}^2+\Delta t\sum_{k=0}^{n}\left\{\left\|\frac{\boldsymbol{\eta}^{k+1}-\boldsymbol{\eta}^k}{\Delta t}\right\|^2+\|\mathbf{r}^{k+1}\|^2\right\} \\ &\quad+2(1+\delta)\,\Delta t\sum_{k=0}^{n}\|\boldsymbol{\phi}^{k+1}\|^2+C\,\Delta t\sum_{k=0}^{n}\left\{\|\boldsymbol{\eta}^{k+1}\|_X^2+\|\mathbf{u}(t^{k+1})-\mathbf{u}(t^k)\|_X^2+\|\boldsymbol{\eta}^{k}\|_X^2\right\}. \end{aligned} \tag{2.32}$$

The discrete Gronwall lemma may be applied to (2.32). Then combining repeated terms in the sums, a simplified bound follows:

$$\begin{aligned} &\|\boldsymbol{\phi}_h^{n+1}\|^2+\Delta t\|\boldsymbol{\phi}_h^{n+1}\|_{A+\delta I}^2+\frac{3\Delta t}{4}\sum_{k=0}^{n+1}\|\boldsymbol{\phi}^{k}\|_{A+\delta I-B}^2 \\ &\quad\le e^{C_2(\delta)T}\left\{\|\boldsymbol{\phi}_h^{0}\|^2+\Delta t\|\boldsymbol{\phi}_h^{0}\|_{A+\delta I}^2+C\,\Delta t\sum_{k=0}^{n+1}\|\boldsymbol{\eta}^{k}\|_X^2\right. \\ &\quad\left.+\Delta t\sum_{k=0}^{n}\left\{\left\|\frac{\boldsymbol{\eta}^{k+1}-\boldsymbol{\eta}^k}{\Delta t}\right\|^2+\|\mathbf{r}^{k+1}\|^2+C\,\|\mathbf{u}(t^{k+1})-\mathbf{u}(t^k)\|_X^2\right\}\right\}, \end{aligned} \tag{2.33}$$

with $C_2(\delta) = 2(1+\delta)(1-2\Delta t(1+\delta))^{-1}$. Bounds for the last three terms in (2.33) can be derived using well known arguments [45, 69]. Indeed, the following inequalities hold:

$$\begin{aligned}
\Delta t \sum_{k=0}^{n} \left\| \frac{\boldsymbol{\eta}^{k+1} - \boldsymbol{\eta}^k}{\Delta t} \right\|^2 &\leq \int_0^{t^{n+1}} \|\boldsymbol{\eta}_t\|^2 \, dt \leq \|\boldsymbol{\eta}_t\|^2_{L^2(0,T;L^2(\Omega))} \\
\Delta t \sum_{k=0}^{n} \|\mathbf{u}(t^{k+1}) - \mathbf{u}(t^k)\|_X^2 &\leq \Delta t^2 \int_0^{t^{n+1}} \|\mathbf{u}_t\|_X^2 \, dt \leq \Delta t^2 \|\mathbf{u}_t\|^2_{L^2(0,T;X)} \\
\Delta t \sum_{k=0}^{n} \|\mathbf{r}^{k+1}\|^2 &\leq \frac{\Delta t^2}{3} \int_0^{t^{n+1}} \|\mathbf{u}_{tt}\|^2 \, dt \leq \frac{\Delta t^2}{3} \|\mathbf{u}_{tt}\|^2_{L^2(0,T;L^2(\Omega))} .
\end{aligned} \tag{2.34}$$

Apply the triangle inequality to $\|\boldsymbol{\phi}_h^0\|^2 + \Delta t \|\boldsymbol{\phi}_h^0\|^2_{A+\delta I}$. Recall $\boldsymbol{\eta}^k = \mathbf{u}(t^k) - \mathbf{v}^k$ with $\mathbf{v}^k \in X_h$ arbitrarily chosen, so take the infimum over $\mathbf{v}^k \in X_h$ on the RHS. Combined with the inequalities in (2.34) it follows

$$\begin{aligned}
&\|\boldsymbol{\phi}_h^{n+1}\|^2 + \Delta t \|\boldsymbol{\phi}_h^{n+1}\|^2_{A+\delta I} + \frac{3\Delta t}{4} \sum_{k=0}^{n+1} \|\boldsymbol{\phi}^k\|^2_{A+\delta I - B} \\
&\qquad \leq C_1^* e^{C_2(\delta)T} \Bigg\{ \|\mathbf{u}(0) - \mathbf{u}^0\|^2 + \Delta t \|\mathbf{u}(0) - \mathbf{u}^0\|^2_{A+\delta I} \\
&\qquad\quad + \inf_{v_h^0 \in X_h} \left\{ \|\boldsymbol{\eta}^0\|^2 + \Delta t \|\boldsymbol{\eta}^0\|^2_{A+\delta I} \right\} \\
&\qquad\quad + \inf_{\mathbf{v}^k \in X_h} \|\boldsymbol{\eta}^k\|_X^2 + \inf_{\mathbf{v} \in X_h} \|\boldsymbol{\eta}_t\|^2_{L^2(0,T;L^2(\Omega))} \\
&\qquad\quad + \Delta t^2 \left(\|\mathbf{u}_t\|^2_{L^2(0,T;X)} + \|\mathbf{u}_{tt}\|^2_{L^2(0,T;L^2(\Omega))} \right) \Bigg\}.
\end{aligned} \tag{2.35}$$

Lemma 2.2.2 can now be applied to replace all norms of type $\|\cdot\|_{A+\delta I-B}$ and $\|\cdot\|_{A+\delta I}$ with the norm $\|\cdot\|_X$. Bound above $\Delta t \inf_{\mathbf{v}^k \in X_h} \sum_{k=0}^{n+1} \|\eta^k\|_X^2 \leq T \max_{k=0,2,\cdots,n+1} \inf_{\mathbf{v}^k \in X_h} \|\eta^k\|_X^2$. One more application of the triangle inequality and rearranging constants yields the final result.

□

In Algorithm 2.2.2 no time-step restriction is needed if $\kappa \leq \gamma \min\{\nu_1, \nu_2\}$, for some positive constant $\gamma = \gamma(\Omega_1, \Omega_2)$. The case of larger κ is less clear. For large κ the analysis indicates that convergence will require $\Delta t \leq O(\frac{\min\{\nu_1,\nu_2\}}{\kappa^2})$ and the error might grow as fast as e^{κ^2}, so that computations for $\kappa >> 1$ may require very small meshes and large numbers of time steps unless $\min\{\nu_1, \nu_2\} >> \kappa$.

The proof of convergence for Algorithm 2.2.3 is technically simpler, and shows optimal convergence in $L^2(0,T;H^1)$ with no time step restriction. κ should have only a small effect on error for the implicit method, while error of the partitioned method may increase proportional to κ, Theorem 2.4.2 next.

Theorem 2.4.2. *(Convergence of the data-passing partitioned scheme)*

Let $\mathbf{u}(t;x) \in X$ *for all* $t \in (0,T)$ *solve (2.1)–(2.4), such that* $\mathbf{u}_t \in L^2(0,T;X)$ *and* $\mathbf{u}_{tt} \in L^2(0,T;L^2(\Omega))$. *Then* $\exists C > 0$ *independent of* h, Δt *such that for any* $n \leq M-1$, *the solution* $\mathbf{u}^{n+1} \in X_h$ *of (2.19) satisfies:*

$$\begin{aligned}
&\|\mathbf{u}(t^{n+1}) - \mathbf{u}^{n+1}\|^2 + \kappa\Delta t\|\mathbf{u}(t^{n+1}) - \mathbf{u}^{n+1}\|_I^2 + \Delta t\sum_{k=0}^{n}\|\mathbf{u}(t^{k+1}) - \mathbf{u}^{k+1}\|_X^2 \\
&\quad\leq C\Big\{\|\mathbf{u}(0) - \mathbf{u}^0\|^2 + \kappa\Delta t\|\mathbf{u}(0) - \mathbf{u}^0\|_I^2 + \Delta t^2\|\mathbf{u}_t\|^2_{L^2(0,T;X)} + \Delta t^2\|\mathbf{u}_{tt}\|^2_{L^2(0,T;L^2(\Omega))} \\
&\qquad + \inf_{\mathbf{v}^0\in X_h}\left\{\|\mathbf{u}(0) - \mathbf{v}^0\|^2 + \Delta t\|\mathbf{u}(0) - \mathbf{v}^0\|_X^2\right\} + \inf_{\mathbf{v}\in X_h}\|(\mathbf{u}(0) - \mathbf{v})_t\|^2 \\
&\qquad + T\max_{k=1,2,\cdots,n+1}\inf_{\mathbf{v}^k\in X_h}\|\mathbf{u}(t^k) - \mathbf{v}^k\|_X^2\Big\}.
\end{aligned}$$

Proof. Restricting test functions to X_h, subtract (2.19) from (2.6), to get the error equation:

$$\begin{aligned}
\big(\mathbf{u}_t(t^{k+1}) - \frac{\mathbf{u}^{k+1}-\mathbf{u}^k}{\Delta t}, \mathbf{v}\big) + \big(A(\mathbf{u}(t^{k+1}) - \mathbf{u}^{k+1}), \mathbf{v}\big) + \kappa\int_I [\mathbf{u}(t^{k+1})][\mathbf{v}]\,ds \\
- \kappa\int_I (u_1^{k+1} - u_2^k)v_1\,ds - \kappa\int_I (u_2^{k+1} - u_1^k)v_2\,ds = 0.
\end{aligned}$$

Define $\mathbf{r}^{k+1} = \mathbf{u}_t(t^{k+1}) - \frac{\mathbf{u}(t^{k+1})-\mathbf{u}(t^k)}{\Delta t}$ and rearrange terms.

$$\begin{aligned}
\big(\mathbf{r}^{k+1}, \mathbf{v}\big) + \big(\frac{\mathbf{u}(t^{k+1}) - \mathbf{u}^{k+1}}{\Delta t} - \frac{\mathbf{u}(t^k) - \mathbf{u}^k}{\Delta t}, \mathbf{v}\big) + \big(A(\mathbf{u}(t^{k+1}) - \mathbf{u}^{k+1}), \mathbf{v}\big) + \kappa\int_I [\mathbf{u}(t^{k+1})][\mathbf{v}]\,ds \\
- \kappa\int_I (u_1^{k+1} - u_2^k)v_1\,ds - \kappa\int_I (u_2^{k+1} - u_1^k)v_2\,ds = 0,\ \forall \mathbf{v} \in X_h.
\end{aligned}$$

Define for each $k = 0, 1, 2, \cdots$ the functions $(\mathbf{u}(t^k) - \mathbf{v}^k) + (\mathbf{v}^k - \mathbf{u}^k) = \boldsymbol{\eta}^k + \boldsymbol{\phi}^k$, where $\mathbf{v}^k \in X_h$ is arbitrary. Then by adding and subtracting $\mathbf{v}^k$ where appropriate,

$$\begin{aligned}
&\frac{1}{\Delta t}\left(\boldsymbol{\phi}^{k+1} - \boldsymbol{\phi}^k, \mathbf{v}\right) + \left(A\boldsymbol{\phi}^{k+1}, \mathbf{v}\right) + \kappa \int_I [\mathbf{u}(t^{k+1})][\mathbf{v}]\, ds \\
&\qquad - \kappa \int_I (u_1^{k+1} - u_2^k) v_1\, ds - \kappa \int_I (u_2^{k+1} - u_1^k) v_2\, ds \\
&\qquad = -\frac{1}{\Delta t}\left(\boldsymbol{\eta}^{k+1} - \boldsymbol{\eta}^k, \mathbf{v}\right) - \left(\mathbf{r}^{k+1}, \mathbf{v}\right) - \left(A\boldsymbol{\eta}^{k+1}, \mathbf{v}\right), \ \forall \mathbf{v} \in X_h.
\end{aligned} \tag{2.36}$$

Choosing $\mathbf{v} = \boldsymbol{\phi}^{k+1}$, (2.36) becomes

$$\begin{aligned}
&\frac{1}{\Delta t}\left(\boldsymbol{\phi}^{k+1} - \boldsymbol{\phi}^k, \boldsymbol{\phi}^{k+1}\right) + \|\boldsymbol{\phi}^{k+1}\|_A^2 + \kappa \int_I [\mathbf{u}(t^{k+1})][\boldsymbol{\phi}^{k+1}]\, ds \\
&\qquad - \kappa \int_I (u_1^{k+1} - u_2^k)\phi_1^{k+1}\, ds - \kappa \int_I (u_2^{k+1} - u_1^k)\phi_2^{k+1}\, ds \\
&\qquad = -\frac{1}{\Delta t}\left(\boldsymbol{\eta}^{k+1} - \boldsymbol{\eta}^k, \boldsymbol{\phi}^{k+1}\right) - \left(\mathbf{r}^{k+1}, \boldsymbol{\phi}^{k+1}\right) - \left(A\boldsymbol{\eta}^{k+1}, \boldsymbol{\phi}^{k+1}\right).
\end{aligned}$$

The first term on the LHS is bounded below as in the proof of Lemma 2.3.1, yielding the new bound

$$\begin{aligned}
&\frac{1}{2\Delta t}\left(\|\boldsymbol{\phi}^{k+1}\|^2 - \|\boldsymbol{\phi}^k\|^2\right) + \|\boldsymbol{\phi}^{k+1}\|_A^2 + \kappa \int_I [\mathbf{u}(t^{k+1})][\boldsymbol{\phi}^{k+1}]\, ds \\
&\qquad - \kappa \int_I (u_1^{k+1} - u_2^k)\phi_1^{k+1}\, ds - \kappa \int_I (u_2^{k+1} - u_1^k)\phi_2^{k+1}\, ds \\
&\qquad \leq -\frac{1}{\Delta t}\left(\boldsymbol{\eta}^{k+1} - \boldsymbol{\eta}^k, \boldsymbol{\phi}^{k+1}\right) - \left(\mathbf{r}^{k+1}, \boldsymbol{\phi}^{k+1}\right) - \left(A\boldsymbol{\eta}^{k+1}, \boldsymbol{\phi}^{k+1}\right).
\end{aligned} \tag{2.37}$$

The interface terms must be handled in a useful way. Algebraically rearranging terms, adding and subtracting $u_1(t^k), u_2(t^k)$ to retain first order accuracy in time it follows

$$\begin{aligned}
&\kappa \int_I [\mathbf{u}(t^{k+1})][\boldsymbol{\phi}^{k+1}]\, ds - \kappa \int_I (u_1^{k+1} - u_2^k)\phi_1^{k+1}\, ds - \kappa \int_I (u_2^{k+1} - u_1^k)\phi_2^{k+1}\, ds \\
&= \kappa \int_I (\mathbf{u}(t^{k+1}) - \mathbf{u}^{k+1}) \cdot \boldsymbol{\phi}^{k+1}\, ds - \kappa \int_I (u_2(t^{k+1}) - u_2(t^k))\phi_1^{k+1}\, ds \\
&- \kappa \int_I (u_1(t^{k+1}) - u_1(t^k))\phi_2^{k+1}\, ds - \kappa \int_I (u_2(t^k) - u_2^k)\phi_1^{k+1}\, ds - \kappa \int_I (u_1(t^k) - u_1^k)\phi_2^{k+1}\, ds.
\end{aligned} \tag{2.38}$$

Now expand (2.38) by substituting $\mathbf{u}(t^j) - \mathbf{u}^j = \boldsymbol{\eta}^j + \boldsymbol{\phi}^j$ where $j = k, k+1$,

$$\begin{aligned}
&\kappa \int_I [\mathbf{u}(t^{k+1})][\boldsymbol{\phi}^{k+1}]\, ds - \kappa \int_I (u_1^{k+1} - u_2^k)\phi_1^{k+1}\, ds - \kappa \int_I (u_2^{k+1} - u_1^k)\phi_2^{k+1}\, ds \\
&\quad = \kappa \|\boldsymbol{\phi}^{k+1}\|_I^2 + \kappa \int_I \boldsymbol{\eta}^{k+1} \cdot \boldsymbol{\phi}^{k+1}\, ds - \kappa \int_I (u_2(t^{k+1}) - u_2(t^k))\phi_1^{k+1}\, ds \\
&\qquad - \kappa \int_I (u_1(t^{k+1}) - u_1(t^k))\phi_2^{k+1}\, ds - \kappa \int_I \eta_2^k \phi_1^{k+1}\, ds - \kappa \int_I \phi_2^k \phi_1^{k+1}\, ds \\
&\qquad\quad - \kappa \int_I \eta_1^k \phi_2^{k+1}\, ds - \kappa \int_I \phi_1^k \phi_2^{k+1}\, ds\,.
\end{aligned} \tag{2.39}$$

Substitution of (2.39) into (2.37) provides a more useful expression to bound $\boldsymbol{\phi}^{k+1}$. After rearranging terms,

$$\begin{aligned}
\frac{1}{2\Delta t}\left(\|\boldsymbol{\phi}^{k+1}\|^2 - \|\boldsymbol{\phi}^k\|^2\right) + \|\boldsymbol{\phi}^{k+1}\|_A^2 + \kappa\|\boldsymbol{\phi}^{k+1}\|_I^2 &\le -\frac{1}{\Delta t}\left(\boldsymbol{\eta}^{k+1} - \boldsymbol{\eta}^k, \boldsymbol{\phi}^{k+1}\right) \\
&\quad - \left(\mathbf{r}^{k+1}, \boldsymbol{\phi}^{k+1}\right) - \left(A\boldsymbol{\eta}^{k+1}, \boldsymbol{\phi}^{k+1}\right) - \kappa \int_I \boldsymbol{\eta}^{k+1} \cdot \boldsymbol{\phi}^{k+1}\, ds \\
&\quad + \kappa \int_I (u_1(t^{k+1}) - u_1(t^k))\phi_2^{k+1}\, ds + \kappa \int_I (u_2(t^{k+1}) - u_2(t^k))\phi_1^{k+1}\, ds \\
&\quad + \kappa \int_I \eta_2^k \phi_1^{k+1}\, ds + \kappa \int_I \phi_2^k \phi_1^{k+1}\, ds + \kappa \int_I \eta_1^k \phi_2^{k+1}\, ds + \kappa \int_I \phi_1^k \phi_2^{k+1}\, ds.
\end{aligned} \tag{2.40}$$

The right hand side of (2.40) must be bounded in a suitable way. The first three terms are the same as in (2.28) and are treated the same way. In fact most of the remaining proof is similar to that of Theorem 2.4.1, apart from properly bounding the interface terms. All but two of these terms contain some factor known to be $O(h)$ or $O(\Delta t)$, so Young's inequality is applied:

$$\begin{aligned}
\kappa \int_I (u_i(t^{k+1}) - u_i(t^k))\phi_j^{k+1}\, ds &\le \kappa \|u_i(t^{k+1}) - u_i(t^k)\|_I \|\phi_j^{k+1}\|_I \\
&\le C(\Omega_j, \nu_j, \kappa)\|u_i(t^{k+1}) - u_i(t^k)\|_I \left(\nu_j^{1/2}\|\nabla\phi_j^{k+1}\|_{\Omega_j}\right) \\
&\le C(\Omega_j, \nu_j, \kappa^2, \epsilon)\|u_i(t^{k+1}) - u_i(t^k)\|_I^2 + \frac{\epsilon}{2}\nu_j\|\nabla\phi_j^{k+1}\|_{\Omega_j}^2 \\
\kappa \int_I \eta_i^{k+1}\phi_j^{k+1}\, ds &\le \kappa \|\eta_i^{k+1}\|_I \|\phi_j^{k+1}\|_I \le C(\Omega_j, \nu_j, \kappa)\|\eta_i^{k+1}\|_I \left(\nu_j^{1/2}\|\nabla\phi_j^{k+1}\|_{\Omega_j}\right) \\
&\le C(\Omega_j, \nu_j, \kappa^2, \epsilon)\|\eta_i^{k+1}\|_I^2 + \frac{\epsilon}{2}\nu_j\|\nabla\phi_j^{k+1}\|_{\Omega_j}^2\,,
\end{aligned}$$

where ϵ is chosen small enough so that all terms occurring on the RHS of (2.40) of the form $\frac{\epsilon}{2}\nu_j\|\nabla\phi_j^{k+1}\|_{\Omega_j}^2$ may be added so as not to exceed $\frac{1}{2}\|\boldsymbol{\phi}^{k+1}\|_A^2$. This leaves only two interface terms to bound. Applying Hölder's and Young's inequalities to these, the bounds

$$\kappa\int_I \phi_1^k\phi_2^{k+1}\,ds + \kappa\int_I \phi_2^k\phi_1^{k+1}\,ds \le \frac{1}{2}\|\boldsymbol{\phi}^{k+1}\|_I^2 + \frac{1}{2}\|\boldsymbol{\phi}^k\|_I^2\,,$$

are applied and subtract both of these terms to the LHS of (2.40) to get the new expression

$$\begin{aligned}\frac{1}{2\Delta t}\big(\|\boldsymbol{\phi}^{k+1}\|^2 - \|\boldsymbol{\phi}^k\|^2\big) + \frac{1}{2}\|\boldsymbol{\phi}^{k+1}\|_A^2 + \frac{\kappa}{2}\big(\|\boldsymbol{\phi}^{k+1}\|_I^2 - \|\boldsymbol{\phi}^k\|_I^2\big)\\ \le C\Big\{\|\frac{\boldsymbol{\eta}^{k+1}-\boldsymbol{\eta}^k}{\Delta t}\|^2 + \|\mathbf{r}^{k+1}\|^2 + \|\nabla\boldsymbol{\eta}^{k+1}\|^2 + \|\boldsymbol{\eta}^{k+1}\|_I^2 + \|\boldsymbol{\eta}^k\|_I^2\\ + \|\mathbf{u}(t^{k+1}) - \mathbf{u}(t^k)\|_I^2\Big\}\,.\end{aligned} \tag{2.41}$$

Multiply through (2.41) by $2\Delta t$ and sum over $k = 0, 1, \cdots, n$ to derive a bound of the form

$$\begin{aligned}\|\boldsymbol{\phi}^{n+1}\|^2 + \kappa\Delta t\|\boldsymbol{\phi}^{n+1}\|_I^2 + \Delta t\sum_{k=0}^{n}\|\boldsymbol{\phi}^{k+1}\|_A^2\\ \le \|\boldsymbol{\phi}^0\|^2 + \kappa\Delta t\|\boldsymbol{\phi}^0\|_I^2 + C\Delta t\sum_{k=0}^{n}\Big\{\|\frac{\boldsymbol{\eta}^{k+1}-\boldsymbol{\eta}^k}{\Delta t}\|^2 + \|\mathbf{r}^{k+1}\|^2\\ + \|\nabla\boldsymbol{\eta}^{k+1}\|^2 + \|\boldsymbol{\eta}^{k+1}\|_I^2 + \|\boldsymbol{\eta}^k\|_I^2 + \|\mathbf{u}(t^{k+1}) - \mathbf{u}(t^k)\|_I^2\Big\}\,.\end{aligned} \tag{2.42}$$

As an application of the Trace Theorem, note that

$$\begin{aligned}\|\mathbf{u}(t^{k+1}) - \mathbf{u}(t^k)\|_I^2 &\le C\,\|\mathbf{u}(t^{k+1}) - \mathbf{u}(t^k)\|_X^2\\ \|\boldsymbol{\eta}^k\|_I^2 &\le C\,\|\boldsymbol{\eta}^k\|_X^2\,.\end{aligned}$$

The rest of the proof follows as for Theorem 2.4.1. The norm $\|\cdot\|_A$ is replaced with $\|\cdot\|_X$ after applying Lemma 2.2.2 with $\delta = 0$. Application of the bounds (2.34) and the triangle inequality finishes the proof.

□

Corollary 2.4.1. *Let $X_h \subset X$ be a finite element space corresponding to continuous piecewise polynomials of degree k. If $\mathbf{u}(\cdot,t)$ is a solution of (2.1)–(2.4) satisfying the assumptions of Theorem 2.4.1, (respectively Theorem 2.4.2) and $\mathbf{u}^0$ approximates $\mathbf{u}(\cdot,0)$ such that*

$$\|\mathbf{u}(\cdot,0) - \mathbf{u}^0\| = O(h^q),$$

then the corresponding approximations (2.17) and (2.19) converge at the rate $O(\Delta t + h^q)$ in the norm

$$\left\{ \Delta t \sum_{k=0}^{M} \|\mathbf{u}(t^k) - \mathbf{u}^k\|_X^2 \right\}^{1/2}.$$

Proof. Applying the results of the respective theorems this follows from finite element analysis, (e.g. [45, 69]). Indeed, the result follows from applying the following interpolation error estimates for $\phi \in X$.

$$\inf_{\mathbf{v}\in X_h} \|\boldsymbol{\phi} - \mathbf{v}\| \leq C\, h^{k+1} \|\boldsymbol{\phi}\|_{W^{k+1}(\Omega)}$$

$$\inf_{\mathbf{v}\in X_h} \|\boldsymbol{\phi} - \mathbf{v}\|_X \leq C\, h^{k} \|\boldsymbol{\phi}\|_{W^{k+1}(\Omega)}$$

$$\inf_{\mathbf{v}\in X_h} \|(\boldsymbol{\phi} - \mathbf{v})_t\| \leq C\, h^{k+1} \|\boldsymbol{\phi}_t\|_{W^{k+1}(\Omega)}.$$

□

2.5 COMPUTATIONAL TESTING

This section investigates the two methods of uncoupling the subdomain problems given in Algorithms 2.2.2 and 2.2.3, the IMEX approach (2.17) and the data passing partitioned approach (2.19). We also solve the fully coupled, monolithic problem (2.13) and use its solution as a baseline for comparison. In Section 2.5.1, the predicted rates of convergence are verified for the two (plus fully implicit) methods on two problems. In Section 2.5.2, computational issues related to dependence of the methods stability and accuracy on the parameters κ, ν_1, and ν_2 are studied. In Section 2.5.3, a brief discussion and a numerical example of a second-order IMEX scheme is presented.

2.5.1 Convergence Rate Verification

Assume $\Omega_1 = [0,1]\times[0,1]$ and $\Omega_2 = [0,1]\times[-1,0]$, so I is the portion of the x-axis from 0 to 1. Then $\mathbf{n}_1 = [0,\ -1]^T$ and $\mathbf{n}_2 = [0,\ 1]^T$. For a, ν_1, ν_2, and κ all arbitrary positive constants, the right hand side function $\mathbf{f}$ is chosen to ensure that

$$\begin{aligned} u_1(t,x,y) &= ax(1-x)(1-y)e^{-t} \\ u_2(t,x,y) &= ax(1-x)(c_1 + c_2 y + c_3 y^2)e^{-t}\,. \end{aligned}$$

The constants c_1, c_2, c_3 are determined from the interface conditions (2.2) and the boundary conditions for u_2. One may verify that with the following choices for c_1, c_2, c_3, u_1 and u_2 will satisfy (2.1)–(2.4) with $g_1 = g_2 = 0$, i. e. when $x \in \{0,1\}$ or $y \in \{-1,1\}$:

$$c_1 = 1 + \frac{\nu_1}{\kappa}\,,\ c_2 = \frac{-\nu_1}{\nu_2}\,,\ c_3 = c_2 - c_1.$$

The numerical analysis performed in Section 2.4 indicates that by choosing κ to be no larger than ν_1, ν_2 the IMEX scheme should perform as well as the implicit scheme. Computational results comparing the performance of the two methods are listed for two test problems:

- Test Problem 1: $a = \nu_1 = \nu_2 = \kappa = 1$.
- Test Problem 2: $a = 4, \nu_1 = 5, \nu_2 = 10, \kappa = 1/4$.

A plot of the approximation computed by the implicit method at $T = 1$ for test problem 1 is given in Figure 2.5.1.

For both problems, computations were performed using the implicit, partition, and IMEX schemes with finite element spaces consisting of continuous piece-wise polynomials of degree 1. While the analysis does not require the meshes on Ω_1 and Ω_2 to match on the interface I, the meshes used for tests herein are chosen to match on I. The code was implemented using the software package `FreeFEM++` [35]. By choosing $\Delta t = h$ the expected convergence rate of $O(\Delta t)$ was achieved by all algorithms for these two test problems. In the following

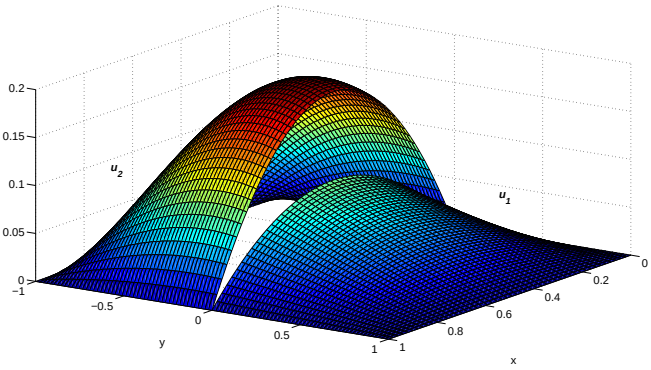

Figure 3: Implicit approximation at $T = 1$, Test Problem 1.

tables and everywhere hereafter, the norm $\|\mathbf{u}\|$ is always the discrete $L^2(0,T;H^1(\Omega))$ norm, given by

$$\|\mathbf{u}\| = \left(\sum_{n=1}^{N} \Delta t |\mathbf{u}(t_n)|_{H^1(\Omega)} \right)^{1/2},$$

where $N = T/\Delta t$ and $|\cdot|_{H^1(\Omega)}$ is the $H^1(\Omega)$ spatial seminorm. Tables 1 and 2 give the errors produced by each of the methods, showing that for these choices of parameters, all three methods compute solutions to very similar levels of accuracy.

The IMEX scheme lags the interface term, and the theory indicates that numerical difficulties may occur if κ is too large, or if the jump $u_1 - u_2$ is large compared to the dissipation rates ν_1, ν_2. Computations for $\nu_1 = \nu_2 = 1$ were also performed while varying κ between 10^{-3} and 10^3, showing the implicit scheme converges optimally choosing $\Delta t = h$ in all cases. These calculations are omitted for brevity. The IMEX scheme fails to converge for $\kappa > 5$ when choosing $\Delta t = h$. For these parameter values the IMEX scheme is expected to require a condition on the time step as outlined in the proof of Theorem 2.4.1. This issue is further explored in Section 2.5.2.

Table 1: Errors for computed approximations, test problem 1

h	Δt	$\|\mathbf{u}(t_n) - \mathbf{u}^n_{imp}\|$	rate	$\|u_1(t_n) - u^n_{1,imp}\|$	rate	$\|u_2(t_n) - u^n_{2,imp}\|$	rate
1/2	1/2	0.339237		0.0981878		0.324717	
1/4	1/4	0.189073	0.84	0.0629993	0.64	0.178269	0.87
1/8	1/8	0.10112	0.90	0.0345772	0.87	0.0950246	0.91
1/16	1/16	0.0522111	0.95	0.0179662	0.94	0.0490226	0.95
1/32	1/32	0.0265096	0.98	0.00913733	0.98	0.0248851	0.98
1/64	1/64	0.0133544	0.99	0.00460509	0.99	0.0125352	0.99
h	Δt	$\|\mathbf{u}(t_n) - \mathbf{u}^n_{part}\|$	rate	$\|u_1(t_n) - u^n_{1,part}\|$	rate	$\|u_2(t_n) - u^n_{2,part}\|$	rate
1/2	1/2	0.341323		0.103661		0.325201	
1/4	1/4	0.191544	0.83	0.0679054	0.61	0.179103	0.86
1/8	1/8	0.102654	0.90	0.0374796	0.86	0.0955673	0.91
1/16	1/16	0.0530381	0.95	0.0195048	0.94	0.0493214	0.95
1/32	1/32	0.0269361	0.98	0.00992551	0.97	0.0250407	0.98
1/64	1/64	0.0135707	0.99	0.00500371	0.99	0.0126145	0.99
h	Δt	$\|\mathbf{u}(t_n) - \mathbf{u}^n_{imex}\|$	rate	$\|u_1(t_n) - u^n_{1,imex}\|$	rate	$\|u_2(t_n) - u^n_{2,imex}\|$	rate
1/2	1/2	0.339893		0.0993662		0.325044	
1/4	1/4	0.189522	0.84	0.0639112	0.64	0.178421	0.87
1/8	1/8	0.101347	0.90	0.0350701	0.87	0.0950854	0.91
1/16	1/16	0.0523184	0.95	0.0182123	0.95	0.0490462	0.96
1/32	1/32	0.0265614	0.98	0.00926006	0.98	0.0248949	0.98
1/64	1/64	0.0133798	0.99	0.0046665	0.99	0.0125397	0.99

In Figure 4, a plot of $\|\mathbf{u}\|$ computed by each of the solution methods for decreasing time step size is given. For these plots, $a = \nu_1 = \nu_2 = 1.0$ and $h = 1/64$. As the size of κ grows, is it observed that the stability of the IMEX method decreases.

2.5.2 Relative Parameter Scaling

The computational results above imply the IMEX scheme will present an attractive alternative to the implicit scheme for problems where decoupling is necessary, so long as energy transfer across I is not too fast, i.e. except when $\kappa >> \min\{\nu_1, \nu_2\}$. To gain a more precise understanding of the time step requirements of the IMEX scheme, consider the case when κ is large compared to ν_2. This corresponds to a high flux of energy into Ω_2 with little diffusion, and thus lagging the interface term requires smaller time steps be taken to maintain stability and accuracy of the scheme. Referring to Theorem 2.4.1, note that choosing $\Delta t < (2+2\delta)^{-1}$ should ensure optimal convergence. The size of δ depends on the relative sizes of κ, ν_1, ν_2. From the proof of Lemma 2.2.2 if $\nu_1 = \nu_2 = 1$ it follows that $\delta = C(\kappa^2)$, and thus the time step size for the IMEX scheme should scale like κ^{-2} for κ sufficiently large.

Table 2: Errors for computed approximations, test problem 2

h	Δt	$\|\mathbf{u}(t_n) - \mathbf{u}^n_{imp}\|$	rate	$\|u_1(t_n) - u^n_{1,imp}\|$	rate	$\|u_2(t_n) - u^n_{2,imp}\|$	rate
1/2	1/2	11.6344		0.393197		11.6277	
1/4	1/4	6.60502	0.82	0.252197	0.64	6.6002	0.82
1/8	1/8	3.53635	0.90	0.13829	0.87	3.53365	0.90
1/16	1/16	1.82584	0.95	0.071831	0.95	1.82443	0.95
1/32	1/32	0.926987	0.98	0.0365283	0.98	0.926267	0.98
1/64	1/64	0.466956	0.99	0.0184091	0.99	0.466593	0.99

h	Δt	$\|\mathbf{u}(t_n) - \mathbf{u}^n_{part}\|$	rate	$\|u_1(t_n) - u^n_{1,part}\|$	rate	$\|u_2(t_n) - u^n_{2,part}\|$	rate
1/2	1/2	11.6345		0.397053		11.6277	
1/4	1/4	6.6052	0.82	0.256811	0.63	6.60021	0.82
1/8	1/8	3.53648	0.90	0.14154	0.86	3.53365	0.90
1/16	1/16	1.82591	0.95	0.0736946	0.94	1.82443	0.95
1/32	1/32	0.927027	0.98	0.0375179	0.97	0.926267	0.98
1/64	1/64	0.466977	0.99	0.0189183	0.99	0.466593	0.99

h	Δt	$\|\mathbf{u}(t_n) - \mathbf{u}^n_{imex}\|$	rate	$\|u_1(t_n) - u^n_{1,imex}\|$	rate	$\|u_2(t_n) - u^n_{2,imex}\|$	rate
1/2	1/2	11.6345		0.39647		11.6277	
1/4	1/4	6.60517	0.82	0.256227	0.63	6.60019	0.82
1/8	1/8	3.53646	0.90	0.141173	0.86	3.53364	0.90
1/16	1/16	1.8259	0.95	0.0734932	0.94	1.82442	0.95
1/32	1/32	0.927021	0.98	0.037413	0.97	0.926266	0.98
1/64	1/64	0.466974	0.99	0.0188648	0.99	0.466593	0.99

Remark 2.5.1. *In the stability plots of Figure 4, one method slightly overestimates the fully implicit solution and one slightly underestimates it. This suggests a possible difference, worthy of further study, in the numerical dissipation introduced by the two approaches. However, this test is too limited to draw general conclusions.*

Using the test problem of Section 4.1 with $a = \nu_1 = \nu_2 = 1$ and $\kappa = 10$ and 100, calculations were performed with $\Delta t = h$, yielding no convergence, for mesh sizes as small as 1/32. For these mesh sizes, the value of Δt is not small enough compared to κ^{-2}. The computations were repeated for fixed $\Delta t = \frac{1}{2\kappa}$ and mesh sizes between 1/2 and 1/32, also yielding no convergence. However, using the fixed time step size of $\Delta t = \frac{1}{2\kappa^2}$, optimal convergence for the IMEX method was recovered as seen in Tables 3 and 4. Results for the fully implicit and partitioned methods are presented as well for comparison.

For the choice $\kappa = 10$, restricting $\Delta t < h^2$ is too restrictive, as seen by the error for the mesh size $h = 1/32$ in Table 3. For $\kappa = 100$, using the scaling $\Delta t < 0.5h^2$ is not restrictive enough, as shown in calculations omitted herein for brevity, on mesh sizes as small as $h = 1/32$. Computational evidence supports that for larger values of κ, the time

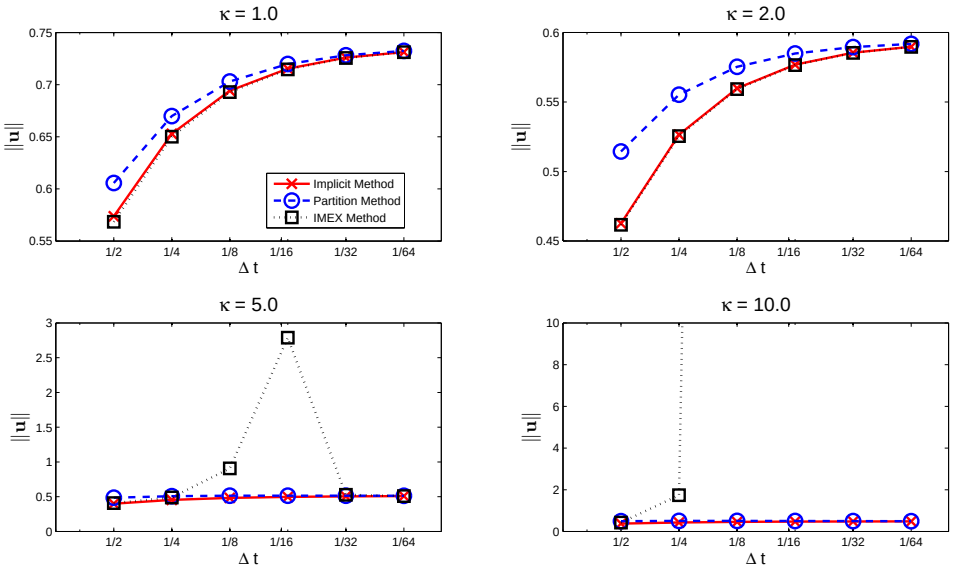

Figure 4: Stability of $\|\mathbf{u}\|$ as $\Delta t \to 0$, different values of κ.

step restriction scales like κ^{-2} and is not dependent on the mesh size.

Theorem 2.4.2 predicts that no timestep restriction is required for convergence of the data passing partitioned time stepping method, but that error may increase proportional to κ. In Table 5 the computational results are listed for the partitioned method applied to the test problem with $a = \nu_1 = \nu_2 = 1$ and $\kappa = 10$, choosing $\Delta t = h$. For these parameters and time step scaling, the IMEX method was shown to be unstable (Figure 4), but the partitioned method is stable and asymptotically approaches the theoretical convergence rate $O(\Delta t)$. The convergence rate does not approach $O(\Delta t)$ as rapidly as when κ is smaller. Table 6 lists the corresponding results using the partitioned method with $\kappa = 100$, and while the convergence rates have degraded in this case compared to $\kappa \leq 10$, there is evidence that the convergence rate may be asymptotically approaching $O(\Delta t)$.

Table 3: Errors for computed approximations, $\kappa = 10.0$, $\Delta t = (2\,\kappa^2)^{-1}$

h	Δt	$\|\mathbf{u}(t_n) - \mathbf{u}^n_{imp}\|$	rate	$\|u_1(t_n) - u^n_{1,imp}\|$	rate	$\|u_2(t_n) - u^n_{2,imp}\|$	rate
1/2	1/200	0.295742		0.129064		0.266094	
1/4	·	0.143320	1.05	0.071672	0.85	0.124112	1.10
1/8	·	0.071857	1.00	0.036764	0.96	0.061740	1.01
1/16	·	0.035946	1.00	0.018489	0.99	0.030826	1.00
1/32	·	0.017967	1.00	0.009254	1.00	0.015400	1.00
h	Δt	$\|\mathbf{u}(t_n) - \mathbf{u}^n_{part}\|$	rate	$\|u_1(t_n) - u^n_{1,part}\|$	rate	$\|u_2(t_n) - u^n_{2,part}\|$	rate
1/2	1/200	0.295704		0.129267		0.265953	
1/4	·	0.143345	1.04	0.071873	0.85	0.124024	1.10
1/8	·	0.071987	0.99	0.036995	0.96	0.061754	1.01
1/16	·	0.036253	0.99	0.018843	0.97	0.030972	1.00
1/32	·	0.018597	0.96	0.009889	0.93	0.015749	0.98
h	Δt	$\|\mathbf{u}(t_n) - \mathbf{u}^n_{imex}\|$	rate	$\|u_1(t_n) - u^n_{1,imex}\|$	rate	$\|u_2(t_n) - u^n_{2,imex}\|$	rate
1/2	1/200	0.295741		0.129068		0.266090	
1/4	·	0.143322	1.05	0.071673	0.85	0.124113	1.10
1/8	·	0.071858	1.00	0.036765	0.96	0.061741	1.01
1/16	·	0.035947	1.00	0.018490	0.99	0.030827	1.00
1/32	·	0.017967	1.00	0.009255	1.00	0.015400	1.00

2.5.3 Second Order Numerical Schemes

The problem can also be discretized using the Crank-Nicolson method, a second order fully implicit method.

Algorithm 2.5.1 (Second-order Implicit Scheme)**.** *Let* $\Delta t > 0$, $\mathbf{f} \in L^2(\Omega)$. *For each* $M \in \mathbb{N}$, $M \leq \frac{T}{\Delta t}$, *given* $\mathbf{u}^k \in X_h$, $k = 0, 1, 2, \cdots, M-1$, *find* $\mathbf{u}^{k+1} \in X_h$ *satisfying*

$$\frac{\mathbf{u}^{k+1} - \mathbf{u}^k}{\Delta t} + A_h\left(\frac{\mathbf{u}^{k+1} + \mathbf{u}^k}{2}\right) + B_h\left(\frac{\mathbf{u}^{k+1} + \mathbf{u}^k}{2}\right) = \mathbf{f}(t^{k+1/2})\,.$$

Second and higher order IMEX schemes are well known, [4], and a commonly employed example is given by Algorithm 2.5.2, where the operator A is discretized using Crank-Nicolson, and the interface operator B is discretized using second order Adams-Bashforth-2. Thus the algorithm is dubbed CNAB2 (ref. [4]), and provides a second order decoupled algorithm with which computations were attempted for the example problem in Section 2.5.1. Using the parameters $a = \nu_1 = \nu_2 = 1$ and $T = 1$ with $\kappa = 0.1$ the second order scheme achieved order $O(\Delta t^2)$ accuracy using a finite element space consisting of continuous piece-wise polynomials of degree 2, shown in Table 7. However, for larger values of κ no convergence was observed using CNAB2 for a reasonable time step size.

Table 4: Errors for computed approximations, $\kappa = 100.0$, $\Delta t = (2\,\kappa^2)^{-1}$

h	Δt	$\|\mathbf{u}(t_n) - \mathbf{u}^n_{imp}\|$	rate	$\|u_1(t_n) - u^n_{1,imp}\|$	rate	$\|u_2(t_n) - u^n_{2,imp}\|$	rate
1/2	$\frac{1}{2\cdot 10^4}$	0.283101		0.130035		0.251470	
1/4	·	0.137155	1.05	0.071969	0.85	0.116756	1.11
1/8	·	0.068752	1.00	0.036872	0.96	0.058029	1.01
1/16	·	0.034391	1.00	0.018537	0.99	0.028967	1.00
1/32	·	0.017189	1.00	0.009277	1.00	0.014471	1.00
h	Δt	$\|\mathbf{u}(t_n) - \mathbf{u}^n_{part}\|$	rate	$\|u_1(t_n) - u^n_{1,part}\|$	rate	$\|u_2(t_n) - u^n_{2,part}\|$	rate
1/2	$\frac{1}{2\cdot 10^4}$	0.283096		0.130060		0.251452	
1/4	·	0.137152	1.05	0.071988	0.85	0.116740	1.11
1/8	·	0.068751	1.00	0.036884	0.96	0.058020	1.01
1/16	·	0.034392	1.00	0.018545	0.99	0.028964	1.00
1/32	·	0.017194	1.00	0.009285	1.00	0.014472	1.00
h	Δt	$\|\mathbf{u}(t_n) - \mathbf{u}^n_{imex}\|$	rate	$\|u_1(t_n) - u^n_{1,imex}\|$	rate	$\|u_2(t_n) - u^n_{2,imex}\|$	rate
1/2	$\frac{1}{2\cdot 10^4}$	0.283101		0.130035		0.251470	
1/4	·	0.137155	1.05	0.071969	0.85	0.116756	1.11
1/8	·	0.068752	1.00	0.036872	0.96	0.058029	1.01
1/16	·	0.034391	1.00	0.018537	0.99	0.028967	1.00
1/32	·	0.017189	1.00	0.009277	1.00	0.014471	1.00

Algorithm 2.5.2 (Second-order IMEX Scheme)**.** *Let* $\Delta t > 0$, $f \in L^2(\Omega)$ *and* $M \leq \frac{T}{\Delta t}$. *Given* $\mathbf{u}^k \in X_h$, $k = 0, 1, 2, \cdots, M-1$, *find* $\mathbf{u}^{k+1} \in X_h$ *for* $M = 1, 2, \cdots, \frac{T}{\Delta t}$ *satisfying*

$$\frac{\mathbf{u}^{k+1} - \mathbf{u}^k}{\Delta t} + A_h\left(\frac{\mathbf{u}^{k+1} + \mathbf{u}^k}{2}\right) + B_h\left(\frac{3}{2}\mathbf{u}^k - \frac{1}{2}\mathbf{u}^{k-1}\right) = \mathbf{f}(t^{k+1/2})\,.$$

Stability results for the second order IMEX algorithm are not available, except for the case A and B commute, i.e. are simultaneously diagonalizable, and some stability analysis can be performed as detailed in Section 2.2.1. Preliminary computational evidence suggests a general theory will not show such a stability result for CNAB2 unless possibly under a restriction on the spatial discretization. Thus a need still exists for development of efficient higher order algorithms. One possibility is to try other second-order methods as presented by Ascher, Ruuth and Wetton [4]. Second-order consistency is expected for CNAB2, so employing the technique of Burman and Fernández [14] to the CNAB2 algorithm may be sufficient, i.e. a penalty term on the boundary followed by defect correction steps to recover consistency. Furthermore, such techniques may extend directly to the fully nonlinear fluid-fluid problem, since recovery of accuracy for both spatial and time discretization errors has been proved by Labovschii [42, 43] for second-order algorithms when solving the full incompressible NSE. These are important open questions for further work.

Table 5: Partitioned method convergence results for $\kappa = 10.0$, $\Delta t = h$

h	$\|\mathbf{u}(t_n) - \mathbf{u}^n_{part}\|$	rate	$\|u_1(t_n) - u^n_{1,part}\|$	rate	$\|u_2(t_n) - u^n_{2,part}\|$	rate
1/2	0.262699		0.146467		0.218078	
1/4	0.173203	0.601	0.108455	0.433	0.135043	0.691
1/8	0.106726	0.699	0.0691402	0.650	0.0813029	0.732
1/16	0.061409	0.797	0.0404435	0.774	0.0462102	0.815
1/32	0.0330993	0.892	0.0219521	0.882	0.0247723	0.899
1/64	0.0171554	0.948	0.0114099	0.944	0.012811	0.951

Table 6: Partitioned method convergence results for $\kappa = 100.0$, $\Delta t = h$

h	$\|\mathbf{u}(t_n) - \mathbf{u}^n_{part}\|$	rate	$\|u_1(t_n) - u^n_{1,part}\|$	rate	$\|u_2(t_n) - u^n_{2,part}\|$	rate
1/2	0.306537		0.195865		0.235801	
1/4	0.237524	0.368	0.161744	0.276	0.173944	0.439
1/8	0.190785	0.316	0.132736	0.285	0.137041	0.344
1/16	0.159422	0.259	0.112014	0.245	0.113438	0.273
1/32	0.128235	0.314	0.0904377	0.309	0.0909134	0.319
1/64	0.0926935	0.468	0.0654566	0.466	0.0656318	0.470

Table 7: Convergence results for second order IMEX

h	Δt	$\|\mathbf{u}(t_n) - \mathbf{u}^n_{imex}\|$	rate	$\|u_1(t_n) - u^n_{1,imex}\|$	rate	$\|u_2(t_n) - u^n_{2,imex}\|$	rate
1/2	1/2	0.167932		0.018283		0.166934	
1/4	1/4	0.068184	1.300	0.005730	1.674	0.067943	1.297
1/8	1/8	0.021351	1.675	0.001669	1.780	0.021286	1.674
1/16	1/16	0.005942	1.845	0.000451	1.886	0.005924	1.845
1/32	1/32	0.001565	1.925	0.000117	1.944	0.001561	1.925

3.0 SEMI-IMPLICIT SPECTRAL DEFERRED CORRECTION

3.1 INTRODUCTION

In this chapter we seek to improve the time accuracy of the partitioned time stepping techniques from Chapter 2. The model problem remains unchanged, but for convenience it is briefly described again here. The domain consists of two subdomains Ω_1 and Ω_2 coupled across an interface I (example in Figure 2). The problem is: *given* $\nu_i > 0, f_i : [0,T] \rightarrow H^1(\Omega_i), u_i(0) \in H^1(\Omega_i)$ *and* $\kappa \in \mathbb{R}$, *find (for* $i = 1,2$*)* $u_i : \overline{\Omega}_i \times [0,T] \rightarrow \mathbb{R}$ *satisfying*

$$
\begin{aligned}
u_{i,t} - \nu_i \Delta u_i &= f_i, \quad \text{in } \Omega_i, && (3.1)\\
-\nu_i \nabla u_i \cdot \hat{n}_i &= \kappa(u_i - u_j), \quad \text{on } I,\ i,j = 1,2\,,\ i \neq j\,, && (3.2)\\
u_i(x,0) &= u_i^0(x), \quad \text{in } \Omega_i, && (3.3)\\
u_i &= g_i, \quad \text{on } \Gamma_i = \partial\Omega_i \setminus I. && (3.4)
\end{aligned}
$$

Let

$$X_i := \{v_i \in H^1(\Omega_i) : v_i = 0 \text{ on } \Gamma_i\}.$$

For $u_i \in X_i$ we denote $\mathbf{u} = (u_1, u_2)$ and $X := \{\mathbf{v} = (v_1, v_2) : v_i \in H^1(\Omega_i) : v_i = 0 \text{ on } \Gamma_i, i = 1,2\}$. A natural subdomain variational formulation for (3.1)-(3.4), obtained by multiplying (3.1) by v_i, integrating and applying the divergence theorem, is to find (for $i,j = 1,2, i \neq j$) $u_i : [0,T] \rightarrow X_i$ satisfying

$$(u_{i,t}, v_i)_{\Omega_i} + (\nu_i \nabla u_i, \nabla v_i)_{\Omega_i} + \int_I \kappa(u_i - u_j) v_i ds = (f_i, v_i)_{\Omega_i}, \text{ for all } v_i \in X_i. \qquad (3.5)$$

The natural monolithic variational formulation for (3.1)-(3.4) is found by summing (3.5) over $i, j = 1, 2$ and $i \neq j$ and is to find $\mathbf{u} : [0, T] \to X$ satisfying

$$(\mathbf{u}_t, \mathbf{v}) + (\nu \nabla \mathbf{u}, \nabla \mathbf{v}) + \int_I \kappa [\mathbf{u}][\mathbf{v}] ds = (f, \mathbf{v}), \forall v \in X, \tag{3.6}$$

where $[\cdot]$ denotes the jump of the indicated quantity across the interface I , $(\cdot, \cdot)$ is the $L^2(\Omega_1 \cup \Omega_2)$ inner product and $\nu = \nu_i$ and $f = f_i$ in Ω_i.

As discussed in Chapter 2, we see that the monolithic problem (3.6) has a global energy that is exactly conserved, but the sub-problems (3.5) do not posses a subdomain energy which behaves similarly due to energy transfer back and forth across the interface I. It is possible for decoupling strategies to become unstable due to the input of non-physical energy as a numerical artifact.

This was one motivation for the work of Chapter 2 in developing partitioned schemes for (3.1)-(3.4), as a model capturing some of the technical difficulties of the coupled fluid-fluid problem. Two first order in time algorithms were analyzed, one an implicit-explicit (IMEX) approach where the interface term in the variational formulation are treated explicitly. The problem can also be discretized using the second and higher order IMEX schemes, [4]. However, stability results for the second order IMEX algorithm are not available. In this chapter, a second order in time, non-overlapping uncoupling method for (3.1)-(3.4) is presented: the two-step Semi-Implicit Spectral Deferred Correction (SISDC) method, based on the IMEX method of Chapter 2. At each step of the method the interface term in (3.5) is advanced in time to give one step black box decoupling of the subdomain problems in Ω_1 and Ω_2.

The main advantage of the deferred correction approach is that a simple low-order method can be employed, and the recovered solution is of high-order accuracy, due to a sequence of deferred correction equations. The general idea of defect correction and deferred correction methods for solving partial differential equations has been known for a long time, see the survey article [10]. The classical deferred correction approach could be seen, e.g., in [31]. However, in 2000 a modification of the classical deferred correction approach was introduced by Dutt, Greengard and Rokhlin, [29]. This allowed the construction of stable

and high-order accurate *spectral deferred correction* methods. In [53] M.L. Minion discusses these spectral deferred correction (SDC) methods in application to an initial value ODE

$$\begin{aligned} \phi'(t) &= F(t, \phi(t)),\ t \in [a, b] \\ \phi(a) &= \phi_a. \end{aligned} \tag{3.7}$$

The solution is written in terms of the Picard integral equation; a polynomial is used to interpolate the subintegrand function and the obtained integral term is replaced by its quadrature approximation. In the case when the right hand side of the ODE can be decomposed into a sum of the stiff and non-stiff terms, a Semi-Implicit SDC method (SISDC) is introduces, which allows to treat the non-stiff terms explicitly and the stiff terms implicitly. These SISDC methods for solving ordinary differential equations are further discussed in [54].

The remainder of this chapter is organized as follows: in Section 3.2, notation and mathematical time-stepping algorithms are described: the family of the higher-order semi-implicit spectral deferred correction methods. Results regarding the stability of the two-step method are presented in Section 3.3. Convergence results are presented in Section 3.4, and computations are performed to investigate stability and accuracy of a two-step SISDC algorithm in Section 3.5.

3.2 METHOD DESCRIPTION, NOTATION AND PRELIMINARIES

This section presents the numerical schemes for (3.1)-(3.4), and provides the necessary definitions and lemmas for the stability and convergence analysis. For $D \subset \Omega$, the Sobolev space $H^k(D) = W^{k,2}(D)$ is equipped with the usual norm $\|\cdot\|_{H^k(D)}$, and semi-norm $|\cdot|_{H^k(D)}$, for $1 \leq k < \infty$, e.g. Adams [1]. The L^2 norm is denoted by $\|\cdot\|_D$. For functions $v(x,t)$ defined for almost every $t \in (0,T)$ on a function space $V(D)$, we define the norms $(1 \leq p \leq \infty)$

$$\|v\|_{L^\infty(0,T;V)} = \operatorname*{ess\,sup}_{0<t<T} \|v(\cdot,t)\|_V \quad \text{and} \quad \|v\|_{L^p(0,T;V)} = \left(\int_0^T \|v\|_V^p dt \right)^{1/p}.$$

The dual space of the Banach space V is denoted V'.

Let the domain $\Omega \subset \mathbb{R}^d$ (typically $d = 2, 3$) have convex, polygonal subdomains Ω_i for $i = 1, 2$ with $\partial\Omega_1 \cap \partial\Omega_2 = \Omega_1 \cap \Omega_2 = I$. Let Γ_i denote the portion of $\partial\Omega_i$ that is not on I, i.e. $\Gamma_i = \partial\Omega_i \setminus I$. For $i = 1, 2$, let $X_i = \{v \in H^1(\Omega_i) : v|_{\Gamma_i} = g_i\}$, let $(\cdot, \cdot)_{\Omega_i}$ denote the standard L^2 inner product on Ω_i, and let $(\cdot, \cdot)_{X_i}$ denote the standard H^1 inner product on Ω_i. Define $X = X_1 \times X_2$ and $L^2(\Omega) = L^2(\Omega_1) \times L^2(\Omega_2)$ for $\mathbf{u}, \mathbf{v} \in X$ with $\mathbf{u} = [u_1, u_2]^T$ and $\mathbf{v} = [v_1, v_2]^T$, define the L^2 inner product

$$(\mathbf{u}, \mathbf{v}) = \sum_{i=1,2} \int_{\Omega_i} u_i v_i \, dx \,,$$

and H^1 inner product

$$(\mathbf{u}, \mathbf{v})_X = \sum_{i=1,2} \left(\int_{\Omega_i} u_i v_i \, dx + \int_{\Omega_i} \nabla u_i \cdot \nabla v_i \, dx \right) ,$$

and the induced norms $\|\mathbf{v}\| = (\mathbf{v}, \mathbf{v})^{1/2}$ and $\|\mathbf{v}\|_X = (\mathbf{v}, \mathbf{v})_X{}^{1/2}$, respectively. The case where $g_i = 0, i = 1, 2$ will be considered here, and can be easily extended to the case of nonhomogeneous Dirichlet conditions on $\partial\Omega_i \setminus I$.

3.2.1 Discrete Formulation

Let $\mathcal{T}_i$ be a triangulation of Ω_i and $\mathcal{T}_h = \mathcal{T}_1 \cup \mathcal{T}_2$. Take $X_{i,h} \subset X_i$ to be conforming finite element spaces for $i = 1, 2$, and define $X_h = X_{1,h} \times X_{2,h} \subset X$. It follows that $X_h \subset X$ is a Hilbert space with corresponding inner product and induced norm. For $\mathbf{u} \in X$, define the operators $A, B : X \to (X)'$ via the Riesz Representation Theorem as

$$\big(A\mathbf{u}, \mathbf{v}\big) = \sum_{i=1,2} \nu_i \int_{\Omega_i} \nabla u_i : \nabla v_i \, dx, \quad \forall \mathbf{v} \in X \text{ and} \tag{3.8}$$

$$\big(B\mathbf{u}, \mathbf{v}\big) = \kappa \int_I [\mathbf{u}] \, [\mathbf{v}] \, ds, \ \forall \mathbf{v} \in X \,. \tag{3.9}$$

The discrete operators $A_h, B_h : X_h \to (X_h)' = X_h$ are defined analogously by restricting (3.8) and (3.9) to $\mathbf{v}_h \in X_h$. With this notation the coupled problem can be written

$$\frac{\partial \mathbf{u}}{\partial t} + A\mathbf{u} + B\mathbf{u} = \mathbf{f}, \ \mathbf{u}(x, 0) = \mathbf{u}_0. \tag{3.10}$$

For $t_k \in [0,T]$, $\mathbf{u}^k$ will denote the discrete approximation to $\mathbf{u}(t_k)$.

Consider the IMEX partitioned time stepping approach for solving (3.10) of Chapter 2, copied here:

Algorithm 3.2.1 (First-order IMEX Scheme). *Let $\Delta t > 0$, $\mathbf{f} \in L^2(\Omega)$. For each $M \in \mathbb{N}, M \leq \frac{T}{\Delta t}$, given $\mathbf{u}^n \in X_h$, $n = 0, 1, 2, \cdots, M-1$, find $\mathbf{u}^{n+1} \in X_h$ satisfying*

$$\frac{\mathbf{u}^{n+1} - \mathbf{u}^n}{\Delta t} + A_h \mathbf{u}^{n+1} + B_h \mathbf{u}^n = \mathbf{f}(t^{n+1}), \tag{3.11}$$

or, in variational form,

$$\left(\frac{\mathbf{u}^{n+1} - \mathbf{u}^n}{\Delta t}, \mathbf{v}\right) + \left(A_h \mathbf{u}^{n+1}, \mathbf{v}\right) + \left(B_h \mathbf{u}^n, \mathbf{v}\right) = \left(\mathbf{f}(t^{n+1}), \mathbf{v}\right), \ \forall \mathbf{v} \in X_h \,. \tag{3.12}$$

This scheme was proven to be stable (provided $\Delta t \leq C \min\{\nu_1, \nu_2\} \kappa^{-2}$) and first order accurate. It will be shown in Section 3.3 that the SISDC method is also stable under these conditions (and higher order accurate).

The SISDC method constructs a sequence of approximations to the sought solution $\mathbf{u}$. The algorithm for the general family of SISDC applied to the model problem (3.10) is as follows.

Algorithm 3.2.2 (General SISDC). *Calculate $\mathbf{u}_0, \mathbf{u}_1, ..., \mathbf{u}_m$ - approximations to $\mathbf{u}$ via*

$$\frac{\mathbf{u}_0^{n+1} - \mathbf{u}_0^n}{\Delta t} + A_h \mathbf{u}_0^{n+1} + B_h \mathbf{u}_0^n = f^{n+1}, \tag{3.13a}$$

$$\frac{\mathbf{u}_{k+1}^{n+1} - \mathbf{u}_{k+1}^n}{\Delta t} + A_h \mathbf{r}_{k+1}^{n+1} + B_h \mathbf{r}_{k+1}^n = \frac{1}{\Delta t} I_n^{n+1}(\mathbf{u}_k), \ \textit{for } k = 0, 1, ..., m-1. \tag{3.13b}$$

Here $\mathbf{r}_{k+1}^i = \mathbf{u}_{k+1}^i - \mathbf{u}_k^i$, $k = 0, 1, ..., m-1$, $i = 0, 1, ..., N$.

$I_n^{n+1}(\mathbf{u}_k)$ is a numerical quadrature approximation to $\int_{t_n}^{t_{n+1}} F(\tau, \mathbf{u}_k(\tau)) d\tau$, where

$$F(t, \mathbf{u}) = f(t) - A_h \mathbf{u}(t) - B_h \mathbf{u}(t).$$

Remark 3.2.1. *Provided the integral terms $I_n^{n+1}(\mathbf{u}_k)$ are computed with the accuracy of order $O((\Delta t)^{k+1})$, after k iterations the above procedure will produce an approximate solution with global accuracy $O((\Delta t)^{k+1})$. If the points $t_m \in [t_n, t_{n+1}]$ are chosen to be Gaussian quadrature nodes, then the integral is being computed with a spectral integration rule, which is the reason for the name **spectral** deferred corrections.*

We will consider the two-step SISDC method and prove its stability and second order temporal accuracy. The method computes an approximation to the solution $\mathbf{u}$ of (3.10). At the first step the initial approximation $\mathbf{u}_0$ is computed via (3.13a). Thus, at the first step we use the Implicit Explicit Algorithm 3.2.1. For the second step we consider (3.13b) with $k = 0$. The second step approximation $\mathbf{u}_1$ satisfies

$$\frac{\mathbf{u}_1^{n+1} - \mathbf{u}_1^n}{\Delta t} + A_h\mathbf{u}_1^{n+1} + B_h\mathbf{u}_1^n = A_h\mathbf{u}_0^{n+1} + B_h\mathbf{u}_0^n + \frac{1}{\Delta t}I_n^{n+1}(\mathbf{u}_0). \tag{3.14}$$

It follows from Remark 3.2.1 that we need the numerical quadrature approximation of the integral term in (3.14) to be of the second order accuracy. We use Gaussian quadrature with one point - midpoint of the interval. Thus, the integral term in (3.14) is replaced by

$$\frac{F(t_n, \mathbf{u}_0) + F(t_{n+1}, \mathbf{u}_0)}{2} = \frac{f^{n+1} + f^n}{2} - \frac{A_h\mathbf{u}_0^{n+1} + A_h\mathbf{u}_0^n}{2} - \frac{B_h\mathbf{u}_0^{n+1} + B_h\mathbf{u}_0^n}{2}. \tag{3.15}$$

Therefore, in the case when the second order accuracy is sought and we only make two steps of the SISDC procedure, the second step equation could be written as:

$$\frac{\mathbf{u}_1^{n+1} - \mathbf{u}_1^n}{\Delta t} + A_h\mathbf{u}_1^{n+1} + B_h\mathbf{u}_1^n = \frac{f^{n+1} + f^n}{2} + \frac{\Delta t}{2}A_h(\frac{\mathbf{u}_0^{n+1} - \mathbf{u}_0^n}{\Delta t}) - \frac{\Delta t}{2}B_h(\frac{\mathbf{u}_0^{n+1} - \mathbf{u}_0^n}{\Delta t}) \tag{3.16}$$

The variational formulation of the two-step Semi-Implicit Spectral Deferred Correction method is:

Algorithm 3.2.3 (Two-Step SISDC Method)**.** *Let* $\Delta t > 0$, $\mathbf{f} \in L^2(\Omega)$. *For each* $M \in \mathbb{N}, M \leq \frac{T}{\Delta t}$, *given* $\mathbf{u}_0^n, \mathbf{u}_1^n \in X_h$, $n = 0, 1, 2, \cdots, M-1$, *find* $\mathbf{u}_0^{n+1}, \mathbf{u}_1^{n+1} \in X_h$ *satisfying*

$$\left(\frac{\mathbf{u}_0^{n+1} - \mathbf{u}_0^n}{\Delta t}, \mathbf{v}\right) + \left(A_h\mathbf{u}_0^{n+1}, \mathbf{v}\right) + \left(B_h\mathbf{u}_0^n, \mathbf{v}\right) = \left(\mathbf{f}^{n+1}, \mathbf{v}\right), \ \forall \mathbf{v} \in X_h \tag{3.17}$$

$$\begin{aligned}\left(\frac{\mathbf{u}_1^{n+1} - \mathbf{u}_1^n}{\Delta t}, \mathbf{v}\right) + \left(A_h\mathbf{u}_1^{n+1}, \mathbf{v}\right) + \left(B_h\mathbf{u}_1^n, \mathbf{v}\right) = \left(\frac{\mathbf{f}^{n+1} + \mathbf{f}^n}{2}, \mathbf{v}\right) \\ + \frac{\Delta t}{2}\left(A_h(\frac{\mathbf{u}_0^{n+1} - \mathbf{u}_0^n}{\Delta t}), \mathbf{v}\right) - \frac{\Delta t}{2}\left(B_h(\frac{\mathbf{u}_0^{n+1} - \mathbf{u}_0^n}{\Delta t}), \mathbf{v}\right), \ \forall \mathbf{v} \in X_h.\end{aligned} \tag{3.18}$$

3.2.2 Analytical Tools

In this section results that will be utilized in the stability and convergence analysis are presented. It is necessary to work with norms induced by the operators A and B, and relate these norms back to $\|\cdot\|$ and $\|\cdot\|_X$. The next lemma serves to introduce useful norms for the numerical analysis and prove equivalence with the $\|\cdot\|_X$-norm. This lemma is restated here but was proved in Section 2.2.2.

Lemma 3.2.1. *Let $\mathbf{v} = (v_1, v_2) \in X$ and $\delta \geq 0$. The following is a norm on X:*

$$\|\mathbf{v}\|_{A+\delta I} = \left\{ \sum_{i=1,2} \nu_i \int_{\Omega_i} |\nabla v_i|^2 \, dx + \delta \sum_{i=1,2} \int_{\Omega_i} |v_i|^2 \, dx \right\}^{1/2}. \tag{3.19}$$

This norm is equivalent to $\|\cdot\|_X$. For $\delta \geq C\,\kappa^2 \max\{\nu_1^{-1}, \nu_2^{-1}\}$,

$$\kappa \int_I [\mathbf{v}]^2 \, ds \leq \sum_{i=1,2} \nu_i \int_{\Omega_i} |\nabla v_i|^2 \, dx + \delta \sum_{i=1,2} \int_{\Omega_i} |v_i|^2 \, dx, \text{ and thus}$$

$$\|\mathbf{v}\|_{A+\delta I-B} = \left\{ \sum_{i=1,2} \nu_i \int_{\Omega_i} |\nabla v_i|^2 \, dx + \delta \sum_{i=1,2} \int_{\Omega_i} |v_i|^2 \, dx - \kappa \int_I |v_1 - v_2|^2 \, ds \right\}^{1/2}$$

is a norm on X equivalent to $\|\cdot\|_X$.

The following discrete Gronwall lemma from [36] will also be utilized in the subsequent analysis.

Lemma 3.2.2. *Let k, M, and $a_\mu, b_\mu, c_\mu, \gamma_\mu$, for integers $\mu > 0$, be nonnegative numbers such that*

$$a_n + k \sum_{\mu=0}^{n} b_\mu \leq k \sum_{\mu=0}^{n} \gamma_\mu a_\mu + k \sum_{\mu=0}^{n} c_\mu + M \text{ for } n \geq 0. \tag{3.20}$$

Suppose that $k\gamma_\mu < 1$, for all μ, and set $\sigma_\mu \equiv (1 - k\gamma_\mu)^{-1}$. Then,

$$a_n + k \sum_{\mu=0}^{n} b_\mu \leq exp\left(k \sum_{\mu=0}^{n} \sigma_\mu \gamma_\mu \right) \left\{ k \sum_{\mu=0}^{n} c_\mu + M \right\} \text{ for } n \geq 0. \tag{3.21}$$

Throughout the chapter we use the following Modified H1 Projection.

Definition 3.2.1 (Modified H1 Projection)**.** *The Modified H1 Projection operator* $P\colon X \to X_h$, $P(\mathbf{u}) = \tilde{\mathbf{u}}$, *satisfies*

$$((I + A + B)(\mathbf{u} - \tilde{\mathbf{u}}), \mathbf{v}^h) = 0, \tag{3.22}$$

for any $\mathbf{v}^h \in X_h$.

Proposition 3.2.3 (Stability of the Modified H1 Projection)**.** *Let* $\mathbf{u}$, $\tilde{\mathbf{u}}$ *satisfy (3.22). Then there exists a constant* $C = C(\kappa, \Omega_1, \Omega_2)$ *such that*

$$\|\tilde{\mathbf{u}}\|^2 + \|\nabla\tilde{\mathbf{u}}\|^2 + (B\tilde{\mathbf{u}}, \tilde{\mathbf{u}}) \leq C\|\mathbf{u}\|_X^2. \tag{3.23}$$

Proof. Take $\mathbf{v}^h = \tilde{\mathbf{u}} \in X_h$ in (3.22). Use Cauchy-Schwarz and Young's inequalities to obtain

$$\begin{aligned}\|\tilde{\mathbf{u}}\|^2 + \|\nabla\tilde{\mathbf{u}}\|^2 + (B\tilde{\mathbf{u}}, \tilde{\mathbf{u}}) \leq \frac{1}{2}\|\tilde{\mathbf{u}}\|^2 + \frac{1}{2}\|\mathbf{u}\|^2 \\ + \frac{1}{2}\|\nabla\tilde{\mathbf{u}}\|^2 + \frac{1}{2}\|\nabla\mathbf{u}\|^2 + (B\mathbf{u}, \tilde{\mathbf{u}}).\end{aligned}$$

Using the trace inequality as in the proof of Lemma 3.2.1 one can show that

$$(B\mathbf{u}, \tilde{\mathbf{u}}) \leq \frac{1}{4}\|\tilde{\mathbf{u}}\|^2 + \frac{1}{4}\|\nabla\tilde{\mathbf{u}}\|^2 + C(\kappa, \Omega_1, \Omega_2)\|\mathbf{u}\|_X^2,$$

which concludes the proof. □

In the error analysis we shall use the error estimate of the Modified H1 Projection (3.22).

Proposition 3.2.4 (Error estimate for the Modified H1 Projection)**.** *The error in the Modified H1 Projection satisfies*

$$\|\mathbf{u} - \tilde{\mathbf{u}}\|^2 + \|\nabla(\mathbf{u} - \tilde{\mathbf{u}})\|^2 + (B(\mathbf{u} - \tilde{\mathbf{u}}), \mathbf{u} - \tilde{\mathbf{u}}) \leq C \inf_{\mathbf{v}^h \in X_h} \|(\mathbf{u} - \mathbf{v}^h)\|_X^2, \tag{3.24}$$

where $C = C(\kappa, \Omega_1, \Omega_2)$.

Proof. Decompose the projection error $\mathbf{u} - \tilde{\mathbf{u}} = \mathbf{u} - I(\mathbf{u}) + (I(\mathbf{u}) - \tilde{\mathbf{u}}) = \boldsymbol{\eta} + \boldsymbol{\phi}$, where $\boldsymbol{\eta} = \mathbf{u} - I(\mathbf{u})$, $\boldsymbol{\phi} = I(\mathbf{u}) - \tilde{\mathbf{u}}$, and $I(\mathbf{u})$ approximates $\mathbf{u}$ in X_h. Take $\mathbf{v}^h = \boldsymbol{\phi} \in X_h$ in (3.22). This gives

$$\|\boldsymbol{\phi}\|^2 + \|\nabla\boldsymbol{\phi}\|^2 + (B\boldsymbol{\phi}, \boldsymbol{\phi}) = -(\boldsymbol{\eta}, \boldsymbol{\phi}) - (\nabla\boldsymbol{\eta}, \nabla\boldsymbol{\phi}) - (B\boldsymbol{\eta}, \boldsymbol{\phi}). \tag{3.25}$$

Using the trace inequality as in the proof of Lemma 3.2.1 and applying the Cauchy-Schwarz and Young's inequalities leads to

$$\|\boldsymbol{\phi}\|^2 + \|\nabla\boldsymbol{\phi}\|^2 + (B\boldsymbol{\phi}, \boldsymbol{\phi}) \leq C\|\boldsymbol{\eta}\|_X^2. \tag{3.26}$$

Since $I(\mathbf{u})$ is an approximation of $\mathbf{u}$ in X_h, we can take infimum over X_h. The proof is concluded by applying the triangle inequality. □

3.3 STABILITY

Stability of the IMEX scheme (Algorithm 3.2.1) was established in [18], see the lemma below.

Lemma 3.3.1. *(IMEX Stability) Let $\mathbf{u}_0^{n+1} \in X^h$ satisfy (3.17) for each $n \leq \frac{T}{\Delta t} - 1$, and $0 < \Delta t < (2\delta + 1)^{-1}$. Then $\exists C_1, C_2 > 0$ independent of h, Δt such that $\mathbf{u}_0^{n+1}$ satisfies:*

$$\left\|\mathbf{u}_0^{n+1}\right\|^2 + \Delta t \sum_{k=0}^{n+1} \|\mathbf{u}_0^k\|_X^2 \leq C_1(\delta) e^{C_2(\delta)T} \left\{ \|\mathbf{u}_0^0\|^2 + \Delta t \|\mathbf{u}_0^0\|_X^2 + \Delta t \sum_{k=0}^{n} \left\|\mathbf{f}(t^{k+1})\right\|^2 \right\}.$$

Hence, the initial approximation $\mathbf{u}_0$ which satisfies (3.17) is stable. We conclude the proof of stability of the SISDC approximations by considering the second step approximation $\mathbf{u}_1$ satisfying (3.18).

Theorem 3.3.2 (Stability of SISDC)**.** *Let $\mathbf{u}_1^{n+1} \in X^h$ satisfy (3.18) for each $n \leq \frac{T}{\Delta t} - 1$, and $0 < \Delta t < (2\delta + 1)^{-1}$. Then $\exists C_1, C_2 > 0$ independent of h, Δt such that $\mathbf{u}_1^{n+1}$ satisfies:*

$$\left\|\mathbf{u}_1^{n+1}\right\|^2 + \Delta t \sum_{k=0}^{n+1} \|\mathbf{u}_1^k\|_X^2 \leq C_1(\delta) e^{C_2(\delta)T} \left\{ \|\mathbf{u}_1^0\|^2 + \Delta t \|\mathbf{u}_1^0\|_X^2 + \Delta t \sum_{k=0}^{n} \left\|\mathbf{f}(t^{k+1})\right\|^2 \right\}.$$

Proof. Choose $\mathbf{v} = \mathbf{u}_1^{n+1}$ in (3.18). Then it follows:

$$\left(\frac{\mathbf{u}_1^{n+1}-\mathbf{u}_1^n}{\Delta t}, \mathbf{u}_1^{n+1}\right) + \left(A_h\mathbf{u}_1^{n+1}, \mathbf{u}_1^{n+1}\right) + \left(B_h\mathbf{u}_1^n, \mathbf{u}_1^{n+1}\right) = \left(\frac{\mathbf{f}^{n+1}+\mathbf{f}^n}{2}, \mathbf{u}_1^{n+1}\right) + \frac{\Delta t}{2}\left(A_h(\frac{\mathbf{u}_0^{n+1}-\mathbf{u}_0^n}{\Delta t}), \mathbf{u}_1^{n+1}\right) - \frac{\Delta t}{2}\left(B_h(\frac{\mathbf{u}_0^{n+1}-\mathbf{u}_0^n}{\Delta t}), \mathbf{u}_1^{n+1}\right).$$

Add $\delta(\mathbf{u}_1^{n+1}, \mathbf{u}_1^{n+1})$ to both sides and apply (3.19). Then apply Young's inequality using the fact that

$$\left(B_h\mathbf{u}_1^n, \mathbf{u}_1^{n+1}\right) \geq -\frac{1}{2}\left(B_h\mathbf{u}_1^{n+1}, \mathbf{u}_1^{n+1}\right) - \frac{1}{2}\left(B_h\mathbf{u}_1^n, \mathbf{u}_1^n\right).$$

Then split the term

$$\|\mathbf{u}_1^{n+1}\|_{A+\delta I}^2 = \frac{1}{2}\|\mathbf{u}_1^{n+1}\|_{A+\delta I}^2 + \frac{1}{2}\left(\|\mathbf{u}_1^{n+1}\|_{A+\delta I}^2 - \|\mathbf{u}_1^n\|_{A+\delta I}^2\right) + \frac{1}{2}\|\mathbf{u}_1^n\|_{A+\delta I}^2.$$

These results together with Lemma 3.2.1 imply the new estimate

$$\frac{1}{2\Delta t}\left(\|\mathbf{u}_1^{n+1}\|^2 - \|\mathbf{u}_1^n\|^2\right) + \frac{1}{2}\|\mathbf{u}_1^{n+1}\|_{A+\delta I-B}^2 + \frac{1}{2}\left(\|\mathbf{u}_1^{n+1}\|_{A+\delta I}^2 - \|\mathbf{u}_1^n\|_{A+\delta I}^2\right) + \frac{1}{2}\|\mathbf{u}_1^n\|_{A+\delta I-B}^2 \leq \left(\frac{\mathbf{f}^{n+1}+\mathbf{f}^n}{2}, \mathbf{u}_1^{n+1}\right) + \delta\|\mathbf{u}_1^{n+1}\|^2 + \frac{1}{4}\|\mathbf{u}_1^{n+1}\|_{A+\delta I-B}^2 + C(\|\mathbf{u}_0^{n+1}\|_X^2 + \|\mathbf{u}_0^n\|_X^2).$$

Rearranging terms,

$$\|\mathbf{u}_1^{n+1}\|^2 + \Delta t\|\mathbf{u}_1^{n+1}\|_{A+\delta I}^2 + \Delta t\sum_{k=0}^{n}\left\{\|\mathbf{u}_1^{k+1}\|_{A+\delta I-B}^2 + \|\mathbf{u}_1^k\|_{A+\delta I-B}^2\right\} \leq \|\mathbf{u}_1^0\|^2 + \Delta t\|\mathbf{u}_1^0\|_{A+\delta I}^2 + \Delta t\sum_{k=0}^{n}(\|\mathbf{u}_0^{k+1}\|_X^2 + \|\frac{\mathbf{f}^{k+1}+\mathbf{f}^k}{2}\|^2) + \Delta t(2\delta+1)\sum_{k=0}^{n}\|\mathbf{u}_1^{k+1}\|^2.$$

Take $\gamma_n \equiv 2\delta + 1$ in Lemma 3.2.2. Choose $C_2(\delta) = 2(2\delta+1)(1-\Delta t(2\delta+1)^{-1})$. Applying Lemma 3.3.1 and Lemma 3.2.1 concludes the proof. □

3.4 CONVERGENCE ANALYSIS

The convergence analysis for Algorithm 3.2.1 was performed in [18], see the theorem below.

Theorem 3.4.1. *(Convergence of the IMEX scheme) Let* $\mathbf{u}(t;x) \in X$ *for all* $t \in (0,T)$ *solve (3.1)–(3.4), such that* $\mathbf{u}_t \in L^2(0,T;X)$ *and* $\mathbf{u}_{tt} \in L^2(0,T;L^2(\Omega))$. *Then* $\exists C_1, C_2 > 0$ *independent of* h, Δt *such that for any* $n \in \{0,1,2,\cdots,M-1 = \frac{T}{\Delta t} - 1\}$ *and* $0 < \Delta t < (2+2\delta)^{-1}$, *the solution* $\mathbf{u}_0^{n+1} \in X_h$ *of (3.17) satisfies:*

$$
\begin{aligned}
&\|\mathbf{u}(t^{n+1}) - \mathbf{u}_0^{n+1}\|^2 + \Delta t\|\mathbf{u}(t^{n+1}) - \mathbf{u}_0^{n+1}\|_X^2 + \frac{3\Delta t}{4}\sum_{k=0}^{n}\|\mathbf{u}(t^{k+1}) - \mathbf{u}_0^{k+1}\|_X^2 \\
&\qquad \leq C_1(\delta)e^{C_2(\delta)T}\Big\{\|\mathbf{u}(0) - \mathbf{u}_0^0\|^2 + \Delta t\|\mathbf{u}(0) - \mathbf{u}_0^0\|_X^2 + \Delta t^2\|\mathbf{u}_t\|_{L^2(0,T;X)}^2 \\
&\qquad + \Delta t^2\|\mathbf{u}_{tt}\|_{L^2(0,T;L^2(\Omega))}^2 \\
&\qquad + \inf_{\mathbf{v}^0 \in X_h}\left\{\|\mathbf{u}(0) - \mathbf{v}^0\|^2 + \Delta t\|\mathbf{u}(0) - \mathbf{v}^0\|_X^2\right\} + \inf_{\mathbf{v} \in X_h}\|(\mathbf{u}(0) - \mathbf{v})_t\|^2 \\
&\qquad + T\max_{k=1,2,\cdots,n+1}\inf_{\mathbf{v}^k \in X_h}\|\mathbf{u}(t^k) - \mathbf{v}^k\|_X^2\Big\}.
\end{aligned}
$$

Corollary 3.4.1. *Let* $X_h \subset X$ *be a finite element space corresponding to continuous piecewise polynomials of degree* k. *If* $\mathbf{u}(\cdot,t)$ *is a solution of (3.1)–(3.4) satisfying the assumptions of Theorem 3.4.1, and* $\mathbf{u}_0^0$ *approximates* $\mathbf{u}(\cdot,0)$ *such that*

$$\|\mathbf{u}(\cdot,0) - \mathbf{u}_0^0\| = O(h^q),$$

then the approximation (3.17) converges at the rate $O(\Delta t + h^q)$ *in the norm*

$$\left\{\Delta t\sum_{k=0}^{M}\|\mathbf{u}(t^k) - \mathbf{u}_0^k\|_X^2\right\}^{1/2}.$$

The rest of this section will be devoted to deriving a bound on the error in the second step approximation $\mathbf{u} - \mathbf{u}_1$. Let $\mathbf{e}_j^i = \mathbf{u}(t_i) - \mathbf{u}_j^i$, $\forall i = 0,1,...,N$, $j = 1,2$. The bounds on $\mathbf{e}_0^i$ have been derived in Theorem 3.4.1. We now need the bounds on $\frac{\mathbf{e}_0^{i+1} - \mathbf{e}_0^i}{\Delta t}$.

Theorem 3.4.2 (IMEX time derivative). *Let* $\mathbf{u}(t;x) \in X$ *for all* $t \in (0,T)$ *solve (3.1)–(3.4), such that* $\mathbf{u}_t \in L^2(0,T;X)$, $\mathbf{u}_{tt} \in L^2(0,T;L^2(\Omega))$ *and* $\mathbf{u}_{ttt} \in L^2(0,T;L^2(\Omega))$. *Then* $\exists C > 0$ *independent of* h, Δt *such that for any* $n \in \{0,1,2,\cdots,M-1 = \frac{T}{\Delta t} - 1\}$ *and* $0 < \Delta t < (2+2\delta)^{-1}$, *the discrete time derivative of the error* $\frac{\mathbf{e}_0^{i+1} - \mathbf{e}_0^i}{\Delta t}$ *satisfies:*

$$\|\frac{\mathbf{e}_0^{n+1} - \mathbf{e}_0^n}{\Delta t}\|^2 + \Delta t \sum_{i=0}^{n} \|\frac{\mathbf{e}_0^{i+1} - \mathbf{e}_0^i}{\Delta t}\|_X^2$$
$$\leq C[\|\mathbf{e}_0^{n+1}\|^2 + \Delta t \sum_{i=0}^{n} \|\mathbf{e}_0^{i+1}\|_X^2].$$

Proof. Restricting test functions to X_h, subtract (3.17) from (3.10) to get the error equation. Let $\mathbf{e}_0^n = \boldsymbol{\eta}^n + \boldsymbol{\phi}^n$, where $\boldsymbol{\eta}^n = \mathbf{u}(t_n) - \mathbf{v}^h$, $\boldsymbol{\phi}^n = \mathbf{v}^h - \mathbf{u}_0^n$, for some $\mathbf{v}^h \in X_h$. Then for $\forall n \geq 0$:

$$\begin{aligned} &(\frac{\boldsymbol{\phi}^{n+1} - \boldsymbol{\phi}^n}{\Delta t}, \mathbf{v}) + (A\boldsymbol{\phi}^{n+1}, \mathbf{v}) + (B(\mathbf{u}(t^{n+1}) - \mathbf{u}_0^n), \mathbf{v}) \\ &= -\left(\frac{\boldsymbol{\eta}^{n+1} - \boldsymbol{\eta}^n}{\Delta t}, \mathbf{v}\right) - (\mathbf{r}^{n+1}, \mathbf{v}) - (A\boldsymbol{\eta}^{n+1}, \mathbf{v}), \ \forall \mathbf{v} \in X_h, \end{aligned} \tag{3.27}$$

where $\mathbf{r}^{n+1} = \mathbf{u}_t(t^{n+1}) - \frac{\mathbf{u}(t^{n+1}) - \mathbf{u}(t^n)}{\Delta t}$.

In order to treat the B-term, add and subtract $B\mathbf{u}(t^k)$; it follows that

$$B\mathbf{u}(t^{n+1}) - B\mathbf{u}_0^n = B(\mathbf{u}(t^{n+1}) - \mathbf{u}(t^n)) + B\boldsymbol{\eta}^n + B\boldsymbol{\phi}^n.$$

Consider (3.27) at the current time level $n+1$ and the previous time level n. Subtract the latter from the current time level, making the same choice $\mathbf{v} = \frac{\boldsymbol{\phi}^{n+1} - \boldsymbol{\phi}^n}{\Delta t}$ in both equations. Denoting $s^{n+1} = \frac{\boldsymbol{\phi}^{n+1} - \boldsymbol{\phi}^n}{\Delta t}$ for $\forall n \geq 0$, we obtain, after dividing by Δt:

$$\begin{aligned} &(\frac{s^{n+1} - s^n}{\Delta t}, s^{n+1}) + (As^{n+1}, s^{n+1}) + \Delta t(B(\frac{\mathbf{u}^{n+1} - 2\mathbf{u}^n + \mathbf{u}^{n-1}}{(\Delta t)^2}), s^{n+1}) \\ &+(B(\frac{\boldsymbol{\eta}^n - \boldsymbol{\eta}^{n-1}}{\Delta t}), s^{n+1}) + (Bs^n, s^{n+1}) = -(\frac{\boldsymbol{\eta}^{n+1} - 2\boldsymbol{\eta}^n + \boldsymbol{\eta}^{n-1}}{(\Delta t)^2}, s^{n+1}) \\ &\qquad -(A(\frac{\boldsymbol{\eta}^{n+1} - \boldsymbol{\eta}^n}{\Delta t}), s^{n+1}) - (\frac{\mathbf{r}^{n+1} - \mathbf{r}^n}{\Delta t}, s^{n+1}). \end{aligned} \tag{3.28}$$

Replacing $\boldsymbol{\phi}$ by s in the IMEX error equation (3.27) results exactly in (3.28), but the regularity assumptions are now needed for $\mathbf{u}_{ttt}$ instead of $\mathbf{u}_{tt}$. Hence, the result analogous

to Theorem 3.4.1 can be obtained by an argument similar to the proof of Theorem 3.4.1. However, the summation is now possible only up to $s = 1$, leaving two extra terms in the right hand side:

$$\|\frac{\mathbf{e}_0^{n+1} - \mathbf{e}_0^n}{\Delta t}\|^2 + \Delta t \sum_{i=0}^{n} \|\frac{\mathbf{e}_0^{i+1} - \mathbf{e}_0^i}{\Delta t}\|_X^2 \leq C[\|\frac{\boldsymbol{\phi}^1 - \boldsymbol{\phi}^0}{\Delta t}\|^2 \tag{3.29}$$
$$+\Delta t\|\nabla(\frac{\boldsymbol{\phi}^1 - \boldsymbol{\phi}^0}{\Delta t})\|^2 + (\Delta t)^2\|\mathbf{u}_{ttt}\|^2_{L^2(0,T;L^2(\Omega))} + \|\mathbf{e}_0^{n+1}\|^2 + \Delta t \sum_{i=0}^{n} \|\mathbf{e}_0^{i+1}\|_X^2].$$

Consider (3.27) at the initial time level $n = 0$. Take $\mathbf{v} = \frac{\boldsymbol{\phi}^1 - \boldsymbol{\phi}^0}{\Delta t} \in X_h$. Choose the initial time level approximation $\mathbf{u}_0^0 \in X_h$ to be the Modified H1 Projection of $\mathbf{u}(x, 0) \in X$: $P(\mathbf{u}(x, 0)) = \mathbf{u}_0^0$. It follows from (3.22) that

$$(A(\boldsymbol{\eta}^0 + \boldsymbol{\phi}^0) + B(\boldsymbol{\eta}^0 + \boldsymbol{\phi}^0), \frac{\boldsymbol{\phi}^1 - \boldsymbol{\phi}^0}{\Delta t}) = -(\boldsymbol{\eta}^0 + \boldsymbol{\phi}^0, \frac{\boldsymbol{\phi}^1 - \boldsymbol{\phi}^0}{\Delta t}).$$

Thus, we obtain from (3.27) that

$$\|\frac{\boldsymbol{\phi}^1 - \boldsymbol{\phi}^0}{\Delta t}\|^2 + \Delta t\|\nabla(\frac{\boldsymbol{\phi}^1 - \boldsymbol{\phi}^0}{\Delta t})\|^2 \tag{3.30}$$
$$+\Delta t(B(\frac{\mathbf{u}^1 - \mathbf{u}^0}{\Delta t}), \frac{\boldsymbol{\phi}^1 - \boldsymbol{\phi}^0}{\Delta t}) + \Delta t(A(\frac{\boldsymbol{\eta}^1 - \boldsymbol{\eta}^0}{\Delta t}), \frac{\boldsymbol{\phi}^1 - \boldsymbol{\phi}^0}{\Delta t}) = 0.$$

Therefore, using Cauchy-Schwarz and Young's inequalities, we get

$$\|\frac{\boldsymbol{\phi}^1 - \boldsymbol{\phi}^0}{\Delta t}\|^2 + \Delta t\|\nabla(\frac{\boldsymbol{\phi}^1 - \boldsymbol{\phi}^0}{\Delta t})\|^2 \leq C(\Delta t)^2\|\mathbf{u}_t\|_X^2.$$

This result combined with (3.29) concludes the proof. □

Finally, we have derived all the intermediate results necessary for the proof of the main theorem of this section.

Theorem 3.4.3 (SISDC error estimate)**.** *Let the conditions of the Theorem 3.4.2 be satisfied. Let also* $\mathbf{u}_t \in L^2(0,T;X)$ *and* $\mathbf{u}_{ttt} \in L^2(0,T;L^2(\Omega))$*. Then* $\exists C > 0$ *independent of* h, Δt *such that for any* $n \in \{0,1,2,\cdots,M-1 = \frac{T}{\Delta t} - 1\}$ *and* $0 < \Delta t < (2+2\delta)^{-1}$*, the second step approximation error* $\mathbf{e}_1^{i+1}$ *satisfies:*

$$\begin{aligned}
&\|\mathbf{u}(t^{n+1}) - \mathbf{u}_1^{n+1}\|^2 + \Delta t\|\mathbf{u}(t^{n+1}) - \mathbf{u}_1^{n+1}\|_X^2 + \Delta t\sum_{k=0}^{n}\|\mathbf{u}(t^{k+1}) - \mathbf{u}_1^{k+1}\|_X^2 \\
&\quad \le C\Big\{\|\mathbf{u}(0) - \mathbf{u}_1^0\|^2 + \Delta t\|\mathbf{u}(0) - \mathbf{u}_1^0\|_X^2 + \Delta t^4\|\mathbf{u}_t\|^2_{L^2(0,T;X)} \\
&\quad + \Delta t^4\|\mathbf{u}_{tt}\|^2_{L^2(0,T;L^2(\Omega))} + \Delta t^4\|\mathbf{u}_{ttt}\|^2_{L^2(0,T;L^2(\Omega))} \\
&\quad + \inf_{\mathbf{v}^0\in X_h}\left\{\|\mathbf{u}(0) - \mathbf{v}^0\|^2 + \Delta t\|\mathbf{u}(0) - \mathbf{v}^0\|_X^2\right\} + \inf_{\mathbf{v}\in X_h}\|(\mathbf{u}(0) - \mathbf{v})_t\|^2 \\
&\quad + T\max_{k=1,2,\cdots,n+1}\inf_{\mathbf{v}^k\in X_h}\|\mathbf{u}(t^k) - \mathbf{v}^k\|_X^2\Big\}.
\end{aligned}$$

Corollary 3.4.2. *Let* $X_h \subset X$ *be a finite element space corresponding to continuous piecewise polynomials of degree* k*. If* $\mathbf{u}(\cdot,t)$ *is a solution of (3.1)–(3.4) satisfying the assumptions of Theorem 3.4.1, and* $\mathbf{u}_0^0, \mathbf{u}_1^0$ *approximates* $\mathbf{u}(\cdot,0)$ *such that*

$$\|\mathbf{u}(\cdot,0) - \mathbf{u}_0^0\| = O(h^q),$$

$$\|\mathbf{u}(\cdot,0) - \mathbf{u}_1^0\| = O(h^q),$$

then the approximation (3.18) converges at the rate $O((\Delta t)^2 + h^q + h^k)$ *in the norm*

$$\left\{\Delta t\sum_{k=0}^{M}\|\mathbf{u}(t^k) - \mathbf{u}_1^k\|_X^2\right\}^{1/2}.$$

Proof. The equation for the true solution (3.10) could be written as

$$\begin{aligned}
(\frac{\mathbf{u}^{n+1} - \mathbf{u}^n}{\Delta t}, \mathbf{v}) + (A\mathbf{u}^{n+1}, \mathbf{v}) + (B\mathbf{u}^n, \mathbf{v}) = \frac{1}{\Delta t}\int_{t_n}^{t_{n+1}} F(\tau,\mathbf{u})d\tau \\
+(A\mathbf{u}^{n+1}, \mathbf{v}) + (B\mathbf{u}^n, \mathbf{v}), \forall \mathbf{v} \in X.
\end{aligned} \tag{3.31}$$

The Gaussian quadrature rule with one point (midpoint of $[t_n, t_{n+1}]$) gives

$$\begin{aligned}
&\frac{1}{\Delta t}\int_{t_n}^{t_{n+1}} F(\tau,\mathbf{u})d\tau = \frac{F(t_n,\mathbf{u}) + F(t_{n+1},\mathbf{u})}{2} + C(\Delta t)^2 F_{tt}(\xi,\mathbf{u}) \\
&= \frac{\mathbf{f}^{n+1} + \mathbf{f}^n}{2} - A(\frac{\mathbf{u}^{n+1} + \mathbf{u}^n}{2}) - B(\frac{\mathbf{u}^{n+1} + \mathbf{u}^n}{2}) + C(\Delta t)^2 F_{tt}(\xi,\mathbf{u}),
\end{aligned} \tag{3.32}$$

for some $\xi \in [t_n, t_{n+1}]$. Hence, it follows from (3.31)-(3.32) that the equation for the true solution $\mathbf{u}$ can be written as:

$$(\frac{\mathbf{u}^{n+1}-\mathbf{u}^n}{\Delta t}, \mathbf{v}) + (A\mathbf{u}^{n+1}, \mathbf{v}) + (B\mathbf{u}^n, \mathbf{v}) = (\frac{\mathbf{f}^{n+1}+\mathbf{f}^n}{2}, \mathbf{v}) \quad (3.33)$$
$$+\frac{\Delta t}{2}(A(\frac{\mathbf{u}^{n+1}-\mathbf{u}^n}{\Delta t}), \mathbf{v}) - \frac{\Delta t}{2}(B(\frac{\mathbf{u}^{n+1}-\mathbf{u}^n}{\Delta t}), \mathbf{v}) + C(\Delta t)^2(F_{tt}(\xi, \mathbf{u}), \mathbf{v}), \forall \mathbf{v} \in X.$$

Subtracting (3.18) from (3.33) gives

$$(\frac{\mathbf{e}_1^{n+1}-\mathbf{e}_1^n}{\Delta t}, \mathbf{v}) + (A\mathbf{e}_1^{n+1}, \mathbf{v}) + (B\mathbf{e}_1^n, \mathbf{v}) = \frac{\Delta t}{2}(A(\frac{\mathbf{e}_0^{n+1}-\mathbf{e}_0^n}{\Delta t}), \mathbf{v}) \quad (3.34)$$
$$-\frac{\Delta t}{2}(B(\frac{\mathbf{e}_0^{n+1}-\mathbf{e}_0^n}{\Delta t}), \mathbf{v}) + C(\Delta t)^2(F_{tt}(\xi, \mathbf{u}), \mathbf{v}), \forall \mathbf{v} \in X_h.$$

Take $\mathbf{v} = \mathbf{e}_1^{n+1}$. The Cauchy-Schwarz and Young inequalities, together with the results of Lemma 3.2.1 and Theorem 3.4.2 complete the proof.

□

3.5 COMPUTATIONAL TESTING

The convergence properties of the two-step SISDC method (Algorithm 3.2.3) are investigated here in the case of a test problem previously discussed in [18] using the first-order in time IMEX method. Emphasis is placed on understanding time accuracy and errors related to the interface. Each iteration of Algorithm 3.2.3 performs a first order in time IMEX half-step followed by a correction half-step to obtain second order in time accuracy. Thus the output of the algorithm is compared between the uncorrected and corrected steps. Comparison of Algorithm 3.2.3 with the classical (coupled) Crank-Nicholson discretization is also provided.

Assume $\Omega_1 = [0,1] \times [0,1]$ and $\Omega_2 = [0,1] \times [-1,0]$, so I is the portion of the x-axis from 0 to 1. Then $\mathbf{n}_1 = [0, -1]^T$ and $\mathbf{n}_2 = [0, 1]^T$. For ν_1, ν_2, and κ all arbitrary positive constants, the right hand side function $\mathbf{f}$ from (3.1) is calculated by differentiating

$$\begin{aligned} u_1(t,x,y) &= x(1-x)(1-y)e^{-t} \\ u_2(t,x,y) &= x(1-x)(1+\frac{\nu_1}{\kappa}-\frac{\nu_1}{\nu_2}y-(1+\frac{\nu_1}{\nu_2}+\frac{\nu_1}{k})y^2)e^{-t}\,. \end{aligned}$$

This choice of $\mathbf{u}$ satisfies the interface conditions (3.2) and the boundary conditions (3.4) with $g_1 = g_2 = 0$. Choosing κ to be no larger than ν_1, ν_2 the IMEX scheme will be stable. Computations were performed using finite element spaces consisting of continuous piece-wise polynomials of degree 2. The code was implemented using the software package `FreeFEM++` [35].

3.5.1 Convergence Rate Study

Computational results are provided choosing parameters $\nu_1 = \nu_2 = 1, \kappa = 0.01, 0.1, 1, 2, 4$. In the following tables, the norm $\|\mathbf{u}\|$ is the discrete $L^2(0,T;H^1(\Omega))$ norm, given by

$$\|\mathbf{u}\| = \left(\sum_{n=1}^{N} \Delta t |\mathbf{u}(t_n)|^2_{H^1(\Omega)} \right)^{1/2}, \tag{3.35}$$

and $\|\mathbf{u}\|_I$ is the discrete $L^2(0,T;L^2(I))$ norm, given by

$$\|\mathbf{u}\|_I = \left(\sum_{n=1}^{N} \Delta t \|\mathbf{u}(t_n)\|^2_{L^2(I)} \right)^{1/2}, \tag{3.36}$$

where $N = T/\Delta t$ and $|\cdot|_{H^1(\Omega)}$ is the $H^1(\Omega)$ spatial seminorm.

Tables 8 - 12 give the errors produced using Algorithm 3.2.3 with $\kappa = 0.01, 0.1, 1, 2, 4$, respectively. The errors are calculated in the norms (3.35),(3.36) in all cases, for both uncorrected and corrected substeps. For each spatial mesh size h the time step size is chosen to be $\Delta t = h$. The errors should then scale proportional to $\Delta t + h^2 = O(h)$ for the uncorrected substeps and $\Delta t^2 + h^2 = O(h^2)$ for the corrected substeps. Convergence of the IMEX scheme (uncorrected substeps) and Algorithm 3.2.3 is clear for $\kappa = 0.1, 1, 2$, consistent with the analysis. The uncorrected substeps show first order convergence in h, while the corrected substeps show very nearly second order convergence in the norm (3.35), consistent with the theory. When $\kappa = 4$ the theory predicts a time step restriction $\Delta t \leq \frac{C}{\kappa^2} = \frac{C}{16}$, explaining the lack of convergence at larger mesh sizes choosing $h = \Delta t$.

Table 8: Errors for computed approximations, $\kappa = 0.01$

FIRST h	**SUBSTEP** Δt	$\|\mathbf{u}(t_n) - \mathbf{u}^n\|$	rate	$\|\mathbf{u}(t_n) - \mathbf{u}^n\|_I$	rate
1/2	1/2	2.39459e+0		1.89181e-1	
1/4	1/4	7.95856e-1	1.59	1.01190e-1	0.90
1/8	1/8	2.47129e-1	1.69	5.21486e-2	0.96
1/16	1/16	8.79092e-2	1.49	2.65604e-2	0.97
1/32	1/32	3.78155e-2	1.23	1.34294e-2	0.98
1/64	1/64	1.80809e-2	1.06	6.75763e-3	0.99
SECOND h	**SUBSTEP** Δt	$\|\mathbf{u}(t_n) - \mathbf{u}^n\|$	rate	$\|\mathbf{u}(t_n) - \mathbf{u}^n\|_I$	rate
1/2	1/2	2.36605e+0		1.30618e-1	
1/4	1/4	7.54202e-1	1.65	2.25005e-2	2.54
1/8	1/8	2.06455e-1	1.87	6.22376e-3	1.85
1/16	1/16	5.36284e-2	1.94	1.74183e-3	1.84
1/32	1/32	1.36432e-2	1.97	4.73823e-4	1.88
1/64	1/64	3.43948e-3	1.99	1.25325e-4	1.92

Application of trace theory suggests asymptotic convergence behavior in $L^2(0,T;L^2(I))$ should mimic that of the global approximations in $L^2(0,T;H^1(\Omega))$. However, this leaves the possibility of approximation errors concentrating near the interface and possibly causing a drop in accuracy of the correction substep of Algorithm 3.2.3, particularly when κ is much larger than $min\{\nu_1,\nu_2\}$ and the true solution will have a large gradient near I. In this case the basic IMEX scheme has a small time step restriction, requiring expensive computations to investigate. The results in Tables 8-12 show an agreement in convergence behavior between $L^2(0,T;L^2(I))$ and $L^2(0,T;H^1(\Omega))$. Table 11 presents an interesting case, as second order convergence is approached quickly in $L^2(0,T;H^1(\Omega))$ as $h, \Delta t \to 0$, whereas in $L^2(0,T;L^2(I))$ smaller mesh sizes and time steps would be required to verify even that convergence on the interface does not plateau below the optimal rate. The data for $\kappa = 4$ reflects the time step restriction inherent in the method, and at mesh sizes larger than $h = 1/64$ the correction substep fails to improve accuracy.

The impact of errors on the interface on accuracy of Algorithm 3.2.3 may be better

Table 9: Errors for computed approximations, $\kappa = 0.1$

FIRST h	**SUBSTEP** Δt	$\|\mathbf{u}(t_n) - \mathbf{u}^n\|$	rate	$\|\mathbf{u}(t_n) - \mathbf{u}^n\|_I$	rate
1/2	1/2	2.66562e-1		2.01643e-2	
1/4	1/4	8.91492e-2	1.58	1.02745e-2	0.97
1/8	1/8	2.74780e-2	1.70	5.23346e-3	0.97
1/16	1/16	9.61081e-3	1.52	2.64604e-3	0.98
1/32	1/32	4.07539e-3	1.24	1.33245e-3	0.99
1/64	1/64	1.93633e-3	1.07	6.69085e-4	0.99
SECOND h	**SUBSTEP** Δt	$\|\mathbf{u}(t_n) - \mathbf{u}^n\|$	rate	$\|\mathbf{u}(t_n) - \mathbf{u}^n\|_I$	rate
1/2	1/2	2.63516e-1		1.40851e-2	
1/4	1/4	8.48811e-2	1.63	2.66683e-3	2.40
1/8	1/8	2.33046e-2	1.86	8.17461e-4	1.71
1/16	1/16	6.06538e-3	1.94	2.46901e-4	1.73
1/32	1/32	1.54660e-3	1.97	7.14203e-5	1.79
1/64	1/64	3.91180e-4	1.98	1.98645e-5	1.85

understood comparing the results above to plots of the error, (interpolated into the finite element space with $h = 1/16$) in Figure 5. The errors are globally distributed for $\kappa = 1, 2$ and concentrated more toward the interface for $\kappa = 4$, both in corrected and uncorrected steps. Since errors are not concentrated at the interface for $\kappa = 2$, the reason for the seemingly anomolous convergence behavior in the correction step in $L^2(0, T; L^2(I))$ in Table 11 is an open question. The concentration of errors near I for $\kappa = 4$ does not help to answer this question, as convergence behavior in this case is dominated by the underlying IMEX scheme. Evidence herein suggests convergence and stability properties of Algorithm 3.2.3 are dominated by the corresponding properties of the IMEX scheme. Extension to problems with boundary layers may present a way to further understand SISDC type methods, emphasizing the difference between interface and global errors. For example, SISDC methods may be tenable for the coupled fluid-fluid problem, (see [42, 43] showing application of defect correction methods to the Navier-Stokes equations).

3.5.2 Comparison of Algorithm 3.2.3 with Crank-Nicholson

In this section the notation and choice of problem are as in Section 3.5.1. The scaling $\Delta t = h$ is again used with globally continuous piece-wise quadratic finite elements. Errors and rates

Table 10: Errors for computed approximations, $\kappa = 1$

FIRST h	**SUBSTEP** Δt	$\|\mathbf{u}(t_n) - \mathbf{u}^n\|$	rate	$\|\mathbf{u}(t_n) - \mathbf{u}^n\|_I$	rate
1/2	1/2	6.66799e-2		1.87087e-2	
1/4	1/4	2.49435e-2	1.42	8.73540e-3	1.10
1/8	1/8	9.28931e-3	1.43	4.07453e-3	1.10
1/16	1/16	3.98260e-3	1.22	1.97159e-3	1.05
1/32	1/32	1.88625e-3	1.08	9.73713e-4	1.02
1/64	1/64	9.28461e-4	1.02	4.84781e-4	1.01
SECOND h	**SUBSTEP** Δt	$\|\mathbf{u}(t_n) - \mathbf{u}^n\|$	rate	$\|\mathbf{u}(t_n) - \mathbf{u}^n\|_I$	rate
1/2	1/2	5.74386e-2		5.78786e-3	
1/4	1/4	1.92132e-2	1.58	1.92903e-3	1.59
1/8	1/8	5.33777e-3	1.85	5.18933e-4	1.89
1/16	1/16	1.40746e-3	1.92	1.38139e-4	1.91
1/32	1/32	3.66342e-4	1.94	3.75883e-5	1.88
1/64	1/64	9.57063e-5	1.94	1.03896e-5	1.86

of convergence both globally and on the interface are listed using the classical, fully coupled and implicit Crank-Nicholson scheme, (Table 13), with parameters $\kappa = 0.01, 0.1, 1, 2$ and $\nu_1 = \nu_2 = 1$. For completeness the Crank-Nicholson algorithm for problem (3.1)-(3.4) is listed as Algorithm 3.5.1.

Algorithm 3.5.1 (Crank-Nicholson Scheme)**.** *Let* $\Delta t > 0$, $\mathbf{f} \in L^2(\Omega)$. *For each* $M \in \mathbb{N}, M \leq \frac{T}{\Delta t}$, *given* $\mathbf{u}^n \in X_h$, $n = 0, 1, 2, \cdots, M-1$, *find* $\mathbf{u}^{n+1} \in X_h$ *satisfying*

$$\begin{aligned}\left(\frac{\mathbf{u}^{n+1} - \mathbf{u}^n}{\Delta t}, \mathbf{v}\right) + \left(A_h\left(\frac{\mathbf{u}^{n+1} + \mathbf{u}^n}{2}\right), \mathbf{v}\right) \\ + \left(B_h\left(\frac{\mathbf{u}^{n+1} + \mathbf{u}^n}{2}\right), \mathbf{v}\right) = \left(\left(\frac{\mathbf{f}(t^{n+1}) + \mathbf{f}(t^n)}{2}\right), \mathbf{v}\right), \ \forall \mathbf{v} \in X_h\,.\end{aligned} \tag{3.37}$$

Second order accuracy is approached using Algorithm 3.5.1. Comparing to Algorithm 3.2.3 in Tables 8 - 11, some improvement is shown in accuracy using the SISDC method over Crank-Nicholson for small κ, particularly on the interface. For $\kappa = 1, 2$ the Crank-Nicholson algorithm yields slightly better accuracy. Interestingly, errors in both substeps using the SISDC scheme and Crank-Nicholson for the chosen problem increase as κ is decreased, probably because the size of ∇u_2 increases, (as does the size of $[\mathbf{u}]$ on I). The improvement in accuracy due to the correction substep using the SISDC method is thus more pronounced

Table 11: Errors for computed approximations, $\kappa = 2$

FIRST h	**SUBSTEP** Δt	$\|\mathbf{u}(t_n) - \mathbf{u}^n\|$	rate	$\|\mathbf{u}(t_n) - \mathbf{u}^n\|_I$	rate
1/2	1/2	5.97678e-2		2.05628e-2	
1/4	1/4	2.33065e-2	1.36	9.46651e-3	1.12
1/8	1/8	7.91217e-3	1.56	3.52150e-3	1.43
1/16	1/16	3.15609e-3	1.33	1.54336e-3	1.19
1/32	1/32	1.45880e-3	1.11	7.45606e-4	1.05
1/64	1/64	7.12773e-4	1.03	3.69198e-4	1.01
SECOND h	**SUBSTEP** Δt	$\|\mathbf{u}(t_n) - \mathbf{u}^n\|$	rate	$\|\mathbf{u}(t_n) - \mathbf{u}^n\|_I$	rate
1/2	1/2	4.73283e-2		6.29809e-3	
1/4	1/4	1.68062e-2	1.49	3.73213e-3	0.75
1/8	1/8	4.42209e-3	1.93	5.94709e-4	2.65
1/16	1/16	1.13583e-3	1.96	4.90307e-5	3.60
1/32	1/32	2.96786e-4	1.94	1.98341e-5	1.31
1/64	1/64	7.80296e-5	1.93	6.89075e-6	1.53

using smaller κ, when the true solution has larger derivatives and the jump on the interface is larger.

Remark 3.5.1. *An alternative SISDC algorithm may be possible with a lessened restriction on the time step, employing a different partitioned scheme from [18], below, in place of the initial IMEX step. This should also help to illuminate the effect of the base partitioned scheme on the overall SISDC method.*

Algorithm 3.5.2 (Data-passing partitioned scheme)**.** *Let* $\Delta t > 0$, $\mathbf{f} \in L^2(\Omega)$. *For each* $M \in \mathbb{N}, M \leq \frac{T}{\Delta t}$, *given* $\mathbf{u}^n \in X_h$, $n = 0, 1, 2, \cdots, M-1$, *find* $\mathbf{u}^{n+1} \in X_h$ *satisfying*

$$\begin{aligned} \left(\frac{u_i^{n+1} - u_i^n}{\Delta t}, v_i\right) + \nu_i \left(\nabla u_i^{n+1}, \nabla v_i\right) + \kappa \int_I (u_i^{n+1} - u_j^n) v_i \, ds \\ = \left(f_i(t^{n+1}), v_i\right), \ i \neq j, \ \forall v_i \in X_{i,h} \, . \end{aligned} \tag{3.38}$$

Table 12: Errors for computed approximations, $\kappa = 4$

FIRST h	**SUBSTEP** Δt	$\|\mathbf{u}(t_n) - \mathbf{u}^n\|$	rate	$\|\mathbf{u}(t_n) - \mathbf{u}^n\|_I$	rate
1/2	1/2	8.94746e-2		4.43531e-2	
1/4	1/4	1.79106e-1	—-	9.93188e-2	—-
1/8	1/8	7.73654e-1	—-	4.20286e-1	—-
1/16	1/16	2.80587e+0	—-	1.43856e+0	—-
1/32	1/32	1.63780e-1	4.10	7.53047e-2	4.26
1/64	1/64	4.73818e-4	8.43	2.28790e-4	8.36
SECOND h	**SUBSTEP** Δt	$\|\mathbf{u}(t_n) - \mathbf{u}^n\|$	rate	$\|\mathbf{u}(t_n) - \mathbf{u}^n\|_I$	rate
1/2	1/2	1.98918e-1		1.07760e-1	
1/4	1/4	8.57831e-1	—-	4.78724e-1	—-
1/8	1/8	6.78714e+0	—-	3.70902e+0	—-
1/16	1/16	41.47450e+0	—-	21.42870e+0	—-
1/32	1/32	3.52984e+0	3.55	1.63776e+0	3.71
1/64	1/64	1.75157e-4	14.30	7.14602e-5	14.48

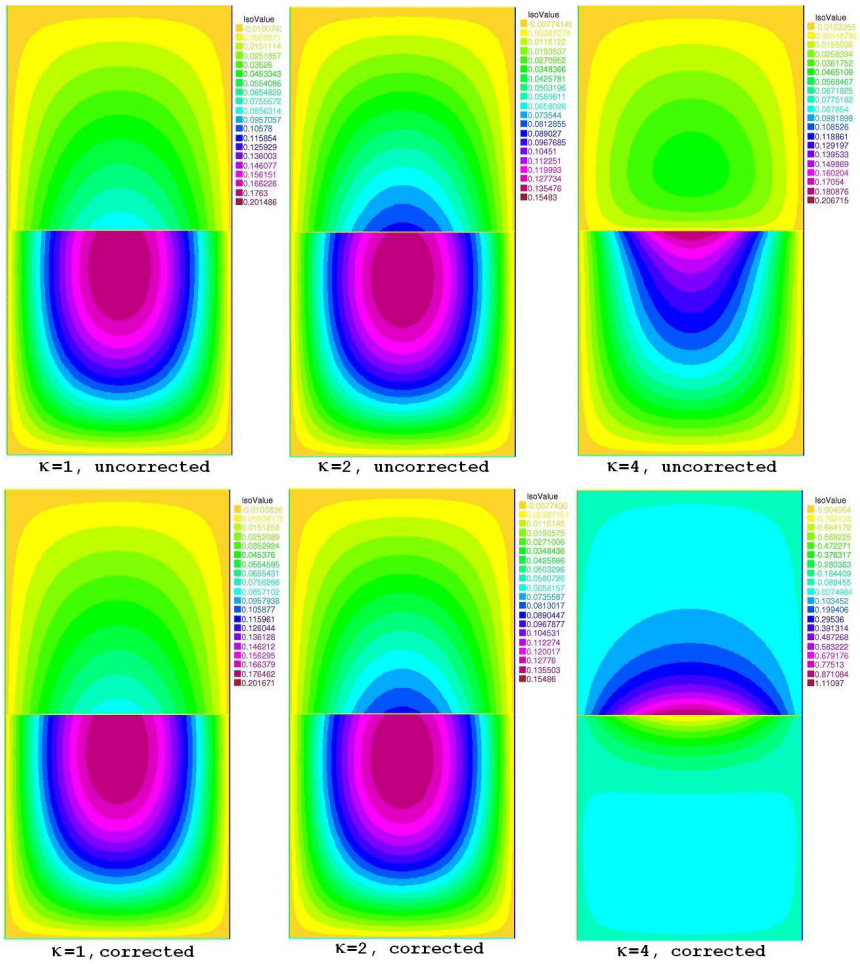

Figure 5: Interpolated SISDC errors at T=1, $h = 1/16$.

Table 13: Errors for computed approximations using Crank-Nicholson.

Data for:	$\kappa = 0.01$				
h	Δt	$\|\mathbf{u}(t_n) - \mathbf{u}^n\|$	rate	$\|\mathbf{u}(t_n) - \mathbf{u}^n\|_I$	rate
1/2	1/2	2.86768e+0		5.25666e-1	
1/4	1/4	8.28172e-1	1.79	9.90764e-2	2.41
1/8	1/8	2.20823e-1	1.91	2.25657e-2	2.13
1/16	1/16	5.69206e-2	1.96	5.48666e-3	2.04
1/32	1/32	1.44421e-2	1.98	1.35979e-3	2.01
1/64	1/64	3.63678e-3	1.99	3.38928e-4	2.00
Data for:	$\kappa = 0.1$				
h	Δt	$\|\mathbf{u}(t_n) - \mathbf{u}^n\|$	rate	$\|\mathbf{u}(t_n) - \mathbf{u}^n\|_I$	rate
1/2	1/2	3.18416e-1		5.63760e-2	
1/4	1/4	9.30861e-2	1.77	1.07763e-2	2.39
1/8	1/8	2.48723e-2	1.90	2.46666e-3	2.13
1/16	1/16	6.41414e-3	1.96	6.00393e-4	2.04
1/32	1/32	1.62758e-3	1.98	1.48833e-4	2.01
1/64	1/64	4.09865e-4	1.99	3.70986e-5	2.00
Data for:	$\kappa = 1.0$				
h	Δt	$\|\mathbf{u}(t_n) - \mathbf{u}^n\|$	rate	$\|\mathbf{u}(t_n) - \mathbf{u}^n\|_I$	rate
1/2	1/2	6.85872e-2		1.13795e-2	
1/4	1/4	2.07551e-2	1.72	2.19941e-3	2.37
1/8	1/8	5.57045e-3	1.90	5.01824e-4	2.13
1/16	1/16	1.43712e-3	1.95	1.21797e-4	2.04
1/32	1/32	3.64604e-4	1.98	3.01616e-5	2.01
1/64	1/64	9.17998e-5	1.99	7.51597e-6	2.00
Data for:	$\kappa = 2.0$				
h	Δt	$\|\mathbf{u}(t_n) - \mathbf{u}^n\|$	rate	$\|\mathbf{u}(t_n) - \mathbf{u}^n\|_I$	rate
1/2	1/2	5.59925e-2		9.36826e-3	
1/4	1/4	1.70320e-2	1.72	1.79221e-3	2.39
1/8	1/8	4.57295e-3	1.90	4.05893e-4	2.14
1/16	1/16	1.17954e-3	1.95	9.82354e-5	2.05
1/32	1/32	2.99198e-4	1.98	2.43058e-5	2.01
1/64	1/64	7.53228e-5	1.99	6.05532e-6	2.01

4.0 TIME STEPPING ALGORITHMS FOR THE NONLINEARLY COUPLED SYSTEM OF ODES

4.1 INTRODUCTION

As a first step toward developing partitioned methods for nonlinear coupling between the atmosphere and ocean the problem is reduced to studying a representative system of ordinary differential equations. If the dynamic core of coupled atmosphere-ocean models are discretized in space a large, coupled system of ODEs in time is obtained of the general form

$$\frac{d\mathbf{x}}{dt} + A(\mathbf{x})\mathbf{x} + \kappa|x_1 - y_1|(x_1 - y_1)[\mathbf{1}\ ,\ \mathbf{0}]^T = \mathbf{f}(t) \tag{4.1}$$

$$\frac{d\mathbf{y}}{dt} + B(\mathbf{y})\mathbf{y} + \kappa|x_1 - y_1|(y_1 - x_1)[\mathbf{1}\ ,\ \mathbf{0}]^T = \mathbf{g}(t), \tag{4.2}$$

subject to $\mathbf{x}(0) = \mathbf{x}_0$ and $\mathbf{y}(0) = \mathbf{y}_0$. Loosely, $\mathbf{x} \in \mathbb{X}$ and $\mathbf{y} \in \mathbb{Y}$ represent the variables associated with the atmosphere and ocean respectively. Their components are ordered so that those at the atmosphere-ocean interface are the sub-vectors x_1 and y_1 respectively, (see Section 4.1.1 for full details and Section 4.1.2-4.1.3 for motivations.)

The practical demands of this and many coupled problems require time stepping methods for (4.1) - (4.2) that (*i*) have strong stability properties, (*ii*) require only uncoupled solves of the individual subsystems at each time step (i.e. partitioned methods), and (*iii*) preserve these good properties when different time steps are used for the individual subsystems (4.1) and (4.2).

We consider herein three partitioned timestepping methods for (4.1) - (4.2) aiming at achieving (i) and (ii) where possible and understanding the limitations the competing conditions (i) and (ii) place on methods. The methods we consider (see Section 4.2.1 for a full description) are:

Algorithm 2.1: the fully implicit and fully coupled method for comparison

Algorithm 2.2: partitioning based on explicit treatment of y_1 in (4.1) and x_1 in (4.2)

Algorithm 2.3: using Algorithm 2.2 with a simple (apparently new) stabilization

Algorithm 2.4: a new and unconditionally stable partitioned method based on using a geometric average of the coupling terms coefficients .

The discretizations of (4.1)-(4.2) we consider take the general form

$$\begin{aligned} \frac{\mathbf{x}^{n+1}-\mathbf{x}^n}{\Delta t} + A(\mathbf{x}^n)\mathbf{x}^{n+1} + \kappa C(\mathbf{x},\mathbf{y}) &= \mathbf{f}^{n+1} \\ \frac{\mathbf{y}^{n+1}-\mathbf{y}^n}{\Delta t} + B(\mathbf{y}^n)\mathbf{y}^{n+1} + \kappa C(\mathbf{y},\mathbf{x}) &= \mathbf{g}^{n+1}. \end{aligned}$$

The main differences occur in how the coupling term $C(\mathbf{x},\mathbf{y})$ is treated. We consider four methods:

- fully implicit (monolithic coupled):
  $C(\mathbf{u},\mathbf{v}) = |u_1^{n+1} - v_1^{n+1}|(u_1^{n+1} - v_1^{n+1})[\mathbf{1}\ ,\ \mathbf{0}]^T$
- a data passing IMEX method
  $C(\mathbf{u},\mathbf{v}) = |u_1^{n} - v_1^{n}|(u_1^{n+1} - v_1^{n})[\mathbf{1}\ ,\ \mathbf{0}]^T$
- a stabilized IMEX method
  $C(\mathbf{u},\mathbf{v}) = |u_1^{n} - v_1^{n}|(u_1^{n+1} - v_1^{n})[\mathbf{1}\ ,\ \mathbf{0}]^T + 2\mu(\kappa)^*\mathbf{u}^{n+1}$
- an IMEX method using geometric averaging to achieve unconditional stability
  $C(\mathbf{u},\mathbf{v}) = \left\{|u_1^{n} - v_1^{n}|u_1^{n+1} - |u_1^{n} - v_1^{n}|^{1/2}|u_1^{n-1} - v_1^{n-1}|^{1/2}v_1^{n}\right\}[\mathbf{1}\ ,\ \mathbf{0}]^T\ .$

We focus directly on the essential difficulty of stability of partitioned time stepping methods. We prove the fully implicit, stabilized IMEX and geometric averaging methods are stable independent of $\kappa, \Delta t$, and the data passing IMEX method is stable under the restriction $\Delta t = O(\kappa^{-2})$. In Section 4.5 we provide numerical experiments which confirm the stability proofs and rates of convergence (expected from stability and the Lax equivalence

theorem). These also explore important issues beyond the stability proofs and point to some important open problems, discussed in Section 4.6.

4.1.1 Model Problem

We shall make several notational simplifications from (4.1),(4.2) that do not affect the stability results. In particular, the notation simplifies when $\mathbb{X}, \mathbb{Y}$ have two components (which can be considered blocks of components). The nonlinearity in $A(\cdot), B(\cdot)$ is essential for the physical behavior but not for stability (since it occurs in skew-symmetric terms) or in algorithms (as it can be extrapolated from previous time levels in standard ways) so we take both to be linear with structure (4.7),(4.8) below. Given functions $f : [0,T] \to \mathbb{R}^2$, $g : [0,T] \to \mathbb{R}^2$, we consider the following initial value problem:

$$\frac{\partial \mathbf{x}(t)}{\partial t} + A\mathbf{x}(t) + \kappa|x_1(t) - y_1(t)|\,(x_1(t) - y_1(t))\,[1 \;\; 0]^T = f(t) \tag{4.3}$$

$$\frac{\partial \mathbf{y}(t)}{\partial t} + B\mathbf{y}(t) + \kappa|y_1(t) - x_1(t)|\,(y_1(t) - x_1(t))\,[1 \;\; 0]^T = g(t) \tag{4.4}$$

$$\mathbf{x}(0) = \mathbf{x}_0 \tag{4.5}$$

$$\mathbf{y}(0) = \mathbf{y}_0 \tag{4.6}$$

where $\mathbf{x} = [x_1 \;\; x_2]^T$, $\mathbf{y} = [y_1 \;\; y_2]^T : [0,T] \to \mathbb{R}^2$ and $A, B \in \mathbb{R}^{2\times 2}$ are fixed, real matrices and $\kappa > 0$ is a fixed parameter. We furthermore assume A, B may be decomposed into the sum of an SPD and a skew-symmetric matrix:

$$A = A_{spd} + A_{sk} \tag{4.7}$$

$$B = B_{spd} + B_{sk}. \tag{4.8}$$

The important features of system (4.3)-(4.4) are evident upon formulation of the corresponding energy equation. Assuming a solution $(\mathbf{x}, \mathbf{y})$ of (4.3)-(4.4), multiply through (4.3) by $\mathbf{x}^T$

and (4.4) by $\mathbf{y}^T$ and integrate the equations over $t \in [0, s]$ for $s \leq T$.

$$\begin{aligned}
\frac{1}{2}|\mathbf{x}(s)|^2 + \int_0^s |\mathbf{x}^T A_{spd}\mathbf{x}|(t)\,dt \;&+\; \kappa \int_0^s |x_1(t) - y_1(t)|\,(x_1(t) - y_1(t))\,x_1(t)\,dt \\
&= \int_0^s \left(\mathbf{x}^T f\right)(t)\,dt + \frac{1}{2}|\mathbf{x}_0|^2 \qquad (4.9)\\
\frac{1}{2}|\mathbf{y}(s)|^2 + \int_0^s |\mathbf{y}^T B_{spd}\mathbf{y}|(t)\,dt \;&+\; \kappa \int_0^s |x_1(t) - y_1(t)|\,(y_1(t) - x_1(t))\,y_1(t)\,dt \\
&= \int_0^s \left(\mathbf{y}^T g\right)(t)\,dt + \frac{1}{2}|\mathbf{y}_0|^2. \qquad (4.10)
\end{aligned}$$

Considering the coupling, κ-terms, neither equation is individually monotone. Summing the equations and combining the coupling integrals one obtains monotone energy estimates and decay (when $\mathbf{f} = \mathbf{g} = 0$). Indeed,

$$\begin{aligned}
\frac{1}{2}\left(|\mathbf{x}(s)|^2 + |\mathbf{y}(s)|^2\right) \;&+\; \int_0^s |\mathbf{x}^T A_{spd}\mathbf{x}|(t) + |\mathbf{y}^T B_{spd}\mathbf{y}|(t)\,dt + \kappa \int_0^s |x_1(t) - y_1(t)|^3\,dt \\
&= \int_0^s \left(\mathbf{x}^T \mathbf{f}\right)(t)\,dt + \int_0^s \left(\mathbf{y}^T \mathbf{g}\right)(t)\,dt + \frac{1}{2}\left(|\mathbf{x}_0|^2 + |\mathbf{y}_0|^2\right) \qquad (4.11)
\end{aligned}$$

where the skew-symmetric components of A and B are eliminated, $\mathbf{x}^T A_{sk}\mathbf{x} = \mathbf{y}^T B_{sk}\mathbf{y} = 0$. The ODE system is dissipative, and the coupling terms act as a penalization on the size of the jump $x_1 - y_1$. As the parameter κ is increased the size of the difference $|x_1(t) - y_1(t)|$ is forced to zero asymptotically. Stability of solutions to the ODE system follows from the energy equation (4.11). Existence and uniqueness of solutions follows immediately (e.g. the limit using successive approximations) as this is a finite system of ODEs and the nonlinearity is locally Lipschitz, (see [57]).

The main difficulty in using semi-implicit time discretizations to decouple the ODE system is clear from examining (4.9) and (4.10). Taken separately, the coupling integrals in these equations are not non-negative in general, as in (4.11), and indeed the size of the solution of $\mathbf{x}(t)$ can only be bounded back in terms of $\mathbf{y}(t)$ and vice-versa. Thus decoupling the equations introduces the possibility of numerical instability, and it becomes the goal of any such decoupling strategy to avoid this.

4.1.2 A Motivating Question: IMEX Stability

One possible approach to decoupling the equations using time stepping is to begin with a fully implicit time discretization of each equation (4.3) and (4.4). Given the approximations $\mathbf{x}^j, \mathbf{y}^j$ for $j = 0, 1, 2, \ldots, n$ we calculate $\mathbf{x}^{n+1}, \mathbf{y}^{n+1}$ by

$$\frac{\mathbf{x}^{n+1} - \mathbf{x}^n}{\Delta t} + A\mathbf{x}^{n+1} + \kappa|x_1^{n+1} - y_1^{n+1}| \left(x_1^{n+1} - y_1^{n+1}\right) [1 \;\; 0]^T = f(t^{n+1}) \tag{4.12}$$

$$\frac{\mathbf{y}^{n+1} - \mathbf{y}^n}{\Delta t} + B\mathbf{y}^{n+1} + \kappa|y_1^{n+1} - x_1^{n+1}| \left(y_1^{n+1} - x_1^{n+1}\right) [1 \;\; 0]^T = g(t^{n+1}) \tag{4.13}$$

Consider first the most natural partitioned discretization:

$$\frac{\mathbf{x}^{n+1} - \mathbf{x}^n}{\Delta t} + A\mathbf{x}^{n+1} + \kappa|x_1^{n} - y_1^{n}| \left(x_1^{n+1} - y_1^{n}\right) [1 \;\; 0]^T = f(t^{n+1}) \tag{4.14}$$

$$\frac{\mathbf{y}^{n+1} - \mathbf{y}^n}{\Delta t} + B\mathbf{y}^{n+1} + \kappa|y_1^{n} - x_1^{n}| \left(y_1^{n+1} - x_1^{n}\right) [1 \;\; 0]^T = g(t^{n+1}). \tag{4.15}$$

Energy estimates are derived by multiplying (4.14) by $\mathbf{x}^{n+1}$ and (4.15) by $\mathbf{y}^{n+1}$, then add the resulting equations:

$$\begin{aligned}
&\frac{1}{\Delta t}\left(|\mathbf{x}^{n+1}|^2 - (\mathbf{x}^{n+1})^T\mathbf{x}^n\right) + \frac{1}{\Delta t}\left(|\mathbf{y}^{n+1}|^2 - (\mathbf{y}^{n+1})^T\mathbf{y}^n\right) + |(\mathbf{x}^{n+1})^T A_{spd}\mathbf{x}^{n+1}| \\
&\quad + |(\mathbf{y}^{n+1})^T B_{spd}\mathbf{y}^{n+1}| + \kappa|x_1^n - y_1^n| \left(x_1^{n+1} - y_1^n\right) x_1^{n+1} + \kappa|x_1^n - y_1^n| \left(y_1^{n+1} - x_1^n\right) y_1^{n+1} \\
&\qquad = \left((\mathbf{x}^{n+1})^T f(t^{n+1})\right) + \left((\mathbf{y}^{n+1})^T g(t^{n+1})\right).
\end{aligned}$$

Using Young's inequality to bound below the nonlinear terms,

$$\begin{aligned}
&\kappa|x_1^n - y_1^n| \left(x_1^{n+1} - y_1^n\right) x_1^{n+1} + \kappa|x_1^n - y_1^n| \left(y_1^{n+1} - x_1^n\right) y_1^{n+1} \\
&\geq \kappa|x_1^n - y_1^n| \left(|x_1^{n+1}|^2 + |y_1^{n+1}|^2\right) - \kappa|x_1^n - y_1^n| \left(|y_1^n||x_1^{n+1}| + |x_1^n||y_1^{n+1}|\right) \\
&\geq \frac{\kappa}{2}|x_1^n - y_1^n| \left(|x_1^{n+1}|^2 + |y_1^{n+1}|^2\right) - \frac{\kappa}{2}|x_1^n - y_1^n| \left(|y_1^n|^2 + |x_1^n|^2\right).
\end{aligned}$$

To prove stability, one hopes to obtain a telescoping series when summing over the index n, but this is not obtained. This is a difficulty associated with the nonlinearity of the coupling. In Chapter 2 it was shown with the linear coupling condition (i.e. $\kappa(x_1 - y_1)[1 \;,\; 0]^T$), strong unconditional stability of the analog of (4.14) and (4.15) holds. For nonlinear coupling this does not appear to be the case in our numerical experiments on (4.14) and (4.15). A more sophisticated algorithm is required to avoid a time step restriction for stability.

The goal is to develop decoupled, unconditionally stable algorithms for use in applications where the computational cost of an implicit solution is prohibitive, and furthermore the cost of the decoupled solve at each time step may still be so expensive as to motivate taking as large a time step as possible. Such applications occur when multiscale, multiphysics, multidomain complex physical systems are modelled using coupled partial differential equations. Implicit time discretization preserves the coupling of the variables, requiring a parallelization strategy for the monolithic problem which results at each time step. Explicit time discretization of the coupling terms yields a system without coupling, and the uncoupled variables may be solved for in parallel. However, using explicit updates in certain applications will allow non-physical energy from the unresolved scales to build up and cause instabilities, unless the time step size is taken to be sufficiently small.

As shown above, one may strategically employ both explicit and implicit updating, known as semi-implicit or implicit-explicit (IMEX) methods. Families of such schemes are known to be stable for certain classes of PDEs, (see [4]), but coupling terms vary in structure among applications and introduce nontrivial complexities. However, viability of semi-implicit time discretizations has been demonstrated for coupled heat equations (see [18]) and in fluid-structure interaction, [14, 16]. A related problem which may benefit from semi-implicit based decoupling strategies is atmosphere-ocean interaction. Herein we introduce unconditionally stable semi-implicit time discretizations for a coupled system of ODE's, motivated by the coupled fluid-fluid problem, resulting in uncoupled systems which may be solved in parallel.

4.1.3 A Motivating Problem: Atmosphere-Ocean Interaction

Numerous computer codes have been developed to simulate some aspects of the global climate, (some are described in [41, 51, 59]). One important part of any such climatology code will model global atmosphere and ocean circulations. At the interface of two fluids a no-slip condition is expected to hold [61], hence these circulations affect each other due to stresses caused by the relative motions of the two fluids at their interface. Due to the large length scale of this problem parallel to the interface, this translates to a severe boundary layer problem. Spatial discretizations of the corresponding partial differential equations re-

quire an unobtainable number of degrees of freedom to resolve all relevant scales of motion. Recently, atmosphere-ocean models have been studied which allow slip with friction at the interface, relaxing the severity of the boundary layers while still maintaining the important physics caused by shear stresses. See [47, 48, 49, 7, 12, 46] for the PDE theory and numerical modelling background.

Consider two fluid domains in $\mathbb{R}^2$, say Ω_1 and Ω_2 which share a common interface I, (Figure 2). The interface I is assumed to remain fixed, the "rigid-lid" hypothesis used in some oceanography models. Let $\mathbf{u}_j : \Omega_j \times [0,T] \to \mathbb{R}^2, j = 1,2$ be the fluid velocities, satisfying the PDE system consisting of the Navier-Stokes equations posed in the two subdomains and coupled at the interface (the pressure may be neglected). Let the kinematic viscocity of the fluid in Ω_i be ν_i, let τ be any tangent vector on I and the velocities on the external boundaries of Ω_i be zero. On I the velocities satisfy a condition which models the effect of tangential shear stresses:

$$-\nu_i \hat{n}_i \cdot \nabla \mathbf{u}_i \cdot \tau = \kappa |\mathbf{u}_i - \mathbf{u}_j| (\mathbf{u}_i - \mathbf{u}_j) \cdot \tau, \qquad \text{on } I,\ i,j = 1,2\,,\ i \neq j. \tag{4.16}$$

The parameter κ is dimensionless and can be tuned to control the amount of friction on I. As $\kappa \to \infty$ the jump in velocity on I will vanish (at times $t > 0$), recovering the case of no-slip between the two fluids. Analogy with the coupled ODE system (4.3)-(4.4) may now be drawn by looking at the variational equation,

$$\int_{\Omega_i} \left\{ \frac{\partial \mathbf{u}_i}{\partial t} \cdot \mathbf{v}_i + \nu_i \nabla \mathbf{u}_i : \nabla \mathbf{v}_i + \mathbf{u}_i \cdot \nabla \mathbf{u}_i \cdot \mathbf{v}_i \right\} dx \\ + \kappa \int_I (\mathbf{u}_i - \mathbf{u}_j) |\mathbf{u}_i - \mathbf{u}_j| \cdot \mathbf{v}_i \, ds = \int_{\Omega_i} \mathbf{f}_i \cdot \mathbf{v}_i \, dx$$

for appropriate divergence-free test functions $\mathbf{v}_i$. Applying a finite element discretization to this variational problem results in a system of ODEs with a structure very similar to that of (4.1)-(4.2).

4.2 METHOD DESCRIPTIONS, NOTATION AND PRELIMINARIES

This section introduces notation convenient for studying the properties of the ODE system (4.3)-(4.4). Also some useful lemmas are proved and methods for the time discretization of the ODE system are defined. We consider $p \times q$ matrices as elements of $\mathbb{R}^{p\times q}$ for natural numbers p, q, equipped with the Euclidean norm, $|\cdot|$. For clarity, in the case $q = 1$ of a column vector, an element $\mathbf{v} \in \mathbb{R}^{p\times 1} \equiv \mathbb{R}^p$ is set in bold, and has components denoted by $v_1, v_2, \ldots, v_p$. The spaces of mappings from the time interval $[0, T]$ to $\mathbb{R}^{p\times q}$ with L^2-integrability in time is

$$L^s(0, T; \mathbb{R}^{p\times q}) = \left\{ \mathbf{v} : [0, T] \to \mathbb{R}^{p\times q} \text{ such that } \int_0^T |\mathbf{v}(t)|^s, dt < \infty \right\}, 1 < s < \infty$$

Norms are induced on $\mathbb{R}^2$ by the SPD matrices $A_{spd}, B_{spd} \in \mathbb{R}^{2\times 2}$ of (4.3)-(4.4). In fact the same norms are induced by A, B. It will be convenient to use the following notation to denote these induced norms.

Definition 4.2.1 (Induced norms)**.** *Let $Q \in \mathbb{R}^{n\times n}$ for $n \in \mathbb{N}$ be an SPD matrix. Then Q induces a norm on $\mathbb{R}^{n\times n}$ defined for all $\mathbf{v} \in \mathbb{R}^1$ by*

$$|\mathbf{v}|_Q = \left\{ \mathbf{v}^T Q \mathbf{v} \right\}^{1/2}. \tag{4.17}$$

Equivalence of the norms induced by A, B with respect to the Euclidean norm is represented using the constants α_1, α_2 and β_1, β_2 where

$$\alpha_1 |\mathbf{v}|_A \leq |\mathbf{v}| \leq \alpha_2 |\mathbf{v}|_A \tag{4.18}$$

$$\beta_1 |\mathbf{v}|_B \leq |\mathbf{v}| \leq \beta_2 |\mathbf{v}|_B \tag{4.19}$$

The SPD components of A and B are used to help prove stability using energy methods. The following lemma is an example of one such usage.

Lemma 4.2.1 (Data bounds)**.** *Let $f, g \in \mathbb{R}^2$ and γ_1, γ_2 be arbitrary positive numbers. Then for any elements $v, w \in \mathbb{R}^2$,*

$$\mathbf{f}^T \mathbf{v} \leq \frac{1}{2\gamma_1} |\mathbf{f}|^2_{A^{-1}_{spd}} + \frac{\gamma_1}{2} |\mathbf{v}|^2_A \tag{4.20}$$

$$\mathbf{g}^T \mathbf{w} \leq \frac{1}{2\gamma_2} |\mathbf{g}|^2_{B^{-1}_{spd}} + \frac{\gamma_2}{2} |\mathbf{w}|^2_B \tag{4.21}$$

Proof. Both A_{spd} and B_{spd} have SPD square roots, and their square roots have inverses which are again SPD. Thus we may write

$$\mathbf{f}^T\mathbf{v} = \mathbf{f}^T(A_{spd}^{-1/2})(A_{spd}^{1/2})\mathbf{v} = (A_{spd}^{-1/2}\mathbf{f})^T(A_{spd}^{1/2}\mathbf{v}).$$

Applying Young's inequality to the expression,

$$\mathbf{f}^T\mathbf{v} \leq |(A_{spd}^{-1/2}\mathbf{f})^T(A_{spd}^{1/2}\mathbf{v})| \leq |A_{spd}^{-1/2}\mathbf{f}||A_{spd}^{1/2}\mathbf{v}| \leq \frac{1}{2\gamma_1}|A_{spd}^{-1/2}\mathbf{f}|^2 + \frac{\gamma_1}{2}|A_{spd}^{1/2}\mathbf{v}|^2.$$

Expanding out these last terms, we achieve the desired result for (4.20):

$$|A_{spd}^{-1/2}\mathbf{f}|^2 = \mathbf{f}^T A_{spd}^{-1/2}A_{spd}^{-1/2}\mathbf{f} = \mathbf{f}^T A_{spd}^{-1}\mathbf{f} = |\mathbf{f}|^2_{A_{spd}^{-1}}$$
$$|A_{spd}^{1/2}\mathbf{v}|^2 = \mathbf{v}^T A_{spd}^{1/2}A_{spd}^{1/2}\mathbf{v} = \mathbf{v}^T A_{spd}\mathbf{v} = |\mathbf{v}|^2_A$$

and the proof of (4.21) is analagous. □

To implement time discretization techniques, the time interval $[0, T]$ is partitioned uniformly by choosing any natural number N and defining $\Delta t = T/N$ and $t^k = k\Delta t$ for $k = 0, 1, 2, \ldots, N$. It is generally assumed the right hand side forcing functions $f(t), g(t)$ are bounded, in $L^2(0, T; \mathbb{R}^2)$. Thus the following useful quantities are well defined.

Definition 4.2.2 (Uniform bound L)**.** *Given initial data* $\mathbf{x}_0, \mathbf{y}_0 \in \mathbb{R}^2$ *and forcing functions* $\mathbf{f}, \mathbf{g} \in L^2(0, T; \mathbb{R}^2)$ *define* L *by*

$$L = |\mathbf{x}_0|^2 + |\mathbf{y}_0|^2 + \sup_{N\in\mathbb{N}} \Delta t \sum_{j=0}^{N-1} \left|\mathbf{f}(t^{j+1})\right|^2_{A_{spd}^{-1}} + \left|\mathbf{g}(t^{j+1})\right|^2_{B_{spd}^{-1}}. \tag{4.22}$$

Furthermore, the following identity is used in the analysis. For $\mathbf{v}^{k+1}, \mathbf{v}^k \in \mathbb{R}^2$,

$$(\mathbf{v}^{k+1})^T\left(\mathbf{v}^{k+1} - \mathbf{v}^k\right) = \frac{1}{2}\left(|\mathbf{v}^{k+1}|^2 - |\mathbf{v}^k|^2 + |\mathbf{v}^{k+1} - \mathbf{v}^k|^2\right). \tag{4.23}$$

4.2.1 Numerical Methods

Denote by $\mathbf{x}^k$ and $\mathbf{y}^k$ the approximation using a time stepping method to the solution values $\mathbf{x}(t^k)$ and $\mathbf{y}(t^k)$, respectively. We begin with a fully implicit and coupled algorithm which admits a relatively easy analysis and is used as a point of reference for the uncoupled algorithms which follow. Using a backward-Euler time discretization of (4.3)-(4.4) at time t^{k+1} results in the following method.

Algorithm 4.2.1 (Implicit method)**.** *Let* $\mathbf{x}^j$, $\mathbf{y}^j$ *be given for* $j = 0, 1, \ldots, k < N$. *Then* $\mathbf{x}^{k+1}$ *and* $\mathbf{y}^{k+1}$ *are calculated by*

$$\frac{1}{\Delta t}(\mathbf{x}^{k+1} - \mathbf{x}^k) + A\mathbf{x}^{k+1} + \kappa \left|x_1^{k+1} - y_1^{k+1}\right| (x_1^{k+1} - y_1^{k+1})[1 \quad 0]^T = \mathbf{f}(t^{k+1}) \tag{4.24}$$

$$\frac{1}{\Delta t}(\mathbf{y}^{k+1} - \mathbf{y}^k) + B\mathbf{y}^{k+1} + \kappa \left|x_1^{k+1} - y_1^{k+1}\right| (y_1^{k+1} - x_1^{k+1})[1 \quad 0]^T = \mathbf{g}(t^{k+1}) \tag{4.25}$$

The next algorithm, discussed already (see Section 4.1.2), decouples the equations for $\mathbf{x}^{k+1}$ and $\mathbf{y}^{k+1}$. For example, in the $\mathbf{x}^{k+1}$-equation (4.24), the term y_1^{k+1} is replaced with y_1^k. Similarly the equation for $\mathbf{y}^{k+1}$ is modified and the resulting algorithm is referred to as the IMEX (*implicit-explicit*) method.

Algorithm 4.2.2 (IMEX method)**.** *Let* $\mathbf{x}^j$, $\mathbf{y}^j$ *be given for* $j = 0, 1, \ldots, k < N$. *Then* $\mathbf{x}^{k+1}$ *and* $\mathbf{y}^{k+1}$ *are calculated by*

$$\frac{1}{\Delta t}(\mathbf{x}^{k+1} - \mathbf{x}^k) + A\mathbf{x}^{k+1} + \kappa \left|x_1^k - y_1^k\right| (x_1^{k+1} - y_1^k)[1 \quad 0]^T = \mathbf{f}(t^{k+1}) \tag{4.26}$$

$$\frac{1}{\Delta t}(\mathbf{y}^{k+1} - \mathbf{y}^k) + B\mathbf{y}^{k+1} + \kappa \left|x_1^k - y_1^k\right| (y_1^{k+1} - x_1^k)[1 \quad 0]^T = \mathbf{g}(t^{k+1}) \tag{4.27}$$

It will be shown that from an analytical and experimental point of view the IMEX method may not exhibit desirable stability properties, and utility of this algorithm in a general context becomes unclear. This motivates the addition of stabilization terms. The terms are added so as not to reintroduce coupling, making the *stabilized IMEX* method no more expensize than unstabilized IMEX.

Algorithm 4.2.3 (Stabilized IMEX method)**.** *Let* $\mathbf{x}^j$, $\mathbf{y}^j$ *be given for* $j = 0, 1, \ldots, k < N$. *Denote by* $\mu(\kappa)^k$ *the quantity* $\mu(\kappa)^k = \kappa^2(\Delta t)\left|x_1^k - y_1^k\right|^2$. *Then* $\mathbf{x}^{k+1}$ *and* $\mathbf{y}^{k+1}$ *are calculated by*

$$\begin{aligned}
\frac{\mathbf{x}^{k+1} - \mathbf{x}^k}{\Delta t} &+ A\mathbf{x}^{k+1} + 2\mu(\kappa)^k\mathbf{x}^{k+1} \\
&+ \kappa\left|x_1^k - y_1^k\right|(x_1^{k+1} - y_1^k)[1 \quad 0]^T = \mathbf{f}(t^{k+1}) \qquad (4.28) \\
\frac{\mathbf{y}^{k+1} - \mathbf{y}^k}{\Delta t} &+ B\mathbf{y}^{k+1} + 2\mu(\kappa)^k\mathbf{y}^{k+1} \\
&+ \kappa\left|x_1^k - y_1^k\right|(y_1^{k+1} - x_1^k)[1 \quad 0]^T = \mathbf{g}(t^{k+1}) \qquad (4.29)
\end{aligned}$$

An alternative to this stabilization technique arises from using a two-step method designed to maintain stability of the algorithm after decoupling, referred to herein as the *geometric averaging* method ("GA method").

Algorithm 4.2.4 (GA method)**.** *Let* $\mathbf{x}^j$, $\mathbf{y}^j$ *be given for* $j = 0, 1, \ldots, k < N$. *Then* $\mathbf{x}^{k+1}$ *and* $\mathbf{y}^{k+1}$ *are calculated by*

$$\begin{aligned}
\frac{1}{\Delta t}(\mathbf{x}^{k+1} - \mathbf{x}^k) + A\mathbf{x}^{k+1} + \kappa\left|x_1^k - y_1^k\right|x_1^{k+1}[1 \quad 0]^T & \\
-\kappa\left|x_1^k - y_1^k\right|^{1/2}\left|x_1^{k-1} - y_1^{k-1}\right|^{1/2} y_1^k[1 \quad 0]^T &= \mathbf{f}(t^{k+1}) \qquad (4.30) \\
\frac{1}{\Delta t}(\mathbf{y}^{k+1} - \mathbf{y}^k) + B\mathbf{y}^{k+1} + \kappa\left|x_1^k - y_1^k\right|y_1^{k+1}[1 \quad 0]^T & \\
-\kappa\left|x_1^k - y_1^k\right|^{1/2}\left|x_1^{k-1} - y_1^{k-1}\right|^{1/2} x_1^k[1 \quad 0]^T &= \mathbf{g}(t^{k+1}) \qquad (4.31)
\end{aligned}$$

4.2.2 Preliminary Results

The linearized algorithms 4.2.2-4.2.4 admit a unique solution at each time step. This becomes clear after writing each of these algorithms in the form $T^n z^{n+1} = \text{data}$, where $z^{n+1} \in \mathbb{R}^4$ is the solution at time step $n+1$ and $T^n \in \mathbb{R}^{4\times 4}$ is a positive definite matrix depending only on z^n. Existence and uniqueness of solutions to Algorithm 4.2.1 may be established using e.g. energy estimates and Brouer's fixed point theorem. To clarify the stability proofs in Section 4.3, in some cases intermediate steps are eliminated by reference to the following lemmas.

Lemma 4.2.2. *The solution* $\mathbf{x}^{j+1}, \mathbf{y}^{j+1}$ *of Algorithm 4.2.2 satisfies the following inequality for* $j = 0, 1, 2, \ldots, N-1$ *:*

$$\begin{aligned}
&\frac{1}{2\Delta t}\left\{|\mathbf{x}^{j+1}|^2 + |\mathbf{y}^{j+1}|^2 - |\mathbf{x}^{j}|^2 - |\mathbf{y}^{j}|^2\right\} + \frac{1}{4\Delta t}\left\{|\mathbf{x}^{j+1} - \mathbf{x}^{j}|^2 + |\mathbf{y}^{j+1} - \mathbf{y}^{j}|^2\right\} \\
&+ \frac{1}{2}\left\{\left|\mathbf{x}^{j+1}\right|_A^2 + \left|\mathbf{y}^{j+1}\right|_B^2\right\} + \kappa\left|x_1^j - y_1^j\right|\left|x_1^{j+1} - y_1^{j+1}\right|^2 \\
&\qquad \le \frac{1}{2}\left\{\left|\mathbf{f}(t^{j+1})\right|_{A_{spd}^{-1}}^2 + \left|\mathbf{g}(t^{j+1})\right|_{B_{spd}^{-1}}^2\right\} \\
&\qquad\qquad + (\Delta t)\kappa^2\left|x_1^j - y_1^j\right|^2\left\{|x_1^{j+1}|^2 + |y_1^{j+1}|^2\right\}. \quad (4.32)
\end{aligned}$$

Proof. At time level $j+1$, left-multiply through (4.26) by $(\mathbf{x}^{j+1})^T$ and (4.27) by $(\mathbf{y}^{j+1})^T$. Then add the resulting equations, apply (4.17) and (4.23) to obtain

$$\begin{aligned}
&\frac{1}{2\Delta t}\left\{|\mathbf{x}^{j+1}|^2 + |\mathbf{y}^{j+1}|^2 - |\mathbf{x}^{j}|^2 - |\mathbf{y}^{j}|^2 + |\mathbf{x}^{j+1} - \mathbf{x}^{j}|^2 + |\mathbf{y}^{j+1} - \mathbf{y}^{j}|^2\right\} \\
&\quad + \left|\mathbf{x}^{j+1}\right|_A^2 + \left|\mathbf{y}^{j+1}\right|_B^2 + \kappa\left|x_1^j - y_1^j\right|\left(x_1^{j+1} - y_1^j\right)x_1^{j+1} + \kappa\left|x_1^j - y_1^j\right|\left(y_1^{j+1} - x_1^j\right)y_1^{j+1} \\
&\qquad = (\mathbf{x}^{j+1})^T\mathbf{f}(t^{j+1}) + (\mathbf{y}^{j+1})^T\mathbf{g}(t^{j+1}).
\end{aligned}$$

Add and subtract x_1^{j+1} and y_1^{j+1} and rearrange the coupling as follows.

$$\begin{aligned}
&\left(x_1^{j+1} - y_1^j\right)x_1^{j+1} + \left(y_1^{j+1} - x_1^j\right)y_1^{j+1} \\
&= \left|x_1^{j+1} - y_1^{j+1}\right|^2 + \left(y_1^{j+1} - y_1^j\right)x_1^{j+1} + \left(x_1^{j+1} - x_1^j\right)y_1^{j+1}.
\end{aligned}$$

The non-negative term is kept on the left hand side of the original equality and others moved to the right hand side. Bound $\mathbf{f}(t^{j+1})$ and $\mathbf{g}(t^{j+1})$ via Lemma 4.2.1:

$$\begin{aligned}
&\frac{1}{2\Delta t}\left\{|\mathbf{x}^{j+1}|^2 + |\mathbf{y}^{j+1}|^2 - |\mathbf{x}^{j}|^2 - |\mathbf{y}^{j}|^2 + |\mathbf{x}^{j+1} - \mathbf{x}^{j}|^2 + |\mathbf{y}^{j+1} - \mathbf{y}^{j}|^2\right\} \\
&\qquad + \frac{1}{2}\left\{\left|\mathbf{x}^{j+1}\right|_A^2 + \left|\mathbf{y}^{j+1}\right|_B^2\right\} + \kappa\left|x_1^j - y_1^j\right|\left|x_1^{j+1} - y_1^{j+1}\right|^2 \\
&\le \frac{1}{2}\left\{\left|\mathbf{f}(t^{j+1})\right|_{A_{spd}^{-1}}^2 + \left|\mathbf{g}(t^{j+1})\right|_{B_{spd}^{-1}}^2\right\} + \kappa\left|x_1^j - y_1^j\right|\left|y_1^{j+1} - y_1^j\right|\left|x_1^{j+1}\right| \\
&\qquad\qquad + \kappa\left|x_1^j - y_1^j\right|\left|x_1^{j+1} - x_1^j\right|\left|y_1^{j+1}\right|.
\end{aligned}$$

Applying Young's inequality,

$$\begin{aligned}
\frac{1}{2\Delta t}\Big\{|\mathbf{x}^{j+1}|^2+|\mathbf{y}^{j+1}|^2-|\mathbf{x}^{j}|^2-|\mathbf{y}^{j}|^2+|\mathbf{x}^{j+1}-\mathbf{x}^{j}|^2+|\mathbf{y}^{j+1}-\mathbf{y}^{j}|^2\Big\}& \\
+\frac{1}{2}\left\{\left|\mathbf{x}^{j+1}\right|_A^2+\left|\mathbf{y}^{j+1}\right|_B^2\right\}+\kappa\left|x_1^j-y_1^j\right|\left|x_1^{j+1}-y_1^{j+1}\right|^2& \\
\leq\frac{1}{2}\left\{\left|\mathbf{f}(t^{j+1})\right|_{A_{spd}^{-1}}^2+\left|\mathbf{g}(t^{j+1})\right|_{B_{spd}^{-1}}^2\right\}+\frac{1}{4\Delta t}\left|y_1^{j+1}-y_1^j\right|^2+\frac{1}{4\Delta t}\left|x_1^{j+1}-x_1^j\right|^2& \\
+(\Delta t)\kappa^2\left|x_1^j-y_1^j\right|^2\left\{|x_1^{j+1}|^2+|y_1^{j+1}|^2\right\}.&
\end{aligned}$$

Bound

$$\frac{1}{4\Delta t}\left|y_1^{j+1}-y_1^j\right|^2+\frac{1}{4\Delta t}\left|x_1^{j+1}-x_1^j\right|^2\leq\frac{1}{4\Delta t}\left|\mathbf{y}^{j+1}-\mathbf{y}^j\right|^2+\frac{1}{4\Delta t}\left|\mathbf{x}^{j+1}-\mathbf{x}^j\right|^2$$

and subsume the terms, proving (4.32). □

4.3 NUMERICAL STABILITY

The following stability lemmas demonstrate many of the key properties of the time discretization methods under study. The implicit method will serve as a benchmark. The proofs employ energy estimates, making evident extension to analogous algorithms for solving systems of PDEs.

The stability proof for the IMEX method will illustrate how instabilities can occur when lagging the coupling terms. Using energy methods to prove stability, the nonlinearity appears to allow for quadratic growth of errors, which are only controlled once the time step size is taken sufficiently small. While not proved here, improved stability results can be shown in special cases, as when A and B are equal, or when they are diagonally dominant. However, we are interested in maintaining the asymptotic stability result seen for the implicit discretization whenever possible, which cannot be guaranteed in general using the IMEX algorithm. Reference to computational experiments (Section 4.5) helps to illustrate the subtle stability properties of the IMEX algorithm.

Lemma 4.3.1 (Stability: IMEX). *Let* $\mathbf{f}$, $\mathbf{g} \in L^2(0,T;\mathbb{R}^2)$, *independent of* $\kappa > 0$. *Assume* Δt *satisfies*

$$\Delta t \left(8\kappa^2 \max\{(\alpha_2)^2, (\beta_2)^2\} L\right) \leq 1, \tag{4.33}$$

where L *is defined by (4.22). Then for* $k = 0, 1, \ldots, N-1$ *the solution* $\mathbf{x}^{k+1}$, $\mathbf{y}^{k+1}$ *of Algorithm 4.2.2 satisfies the following bound independent of* Δt *and* κ*:*

$$\begin{aligned} &|\mathbf{x}^{k+1}|^2 + |\mathbf{y}^{k+1}|^2 + \frac{1}{2}\sum_{j=0}^{k} \left\{|\mathbf{x}^{j+1} - \mathbf{x}^j|^2 + |\mathbf{y}^{j+1} - \mathbf{y}^j|^2\right\} \\ &\quad + \frac{\Delta t}{2}\sum_{j=0}^{k} \left\{ \left|\mathbf{x}^{j+1}\right|_A^2 + \left|\mathbf{y}^{j+1}\right|_B^2 + 4\kappa \left|x_1^j - y_1^j\right| \left|x_1^{j+1} - y_1^{j+1}\right|^2 \right\} \leq L. \end{aligned} \tag{4.34}$$

Proof. Using Lemma 4.2.2, the inequality (4.32) holds at each time step $j+1$. The data up to time step j will be known, thus an inductive argument may be used to control the size of the terms by making Δt sufficiently small. First, we simplify by noting

$$\begin{aligned} \left|x_1^j - y_1^j\right|^2 \left\{|x_1^{j+1}|^2 + |y_1^{j+1}|^2\right\} &\leq 2\left\{|\mathbf{x}^j|^2 + |\mathbf{y}^j|^2\right\}\left\{|\mathbf{x}^{j+1}|^2 + |\mathbf{y}^{j+1}|^2\right\} \\ &\leq 2C\left\{|\mathbf{x}^j|^2 + |\mathbf{y}^j|^2\right\}\left\{|\mathbf{x}^{j+1}|_A^2 + |\mathbf{y}^{j+1}|_B^2\right\} \end{aligned}$$

where $C = \max\{(\alpha_2)^2, (\beta_2)^2\}$, coming from (4.18)-(4.19). To prove the inductive hypothesis, take first $j = 0$, and inserting into (4.32) one obtains

$$\begin{aligned} &\frac{1}{2\Delta t}\left\{|\mathbf{x}^1|^2 + |\mathbf{y}^1|^2 - |\mathbf{x}^0|^2 - |\mathbf{y}^0|^2\right\} + \frac{1}{4\Delta t}\left\{|\mathbf{x}^1 - \mathbf{x}^0|^2 + |\mathbf{y}^1 - \mathbf{y}^0|^2\right\} \\ &\qquad + \frac{1}{2}\left\{\left|\mathbf{x}^1\right|_A^2 + \left|\mathbf{y}^1\right|_B^2\right\} + \kappa\left|x_1^0 - y_1^0\right|\left|x_1^1 - y_1^1\right|^2 \\ &\leq \frac{1}{2}\left\{\left|\mathbf{f}(t^1)\right|_{A_{spd}^{-1}}^2 + \left|\mathbf{g}(t^1)\right|_{B_{spd}^{-1}}^2\right\} + (\Delta t) 2\,\kappa^2\, C\left\{|\mathbf{x}^0|^2 + |\mathbf{y}^0|^2\right\}\left\{|\mathbf{x}^1|_A^2 + |\mathbf{y}^1|_B^2\right\} \end{aligned}$$

so that restricting

$$(\Delta t) 2\,\kappa^2\, C\left\{|\mathbf{x}^0|^2 + |\mathbf{y}^0|^2\right\} \leq \frac{1}{4} \tag{4.35}$$

it follows

$$\begin{aligned} &\frac{1}{2\Delta t}\left\{|\mathbf{x}^1|^2 + |\mathbf{y}^1|^2 - |\mathbf{x}^0|^2 - |\mathbf{y}^0|^2\right\} + \frac{1}{4\Delta t}\left\{|\mathbf{x}^1 - \mathbf{x}^0|^2 + |\mathbf{y}^1 - \mathbf{y}^0|^2\right\} \\ &\qquad + \frac{1}{2}\left\{\left|\mathbf{x}^1\right|_A^2 + \left|\mathbf{y}^1\right|_B^2\right\} + \kappa\left|x_1^0 - y_1^0\right|\left|x_1^1 - y_1^1\right|^2 \\ &\leq \frac{1}{2}\left\{\left|\mathbf{f}(t^1)\right|_{A_{spd}^{-1}}^2 + \left|\mathbf{g}(t^1)\right|_{B_{spd}^{-1}}^2\right\} + \frac{1}{4}\left\{|\mathbf{x}^1|_A^2 + |\mathbf{y}^1|_B^2\right\}. \end{aligned}$$

These arguments are true, noting the restriction (4.35) holds because of assumption (4.33). Subsume the extra terms on the right hand side, and the desired bound results,

$$\begin{aligned}&\frac{1}{2\Delta t}\left\{|\mathbf{x}^1|^2+|\mathbf{y}^1|^2-|\mathbf{x}^0|^2-|\mathbf{y}^0|^2\right\}+\frac{1}{4\Delta t}\left\{|\mathbf{x}^1-\mathbf{x}^0|^2+|\mathbf{y}^1-\mathbf{y}^0|^2\right\}+\frac{1}{4}\left|\mathbf{x}^1\right|_A^2\\&+\frac{1}{4}\left|\mathbf{y}^1\right|_B^2+\kappa\left|x_1^0-y_1^0\right|\left|x_1^1-y_1^1\right|^2\leq\frac{1}{2}\left\{\left|\mathbf{f}(t^1)\right|_{A_{spd}^{-1}}^2+\left|\mathbf{g}(t^1)\right|_{B_{spd}^{-1}}^2\right\}.\end{aligned}\tag{4.36}$$

That case k implies case $k+1$ in general follows by using the time step restriction (4.33). For completeness, we show this explicitly. Assume that

$$\begin{aligned}&|\mathbf{x}^k|^2+|\mathbf{y}^k|^2+\frac{1}{2}\sum_{j=0}^{k-1}\left\{|\mathbf{x}^{j+1}-\mathbf{x}^j|^2+|\mathbf{y}^{j+1}-\mathbf{y}^j|^2\right\}\\&+\frac{\Delta t}{2}\sum_{j=0}^{k-1}\left\{\left|\mathbf{x}^{j+1}\right|_A^2+\left|\mathbf{y}^{j+1}\right|_B^2\right\}+2\kappa\,\Delta t\sum_{j=0}^{k-1}\left|x_1^j-y_1^j\right|\left|x_1^{j+1}-y_1^{j+1}\right|^2\\&\leq|\mathbf{x}_0|^2+|\mathbf{y}_0|^2+\Delta t\sum_{j=0}^{k-1}\left\{\left|\mathbf{f}(t^{j+1})\right|_{A_{spd}^{-1}}^2+\left|\mathbf{g}(t^{j+1})\right|_{B_{spd}^{-1}}^2\right\}\leq L.\end{aligned}\tag{4.37}$$

Then it follows

$$\begin{aligned}C\,\Delta t\,\kappa^2|x_1^k-y_1^k|^2&\leq 2C\,\Delta t\,\kappa^2\left(|\mathbf{x}^k|^2+|\mathbf{y}^k|^2\right)\\\Rightarrow C\,\Delta t\,\kappa^2|x_1^k-y_1^k|^2&\leq 2C\,\Delta t\,\kappa^2 L\leq\frac{1}{4},\end{aligned}\tag{4.38}$$

by assumption (4.33). In (4.32) take $j=k$, multiply through by $2\Delta t$, and add the result to (4.37). This yields

$$\begin{aligned}&|\mathbf{x}^{k+1}|^2+|\mathbf{y}^{k+1}|^2+\frac{1}{2}\sum_{j=0}^{k}\left\{|\mathbf{x}^{j+1}-\mathbf{x}^j|^2+|\mathbf{y}^{j+1}-\mathbf{y}^j|^2\right\}+\Delta t\left\{\left|\mathbf{x}^{k+1}\right|_A^2+\left|\mathbf{y}^{k+1}\right|_B^2\right\}\\&+\frac{\Delta t}{2}\sum_{j=0}^{k-1}\left\{\left|\mathbf{x}^{j+1}\right|_A^2+\left|\mathbf{y}^{j+1}\right|_B^2\right\}+2\kappa\,\Delta t\sum_{j=0}^{k}\left|x_1^j-y_1^j\right|\left|x_1^{j+1}-y_1^{j+1}\right|^2\\&\leq|\mathbf{x}_0|^2+|\mathbf{y}_0|^2+\Delta t\sum_{j=0}^{k}\left\{\left|\mathbf{f}(t^{j+1})\right|_{A_{spd}^{-1}}^2+\left|\mathbf{g}(t^{j+1})\right|_{B_{spd}^{-1}}^2\right\}\\&+2\Delta t^2\,\kappa^2|x_1^k-y_1^k|^2\left(|x_1^{k+1}|^2+|y_1^{k+1}|^2\right)\\&\leq L+2\Delta t^2\,\kappa^2|x_1^k-y_1^k|^2C\left\{\left|\mathbf{x}^{k+1}\right|_A^2+\left|\mathbf{y}^{k+1}\right|_B^2\right\}.\end{aligned}$$

Applying (4.38),

$$
\begin{aligned}
&|\mathbf{x}^{k+1}|^2 + |\mathbf{y}^{k+1}|^2 + \frac{1}{2}\sum_{j=0}^{k}\left\{|\mathbf{x}^{j+1}-\mathbf{x}^{j}|^2 + |\mathbf{y}^{j+1}-\mathbf{y}^{j}|^2\right\} + \Delta t\,\left\{\left|\mathbf{x}^{k+1}\right|_A^2 + \left|\mathbf{y}^{k+1}\right|_B^2\right\} \\
&+ \frac{\Delta t}{2}\sum_{j=0}^{k-1}\left\{\left|\mathbf{x}^{j+1}\right|_A^2 + \left|\mathbf{y}^{j+1}\right|_B^2\right\} + 2\kappa\,\Delta t\sum_{j=0}^{k}\left|x_1^j - y_1^j\right|\left|x_1^{j+1} - y_1^{j+1}\right|^2 \\
&\leq L + \frac{\Delta t}{2}\left\{\left|\mathbf{x}^{k+1}\right|_A^2 + \left|\mathbf{y}^{k+1}\right|_B^2\right\},
\end{aligned}
$$

and rearranging terms, the result follows,

$$
\begin{aligned}
&|\mathbf{x}^{k+1}|^2 + |\mathbf{y}^{k+1}|^2 + \frac{1}{2}\sum_{j=0}^{k}\left\{|\mathbf{x}^{j+1}-\mathbf{x}^{j}|^2 + |\mathbf{y}^{j+1}-\mathbf{y}^{j}|^2\right\} \\
&+ \frac{\Delta t}{2}\sum_{j=0}^{k}\left\{\left|\mathbf{x}^{j+1}\right|_A^2 + \left|\mathbf{y}^{j+1}\right|_B^2\right\} + 2\kappa\,\Delta t\sum_{j=0}^{k}\left|x_1^j - y_1^j\right|\left|x_1^{j+1} - y_1^{j+1}\right|^2 \leq L.
\end{aligned}
$$

□

An alternative to restricting the time step size is the addition of stabilizing terms. The proof of Lemma 4.3.2 contains the key ideas making this possible.

Lemma 4.3.2 (Stability: stabilized IMEX)**.** *Let* $\mathbf{f}$, $\mathbf{g} \in L^2(0,T;\mathbb{R}^2)$, *independent of* $\kappa > 0$. *Then for* $k = 0, 1, \ldots, N-1$ *the solution* $\mathbf{x}^{k+1}$, $\mathbf{y}^{k+1}$ *of Algorithm 4.2.2 satisfies the following bound independent of* Δt *and* κ*:*

$$
\begin{aligned}
&|\mathbf{x}^{k+1}|^2 + |\mathbf{y}^{k+1}|^2 \\
&+ \sum_{j=0}^{k}\left\{|\mathbf{x}^{j+1}-\mathbf{x}^{j}|^2 + |\mathbf{y}^{j+1}-\mathbf{y}^{j}|^2 + 2(\Delta t)\mu(\kappa)^j\left(|\mathbf{x}^{j+1}|^2 + |\mathbf{y}^{j+1}|^2\right)\right\} \\
&+ \Delta t\sum_{j=0}^{k}\left\{\left|\mathbf{x}^{j+1}\right|_A^2 + \left|\mathbf{y}^{j+1}\right|_B^2 + 2\kappa\left|x_1^j - y_1^j\right|\left|x_1^{j+1} - y_1^{j+1}\right|^2\right\} \leq L.
\end{aligned}
\tag{4.39}
$$

where L *is defined by (4.22).*

Proof. Algorithms 4.2.2 and 4.2.3 differ only by the addition of one stabilization term for both the $\mathbf{x}^{k+1}$ and $\mathbf{y}^{k+1}$ equations. Thus the inequality (4.32) from the proof of Lemma 4.3.2 is easily modified to generate a new inequality valid for the stabilized IMEX method. At time t^{j+1} we obtain

$$\begin{aligned}
&\frac{1}{2\Delta t}\left\{|\mathbf{x}^{j+1}|^2+|\mathbf{y}^{j+1}|^2-|\mathbf{x}^{j}|^2-|\mathbf{y}^{j}|^2\right\}+\frac{1}{4\Delta t}\left\{|\mathbf{x}^{j+1}-\mathbf{x}^{j}|^2+|\mathbf{y}^{j+1}-\mathbf{y}^{j}|^2\right\}\\
&+2\mu(\kappa)^j\left\{|\mathbf{x}^{j+1}|^2+|\mathbf{y}^{j+1}|^2\right\}+\frac{1}{2}\left\{\left|\mathbf{x}^{j+1}\right|_A^2+\left|\mathbf{y}^{j+1}\right|_B^2\right\}+\kappa\left|x_1^j-y_1^j\right|\left|x_1^{j+1}-y_1^{j+1}\right|^2\\
&\leq\frac{1}{2}\left\{\left|\mathbf{f}(t^{j+1})\right|^2_{A^{-1}_{spd}}+\left|\mathbf{g}(t^{j+1})\right|^2_{B^{-1}_{spd}}\right\}+(\Delta t)\kappa^2\left|x_1^j-y_1^j\right|^2\left\{|x_1^{j+1}|^2+|y_1^{j+1}|^2\right\}.
\end{aligned}$$

Bound $|x_1^{j+1}|^2+|y_1^{j+1}|^2\leq|\mathbf{x}^{j+1}|^2+|\mathbf{y}^{j+1}|^2$, and recalling $\mu(\kappa)^j=\Delta t\kappa^2|x_1^j-y_1^j|^2$,

$$\begin{aligned}
&\frac{1}{2\Delta t}\left\{|\mathbf{x}^{j+1}|^2+|\mathbf{y}^{j+1}|^2-|\mathbf{x}^{j}|^2-|\mathbf{y}^{j}|^2\right\}+\frac{1}{4\Delta t}\left\{|\mathbf{x}^{j+1}-\mathbf{x}^{j}|^2+|\mathbf{y}^{j+1}-\mathbf{y}^{j}|^2\right\}\\
&+2\mu(\kappa)^j\left\{|\mathbf{x}^{j+1}|^2+|\mathbf{y}^{j+1}|^2\right\}+\frac{1}{2}\left\{\left|\mathbf{x}^{j+1}\right|_A^2+\left|\mathbf{y}^{j+1}\right|_B^2\right\}+\kappa\left|x_1^j-y_1^j\right|\left|x_1^{j+1}-y_1^{j+1}\right|^2\\
&\qquad\leq\frac{1}{2}\left\{\left|\mathbf{f}(t^{j+1})\right|^2_{A^{-1}_{spd}}+\left|\mathbf{g}(t^{j+1})\right|^2_{B^{-1}_{spd}}\right\}+\mu(\kappa)^j\left\{|\mathbf{x}^{j+1}|^2+|\mathbf{y}^{j+1}|^2\right\}.
\end{aligned}$$

After subtracting $\mu(\kappa)^j\left\{|\mathbf{x}^{j+1}|^2+|\mathbf{y}^{j+1}|^2\right\}$ to the left hand side, the rest of the proof follows by summing over the index j. □

The two step algorithm removes the need for stabilizations or time step restrictions.

Lemma 4.3.3 (Stability: GA)**.** *Let* $\mathbf{f}$, $\mathbf{g}\in L^2(0,T;\mathbb{R}^2)$, *independent of* $\kappa>0$. *Then for* $k=0,1,\ldots,N-1$ *the solution* $\mathbf{x}^{k+1}$, $\mathbf{y}^{k+1}$ *of Algorithm 4.2.4 satisfies the following bound independent of* Δt *and* κ*:*

$$\begin{aligned}
&|\mathbf{x}^{k+1}|^2+|\mathbf{y}^{k+1}|^2+\sum_{j=0}^{k}\left\{|\mathbf{x}^{j+1}-\mathbf{x}^{j}|^2+|\mathbf{y}^{j+1}-\mathbf{y}^{j}|^2\right\}\\
&+\Delta t\sum_{j=0}^{k}\left\{\left|\mathbf{x}^{j+1}\right|_A^2+\left|\mathbf{y}^{j+1}\right|_B^2\right\}+\Delta t\,\kappa\left|x_1^k-y_1^k\right|\left\{|x_1^{k+1}|^2+|y_1^{k+1}|^2\right\}\\
&\leq L+\Delta t\,\kappa\left|x_1^0-y_1^0\right|\left\{|x_1^1|^2+|y_1^1|^2\right\}.
\end{aligned}\tag{4.40}$$

where L *is defined by (4.22).*

Proof. At time level $j+1$, left-multiply through (4.30) by $(\mathbf{x}^{j+1})^T$ and (4.31) by $(\mathbf{y}^{j+1})^T$. Then add the resulting equations, apply (4.23) and (4.17) to obtain

$$\begin{aligned}
&\frac{1}{2\Delta t}\left\{|\mathbf{x}^{j+1}|^2+|\mathbf{y}^{j+1}|^2-|\mathbf{x}^{j}|^2-|\mathbf{y}^{j}|^2+|\mathbf{x}^{j+1}-\mathbf{x}^{j}|^2+|\mathbf{y}^{j+1}-\mathbf{y}^{j}|^2\right\}\\
&\quad+\left|\mathbf{x}^{j+1}\right|_A^2+\left|\mathbf{y}^{j+1}\right|_B^2+\kappa\left|x_1^j-y_1^j\right|\left|x_1^{j+1}\right|^2-\kappa\left|x_1^j-y_1^j\right|^{1/2}\left|x_1^{j-1}-y_1^{j-1}\right|^{1/2}x_1^{j+1}y_1^j\\
&\quad+\kappa\left|x_1^j-y_1^j\right|\left|y_1^{j+1}\right|^2-\kappa\left|x_1^j-y_1^j\right|^{1/2}\left|x_1^{j-1}-y_1^{j-1}\right|^{1/2}y_1^{j+1}x_1^j\\
&\quad=(\mathbf{x}^{j+1})^T\mathbf{f}(t^{j+1})+(\mathbf{y}^{j+1})^T\mathbf{g}(t^{j+1}).
\end{aligned}$$

Using Young's inequality the following bounds are derived:

$$\begin{aligned}
\kappa\left|x_1^j-y_1^j\right|^{1/2}\left|x_1^{j-1}-y_1^{j-1}\right|^{1/2}\left|x_1^{j+1}y_1^j\right|&\le\frac{\kappa}{2}\left|x_1^j-y_1^j\right|\left|x_1^{j+1}\right|^2+\frac{\kappa}{2}\left|x_1^{j-1}-y_1^{j-1}\right|\left|y_1^j\right|^2\\
\kappa\left|x_1^j-y_1^j\right|^{1/2}\left|x_1^{j-1}-y_1^{j-1}\right|^{1/2}\left|y_1^{j+1}x_1^j\right|&\le\frac{\kappa}{2}\left|x_1^j-y_1^j\right|\left|y_1^{j+1}\right|^2+\frac{\kappa}{2}\left|x_1^{j-1}-y_1^{j-1}\right|\left|x_1^j\right|^2
\end{aligned}$$

After bounding the right hand side, it follows

$$\begin{aligned}
&\frac{1}{2\Delta t}\left\{|\mathbf{x}^{j+1}|^2+|\mathbf{y}^{j+1}|^2-|\mathbf{x}^{j}|^2-|\mathbf{y}^{j}|^2+|\mathbf{x}^{j+1}-\mathbf{x}^{j}|^2+|\mathbf{y}^{j+1}-\mathbf{y}^{j}|^2\right\}\\
&\quad+\frac{\kappa}{2}\left|x_1^j-y_1^j\right|\left|x_1^{j+1}\right|^2-\frac{\kappa}{2}\left|x_1^{j-1}-y_1^{j-1}\right|\left|x_1^j\right|^2+\frac{1}{2}\left\{\left|\mathbf{x}^{j+1}\right|_A^2+\left|\mathbf{y}^{j+1}\right|_B^2\right\}\\
&\quad+\frac{\kappa}{2}\left|x_1^j-y_1^j\right|\left|y_1^{j+1}\right|^2-\frac{\kappa}{2}\left|x_1^{j-1}-y_1^{j-1}\right|\left|y_1^j\right|^2\le\left\{\left|\mathbf{f}(t^{j+1})\right|_{A_{spd}^{-1}}^2+\left|\mathbf{g}(t^{j+1})\right|_{B_{spd}^{-1}}^2\right\}.
\end{aligned}$$

Multiply through by $2\Delta t$, sum over $j=1,2,\ldots,k$ and the result follows. □

4.4 CONVERGENCE OF THE NUMERICAL METHODS

Consistency of the numerical methods will first be established. It is assumed the solution to the ODE system (4.3)-(4.4) is sufficiently smooth. Consistency of the methods then follows from Taylor's theorem.

Lemma 4.4.1 (Consistency: IMEX,Stabilized IMEX)**.** *Let* $\mathbf{x}, \mathbf{y}$ *be the solution to (4.3)-(4.4), with continuous second derivatives for* $t \in [0,T]$*. Let* τ^{n+1} *denote the local truncation error at time step* t^{n+1} *for Algorithm 4.2.2, (4.2.3). Then Algorithm 4.2.2, (4.2.3), is consistent of order one, satisfying*

$$\max_{n=0,\ldots,N-1} \left|\tau^{n+1}\right| \leq \frac{3}{2}(1+C\kappa)\,\Delta t \max_{t\in[0,T]} \left\{ \left|\frac{d^2}{dt^2}\mathbf{x}(t)\right| + \left|\frac{d^2}{dt^2}\mathbf{y}(t)\right| \right\} \quad \textit{IMEX} \tag{4.41}$$

$$\begin{aligned} \max_{n=0,\ldots,N-1} \left|\tau^{n+1}\right| &\leq \frac{3}{2}(1+C\kappa)\,\Delta t \max_{t\in[0,T]} \left\{ \left|\frac{d^2}{dt^2}\mathbf{x}(t)\right| + \left|\frac{d^2}{dt^2}\mathbf{y}(t)\right| \right\} \\ &+ \Delta t\, C^2\kappa^2 \max_{t\in[0,T]} \{|\mathbf{x}(t)| + |\mathbf{y}(t)|\} \quad \textit{Stabilized IMEX} \end{aligned} \tag{4.42}$$

where $C = 2\max_{t\in[0,T]} |x_1(t)| + |y_1(t)|$.

Proof. The truncation errors for the $\mathbf{x}^{n+1}$ and $\mathbf{y}^{n+1}$ equations may be considered independently. Denote by τ_x^{n+1} the truncation error derived by inserting $\mathbf{x}(t^{n+1})$ into the discrete equation (4.26),

$$\begin{aligned} \tau_x^{n+1} &= \frac{1}{\Delta t}(\mathbf{x}(t^{n+1}) - \mathbf{x}(t^n)) + A\mathbf{x}(t^{n+1}) \\ &\quad + \kappa\,|x_1(t^n) - y_1(t^n)|\,(x_1(t^{n+1}) - y_1(t^n))[1 \quad 0]^T - \mathbf{f}(t^{n+1}). \end{aligned}$$

Subtract the corresponding expression derived from the ODE equation (4.3)

$$\begin{aligned} 0 &= \frac{d}{dt}\mathbf{x}(t^{n+1}) + A\mathbf{x}(t^{n+1}) \\ &\quad + \kappa\left|x_1(t^{n+1}) - y_1(t^{n+1})\right|(x_1(t^{n+1}) - y_1(t^{n+1}))[1 \quad 0]^T - \mathbf{f}(t^{n+1}) \end{aligned}$$

and it is clear the truncation error satisfies

$$\begin{aligned} \tau_x^{n+1} &= \frac{\mathbf{x}(t^{n+1}) - \mathbf{x}(t^n)}{\Delta t} - \frac{d}{dt}\mathbf{x}(t^{n+1}) + \kappa\left|x_1(t^{n+1}) - y_1(t^{n+1})\right|\left(y_1(t^{n+1}) - y_1(t^n)\right) \\ &\quad + \kappa\left(|x_1(t^n) - y_1(t^n)| - \left|x_1(t^{n+1}) - y_1(t^{n+1})\right|\right)\left(x_1(t^{n+1}) - y_1(t^n)\right). \end{aligned}$$

The error in estimating the discrete derivative is bounded as follows.

$$\begin{aligned} &\left|\frac{1}{\Delta t}(\mathbf{x}(t^{n+1}) - \mathbf{x}(t^n)) - \frac{d}{dt}\mathbf{x}(t^{n+1})\right| \\ &\leq \left|\frac{1}{\Delta t}(\mathbf{x}(t^{n+1}) - \mathbf{x}(t^n)) - \frac{d}{dt}\mathbf{x}(t^n)\right| + \left|\frac{d}{dt}\mathbf{x}(t^n) - \frac{d}{dt}\mathbf{x}(t^{n+1})\right| \\ &\leq \frac{1}{\Delta t}\int_{t^n}^{t^{n+1}} (t^{n+1} - s)\left|\frac{d^2}{dt^2}\mathbf{x}(s)\right| ds + \Delta t \max_{t\in[t^n,t^{n+1}]}\left|\frac{d^2}{dt^2}\mathbf{x}(t)\right| \\ &\leq \frac{\Delta t^2}{2\Delta t}\max_{t\in[t^n,t^{n+1}]}\left|\frac{d^2}{dt^2}\mathbf{x}(s)\right| ds + \Delta t \max_{t\in[t^n,t^{n+1}]}\left|\frac{d^2}{dt^2}\mathbf{x}(t)\right|. \end{aligned}$$

Therefore,

$$
\begin{aligned}
|\tau_x^{n+1}| &\leq \frac{3}{2}\Delta t \max_{t\in[0,T]} \left|\frac{d^2}{dt^2}\mathbf{x}(t)\right| + \kappa\,\Delta t \left|x_1(t^{n+1}) - y_1(t^{n+1})\right| \max_{t\in[t^n,t^{n+1}]} |\frac{d}{dt}y_1(t)| \\
&+ \kappa \left|(x_1(t^{n+1}) - x_1(t^n)) - (y_1(t^{n+1}) - y_1(t^n))\right| \left|x_1(t^{n+1}) - y_1(t^n)\right| \\
&\leq \frac{3}{2}\Delta t \max_{t\in[0,T]} \left|\frac{d^2}{dt^2}\mathbf{x}(t)\right| + \kappa\,\Delta t \max_{t\in[t^n,t^{n+1}]} \{|x_1(t)| + |y_1(t)|\}\, |\frac{d}{dt}y_1(t)| \\
&+ \kappa\,\Delta t \max_{t\in[t^n,t^{n+1}]} \{|x_1(t)| + |y_1(t)|\} \left\{ |\frac{d}{dt}x_1(t)| + |\frac{d}{dt}y_1(t)| \right\}.
\end{aligned}
$$

The corresponding result for τ_y^{n+1} is analogously derived. These bounds hold at each time step, so taking the maximum over $n = 0, 1, \ldots, N-1$ gives the final result for the IMEX scheme. The stabilized IMEX result may be derived by adding in the error due to the stabilization terms. For example,

$$
\begin{aligned}
2\mu(\kappa)^n |\mathbf{x}(t^{n+1})| &\leq \Delta t\ 2\kappa^2 \left\{|x_1(t^n)| + |y_1(t^n)|\right\}^2 |\mathbf{x}(t^{n+1})| \\
&\leq \Delta t\ 2\kappa^2 \max_{t\in[t^n,t^{n+1}]} \left\{|x_1(t)| + |y_1(t)|\right\}^2 |\mathbf{x}(t)| \\
&\leq \Delta t\ \kappa^2 C^2 \max_{t\in[t^n,t^{n+1}]} |\mathbf{x}(t)|.
\end{aligned}
$$

□

Lemma 4.4.2 (Consistency: GA)**.** *Let* $\mathbf{x}, \mathbf{y}$ *be the solution to (4.3)-(4.4), with continuous second derivatives for* $t \in [0, T]$*. Let* τ^{n+1} *denote the local truncation error at time step* t^{n+1} *for Algorithm 4.2.4. Then Algorithm 4.2.4 is consistent of order one, satisfying*

$$
\max_{n=0,\ldots,N-1} \left|\tau^{n+1}\right| \leq \frac{3}{2}(1 + C\kappa)\,\Delta t \max_{t\in[0,T]} \left\{ \left|\frac{d^2}{dt^2}\mathbf{x}(t)\right| + \left|\frac{d^2}{dt^2}\mathbf{y}(t)\right| \right\} \tag{4.43}
$$

where $C = 4 \max_{t\in[0,T]} |x_1(t)| + |y_1(t)|$.

Proof. The truncation errors for the $\mathbf{x}^{n+1}$ and $\mathbf{y}^{n+1}$ equations may be considered independently. Denote by τ_x^{n+1} the truncation error derived by inserting $\mathbf{x}(t^{n+1})$ into the discrete equation (4.30), subtract the corresponding expression derived from the ODE equation (4.3) and it is clear the truncation error satisfies

$$\begin{aligned}
\tau_x^{n+1} &= \frac{\mathbf{x}(t^{n+1}) - \mathbf{x}(t^n)}{\Delta t} - \frac{d}{dt}\mathbf{x}(t^{n+1}) + \kappa \left|x_1(t^{n+1}) - y_1(t^{n+1})\right| \left(y_1(t^{n+1}) - y_1(t^n)\right) \\
&+ \kappa \left(\left|x_1(t^n) - y_1(t^n)\right| - \left|x_1(t^{n+1}) - y_1(t^{n+1})\right|\right) x_1(t^{n+1}) \\
&+ \kappa \left(\left|x_1(t^{n+1}) - y_1(t^{n+1})\right| - \left|x_1(t^n) - y_1(t^n)\right|^{1/2} \left|x_1(t^{n-1}) - y_1(t^{n-1})\right|^{1/2}\right) y_1(t^n).
\end{aligned}$$

More compact notation will be used, setting $\lambda^n = x_1(t^n) - y_1(t^n)$. Only the last error term differs from the IMEX case above. To show the consistency of this term, first add and subtract the algebraic average $(|\lambda^n| + |\lambda^{n-1}|)/2$:

$$\begin{aligned}
&\left(\left|\lambda^{n+1}\right| - \left|\lambda^n\right|^{1/2} \left|\lambda^{n-1}\right|^{1/2}\right) y_1(t^n) \\
&= \left(\left|\lambda^{n+1}\right| - \frac{|\lambda^n| + |\lambda^{n-1}|}{2}\right) y_1(t^n) + \left(\frac{|\lambda^n| + |\lambda^{n-1}|}{2} - \left|\lambda^n\right|^{1/2} \left|\lambda^{n-1}\right|^{1/2}\right) y_1(t^n) \\
&\le \left|\left|\lambda^{n+1}\right| - \frac{|\lambda^n| + |\lambda^{n-1}|}{2}\right| |y_1(t^n)| + \left|\frac{|\lambda^n| + |\lambda^{n-1}|}{2} - \left|\lambda^n\right|^{1/2} \left|\lambda^{n-1}\right|^{1/2}\right| |y_1(t^n)| \\
&= \left|\left|\lambda^{n+1}\right| - \frac{|\lambda^n| + |\lambda^{n-1}|}{2}\right| |y_1(t^n)| + \frac{1}{2}\left||\lambda^n| + \left|\lambda^{n-1}\right| - 2\left|\lambda^n\right|^{1/2} \left|\lambda^{n-1}\right|^{1/2}\right| |y_1(t^n)|.
\end{aligned}$$

Using the mean value theorem, it can be shown

$$\left|\left|\lambda^{n+1}\right| - \frac{|\lambda^n| + |\lambda^{n-1}|}{2}\right| |y_1(t^n)| \le \Delta t \max_{t \in [t^{n-1}, t^{n+1}]} \left\{ \left|\frac{d}{dt} x_1(t)\right| + \left|\frac{d}{dt} y_1(t)\right| \right\} |y_1(t)|.$$

Some algebraic manipulation helps to bound the last terms above:

$$\begin{aligned}
&\frac{1}{2}\left||\lambda^n| + \left|\lambda^{n-1}\right| - 2\left|\lambda^n\right|^{1/2} \left|\lambda^{n-1}\right|^{1/2}\right| |y_1(t^n)| \\
&= \frac{1}{2}\left|\left|\lambda^n\right|^{1/2} - \left|\lambda^{n-1}\right|^{1/2}\right|^2 |y_1(t^n)| \\
&\le \frac{1}{2}\left||\lambda^n| - \left|\lambda^{n-1}\right|\right| |y_1(t^n)| \\
&\le \frac{1}{2}\left|(x_1(t^n) - x_1(t^{n-1})) - (y_1(t^n) - y_1(t^{n-1}))\right| |y_1(t^n)| \\
&\le \frac{1}{2}\left\{\left|x_1(t^n) - x_1(t^{n-1})\right| + \left|y_1(t^n) - y_1(t^{n-1})\right|\right\} |y_1(t^n)|
\end{aligned}$$

and applying the mean value theorem again,

$$\begin{aligned}&\frac{1}{2}\left\{\left|x_1(t^n)-x_1(t^{n-1})\right|+\left|y_1(t^n)-y_1(t^{n-1})\right|\right\}|y_1(t^n)|\\&\leq \Delta t\,\frac{1}{2}\max_{t\in[t^{n-1},t^n]}\left\{\left|\frac{d}{dt}x_1(t)\right|+\left|\frac{d}{dt}y_1(t)\right|\right\}|y_1(t)|.\end{aligned}$$

Combining the above results,

$$\begin{aligned}|\tau_x^{n+1}|\leq{}&\frac{3}{2}\Delta t\max_{t\in[0,T]}\left|\frac{d^2}{dt^2}\mathbf{x}(t)\right|+\kappa\,\Delta t\max_{t\in[t^n,t^{n+1}]}\{|x_1(t)|+|y_1(t)|\}\,|\frac{d}{dt}y_1(t)|\\&+\frac{5\kappa}{2}\,\Delta t\max_{t\in[t^n,t^{n+1}]}\{|x_1(t)|+|y_1(t)|\}\left\{|\frac{d}{dt}x_1(t)|+|\frac{d}{dt}y_1(t)|\right\}.\end{aligned}$$

The corresponding result for τ_y^{n+1} is analogously derived. These bounds hold at each time step, so taking the maximum over $n = 0, 1, \ldots, N-1$ gives the final result for the GA scheme. □

Convergence of the single step algorithms now follows from the Lax equivalence theorem, (see also [3]). The foremost interest is development of stable, decoupled algorithms which may be extended to the study of coupled systems of PDEs. The following result is to gain only an intuition into the convergence properties which can be expected in general of Algorithms 4.2.1-4.2.4. Numerical examples indicative of typical convergence behaviors for the algorithms are provided in Section 4.5.

Theorem 4.4.3 (Convergence.)**.** *Let* $\mathbf{f}, \mathbf{g} \in L^2(0,T;\mathbb{R}^2)$, $\kappa > 0$ *and* $A, B \in \mathbb{R}^{2\times 2}$ *satisfying (4.7)-(4.8). For each respective one-step algorithm, assume* Δt *satisfies the assumptions of the corresponding stability lemma. Assume the solution of the ODE system (4.3)-(4.4) has regularity as required by the corresponding consistency lemma. Then there exists* $C > 0$*, a generic constant depending on* $\mathbf{f}, \mathbf{g}, A, B$*, independent of* κ*, such that if*

$$\Delta t(1+\kappa) < C \tag{4.44}$$

then the algorithm converges to the solution of the ODE system, and the accuracy is $O(\Delta t)$*.*

Proof. Each algorithm may be written in the form

$$\frac{\mathbf{u}^{n+1}-\mathbf{u}^n}{\Delta t}+G(t^{n+1},\mathbf{u}^{n+1},\mathbf{u}^n)=0$$

with $\mathbf{u}^{n+1}\in\mathbb{R}^4$ the solution at time step $n+1$ of the numerical algorithm, (G depends on the algorithm). Let $\mathbf{u}(t^{n+1})$ be the solution of the ODE system at time t^{n+1}. Under the assumptions required for stability (Lemmas 4.3.1-4.3.2) and the regularity assumptions on $\mathbf{u}(t)$ required for consistency, G satisfies the following Lipschitz bounds for some fixed positive constants L_1, L_2:

$$\begin{aligned}&\left|G(t^{n+1},\mathbf{u}(t^{n+1}),\mathbf{u}(t^n))-G(t^{n+1},\mathbf{u}^{n+1},\mathbf{u}^n)\right|\\&\qquad\le L_1\left|\mathbf{u}(t^{n+1})-\mathbf{u}^{n+1}\right|+L_2\left|\mathbf{u}(t^n)-\mathbf{u}^n\right|.\end{aligned}$$

Using the notation τ^{n+1} for the consistency error at time t^{n+1} it follows

$$\begin{aligned}&\max_{n=1,2,\dots,N-1}|\tau^{n+1}|=\max_{n=1,2,\dots,N-1}\left|\tau^{n+1}-\frac{\mathbf{u}^{n+1}-\mathbf{u}^n}{\Delta t}+G(t^{n+1},\mathbf{u}^{n+1},\mathbf{u}^n)\right|\\&\ge\left|\frac{\mathbf{u}(t^{n+1})-\mathbf{u}(t^n)}{\Delta t}+G(t^{n+1},\mathbf{u}(t^{n+1}),\mathbf{u}(t^n))-\frac{\mathbf{u}^{n+1}-\mathbf{u}^n}{\Delta t}-G(t^{n+1},\mathbf{u}^{n+1},\mathbf{u}^n)\right|\\&\ge\frac{|\mathbf{u}(t^{n+1})-\mathbf{u}^{n+1}|}{\Delta t}-\frac{|\mathbf{u}(t^n)-\mathbf{u}^n|}{\Delta t}-|G(t^{n+1},\mathbf{u}(t^{n+1}),\mathbf{u}(t^n))-G(t^{n+1},\mathbf{u}^{n+1},\mathbf{u}^n)|.\end{aligned}$$

Thus after rearranging terms in the inequality,

$$\begin{aligned}|\mathbf{u}(t^{n+1})-\mathbf{u}^{n+1}|&\le|\mathbf{u}(t^n)-\mathbf{u}^n|+\Delta t\left(\max_{n=1,2,\dots,N-1}|\tau^{n+1}|\right)\\&\quad+\Delta t\,|G(t^{n+1},\mathbf{u}(t^{n+1}),\mathbf{u}(t^n))-G(t^{n+1},\mathbf{u}^{n+1},\mathbf{u}^n)|\\&\le|\mathbf{u}(t^n)-\mathbf{u}^n|+\Delta t\left(\max_{n=1,2,\dots,N-1}|\tau^{n+1}|\right)\\&\quad+\Delta t\,L_1\left|\mathbf{u}(t^{n+1})-\mathbf{u}^{n+1}\right|+\Delta t\,L_2\left|\mathbf{u}(t^n)-\mathbf{u}^n\right|.\end{aligned}$$

Here the time step restriction is imposed. Take, for example, $\Delta t L_1<1/2$. It can be shown for each algorithm this is equivalent to the time step restriction (4.44), for an appropriate $C>0$. Therefore,

$$\begin{aligned}&(1-\Delta t\,L_1)|\mathbf{u}(t^{n+1})-\mathbf{u}^{n+1}|\le(1+\Delta t\,L_2)|\mathbf{u}(t^n)-\mathbf{u}^n|+\Delta t\left(\max_{n=1,2,\dots,N-1}|\tau^{n+1}|\right)\\&\Rightarrow|\mathbf{u}(t^{n+1})-\mathbf{u}^{n+1}|\le\frac{1+\Delta t\,L_2}{1-\Delta t\,L_1}|\mathbf{u}(t^n)-\mathbf{u}^n|+\frac{\Delta t}{1-1/2}\left(\max_{n=1,2,\dots,N-1}|\tau^{n+1}|\right).\end{aligned}$$

For convenience, define s by

$$s = \frac{1 + \Delta t\, L_2}{1 - \Delta t\, L_1}$$

and recursively the following bounds are derived:

$$\begin{aligned}
|\mathbf{u}(t^{n+1}) - \mathbf{u}^{n+1}| &\leq s|\mathbf{u}(t^n) - \mathbf{u}^n| + 2\Delta t \left(\max_{n=1,2,\ldots,N-1} |\tau^{n+1}| \right) \\
&\leq s^2|\mathbf{u}(t^{n-1}) - \mathbf{u}^{n-1}| + 2\Delta t(1+s) \left(\max_{n=1,2,\ldots,N-1} |\tau^{n+1}| \right) \\
&\leq s^{n+1}|\mathbf{u}(0) - \mathbf{u}^0| + 2\Delta t \left(\sum_{j=0}^{n} s^j \right) \left(\max_{n=1,2,\ldots,N-1} |\tau^{n+1}| \right) \\
&\leq 2\Delta t \frac{s^{n+1} - 1}{s - 1} \left(\max_{n=1,2,\ldots,N-1} |\tau^{n+1}| \right),
\end{aligned}$$

since $\mathbf{u}(0) = \mathbf{u}^0$. From the definition of s,

$$\begin{aligned}
|\mathbf{u}(t^{n+1}) - \mathbf{u}^{n+1}| &\leq 2\frac{s^{n+1} - 1}{L_1 + L_2} \left(\max_{n=1,2,\ldots,N-1} |\tau^{n+1}| \right) \\
&\leq \frac{2}{L_1 + L_2} \exp\left(2T(L_1 + L_2)\right) \left(\max_{n=1,2,\ldots,N-1} |\tau^{n+1}| \right).
\end{aligned}$$

□

4.5 NUMERICAL EXPERIMENTS

The matrices A and B of (4.3)-(4.4) are taken to be

$$A = \eta \begin{bmatrix} 4 & 2 \\ 2 & 2 \end{bmatrix} + \omega \begin{bmatrix} 0 & -1 \\ 1 & 0 \end{bmatrix}$$

$$B = \eta \begin{bmatrix} 9 & 3 \\ 3 & 2 \end{bmatrix} + \omega \begin{bmatrix} 0 & -1 \\ 1 & 0 \end{bmatrix}$$

where $\eta, \omega \in \mathbb{R}$ are to be specified later. Assuming a global time interval $[0, T]$ for the problem and uniform time discretization with step size $\Delta t = T/N$, let $\mathbf{x}, \mathbf{y} : [0, T] \to \mathbb{R}^2$

be the solution of the ODE system. Assume $\mathbf{x}^j, \mathbf{y}^j \in \mathbb{R}^2$ are the approximations at time $t^j = j\Delta t$ to $\mathbf{x}(t^j), \mathbf{y}(t^j)$, respectively. The following errors occur in the tests.

$$\begin{aligned} E(t^j) &= \left(\left| \mathbf{x}(t^j) - \mathbf{x}^j \right|^2 + \left| \mathbf{y}(t^j) - \mathbf{y}^j \right|^2 \right)^{1/2} \\ error &= \left(\Delta t \sum_{j=0}^{N} E(t^j)^2 \right)^{1/2}. \end{aligned}$$

4.5.1 Convergence Testing

It is expected that the choices of parameters η, ω, κ will play a large role in the relative size of errors and convergence properties of the decoupled algorithms. However, the implicit algorithm should have consistently superior performance in all respects, and is thus used as a benchmark. To demonstrate the convergence properties of all algorithms the solution of the ODE system is taken to be $\mathbf{x}(t) = \cos(t)[1 \;\; 1]^T$ and $\mathbf{y}(t) = -\sin(t)[1 \;\; 1]^T$. The right hand side forcing functions $\mathbf{f}(t), \mathbf{g}(t)$ in the ODE system are calculated by inserting this choice of $\mathbf{x}(t), \mathbf{y}(t)$ into (4.3)-(4.4). Using $\eta = 1$, errors and convergence rates are calculated for each combination of the parameter values $\omega = 1, 100$ and $\kappa = 1, 1000$.

The implicit method shows the expected first order convergence rate, regardless of parameter choices; no time step restriction is needed. Increasing κ causes an increase in the error, though relatively small. An interesting observation is that smaller errors are observed using larger ω, indicating the solution is easier to estimate using a large skew-symmetric component in this case. Errors using the implicit method are close to those of the decoupled methods for $\kappa = 1$. When $\kappa = 1000$, the errors using the implicit method are in many cases a few orders of magnitude smaller than using the decoupled methods. It is not yet clear what scaling of κ would be most interesting for the atmosphere-ocean problem. As one example, numerical work by Bresch and Koko [12] studying two coupled fluids uses $\kappa = 2.45 \cdot 10^{-3}$.

Using the larger κ value is the most obvious source of difficulty, demonstrating one possible challenge for decoupled algorithms. Where for $\kappa = 1000$ and $\omega = 100$ the implicit algorithm generates smaller errors than for $\omega = 1$, the opposite effect is seen at the larger step sizes for both Algorithm 4.2.2 and 4.2.4, as a smaller time step size is required for convergence. Algorithm 4.2.3 behaves more like the implicit algorithm in this respect. Stability problems

may degrade performance of Algorithms 4.2.2,4.2.4 in these cases, though it is not clear, (see Section 4.5.2).

The results confirm predictions for Algorithm 4.2.3 that the consistency error is largest amongst the algorithms studied. The offsetting advantage is in the unconditional stability of the algorithm. For some problems the stabilized algorithm may have better accuracy than Algorithms 4.2.2, 4.2.4 but not this has not been observed. Indeed, errors for $\kappa = 1000$ are large and convergence is slow. The asymptotic convergence rate of order one was finally observed using time steps $\approx 10^{-7}$.

The decoupled algorithms converge optimally for $\kappa = 1$. In particular, Algorithms 4.2.2, 4.2.4 prove to make good choices of decoupled algorithms using large time step sizes for $\kappa = O(1)$. Errors are generally largest using Algorithm 4.2.3 for this test problem. However, the size of the jump $x_1 - y_1$ in the coupling terms does not decrease with increasing κ for this test problem, as when $\mathbf{f}, \mathbf{g}$ are chosen κ-independent. An interesting case is zero forcing, where (for $t > 0$) the size of the coupling terms decreases with increasing κ.

4.5.2 A Study of Discrete Asymptotic Stability

Only energetic stability of the decoupled algorithms has been addressed in the analysis. Asymptotic stability is of interest for the decoupled algorithms studied herein, as the matrices A, B and parameter κ will effect the eigenvalues of the system, and large time steps are desirable. In the present context, discrete asymptotic stability means that if $\mathbf{f} = \mathbf{g} = 0$, the discrete solution will exhibit a monotonic decay of energy regardless of any parameter choices, as for the true solution. This differs from the typical A-stability definition (Dahlquist, [24]) mainly in the requirement of monotonic decay.

Algorithms 4.2.1 and 4.2.3 will have this property, evident from their stability proofs. However, it is not clear for Algorithms 4.2.2 , 4.2.4. A numerical example will clarify the situation. Take $\eta = 1/100$, $\omega = 1$, $\kappa = 100$ with initial conditions $\mathbf{x}_0 = [2 \quad -2]^T$ and $\mathbf{y}_0 = [-1 \quad 1]^T$. Choose final time $T = 1$ and $N = 10$ time steps. The Euclidean norm of the approximations using each algorithm is plotted in Figure 6 for this problem, at each time step. Asymptotic stability is studied by setting $\mathbf{f} = \mathbf{g} = 0$ and examining the plot. Algorithms

4.2.1 and 4.2.3 show the expected monotonic decrease in norm. The plot provides a good illustration of the excessive dissipation inherent to Algorithm 4.2.3 for large κ. It is clear that both Algorithm 4.2.2 and Algorithm 4.2.4 are not asymptotically stable in the sense described above. This leads to a natural next step in the study of decoupled algorithms: to combine the asymptotically stable nature of Algorithm 4.2.3 and smaller consistency errors of Algorithms 4.2.2, 4.2.4 somehow in hope of achieving improved convergence results. Such a result could reasonably inspire analogous algorithms for the type of difficult, long-time calculations necessary in applications such as atmosphere-ocean interaction.

4.6 CONSIDERATIONS FOR FURTHER STUDY.

Concerning stability analysis, it is not completely clear which particular type of stability is most important for the motivating application. Energetic stability, zero-stability and asymptotic stability are all seen as important. The numeric results indicate the unconditional, energetic stability of Algorithms 4.2.3, 4.2.4 is not sufficient to guarantee the rate of convergence for large time steps, including for the asymptotically stable Algorithm 4.2.3. This could be attributed to a lack of "unconditional" zero-stability, meaning no restriction on the time step size for which the zero-stability bound (see [3]) holds, which would guarantee convergence rates at large time steps by the Lax equivalence theorem. In particular, the algorithms are all based upon modification of the fully implicit time discretization, for which it is not known if the zero-stability bound could require a time step restriction. However, in numerical testing the fully implicit algorithm appears to be unconditionally convergent.

Energetic stability of Algorithm 4.2.2 is an important open question. Energetic blow-up has not thus far been observed. This algorithm has often exhibited better behavior than other decoupled algorithms.

Numerical testing suggests large time steps can not be used with decoupled algorithms except for κ below some value depending on the problem. The dependence of stability properties of uncoupling algorithms upon κ is a very important open problem. We have given some preliminary results and experiments, but do not believe either to be sharp. Thus

a list of questions arises.

- What are the most important stability considerations in developing decoupled algorithms?
- Is an unconditional zero-stability result ever possible for the implicit algorithm?
- May Algorithm 4.2.2 ever exhibit energetic instability? How may stability of this algorithm best be characterized?

Table 14: Errors and convergence rates for test problem 1.

		Alg.	4.2.1	Alg.	4.2.2	Alg.	4.2.3	Alg.	4.2.4
κ, ω	Δt	error	rate	error	rate	error	rate	error	rate
	0.6284	0.3015	—	0.5877	—	0.9561	—	0.5976	—
	0.3142	0.1570	0.942	0.2978	0.981	0.6091	0.651	0.3106	0.944
	0.1571	0.0803	0.967	0.1533	0.958	0.3664	0.733	0.1630	0.930
1,	0.0785	0.0461	0.983	0.0780	0.972	0.2044	0.842	0.0842	0.952
1	0.0393	0.0204	0.991	0.0394	0.986	0.1084	0.915	0.0430	0.972
	0.0196	0.0102	0.996	0.0198	0.993	0.0559	0.956	0.0217	0.984
	0.6284	0.0106	—	0.0284	—	0.0682	—	0.0273	—
	0.3142	0.0054	0.988	0.0147	0.952	0.0339	1.009	0.0153	0.836
	0.1571	0.0027	0.997	0.0074	0.985	0.0169	1.005	0.0081	0.912
100,	0.0785	0.0013	0.999	0.0037	0.995	0.0084	1.003	0.0041	0.988
1	0.0393	0.0007	1.000	0.0019	0.998	0.0042	1.002	0.0021	0.995
	0.0196	0.0003	1.000	0.0009	0.999	0.0021	1.001	0.0010	0.998
	0.6284	0.3042	—	7.1916	—	396.90	—	7.6946	—
	0.3142	0.1582	0.943	19.392	-1.44	261.12	0.604	19.683	-1.356
	0.1571	0.0809	0.968	16.066	0.273	167.93	0.637	8.0611	1.288
	0.0785	0.0409	0.983	8.5695	0.907	97.310	0.787	7.7455	0.058
1,	0.0393	0.0206	0.991	8.1615	0.070	52.987	0.877	7.6964	0.009
1000	0.0196	0.0103	0.996	6.9940	0.223	27.607	0.941	6.0873	0.338
	0.0098	0.0048	1.103	5.7246	0.384	14.091	0.971	5.0520	0.363
	0.0049	0.0024	0.999	4.6289	0.307	7.4609	0.917	4.1606	0.280
	0.0025	0.0012	0.999	3.6118	0.358	4.6689	0.676	5.3596	-0.365
	0.0012	0.0006	1.000	2.5052	0.528	3.6698	0.347	0.7266	2.883
	0.0006	0.0003	1.000	0.4781	2.390	2.9854	0.298	0.3936	0.884
	0.0003	0.0002	1.000	0.2492	0.940	2.8656	0.059	0.2049	0.942
	0.6284	0.1139	—	21.734	—	22.258	—	20.121	—
	0.3142	0.0597	0.932	13.750	0.661	29.820	-0.422	10.153	0.987
	0.1571	0.0307	0.961	28.170	-1.035	30.976	-0.055	10.201	-0.007
100,	0.0785	0.0155	0.981	30.922	-0.135	29.898	0.051	20.373	-0.998
1000	0.0393	0.0078	0.990	34.408	-0.154	27.184	0.137	12.925	0.657
	0.0196	0.0039	0.995	36.142	-0.071	21.041	0.370	9.0967	0.507
	0.0098	0.0020	0.997	33.656	0.103	13.098	0.684	5.6369	0.691
	0.0049	0.0010	0.999	26.705	0.334	7.3666	0.830	13.114	-1.218
	0.0025	0.0005	0.999	17.479	0.612	4.6157	0.674	17.251	-0.396
	0.0012	0.0002	1.000	7.4980	1.221	3.5416	0.382	0.0392	8.781
	0.0006	0.0001	1.000	0.0184	8.673	2.7200	0.381	0.0197	0.995
	0.0003	5.0e-5	1.000	0.0092	1.000	2.5364	0.101	0.0099	0.995

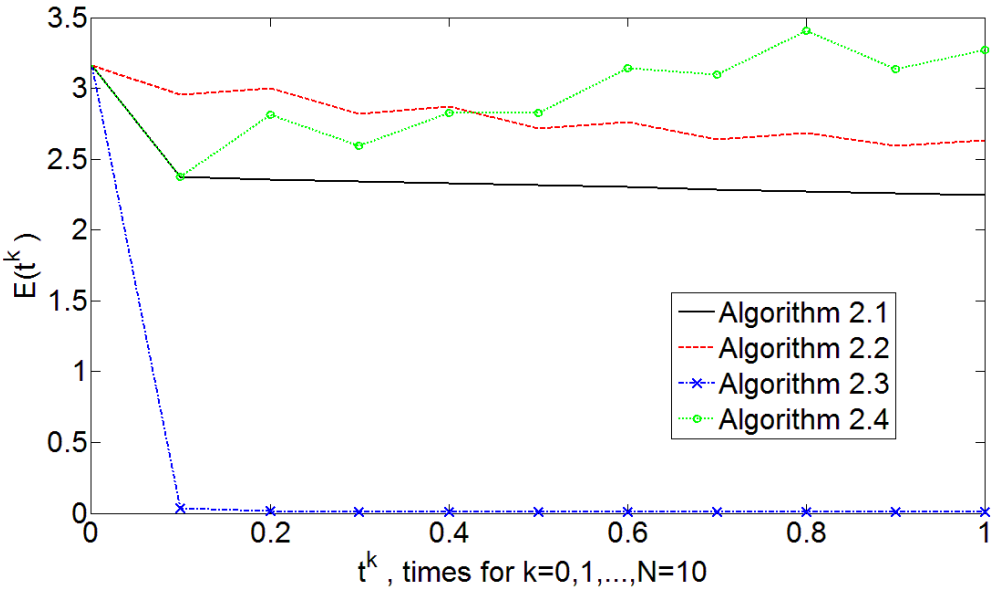

Figure 6: Euclidean norm of numerical approximations.

5.0 PARTITIONED TIME STEPPING FOR COUPLED FLUIDS

5.1 INTRODUCTION

This chapter will build upon the results of Chapters 2-4 by considering partitioned methods for the system of partial differential equations resulting from two coupled Navier-Stokes fluids as one component of the dynamic core of climate models. The dynamic core in atmosphere-ocean interaction is a critical component of climatology models and has attracted the interest of many mathematical researchers due to the richness of the theory and technical complexities of efficiently computing approximations to the coupled system using only (uncoupled) atmosphere and ocean solves, (see e.g. [7, 12, 47, 48, 49]). Motivated by this problem we consider uncoupled or "partitioned" methods for two fluids coupled across their shared interface I by a rigid-lid coupling condition, i.e. no penetration and a slip with friction condition allowing a jump in the tangential velocities across I. This *rigid-lid* assumption is used in many oceanography models, [55, 70].

The coupling between the atmosphere and the ocean dynamics occurs in the nonlinear interface condition (5.2) below. We have discovered (Chapter 2) that the nonlinearity in (5.2) cannot be treated in the most natural way (which is stable if (5.2) is linear). We give in (5.17)-(5.18) below an uncoupled and surprising (to us) discretization for the nonlinear condition (5.2) which has no analog for the linear version of (5.2) and which yields an unconditionally stable partitioned method for the fully coupled problem (5.1) - (5.6) below.

To reduce the dynamic core of the coupled atmosphere-ocean problem to its simplest form which still retains the essential difficulty of the coupling condition, let the domain consist of two subdomains Ω_1 and Ω_2 of $\mathbb{R}^d, d = 2, 3$ with outward unit normal vectors $\hat{n}_1$ and $\hat{n}_2$, respectively, coupled across an interface I (example in Figure 2 below). The

problem is: *given* $\nu_i > 0, f_i : [0,T] \to H^1(\Omega_i), u_i(0) \in H^1(\Omega_i)$ *and* $\kappa \in \mathbb{R}$, *find (for* $i = 1, 2$*)* $u_i : \overline{\Omega}_i \times [0,T] \to \mathbb{R}^d$ *and* $p_i : \overline{\Omega}_i \times [0,T] \to \mathbb{R}$ *satisfying*

$$
\begin{aligned}
u_{i,t} + u_i \cdot \nabla u_i - \nu_i \Delta u_i + \nabla p_i &= f_i, \quad \text{in } \Omega_i, && (5.1)\\
-\nu_i \hat{n}_i \cdot \nabla u_i \cdot \tau &= \kappa |u_i - u_j|(u_i - u_j) \cdot \tau, && (5.2)\\
\text{on} \quad I &\quad , \text{for } i, j = 1, 2 \, , \; i \neq j \, , \\
u_i \cdot \hat{n}_i &= 0 \text{ on } I, \; i = 1, 2 && (5.3)\\
\nabla \cdot u_i &= 0 \, , \text{ in } \Omega_i && (5.4)\\
u_i(x, 0) &= u_i^0(x), \quad \text{in } \Omega_i, && (5.5)\\
u_i &= 0, \quad \text{on } \Gamma_i = \partial\Omega_i \setminus I. && (5.6)
\end{aligned}
$$

Here τ may be any tangent vector on I. The lateral boundary conditions on Ω_i, (5.6), are not essential for our study. We focus on (5.2). Let

$$
\begin{aligned}
X_i &:= \{v_i \in H^1(\Omega_i)^d : v_i = 0 \text{ on } \Gamma_i = \partial\Omega_i \setminus I, v_i \cdot \hat{n}_i = 0 \text{ on } I\} \\
Q_i &:= \left\{ q_i \in L^2(\Omega_i)^d : \int_{\Omega_i} q_i \, d\Omega_i = 0 \right\}.
\end{aligned}
$$

For $u_i \in X_i$ we denote $\mathbf{u} = (u_1, u_2)$ and $X := \{\mathbf{v} = (v_1, v_2) : v_i \in X_i, \, i = 1, 2\}$. Similarly, for $q_i \in Q_i$ we denote $\mathbf{q} = (q_1, q_2)$ and $Q := \{\mathbf{q} = (q_1, q_2) : q_i \in Q_i, \, i = 1, 2\}$. A natural subdomain variational formulation for (5.1)-(5.6), obtained by multiplying (5.1) by v_i and (5.4) by q_i, integrating and applying the divergence theorem, is to find (for $i, j = 1, 2, i \neq j$) $u_i : [0,T] \to X_i$ and $p_i : [0,T] \to Q_i$ satisfying

$$
\begin{aligned}
(u_{i,t}, v_i)_{\Omega_i} + (\nu_i \nabla u_i, \nabla v_i)_{\Omega_i} + (u_i \cdot \nabla u_i, v_i)_{\Omega_i} - (p_i, \nabla \cdot v_i)_{\Omega_i} \\
+ \int_I \kappa |u_i - u_j|(u_i - u_j) v_i ds = (f_i, v_i)_{\Omega_i}, \; \forall \, v_i \in X_i \qquad (5.7)\\
(\nabla \cdot u_i, q_i)_{\Omega_i} = 0 \, , \; \forall q_i \in Q_i.
\end{aligned}
$$

Let $[\cdot]$ denote the jump of the indicated quantity across the interface I , $(\cdot, \cdot)$ the $L^2(\Omega_1 \cup \Omega_2)$ inner product and $\nu = \nu_i$ and $f = f_i$ in Ω_i. The natural coupled or monolithic variational

formulation for (5.1)-(5.6) is found by summing (5.7) over $i, j = 1, 2$ and $i \neq j$ and is to find $\mathbf{u} : [0, T] \to X$ and $\mathbf{p} : [0, T] \to Q$ satisfying

$$\begin{aligned}(\mathbf{u}_t, \mathbf{v}) + (\nu \nabla \mathbf{u}, \nabla \mathbf{v}) + (\mathbf{u} \cdot \nabla \mathbf{u}, \mathbf{v}) - (\mathbf{p}, \nabla \cdot \mathbf{v}) \\ + \int_I \kappa \, |[\mathbf{u}]| \, [\mathbf{u}][\mathbf{v}] ds = (f, \mathbf{v}), \forall v \in X, \\ (\nabla \cdot \mathbf{u}, \mathbf{q}) = 0 \, , \, \forall \mathbf{q} \in Q.\end{aligned} \tag{5.8}$$

We note that a realistic atmosphere-ocean model would contain many more terms including (typically) some eddy-viscocity term representing the effects of unresolved turbulent fluctuations on resolved scales. Without such a term there is an interesting theoretical question as to whether *weak* solutions of (5.1) - (5.6) possess enough regularity for their traces to be well defined in $L^3(I)$. We focus on algorithmic issues herein and suppose that the solution to (5.1) - (5.6) approximated is a strong solution.

5.1.1 Partitioned Stability

The simplest and most natural partitioned method for (5.1) - (5.6) is to extrapolate from past time values the speed $|u_i - u_j|$ in the friction coefficient, pass the previous, known interface velocity u_j across I to the problem in Ω_i and solve the problem in Ω_i. The natural extension of the partitioned method Algorithm 2.2.3 from Chapter 2 to using nonlinear coupling is given as follows. For final time T and time step size $\Delta t/N$, find $u_i^{n+1} \in X_i^h \subset X_i$, $p_i^{n+1} \in Q_i^h \subset Q_i$ for $i, j = 1, 2$, $i \neq j$ satisfying

$$\begin{aligned}\left(\frac{u_i^{n+1} - u_i^n}{\Delta t}, v_i \right)_{\Omega_i} + (\nu_i \nabla u_i^{n+1}, \nabla v_i)_{\Omega_i} + (u_i^{n+1} \cdot \nabla u_i^{n+1}, v_i)_{\Omega_i} \\ -(p_i^{n+1}, \nabla \cdot v_i)_{\Omega_i} + \kappa \int_I |u_i^n - u_j^n| (u_i^{n+1} - u_j^n) v_i ds = (f_i(t^{n+1}), v_i)_{\Omega_i}, \ \forall \, v_i \in X_i^h \\ (\nabla \cdot u_i^{n+1}, q_i)_{\Omega_i} = 0 \, , \, \forall q_i \in Q_i^h,\end{aligned} \tag{5.9}$$

In the case of linear coupling (without $|u_i^n - u_j^n|$), (5.9) can be proven (a simple modification of the results in Chapter 2) to be unconditionally stable. We also present strong numerical evidence in Section 5.4 that (5.9) is in fact unstable for the nonlinear problem unless Δt is taken very small. The development of a partitioned discretization method which is unconditionally and nonlinearly stable for large time steps for the nonlinear interface condition (5.2)

is the main motivation of this chapter. We show that replacing the term $u_j^n|u_i^n - u_j^n|$ in (5.9) by using a *geometric averaging* of the jump,

$$u_j^n|u_i^n - u_j^n|^{1/2}|u_i^{n-1} - u_j^{n-1}|^{1/2},$$

gives this partitioned method.

The remainder of this chapter is organized as follows: in Section 5.2, the mathematical setting and notation are described, and the partitioned time-stepping algorithm is presented. Theoretical results regarding the stability and convergence of the method are presented in Section 5.3. Unconditional stability of the proposed numerical method is proven and an optimal error estimate is derived. A remark is included discussing the expected dissipation of the decoupled algorithm. Numerical results that support the theoretical results are presented in Section 5.4. Convergence rates are demonstrated for an academic test, as well as a problem representing the flow of air over a container of water. For this problem, it is furthermore shown that with certain parameter choices the unmodified IMEX discretization (5.9) is unstable for a range of time step sizes, but our proposed method is stable.

5.1.2 Related Work

A standard simplification of the interface condition (5.5) used in some climate models, (e.g. [70]), is to represent the "wind shear stress" or "momentum flux" by a relationship of the form

$$\rho_O \nu_O \nabla u_O \cdot \hat{n}_O = C_D \rho_a |u_a| u_a$$

where ρ_O, ρ_a are densities of the ocean and atmosphere, respectively, ν_O is the kinematic viscocity of the ocean, u_O and u_a are the velocities of the ocean and atmosphere, respectively, $\hat{n}_O$ is the unit outward normal vector of the ocean domain and C_D is a (dimensionless) drag coefficient. The velocity jump $u_a - u_O$ does not appear as it would using (5.2) since the ocean velocity is assumed to be negligible compared to the air velocity near the interface. The atmosphere and ocean are updated by an explicit update of the ocean to compute the momentum flux, which is then mapped conservatively to the atmosphere mesh.

An atmosphere-ocean system, more physically refined than (5.1) - (5.6) but sharing the same mathematical structure for the dynamic core and coupling, is studied by Lions, Temam and Wang in a series of papers performing a thorough mathematical analysis [47, 48, 49]. The coupling condition (5.2) is a more physically relevant representation of the momentum flux across the interface, taking into account when the ocean surface flow may be influencing the surface air current. Bresch and Koko [12] introduce some decoupling algorithms for a model akin to (5.1)-(5.6). In it, the monolithic, coupled problem at each step is solved by preconditioned iterative methods, uncoupling can occur in the residual calculation and in the preconditioning step.

Often systems of ODEs or PDEs may be decomposed into a sum of linear, stiff terms and other less stiff (possibly nonlinear) terms. Stable, consistent methods for such ODEs were derived by using implicit treatment of stiff terms and explicit treatment of the remaining terms, the so called additive Runge-Kutta methods, [23]. Kennedy and Carpenter exhibited the utility of this idea for convection-diffusion-reaction equations, [40], and in [4] implicit-explicit (IMEX) methods of up to fourth order have been developed for some classes of PDEs. These methods seek to reduce the time step restriction on an explicit method for stability by implicit treatment of stiff terms while reducing computational cost through explicit updating of other terms, particularly nonlinear terms.

One application of the IMEX approach is to use explicit updates of the terms responsible for coupling across I, giving semi-implicit partitioned methods. A straight-forward partitioning approach for some coupled problems may result in an unstable or conditionally stable method, as demonstrated for the fluid-structure interaction problem, see [14, 16].

5.2 METHOD DESCRIPTION, NOTATION AND PRELIMINARIES

This section presents the numerical scheme for (5.1)-(5.6), and provides the necessary definitions and lemmas for the stability and convergence analysis. For $D \subset \Omega$, the Sobolev space $H^k(D) = W^{k,2}(D)$ is equipped with the usual norm $\|\cdot\|_{H^k(D)}$, and semi-norm $|\cdot|_{H^k(D)}$, for $1 \leq k < \infty$, e.g. Adams [1]. The L^2 norm is denoted by $\|\cdot\|_D$. For functions $v(x,t)$ defined

for almost every $t \in (0,T)$ on a function space $V(D)$, we define the norms $(1 \le p \le \infty)$

$$\|v\|_{L^\infty(0,T;V)} = \operatorname*{ess\,sup}_{0<t<T} \|v(\cdot,t)\|_V \quad \text{and} \quad \|v\|_{L^p(0,T;V)} = \left(\int_0^T \|v\|_V^p dt \right)^{1/p}.$$

The dual space of the Banach space V is denoted V'.

Let the domain $\Omega \subset \mathbb{R}^d$ $(d = 2, 3)$ have convex, polygonal subdomains Ω_i for $i = 1, 2$ with $\partial\Omega_1 \cap \partial\Omega_2 = \Omega_1 \cap \Omega_2 = I$. Let Γ_i denote the portion of $\partial\Omega_i$ that is not on I, i.e. $\Gamma_i = \partial\Omega_i \setminus I$. For $i = 1, 2$, let

$$X_i = \left\{ v \in H^1(\Omega_i)^d \mid v|_{\Gamma_i} = g_i \text{ and } v \cdot \hat{n}_i = 0 \text{ on } I \right\}.$$

Let $(\cdot,\cdot)_{\Omega_i}$ denote the standard L^2 inner product on Ω_i, and let $(\cdot,\cdot)_{X_i}$ denote the standard H^1 inner product on Ω_i. The case $g_i = 0$, $i = 1, 2$ is considered in this thesis. The space $Q_i = L_0^2(\Omega_i)$ consists of L^2 functions on Ω_i with average value zero. Divergence free spaces are

$$V_i = \left\{ v \in X_i : \int_{\Omega_i} q \nabla \cdot v \, d\Omega_i = 0 \ , \ \forall q \in Q_i \right\}.$$

Define $X = X_1 \times X_2$, $L^2(\Omega) = L^2(\Omega_1) \times L^2(\Omega_2)$, $Q = Q_1 \times Q_2$ and $V = V_1 \times V_2$. For $\mathbf{u}, \mathbf{v} \in X$ with $\mathbf{u} = [u_1, u_2]^T$ and $\mathbf{v} = [v_1, v_2]^T$, define the L^2 inner product

$$(\mathbf{u}, \mathbf{v}) = \sum_{i=1,2} \int_{\Omega_i} u_i v_i \, dx \,,$$

and H^1 inner product

$$(\mathbf{u}, \mathbf{v})_X = \sum_{i=1,2} \left(\int_{\Omega_i} u_i v_i \, dx + \int_{\Omega_i} \nabla u_i \cdot \nabla v_i \, dx \right),$$

and the induced norms $\|\mathbf{v}\| = (\mathbf{v}, \mathbf{v})^{1/2}$ and $\|\mathbf{v}\|_X = (\mathbf{v}, \mathbf{v})_X{}^{1/2}$, respectively. A fundamental norm to be used is that of $L^3(I)$, denoted simply by $\|\cdot\|_I$.

For functions $u, v, w \in X_i, i = 1, 2$ we define the explicitly skew-symmetrized nonlinear form on Ω_i by

$$c_i(u; v, w) = \frac{1}{2}(u \cdot \nabla v, w)_{\Omega_i} - \frac{1}{2}(u \cdot \nabla w, v)_{\Omega_i}. \tag{5.10}$$

It can be shown this is equal to the convective form $(u \cdot \nabla v, w)_{\Omega_i}$ since $u \cdot \hat{n} = 0$ on I. The following standard bounds are used in the analysis.

Lemma 5.2.1. *Let $u, v, w \in H^1(\Omega_i)$ for $i = 1, 2$ with $\Omega_i \subset \mathbb{R}^d$, $d = 2, 3$. Then there exists $C = C(\Omega_i) > 0$, a finite constant such that*

$$
\begin{aligned}
c_i(u; v, w) &\leq C \|u\|_{\Omega_i}^{1/2} \|\nabla u\|_{\Omega_i}^{1/2} \|\nabla v\|_{\Omega_i} \|\nabla w\|_{\Omega_i} && (5.11)\\
\int_I u|[v]| \cdot w \, ds &\leq \|u\|_I \|[v]\|_I \|w\|_I && (5.12)\\
\|u\|_I &\leq C \|u\|_{\Omega_i}^{1/4} \|\nabla u\|_{\Omega_i}^{3/4} && (5.13)
\end{aligned}
$$

Proof. The first bound is standard, e.g. [45], and the second bound is an application of Hölder's inequality. The inequality (5.13) follows from Sobolev space theory. Note $u = 0$ on $\partial\Omega_i \setminus I$ and hence $\|u_i\|_{L^3(I)} = \|u_i\|_{L^3(\partial\Omega_i)}$. Then the result follows from (e.g.) Galdi, [32] with the Poincaré - Friedrichs inequality. □

Lemma 5.2.2. *Let $i, j \in \{1, 2\}$ and $\{\alpha_1, \alpha_2, \beta_1, \beta_2\}$ arbitrary positive real numbers. For functions $u_i \in X_i$, $v_j \in X_j$, $\mathbf{w} \in X$ the following bounds hold.*

$$
\begin{aligned}
\kappa \int_I |u_i||[\mathbf{w}]||v_j| \, ds &\leq C \frac{\kappa^2}{4} \|u_i\|_I^2 \|[\mathbf{w}]\|_I^2 + \frac{\alpha_j^3}{\nu_j^3} \|v_j\|_{\Omega_j}^2 + \frac{\nu_j}{2\alpha_j} \|\nabla v_j\|_{\Omega_j}^2 && (5.14)\\
\kappa \int_I |u_i||[\mathbf{w}]||v_j| \, ds &\leq C \frac{\kappa^4 \alpha_i^3}{\nu_i^3} \|[\mathbf{w}]\|_I^4 \|u_i\|_{\Omega_i}^2 + \frac{\nu_i}{4\alpha_i} \|\nabla u_i\|_{\Omega_i}^2 \\
&\quad + C \frac{\kappa^4 \beta_j^3}{\nu_j^3} \|[\mathbf{w}]\|_I^4 \|v_j\|_{\Omega_j}^2 + \frac{\nu_j}{4\beta_j} \|\nabla v_j\|_{\Omega_j}^2 && (5.15)\\
\kappa \int_I |u_i||[\mathbf{w}]||v_j| \, ds &\leq C\kappa^4 \|u_i\|_I^4 \left\{ \frac{\alpha_1^3}{\nu_1^3} \|w_1\|_{\Omega_1}^2 + \frac{\alpha_2^3}{\nu_2^3} \|w_2\|_{\Omega_2}^2 + \frac{2\beta_j^3}{\nu_j^3} \|v_j\|_{\Omega_j}^2 \right\} \\
&\quad + \frac{1}{4} \left\{ \frac{\nu_1}{\alpha_1} \|\nabla w_1\|_{\Omega_1}^2 + \frac{\nu_2}{\alpha_2} \|\nabla w_2\|_{\Omega_2}^2 + \frac{2\nu_j}{\beta_j} \|\nabla v_j\|_{\Omega_j}^2 \right\} && (5.16)
\end{aligned}
$$

Proof. To prove the above inequalities one begins in each case applying (5.12), followed by application of (5.13) and Young's inequality. In the first case,

$$
\begin{aligned}
\kappa \int_I |u_i||[\mathbf{w}]||v_j| \, ds &\leq C\kappa \|u_i\|_I \|[\mathbf{w}]\|_I \|v_j\|_{\Omega_j}^{1/4} \|\nabla v_j\|_{\Omega_j}^{3/4} \\
&\leq C \frac{\kappa^2}{4} \|u_i\|_I^2 \|[\mathbf{w}]\|_I^2 + \|v_j\|_{\Omega_j}^{1/2} \|\nabla v_j\|_{\Omega_j}^{3/2} \\
&\leq C \frac{\kappa^2}{4} \|u_i\|_I^2 \|[\mathbf{w}]\|_I^2 + \frac{1}{4s^3} \|v_j\|_{\Omega_j}^2 + \frac{3s}{4} \|\nabla v_j\|_{\Omega_j}^2 \\
&\leq C \frac{\kappa^2}{4} \|u_i\|_I^2 \|[\mathbf{w}]\|_I^2 + \frac{27\alpha_j^3}{32\nu_j^3} \|v_j\|_{\Omega_j}^2 + \frac{\nu_j}{2\alpha_j} \|\nabla v_j\|_{\Omega_j}^2 ,
\end{aligned}
$$

choosing $s = 2\nu_j/3\alpha_j$. Simplify using $27/32 < 1$ for convenience, thus proving (5.14). In the second case,

$$\begin{aligned}
\kappa \int_I |u_i||[\mathbf{w}]||v_j|\,ds &\le \kappa \|u_i\|_I \|[\mathbf{w}]\|_I \|v_j\|_I \\
&\le \frac{\kappa}{2}\|u_i\|_I^2 \|[\mathbf{w}]\|_I + \frac{\kappa}{2}\|[\mathbf{w}]\|_I \|v_j\|_I^2 \\
&\le C\frac{\kappa}{2}\|u_i\|_{\Omega_i} 1/2 \|\nabla u_i\|_{\Omega_i}^{3/2} \|[\mathbf{w}]\|_I + C\frac{\kappa}{2}\|v_j\|_{\Omega_j}^{1/2}\|\nabla v_j\|_{\Omega_j}^{3/2}\|[\mathbf{w}]\|_I \\
&\le C\frac{\kappa^4}{4s_i^3}\|[\mathbf{w}]\|_I^4 \|u_i\|_{\Omega_i}^2 + \frac{3s_i}{4}\|\nabla u_i\|_{\Omega_i}^2 \\
&+ C\frac{\kappa^4}{4s_j^3}\|[\mathbf{w}]\|_I^4 \|v_j\|_{\Omega_j}^2 + \frac{3s_j}{4}\|\nabla v_j\|_{\Omega_j}^2,
\end{aligned}$$

then choose $s_i = \nu_i/3\alpha_i$ and $s_j = \nu_j/3\beta_j$, proceeding as above to prove (5.15). To prove (5.16) we note

$$\begin{aligned}
\kappa \int_I |u_i||[\mathbf{w}]||v_j|\,ds &\le \kappa \|u_i\|_I (\|w_1\|_I + \|w_2\|_I)\|v_j\|_I \\
&\le \frac{\kappa}{2}\|u_i\|_I \|w_1\|_I^2 + \frac{\kappa}{2}\|u_i\|_I \|w_2\|_I^2 + \kappa\|u_i\|_I\|v_j\|_I^2 \\
&\le C\frac{\kappa}{2}\|u_i\|_I \left\{\|w_1\|_{\Omega_1}^{1/2}\|\nabla w_1\|_{\Omega_1}^{3/2} + \|w_2\|_{\Omega_2}^{1/2}\|\nabla w_2\|_{\Omega_2}^{3/2} + \|v_j\|_{\Omega_j}^{1/2}\|\nabla v_j\|_{\Omega_j}^{3/2}\right\}
\end{aligned}$$

and the result follows from these inequalities:

$$\begin{aligned}
C\frac{\kappa}{2}\|u_i\|_I \|w_1\|_{\Omega_1}^{1/2}\|\nabla w_1\|_{\Omega_1}^{3/2} &\le C\frac{\kappa^4\alpha_1^3}{\nu_1^3}\|u_i\|_I^4\|w_1\|_{\Omega_1}^2 + \frac{\nu_1}{4\alpha_1}\|\nabla w_1\|_{\Omega_1}^2 \\
C\frac{\kappa}{2}\|u_i\|_I \|w_2\|_{\Omega_2}^{1/2}\|\nabla w_2\|_{\Omega_2}^{3/2} &\le C\frac{\kappa^4\alpha_2^3}{\nu_2^3}\|u_i\|_I^4\|w_2\|_{\Omega_2}^2 + \frac{\nu_2}{4\alpha_2}\|\nabla w_2\|_{\Omega_2}^2 \\
C\frac{\kappa}{2}\|u_i\|_I \|v_j\|_{\Omega_j}^{1/2}\|\nabla v_j\|_{\Omega_j}^{3/2} &\le C\frac{\kappa^4\beta_j^3}{\nu_j^3}\|u_i\|_I^4\|v_j\|_{\Omega_j}^2 + \frac{\nu_j}{4\beta_j}\|\nabla v_j\|_{\Omega_j}^2
\end{aligned}$$

□

For $t^n \in [0,T]$, $\mathbf{u}^n$ will denote the discrete approximation to $\mathbf{u}(t^n)$, where the discrete times t^n are calculated from the uniform time step size $\Delta t = T/N$ by $t^n = n\Delta t$, $n = 0,1,\ldots,N$. Then the approximations $u_1^n \in V_{1,h}$ and $u_2^n \in V_{2,h}$ for $n = 2,3,\ldots,N$ are calculated using Algorithm 5.2.1. It should be noted that this algorithm requires the two initial values $\mathbf{u}^0$ and $\mathbf{u}^1$.

Algorithm 5.2.1 (Partitioned Scheme). *Let* $\Delta t > 0$, $\mathbf{f} \in H^{-1}(\Omega)$. *Given* $\mathbf{u}^{n-1}, \mathbf{u}^n \in V_h$, $n \in \{1, 2, \cdots, N-1\}$, *find* $u_1^{n+1} \in V_{1,h}$ *satisfying*

$$\begin{aligned}\left(\frac{u_1^{n+1} - u_1^n}{\Delta t}, v_1\right)_{\Omega_1} &+ \nu_1 \left(\nabla u_1^{n+1}, \nabla v_1\right)_{\Omega_1} + c_1\left(u_1^{n+1}; u_1^{n+1}, v_1\right) \\ &+ \kappa \int_I |[\mathbf{u}^n]| u_1^{n+1} \cdot v_1 \, ds - \kappa \int_I |[\mathbf{u}^n]|^{1/2} |[\mathbf{u}^{n-1}]|^{1/2} u_2^n \cdot v_1 \, ds \\ &= \left(f_1(t^{n+1}), v_1\right)_{\Omega_1}, \ \forall v_1 \in V_{1,h}.\end{aligned} \tag{5.17}$$

and $u_2^{n+1} \in V_{2,h}$ *satisfying*

$$\begin{aligned}\left(\frac{u_2^{n+1} - u_2^n}{\Delta t}, v_2\right)_{\Omega_2} &+ \nu_2 \left(\nabla u_2^{n+1}, \nabla v_2\right)_{\Omega_2} + c_2\left(u_2^{n+1}; u_2^{n+1}, v_2\right) \\ &+ \kappa \int_I |[\mathbf{u}^n]| u_2^{n+1} \cdot v_2 \, ds - \kappa \int_I |[\mathbf{u}^n]|^{1/2} |[\mathbf{u}^{n-1}]|^{1/2} u_1^n \cdot v_2 \, ds \\ &= \left(f_2(t^{n+1}), v_2\right)_{\Omega_2}, \ \forall v_2 \in V_{2,h}.\end{aligned} \tag{5.18}$$

The main feature of this algorithm is the use of the geometric average $|[\mathbf{u}^n]|^{1/2}|[\mathbf{u}^{n-1}]|^{1/2}$ in the coupling terms. This will be shown to have a stabilizing effect for the algorithm. Hence Algorithm 5.2.1 will often be referred to as the geometric averaging method, or *GA method*.

5.3 NUMERICAL ANALYSIS

Stability of the partitioned scheme (Algorithm 5.2.1) is established below. The polarization identity is used in the stability and convergence proofs:

$$(w^{j+1} - w^j) \cdot w^{j+1} = \frac{1}{2}\left(|w^{j+1}|^2 + |w^{j+1} - w^j|^2 - |w^j|^2\right) \tag{5.19}$$

Lemma 5.3.1. *(Partitioned Stability) Let $u_1^j \in X_{1,h}$ satisfy (5.17) for each $j \in \{0, 1, \cdots, n\}$, and $u_2^j \in X_{2,h}$ satisfy (5.18) for each $j \in \{0, 1, \cdots, n\}$. Then Algorithm 5.2.1 satisfies the following energy equality at time step $n+1$:*

$$\begin{aligned}
\left\|\mathbf{u}^{n+1}\right\|^2 + \sum_{j=1}^{n} \left\|\mathbf{u}^{j+1} - \mathbf{u}^j\right\|^2 + 2\Delta t \sum_{j=1}^{n} \left(\nu_1 \left\|\nabla u_1^{j+1}\right\|_{\Omega_1}^2 + \nu_2 \left\|\nabla u_2^{j+1}\right\|_{\Omega_2}^2\right) \\
+ \kappa\, \Delta t \sum_{j=1}^{n} \int_I \left| |[\mathbf{u}^j]|^{1/2} u_1^{j+1} - |[\mathbf{u}^{j-1}]|^{1/2} u_2^j \right|^2 ds \\
+ \kappa\, \Delta t \sum_{j=1}^{n} \int_I \left| |[\mathbf{u}^j]|^{1/2} u_2^{j+1} - |[\mathbf{u}^{j-1}]|^{1/2} u_1^j \right|^2 ds \\
+ \kappa \Delta t \int_I |[\mathbf{u}^n]| \left(\left|u_1^{n+1}\right|^2 + \left|u_2^{n+1}\right|^2\right) ds \\
= \left\|\mathbf{u}^1\right\|^2 + \kappa \Delta t \int_I |[\mathbf{u}^0]| \left(\left|u_1^1\right|^2 + \left|u_2^1\right|^2\right) ds \\
+ 2\Delta t \sum_{j=1}^{n} \left\{ \left(f_1(t^{j+1}), u_1^{j+1}\right)_{\Omega_1} + \left(f_2(t^{j+1}), u_2^{j+1}\right)_{\Omega_2} \right\}. \quad (5.20)
\end{aligned}$$

Furthermore, the algorithm is unconditionally stable, satisfying:

$$\begin{aligned}
\left\|\mathbf{u}^{n+1}\right\|^2 + \sum_{j=1}^{n} \left\|\mathbf{u}^{j+1} - \mathbf{u}^j\right\|^2 + \Delta t \sum_{j=1}^{n} \left(\nu_1 \left\|\nabla u_1^{j+1}\right\|_{\Omega_1}^2 + \nu_2 \left\|\nabla u_2^{j+1}\right\|_{\Omega_2}^2\right) \\
+ \kappa \Delta t \int_I |[\mathbf{u}^n]| \left(\left|u_1^{n+1}\right|^2 + \left|u_2^{n+1}\right|^2\right) ds \\
\leq \left\|\mathbf{u}^1\right\|^2 + \kappa \Delta t \int_I |[\mathbf{u}^0]| \left(\left|u_1^1\right|^2 + \left|u_2^1\right|^2\right) ds \\
+ \sum_{j=1}^{n} \left(\frac{\Delta t}{\nu_1} \left\|f_1(t^{j+1})\right\|_{V_1'}^2 + \frac{\Delta t}{\nu_2} \left\|f_2(t^{j+1})\right\|_{V_2'}^2 \right). \quad (5.21)
\end{aligned}$$

Remark 5.3.1 (Discrete energy)**.** *The discrete energy equation (5.20) includes the following exact "kinetic energy" of the discretization, denoted by KE^{n+1}:*

$$KE^{n+1} = \left\|\mathbf{u}^{n+1}\right\|^2 + \kappa \Delta t \int_I |[\mathbf{u}^n]| \left(\left|u_1^{n+1}\right|^2 + \left|u_2^{n+1}\right|^2\right) ds.$$

The corresponding "energy dissipation" of the method, denoted by ϵ^{n+1} is

$$\epsilon^{n+1} = 2\Delta t \sum_{j=1}^{n} \left(\nu_1 \left\| \nabla u_1^{j+1} \right\|_{\Omega_1}^2 + \nu_2 \left\| \nabla u_2^{j+1} \right\|_{\Omega_2}^2 \right) + \kappa \, \Delta t \sum_{j=1}^{n} \int_I \left| |[\mathbf{u}^j]|^{1/2} u_1^{j+1} - |[\mathbf{u}^{j-1}]|^{1/2} u_2^j \right|^2 ds + \kappa \, \Delta t \sum_{j=1}^{n} \int_I \left| |[\mathbf{u}^j]|^{1/2} u_2^{j+1} - |[\mathbf{u}^{j-1}]|^{1/2} u_1^j \right|^2 ds.$$

Proof. . Let $j \in \{1, 2, \ldots, N-1\}$ and consider (5.17) with $n = j$. Setting $v_1 = u_1^{j+1}$, (5.17) yields

$$\left(\frac{u_1^{j+1} - u_1^j}{\Delta t}, u_1^{j+1} \right)_{\Omega_1} + \nu_1 \left\| \nabla u_1^{j+1} \right\|_{\Omega_1}^2 + \kappa \int_I |u_1^{j+1}|^2 |[\mathbf{u}^j]| \, ds - \kappa \int_I u_2^j \cdot u_1^{j+1} |[\mathbf{u}^j]|^{1/2} |[\mathbf{u}^{j-1}]|^{1/2} \, ds = \left(f_1(t^{j+1}), u_1^{j+1} \right)_{\Omega_1}. \quad (5.22)$$

Similarly, choosing $v_2 = u_2^{j+1}$ in (5.18) yields

$$\left(\frac{u_2^{j+1} - u_2^j}{\Delta t}, u_2^{j+1} \right)_{\Omega_2} + \nu_2 \left\| \nabla u_2^{j+1} \right\|_{\Omega_2}^2 + \kappa \int_I |u_2^{j+1}|^2 |[\mathbf{u}^j]| \, ds - \kappa \int_I u_1^j \cdot u_2^{j+1} |[\mathbf{u}^j]|^{1/2} |[\mathbf{u}^{j-1}]|^{1/2} \, ds = \left(f_2(t^{j+1}), u_2^{j+1} \right)_{\Omega_2}. \quad (5.23)$$

Applying the identity (5.19) to the first terms on the left hand side of (5.22)-(5.23) and adding, it follows that

$$\begin{aligned} &\frac{1}{2\Delta t} \left(\left\| u_1^{j+1} \right\|_{\Omega_1}^2 - \left\| u_1^j \right\|_{\Omega_1}^2 + \left\| u_1^{j+1} - u_1^j \right\|_{\Omega_1}^2 + \left\| u_2^{j+1} \right\|_{\Omega_2}^2 - \left\| u_2^j \right\|_{\Omega_2}^2 + \left\| u_2^{j+1} - u_2^j \right\|_{\Omega_2}^2 \right) \\ &\quad + \nu_1 \left\| \nabla u_1^{j+1} \right\|_{\Omega_1}^2 + \nu_2 \left\| \nabla u_2^{j+1} \right\|_{\Omega_2}^2 + \kappa \int_I \left| u_1^{j+1} \right|^2 \left| [\mathbf{u}^j] \right| \, ds + \kappa \int_I \left| u_2^{j+1} \right|^2 \left| [\mathbf{u}^j] \right| \, ds \\ &\quad - \kappa \int_I u_2^j \cdot u_1^{j+1} \left| [\mathbf{u}^j] \right|^{1/2} \left| [\mathbf{u}^{j-1}] \right|^{1/2} \, ds - \kappa \int_I u_1^j \cdot u_2^{j+1} \left| [\mathbf{u}^j] \right|^{1/2} \left| [\mathbf{u}^{j-1}] \right|^{1/2} \, ds \\ &\quad = \left(f_1(t^{j+1}), u_1^{j+1} \right)_{\Omega_1} + \left(f_2(t^{j+1}), u_2^{j+1} \right)_{\Omega_2}. \end{aligned} \quad (5.24)$$

Applying (5.19) with $w^{j+1} = u_1^{j+1}|[\mathbf{u}^j]|^{1/2}$ and $w^j = u_2^j|[\mathbf{u}^{j-1}]|^{1/2}$, the following two interface integrals may be expressed in a different way:

$$\begin{aligned}
&\kappa \int_I \left|u_1^{j+1}\right|^2 \left|[\mathbf{u}^j]\right| \, ds - \kappa \int_I u_2^j \cdot u_1^{j+1} \left|[\mathbf{u}^j]\right|^{1/2} \left|[\mathbf{u}^{j-1}]\right|^{1/2} \, ds \\
&= \kappa \int_I w^{j+1} \cdot w^{j+1} - w^{j+1} \cdot w^j \, ds = \kappa \int_I w^{j+1} \cdot (w^{j+1} - w^j) \, ds \\
&= \frac{\kappa}{2} \int_I \left|u_1^{j+1}\right|^2 \left|[\mathbf{u}^j]\right| \, ds - \frac{\kappa}{2} \int_I \left|u_2^j\right|^2 \left|[\mathbf{u}^{j-1}]\right| \, ds \\
&+ \frac{\kappa}{2} \int_I \left|u_1^{j+1}|[\mathbf{u}^j]|^{1/2} - u_2^j|[\mathbf{u}^{j-1}]|^{1/2}\right|^2 \, ds.
\end{aligned}$$

This expression is inserted into (5.24) and the remaining two interface integrals are treated analogously:

$$\begin{aligned}
&\frac{1}{2\Delta t}\left(\left\|u_1^{j+1}\right\|_{\Omega_1}^2 - \left\|u_1^j\right\|_{\Omega_1}^2 + \left\|u_2^{j+1}\right\|_{\Omega_2}^2 - \left\|u_2^j\right\|_{\Omega_2}^2\right) \\
&+ \frac{1}{2\Delta t}\left(\left\|u_1^{j+1} - u_1^j\right\|_{\Omega_1}^2 + \left\|u_2^{j+1} - u_2^j\right\|_{\Omega_2}^2\right) + \nu_1 \left\|\nabla u_1^{j+1}\right\|_{\Omega_1}^2 + \nu_2 \left\|\nabla u_2^{j+1}\right\|_{\Omega_2}^2 \\
&+ \frac{\kappa}{2} \int_I \left\{\left|u_1^{j+1}\right|^2 + \left|u_2^{j+1}\right|^2\right\} \left|[\mathbf{u}^j]\right| \, ds - \frac{\kappa}{2} \int_I \left\{\left|u_1^j\right|^2 + \left|u_2^j\right|^2\right\} \left|[\mathbf{u}^{j-1}]\right| \, ds \\
&+ \frac{\kappa}{2} \int_I \left|u_1^{j+1}|[\mathbf{u}^j]|^{1/2} - u_2^j|[\mathbf{u}^{j-1}]|^{1/2}\right|^2 \, ds \\
&+ \frac{\kappa}{2} \int_I \left|u_2^{j+1}|[\mathbf{u}^j]|^{1/2} - u_1^j|[\mathbf{u}^{j-1}]|^{1/2}\right|^2 \, ds \\
&= \left(f_1(t^{j+1}), u_1^{j+1}\right)_{\Omega_1} + \left(f_2(t^{j+1}), u_2^{j+1}\right)_{\Omega_2}.
\end{aligned} \tag{5.25}$$

Multiply through (5.25) by $2\Delta t$, and summing over $j = 1, 2, \ldots, n$ proves the energy equation (5.20). To prove (5.21), bound the right hand side of (5.25) by:

$$\begin{aligned}
&\left(f_1(t^{j+1}), u_1^{j+1}\right)_{\Omega_1} + \left(f_2(t^{j+1}), u_2^{j+1}\right)_{\Omega_2} \\
&\qquad \leq \frac{1}{2\nu_1} \left\|f_1(t^{j+1})\right\|_{V_1'}^2 + \frac{1}{2\nu_2} \left\|f_2(t^{j+1})\right\|_{V_2'}^2 \\
&\qquad\qquad + \frac{\nu_1}{2} \left\|\nabla u_1^{j+1}\right\|_{\Omega_1}^2 + \frac{\nu_2}{2} \left\|\nabla u_2^{j+1}\right\|_{\Omega_2}^2.
\end{aligned} \tag{5.26}$$

Insert (5.26) into (5.25), and the desired result follows by multiplying through by $2\Delta t$ and summing over $j = 1, 2, \ldots, n$. □

Theorem 5.3.2 (Convergence of Algorithm 5.2.1)**.** *Let $u_1^k \in X_{1,h}$ satisfy (5.17) for each $n \in \{0,1,2,\cdots,n \le N\}$, and $u_2^n \in X_{2,h}$ satisfy (5.18) for each $k \in \{0,1,2,\cdots,n \le N\}$. Let $\tilde{\nu} = \max\{\nu_1^{-1}, \nu_2^{-1}\}$, $\hat{\nu} = \max\{\nu_1, \nu_2\}$, and let*

$$D^{n+1} = \tilde{\nu}^3 \left(1 + \kappa^4 E^{n+1} + \left\|\nabla \mathbf{u}(t^{n+1})\right\|^4\right),$$

where $E^{n+1} = \max_{j=0,1,\ldots,n+1}\{\max\{\|\mathbf{u}(t^j)\|_I^4, \|\mathbf{u}^j\|_I^4\}\}$. Assume $\Delta t \le 1/D^{n+1}$, and that $(\mathbf{u}, \mathbf{p})$ is a strong solution of the coupled NSE system (5.1)-(5.6) with $\mathbf{u}_t \in L^2(0,T;X)$ and $\mathbf{u}_{tt} \in L^2(0,T;L^2(\Omega))$. Then the solution $\mathbf{u}^{n+1}$ of Algorithm 5.2.1 satisfies:

$$\begin{aligned}
&\left\|\mathbf{u}(t^{n+1}) - \mathbf{u}^{n+1}\right\|^2 \\
&\quad + \frac{\Delta t}{2}\left(\nu_1 \sum_{k=1}^{n} \left\|\nabla(u_1(t^{k+1}) - u_1^{k+1})\right\|_{\Omega_1}^2 + \nu_2 \sum_{k=1}^{n} \left\|\nabla(u_2(t^{k+1}) - u_2^{k+1})\right\|_{\Omega_2}^2\right) \\
&\le C \exp\left(\Delta t \sum_{n=1}^{j} \frac{D^{n+1}}{1 - \Delta t\, D^{n+1}}\right)\Bigg\{\left\|\mathbf{u}(t^1) - \mathbf{u}^1\right\|^2 + \inf_{\mathbf{v}^1 \in V_h}\left\|\mathbf{u}(t^1) - \mathbf{v}^1\right\|^2 \\
&\quad + \Delta t\, \nu_1 \Bigg(\left\|\nabla(u_1(t^1) - u_1^1)\right\|_{\Omega_1}^2 + \frac{1}{2}\left\|\nabla(u_1(t^0) - u_1^0)\right\|_{\Omega_1}^2 \\
&\qquad + \inf_{v_1^1 \in V_{1,h}}\left\|\nabla(u_1(t^1) - v_1^1)\right\|_{\Omega_1}^2 + \frac{1}{2}\inf_{v_1^0 \in V_{1,h}}\left\|\nabla(u_1(t^0) - v_1^0)\right\|_{\Omega_1}^2\Bigg) \\
&\quad + \Delta t\, \nu_2 \Bigg(\left\|\nabla(u_2(t^1) - u_2^1)\right\|_{\Omega_2}^2 + \frac{1}{2}\left\|\nabla(u_2(t^0) - u_2^0)\right\|_{\Omega_2}^2 \\
&\qquad + \inf_{v_2^1 \in V_{2,h}}\left\|\nabla(u_2(t^1) - v_2^1)\right\|_{\Omega_2}^2 + \frac{1}{2}\inf_{v_2^0 \in V_{2,h}}\left\|\nabla(u_2(t^0) - v_2^0)\right\|_{\Omega_2}^2\Bigg) \\
&\quad + \Delta t^2 \left\|\mathbf{u}_{tt}\right\|_{L^2(0,T;L^2(\Omega))}^2 + \inf_{\mathbf{v} \in V_h}\left\|(\mathbf{u} - \mathbf{v})_t\right\|_{L^2(0,T;L^2(\Omega))}^2 + \inf_{\mathbf{q} \in Q_h}\left\|\mathbf{p} - \mathbf{q}\right\|_{L^2(0,T;L^2(\Omega))}^2 \\
&\quad + \kappa^2 \Delta t^2 \left\|\mathbf{u}_t\right\|_{L^2(0,T;X)}^2 + T \max_{k=2,\ldots,n+1}\left(\inf_{\mathbf{v}^k \in V_h}\left\|\nabla(\mathbf{u}(t^k) - \mathbf{v}^k)\right\|^2\right)\Bigg\},
\end{aligned} \tag{5.27}$$

where C has the following dependence on κ, ν_1, and ν_2:

$$C = \mathcal{O}\left(\max\{\hat{\nu}, \tilde{\nu}, (1 + \Delta t \kappa^4)\tilde{\nu}^3, \kappa^2\}\right).$$

Proof. . To prove convergence we will consider the error equations on each subdomain independently first. The resulting error bounds from the two subdomains will then be summed. Begin by taking the variational formulation for the true solution $u_1(t^{n+1})$ on Ω_1 and subtracting (5.17),

$$\begin{aligned}
&\frac{1}{\Delta t}\left((u_1(t^{n+1})-u_1^{n+1})-(u_1(t^n)-u_1^n),v_1\right)_{\Omega_1}+\nu_1\left(\nabla(u_1(t^{n+1})-u_1^{n+1}),\nabla v_1\right)_{\Omega_1}\\
&\quad+c_1\left(u_1(t^{n+1});u_1(t^{n+1}),v_1\right)-c_1\left(u_1^{n+1};u_1^{n+1},v_1\right)-\left(p_1(t^{n+1}),\nabla\cdot v_1\right)_{\Omega_1}\\
&\quad+\kappa\int_I u_1(t^{n+1})|[\mathbf{u}(t^{n+1})]|\cdot v_1\,ds-\kappa\int_I u_1^{n+1}|[\mathbf{u}^n]|\cdot v_1\,ds\\
&\quad+\kappa\int_I u_2^n|[\mathbf{u}^n]|^{1/2}|[\mathbf{u}^{n-1}]|^{1/2}\cdot v_1\,ds-\kappa\int_I u_2(t^{n+1})|[\mathbf{u}(t^{n+1})]|\cdot v_1\,ds\\
&\quad=\left(\frac{u_1(t^{n+1})-u_1(t^n)}{\Delta t}-\frac{\partial u_1(t^{n+1})}{\partial t},v_1\right)_{\Omega_1},\ \forall v_1\in V_{1,h}.
\end{aligned}$$

Errors are decomposed using the equation

$$u_i(t^j)-u_i^j=(u_i(t^j)-\tilde{u}_i^j)+(\tilde{u}_i^j-u_i^j)=\eta_i^j+\phi_i^j$$

where $\eta_i^j\in V_i$ and $\phi_i^j\in V_{h,i}$ with $\tilde{u}_i^j\in V_{h,i}$ arbitrarily chosen. We also subtract an arbitrarily chosen $q_i^j\in Q_{h,i}$ from the pressure for free. Thus choosing $v_1=\phi_1^{n+1}$ the above error equation is rewritten as

$$\begin{aligned}
&\frac{1}{\Delta t}\left(\eta_1^{n+1}-\eta_1^n,\phi_1^{n+1}\right)_{\Omega_1}+\frac{1}{\Delta t}\left(\phi_1^{n+1}-\phi_1^n,\phi_1^{n+1}\right)_{\Omega_1}+\nu_1\left(\nabla\eta_1^{n+1},\nabla\phi_1^{n+1}\right)_{\Omega_1}+\nu_1\|\nabla\phi_1^{n+1}\|_{\Omega_1}^2\\
&\quad+c_1\left(u_1(t^{n+1});u_1(t^{n+1}),\phi_1^{n+1}\right)-c_1\left(u_1^{n+1};u_1^{n+1},\phi_1^{n+1}\right)-\left(p_1(t^{n+1})-q_1^{n+1},\nabla\cdot\phi_1^{n+1}\right)_{\Omega_1}\\
&\quad+\kappa\int_I u_1(t^{n+1})|[\mathbf{u}(t^{n+1})]|\cdot\phi_1^{n+1}\,ds-\kappa\int_I u_1^{n+1}|[\mathbf{u}^n]|\cdot\phi_1^{n+1}\,ds\\
&\quad+\kappa\int_I u_2^n|[\mathbf{u}^n]|^{1/2}|[\mathbf{u}^{n-1}]|^{1/2}\cdot\phi_1^{n+1}\,ds-\kappa\int_I u_2(t^{n+1})|[\mathbf{u}(t^{n+1})]|\cdot\phi_1^{n+1}\,ds\\
&\quad=\left(R_1^{n+1},\phi_1^{n+1}\right)_{\Omega_1},
\end{aligned}$$

where $R_j^{n+1} = \frac{u_j(t^{n+1}) - u_j(t^n)}{\Delta t} - \frac{\partial u_j(t^{n+1})}{\partial t}$, for $j = 1, 2$. The goal is to bound ϕ_1^{n+1}, hence we move many terms to the right hand side. Apply (5.19) on the left hand side:

$$\begin{aligned}
&\frac{1}{2\Delta t}\left(\|\phi_1^{n+1}\|_{\Omega_1}^2 - \|\phi_1^n\|_{\Omega_1}^2 + \|\phi_1^{n+1} - \phi_1^n\|_{\Omega_1}^2\right) + \nu_1\|\nabla\phi_1^{n+1}\|_{\Omega_1}^2 \\
&\quad + \left\{\kappa\int_I u_1(t^{n+1})|[\mathbf{u}(t^{n+1})]|\cdot\phi_1^{n+1}\,ds - \kappa\int_I u_1^{n+1}|[\mathbf{u}^n]|\cdot\phi_1^{n+1}\,ds\right\} \\
&\quad + \left\{\kappa\int_I u_2^n|[\mathbf{u}^n]|^{1/2}|[\mathbf{u}^{n-1}]|^{1/2}\cdot\phi_1^{n+1}\,ds - \kappa\int_I u_2(t^{n+1})|[\mathbf{u}(t^{n+1})]|\cdot\phi_1^{n+1}\,ds\right\} \\
&\quad = -\frac{1}{\Delta t}\left(\eta_1^{n+1} - \eta_1^n, \phi_1^{n+1}\right)_{\Omega_1} - \nu_1\left(\nabla\eta_1^{n+1}, \nabla\phi_1^{n+1}\right)_{\Omega_1} \\
&\quad + \left(p_1(t^{n+1}) - q_1^{n+1}, \nabla\cdot\phi_1^{n+1}\right)_{\Omega_1} \\
&\quad - c_1\left(u_1(t^{n+1}); u_1(t^{n+1}), \phi_1^{n+1}\right) + c_1\left(u_1^{n+1}; u_1^{n+1}, \phi_1^{n+1}\right) + \left(R_1^{n+1}, \phi_1^{n+1}\right)_{\Omega_1}.
\end{aligned} \tag{5.28}$$

Bounds for the non-interface terms follow as in the standard NSE case, (see e.g. [45]). The interface terms require special treatment. First, note that by adding and subtracting terms in sequence one may derive the following expression:

$$\begin{aligned}
\kappa\int_I u_1(t^{n+1})|[\mathbf{u}(t^{n+1})]|\cdot\phi_1^{n+1}\,ds - \kappa\int_I u_1^{n+1}|[\mathbf{u}^n]|\cdot\phi_1^{n+1}\,ds& \\
= \kappa\int_I u_1(t^{n+1})\left(|[\mathbf{u}(t^{n+1})]| - |[\mathbf{u}(t^n)]|\right)\cdot\phi_1^{n+1}\,ds& \\
+ \kappa\int_I u_1(t^{n+1})\left(|[\mathbf{u}(t^n)]| - |[\tilde{\mathbf{u}}^n]|\right)\cdot\phi_1^{n+1}\,ds& \\
+ \kappa\int_I u_1(t^{n+1})\left(|[\tilde{\mathbf{u}}^n]| - |[\mathbf{u}^n]|\right)\cdot\phi_1^{n+1}\,ds& \\
+ \kappa\int_I \eta_1^{n+1}|[\mathbf{u}^n]|\cdot\phi_1^{n+1}\,ds + \kappa\int_I |\phi_1^{n+1}|^2|[\mathbf{u}^n]|\,ds.&
\end{aligned} \tag{5.29}$$

The splitting used for the remaining pair of interface integrals is more complicated due to the product $|[\mathbf{u}^n]|^{1/2}|[\mathbf{u}^{n-1}]|^{1/2}$. The key is to recognize an error of $O(\Delta t)$ is committed in replacing the product $|[\mathbf{u}(t^n)]|^{1/2}|[\mathbf{u}(t^{n-1})]|^{1/2}$ with the average $\frac{1}{2}(|[\mathbf{u}(t^n)]| + |[\mathbf{u}(t^{n-1})]|)$. We

proceed as follows.

$$
\begin{aligned}
&\kappa \int_I u_2^n |[\mathbf{u}^n]|^{1/2} |[\mathbf{u}^{n-1}]|^{1/2} \cdot \phi_1^{n+1}\, ds - \kappa \int_I u_2(t^{n+1}) |[\mathbf{u}(t^{n+1})]| \cdot \phi_1^{n+1}\, ds \\
&= \kappa \int_I u_2^n \left\{ |[\mathbf{u}^n]|^{1/2} |[\mathbf{u}^{n-1}]|^{1/2} - \frac{1}{2}(|[\mathbf{u}^n]| + |[\mathbf{u}^{n-1}]|) \right\} \cdot \phi_1^{n+1}\, ds \\
&+ \frac{1}{2}\kappa \int_I u_2^n \left\{ (|[\mathbf{u}^n]| + |[\mathbf{u}^{n-1}]|) - (|[\tilde{\mathbf{u}}^n]| + |[\tilde{\mathbf{u}}^{n-1}]|) \right\} \cdot \phi_1^{n+1}\, ds \\
&+ \frac{1}{2}\kappa \int_I u_2^n \left\{ (|[\tilde{\mathbf{u}}^n]| + |[\tilde{\mathbf{u}}^{n-1}]|) - (|[\mathbf{u}(t^n)]| + |[\mathbf{u}(t^{n-1})]|) \right\} \cdot \phi_1^{n+1}\, ds \\
&+ \kappa \int_I u_2^n \left\{ \frac{1}{2}(|[\mathbf{u}(t^n)]| + |[\mathbf{u}(t^{n-1})]|) - |[\mathbf{u}(t^{n+1})]| \right\} \cdot \phi_1^{n+1}\, ds \\
&- \kappa \int_I \phi_2^n |[\mathbf{u}(t^{n+1})]| \cdot \phi_1^{n+1}\, ds - \kappa \int_I \eta_2^n |[\mathbf{u}(t^{n+1})]| \cdot \phi_1^{n+1}\, ds \\
&+ \kappa \int_I (u_2(t^n) - u_2(t^{n+1})) |[\mathbf{u}(t^{n+1})]| \cdot \phi_1^{n+1}\, ds
\end{aligned}
\tag{5.30}
$$

Using (5.29)–(5.30), substitution for the interface integrals in (5.28) is performed. The last term of (5.29) is positive and may be kept on the left hand side of (5.28), but all other interface terms are now moved to the right hand side, and bounded. Applying the reverse triangle inequality and the equality $[a] - [b] = [a - b]$ for $a, b \in X$, we first note

$$
\big| |[\mathbf{u}(t^j)]| - |[\tilde{\mathbf{u}}^j]| \big| \le |[\boldsymbol{\eta}^j]| \quad \text{and} \quad \big| |[\tilde{\mathbf{u}}^j]| - |[\mathbf{u}^j]| \big| \le |[\boldsymbol{\phi}^j]|.
$$

Thus (5.28)–(5.30) yield the following error inequality:

$$
\begin{aligned}
&\frac{1}{2\Delta t} \left(\|\phi_1^{n+1}\|_{\Omega_1}^2 - \|\phi_1^n\|_{\Omega_1}^2 + \|\phi_1^{n+1} - \phi_1^n\|_{\Omega_1}^2 \right) + \nu_1 \|\nabla \phi_1^{n+1}\|_{\Omega_1}^2 + \kappa \int_I |\phi_1^{n+1}|^2 |[\mathbf{u}^n]|\, ds \\
&\le -\frac{1}{\Delta t} \left(\eta_1^{n+1} - \eta_1^n, \phi_1^{n+1} \right)_{\Omega_1} - \nu_1 \left(\nabla \eta_1^{n+1}, \nabla \phi_1^{n+1} \right)_{\Omega_1} + \left(p_1(t^{n+1}) - q_1^{n+1}, \nabla \cdot \phi_1^{n+1} \right)_{\Omega_1} \\
&- c_1 \left(u_1(t^{n+1}); u_1(t^{n+1}), \phi_1^{n+1} \right) + c_1 \left(u_1^{n+1}; u_1^{n+1}, \phi_1^{n+1} \right) + \left(R_1^{n+1}, \phi_1^{n+1} \right)_{\Omega_1} \\
&+ I_1 + I_2 + I_3 + I_4,
\end{aligned}
\tag{5.31}
$$

where the I_j-terms denote the following interface integrals.

$$
\begin{aligned}
I_1 = \kappa &\int_I |u_1(t^{n+1})| |[\mathbf{u}(t^{n+1}) - \mathbf{u}(t^n)]| |\phi_1^{n+1}|\, ds + \kappa \int_I |u_1(t^{n+1})| |[\boldsymbol{\eta}^n]| |\phi_1^{n+1}|\, ds \\
&+ \kappa \int_I |u_2(t^n) - u_2(t^{n+1})| |[\mathbf{u}(t^{n+1})]| |\phi_1^{n+1}|\, ds + \kappa \int_I |\eta_1^{n+1}| |[\mathbf{u}^n]| |\phi_1^{n+1}|\, ds \\
&+ \frac{1}{2}\kappa \int_I |u_2^n| (|[\boldsymbol{\eta}^n]| + |[\boldsymbol{\eta}^{n-1}]|) |\phi_1^{n+1}|\, ds + \kappa \int_I |\eta_2^n| |[\mathbf{u}(t^{n+1})]| |\phi_1^{n+1}|\, ds
\end{aligned}
$$

$$I_2 = \frac{1}{2}\kappa \int_I |u_2^n|(|[\boldsymbol{\phi}^n]| + |[\boldsymbol{\phi}^{n-1}]|)|\phi_1^{n+1}|\,ds + \kappa \int_I |u_1(t^{n+1})||[\boldsymbol{\phi}^n]||\phi_1^{n+1}|\,ds$$
$$+ \kappa \int_I |\phi_2^n||[\mathbf{u}(t^{n+1})]||\phi_1^{n+1}|\,ds$$
$$I_3 = \kappa \int_I |u_2^n| \left| \frac{1}{2}(|[\mathbf{u}(t^n)]| + |[\mathbf{u}(t^{n-1})]|) - |[\mathbf{u}(t^{n+1})]| \right| |\phi_1^{n+1}|\,ds$$
$$I_4 = \kappa \int_I |u_2^n| \left| |[\mathbf{u}^n]|^{1/2}|[\mathbf{u}^{n-1}]|^{1/2} - \frac{1}{2}(|[\mathbf{u}^n]| + |[\mathbf{u}^{n-1}]|) \right| |\phi_1^{n+1}|\,ds$$

The application of Hölder's inequality, Young's inequality, and (5.11) to the non-interface terms of (5.31) gives the estimate

$$\begin{aligned}
&\frac{1}{2\Delta t}\left(\|\phi_1^{n+1}\|_{\Omega_1}^2 - \|\phi_1^n\|_{\Omega_1}^2 + \|\phi_1^{n+1} - \phi_1^n\|_{\Omega_1}^2\right) + \nu_1\|\nabla\phi_1^{n+1}\|_{\Omega_1}^2 + \kappa\int_I |\phi_1^{n+1}|^2|[\mathbf{u}^n]|\,ds \\
&\le \frac{\nu_1}{2\varepsilon_2}\left\|\nabla\eta_1^{n+1}\right\|_{\Omega_1}^2 + \frac{1}{4\varepsilon_3^3\nu_1^3}\left\|\nabla u_1(t^{n+1})\right\|_{\Omega_1}^4\left\|\phi_1^{n+1}\right\|_{\Omega_1}^2 + \frac{d}{2\varepsilon_2\nu_1}\|p_1(t^{n+1}) - q_1^{n+1}\|_{L^2(\Omega_1)}^2 \\
&+ \left(2\varepsilon_1 + \varepsilon_2 + \frac{3\varepsilon_3}{4}\right)\nu_1\left\|\nabla\phi_1^{n+1}\right\|_{\Omega_1}^2 + \frac{C}{2\varepsilon_1\nu_1}\left(\left\|\frac{\eta_1^{n+1} - \eta_1^n}{\Delta t}\right\|_{V_1'}^2 + \left\|R_1^{n+1}\right\|_{V_1'}^2\right. \\
&\qquad \left. + \|\nabla u_1(t^{n+1})\|_{\Omega_1}^2\|\nabla\eta_1^{n+1}\|_{\Omega_1}^2 + \left\|u_1^{n+1}\right\|_{\Omega_1}\left\|\nabla u_1^{n+1}\right\|_{\Omega_1}\left\|\nabla\eta_1^{n+1}\right\|_{\Omega_1}^2\right) \\
&+ I_1 + I_2 + I_3 + I_4,
\end{aligned} \tag{5.32}$$

for constants C and $\varepsilon_i, i = 1,2,3$ independent of ν_1. The interface integrals are bounded using Lemma 5.2.2, with particular attention paid to the constants involving κ, ν_1, ν_2 and terms with $\left\|\nabla\phi_1^{n+1}\right\|_{\Omega_1}^2$ or $\left\|\phi_1^{n+1}\right\|_{\Omega_1}^2$. In the term I_1, each piece is bounded using (5.14) with $\alpha_1 = 192$. Then the first two terms of I_2 are bounded using (5.16) with $\alpha_1 = 16$, $\alpha_2 = 32$, $\beta_1 = 96$ and the last term using (5.15) with $\alpha_2 = 8$ and $\beta_1 = 48$. Some basic inequalities can be used to simplify I_3, I_4 and derive corresponding error estimates. Applying the reverse triangle inequality for I_3 yields

$$\begin{aligned}
&\left|\frac{1}{2}(|[\mathbf{u}(t^n)]| + |[\mathbf{u}(t^{n-1})]|) - |[\mathbf{u}(t^{n+1})]|\right| \\
&\le \frac{1}{2}\left||[\mathbf{u}(t^n)]| - |[\mathbf{u}(t^{n+1})]\right| + \frac{1}{2}\left||[\mathbf{u}(t^{n-1})]| - |[\mathbf{u}(t^{n+1})]|\right| \\
&\le \frac{1}{2}\left|[\mathbf{u}(t^n) - \mathbf{u}(t^{n+1})]\right| + \frac{1}{2}\left|[\mathbf{u}(t^{n-1}) - \mathbf{u}(t^{n+1})]\right|.
\end{aligned} \tag{5.33}$$

I_4 is bounded by first noting

$$\begin{aligned}\left|\,|[\mathbf{u}^n]|^{1/2}|[\mathbf{u}^{n-1}]|^{1/2}-\frac{1}{2}(|[\mathbf{u}^n]|+|[\mathbf{u}^{n-1}]|)\right| &= \frac{1}{2}\left|\,|[\mathbf{u}^n]|^{1/2}-|[\mathbf{u}^{n-1}]|^{1/2}\right|^2\\ &\le \frac{1}{2}\left|\,|[\mathbf{u}^n]|^{1/2}-|[\mathbf{u}^{n-1}]|^{1/2}\right|\left|\,|[\mathbf{u}^n]|^{1/2}+|[\mathbf{u}^{n-1}]|^{1/2}\right|\\ &= \frac{1}{2}\left|\,|[\mathbf{u}^n]|-|[\mathbf{u}^{n-1}]|\right| \le \frac{1}{2}\left|[\mathbf{u}^n-\mathbf{u}^{n-1}]\right|.\end{aligned}$$

Add and subtract $\mathbf{u}(t^n)-\mathbf{u}(t^{n-1})$,

$$\begin{aligned}&\left|\,|[\mathbf{u}^n]|^{1/2}|[\mathbf{u}^{n-1}]|^{1/2}-\frac{1}{2}(|[\mathbf{u}^n]|+|[\mathbf{u}^{n-1}]|)\right|\\ &\le \frac{1}{2}\left|[(\mathbf{u}^n-\mathbf{u}(t^{n-1}))+(\mathbf{u}(t^{n-1})-\mathbf{u}^{n-1})]\right|+\frac{1}{2}\left|[\mathbf{u}(t^n)-\mathbf{u}(t^{n-1})]\right|\\ &\le \frac{1}{2}\Big\{\,|[\boldsymbol{\phi}^n]|+\left|[\boldsymbol{\phi}^{n-1}]\right|+|[\boldsymbol{\eta}^n]|+\left|[\boldsymbol{\eta}^{n-1}]\right|+\left|[\mathbf{u}(t^n)-\mathbf{u}(t^{n-1})]\right|\Big\}.\end{aligned}\tag{5.34}$$

The results (5.33)–(5.34) are then bounded using the same approach as particular terms in I_1 and I_2. For example, I_3 can be bounded in the same manner as the first term from I_1, while the first term from I_4 is bounded the same way as the first term of I_2. Thus, the interface terms are bounded by

$$\begin{aligned}&I_1+I_2+I_3+I_4\\ &\le \frac{\nu_1}{16}\left\|\nabla\phi_1^{n+1}\right\|_{\Omega_1}^2+C\nu_1^{-3}\left(1+\kappa^4\left(48\left\|u_2^n\right\|_I^4+12\left\|[\mathbf{u}(t^{n+1})]\right\|_I^4\right)\right)\left\|\phi_1^{n+1}\right\|_{\Omega_1}^2\\ &+\frac{\nu_1}{16}\left(\|\nabla\phi_1^n\|_{\Omega_1}^2+\left\|\nabla\phi_1^{n-1}\right\|_{\Omega_1}^2\right)+\frac{\nu_2}{16}\left(\|\nabla\phi_2^n\|_{\Omega_2}^2+\left\|\nabla\phi_2^{n-1}\right\|_{\Omega_2}^2\right)+C\kappa^2L^{n+1}P^{n+1}\\ &+C\kappa^4M^{n+1}\left\{\nu_1^{-3}\left(\|\phi_1^n\|_{\Omega_1}^2+\left\|\phi_1^{n-1}\right\|_{\Omega_1}^2\right)+\nu_2^{-3}\left(\|\phi_2^n\|_{\Omega_2}^2+\left\|\phi_2^{n-1}\right\|_{\Omega_2}^2\right)\right\},\end{aligned}\tag{5.35}$$

where C is a constant independent of κ,ν_1, and ν_2. The quantities L^{n+1}, M^{n+1} and P^{n+1} are defined by:

$$\begin{aligned}L^{n+1} &= \left\|u_1(t^{n+1})\right\|_I^2+\left\|u_2(t^{n+1})\right\|_I^2+\|u_1^n\|_I^2+\|u_2^n\|_I^2,\\ M^{n+1} &= \left\|u_1(t^{n+1})\right\|_I^4+\left\|u_2(t^{n+1})\right\|_I^4+\|u_1^n\|_I^4+\|u_2^n\|_I^4,\\ \text{and } P^{n+1} &= \left\|u_1(t^{n+1})-u_1(t^n)\right\|_I^2+\left\|u_2(t^{n+1})-u_2(t^n)\right\|_I^2\\ &\quad+\left\|u_1(t^{n+1})-u_1(t^{n-1})\right\|_I^2+\left\|u_2(t^{n+1})-u_2(t^{n-1})\right\|_I^2\\ &\quad+\|\eta_1^n\|_I^2+\|\eta_2^n\|_I^2+\left\|\eta_1^{n-1}\right\|_I^2+\left\|\eta_2^{n-1}\right\|_I^2+\left\|\eta_1^{n+1}\right\|_I^2+\left\|\eta_2^{n+1}\right\|_I^2.\end{aligned}$$

(The last term in the definition of P^{n+1} is auxiliary, it is included in the definition for use in the estimate on Ω_2.) Then, with choices for $\varepsilon_1, \varepsilon_2, \varepsilon_3$ satisfying $2\varepsilon_1 + \varepsilon_2 + 3\varepsilon_3/4 = 1/16$, (5.32) can be bounded as follows:

$$\begin{aligned}
&\frac{1}{2\Delta t}\left(\|\phi_1^{n+1}\|_{\Omega_1}^2 - \|\phi_1^n\|_{\Omega_1}^2 + \|\phi_1^{n+1} - \phi_1^n\|_{\Omega_1}^2\right) + \frac{7\nu_1}{8}\|\nabla\phi_1^{n+1}\|_{\Omega_1}^2 \\
&\leq C\nu_1^{-3}\left\{1 + \|\nabla u_1(t^{n+1})\|_{\Omega_1}^4 + \kappa^4\left(\|u_2^n\|_I^4 + \left\|[\mathbf{u}(t^{n+1})]\right\|_I^4\right)\right\}\left\|\phi_1^{n+1}\right\|_{\Omega_1}^2 \\
&+ C\nu_1^{-1}\left(\left\|\frac{\eta_1^{n+1} - \eta_1^n}{\Delta t}\right\|_{V_1'}^2 + \|R_1^{n+1}\|_{V_1'}^2 + \|p_1(t^{n+1}) - q_1^{n+1}\|_{\Omega_1}^2\right) \\
&+ \frac{\nu_1}{16}\left(\|\nabla\phi_1^n\|_{\Omega_1}^2 + \left\|\nabla\phi_1^{n-1}\right\|_{\Omega_1}^2\right) + \frac{\nu_2}{16}\left(\|\nabla\phi_2^n\|_{\Omega_2}^2 + \left\|\nabla\phi_2^{n-1}\right\|_{\Omega_2}^2\right) + C\kappa^2 L^{n+1}P^{n+1} \\
&+ C\kappa^4 M^{n+1}\left\{\nu_1^{-3}\left(\|\phi_1^n\|_{\Omega_1}^2 + \left\|\phi_1^{n-1}\right\|_{\Omega_1}^2\right) + \nu_2^{-3}\left(\|\phi_2^n\|_{\Omega_2}^2 + \left\|\phi_2^{n-1}\right\|_{\Omega_2}^2\right)\right\} \\
&+ C\left(\nu_1 + \nu_1^{-1}\|\nabla u_1(t^{n+1})\|_{\Omega_1}^2 + \nu_1^{-1}\left\|u_1^{n+1}\right\|_{\Omega_1}\left\|\nabla u_1^{n+1}\right\|_{\Omega_1}\right)\|\nabla\eta_1^{n+1}\|_{\Omega_1}^2.
\end{aligned} \tag{5.36}$$

Let S_{n+1} denote

$$\begin{aligned}
S_{n+1} = \left\|\mathbf{u}^1\right\|^2 + \kappa\Delta t\int_I \left|[\mathbf{u}^0]\right|\left(\left|u_1^1\right|^2 + \left|u_2^1\right|^2\right)ds \\
+ \sum_{j=1}^n\left(\frac{\Delta t}{\nu_1}\left\|f_1(t^{j+1})\right\|_{V_1'}^2 + \frac{\Delta t}{\nu_2}\left\|f_2(t^{j+1})\right\|_{V_2'}^2\right),
\end{aligned} \tag{5.37}$$

i.e., the right-hand side of the stability estimate (5.21). Also, let $\hat{\nu} := \max\{\nu_1, \nu_2\}$ and $\tilde{\nu} := \max\{\nu_1^{-1}, \nu_2^{-1}\}$. Then (5.36) can be simplified to

$$\begin{aligned}
&\frac{1}{2\Delta t}\left(\|\phi_1^{n+1}\|_{\Omega_1}^2 - \|\phi_1^n\|_{\Omega_1}^2 + \|\phi_1^{n+1} - \phi_1^n\|_{\Omega_1}^2\right) + \frac{7\nu_1}{8}\|\nabla\phi_1^{n+1}\|_{\Omega_1}^2 \\
&\leq C\nu_1^{-3}\left\{1 + \|\nabla u_1(t^{n+1})\|_{\Omega_1}^4 + \kappa^4\left(\|u_2^n\|_I^4 + \left\|[\mathbf{u}(t^{n+1})]\right\|_I^4\right)\right\}\left\|\phi_1^{n+1}\right\|_{\Omega_1}^2 \\
&+ C\nu_1^{-1}\left(\left\|\frac{\eta_1^{n+1} - \eta_1^n}{\Delta t}\right\|_{V_1'}^2 + \|R_1^{n+1}\|_{V_1'}^2 + \|p_1(t^{n+1}) - q_1^{n+1}\|_{\Omega_1}^2\right) \\
&+ \frac{\nu_1}{16}\left(\|\nabla\phi_1^n\|_{\Omega_1}^2 + \left\|\nabla\phi_1^{n-1}\right\|_{\Omega_1}^2\right) + \frac{\nu_2}{16}\left(\|\nabla\phi_2^n\|_{\Omega_2}^2 + \left\|\nabla\phi_2^{n-1}\right\|_{\Omega_2}^2\right) \\
&+ C\kappa^2 L^{n+1}P^{n+1} + C\kappa^4 M^{n+1}\tilde{\nu}^3\left(\|\boldsymbol{\phi}^n\|^2 + \left\|\boldsymbol{\phi}^{n-1}\right\|^2\right) \\
&+ C\left(\nu_1 + \nu_1^{-1}\|\nabla u_1(t^{n+1})\|_{\Omega_1}^2 + \nu_1^{-1}S_{n+1}^{1/2}\left\|\nabla u_1^{n+1}\right\|_{\Omega_1}\right)\|\nabla\eta_1^{n+1}\|_{\Omega_1}^2.
\end{aligned} \tag{5.38}$$

Proceeding further requires estimates for the solution on Ω_2. This analysis is done in the same manner as above for Ω_1 using (5.18), and a similar estimate is derived:

$$\begin{aligned}
&\frac{1}{2\Delta t}\left(\|\phi_2^{n+1}\|_{\Omega_2}^2-\|\phi_2^n\|_{\Omega_2}^2+\|\phi_2^{n+1}-\phi_2^n\|_{\Omega_2}^2\right)+\frac{7\nu_2}{8}\|\nabla\phi_2^{n+1}\|_{\Omega_2}^2\\
&\leq C\nu_2^{-3}\left\{1+\|\nabla u_2(t^{n+1})\|_{\Omega_2}^4+\kappa^4\left(\|u_1^n\|_I^4+\left\|[\mathbf{u}(t^{n+1})]\right\|_I^4\right)\right\}\left\|\phi_2^{n+1}\right\|_{\Omega_2}^2\\
&+C\nu_2^{-1}\left(\left\|\frac{\eta_2^{n+1}-\eta_2^n}{\Delta t}\right\|_{V_2'}^2+\|R_2^{n+1}\|_{V_2'}^2+\|p_2(t^{n+1})-q_2^{n+1}\|_{\Omega_2}^2\right)\\
&+\frac{\nu_1}{16}\left(\|\nabla\phi_1^n\|_{\Omega_1}^2+\left\|\nabla\phi_1^{n-1}\right\|_{\Omega_1}^2\right)+\frac{\nu_2}{16}\left(\|\nabla\phi_2^n\|_{\Omega_2}^2+\left\|\nabla\phi_2^{n-1}\right\|_{\Omega_2}^2\right)\\
&+C\kappa^2L^{n+1}P^{n+1}+C\kappa^4M^{n+1}\tilde{\nu}^3\left(\|\boldsymbol{\phi}^n\|^2+\left\|\boldsymbol{\phi}^{n-1}\right\|^2\right)\\
&+C\left(\nu_2+\nu_2^{-1}\|\nabla u_2(t^{n+1})\|_{\Omega_2}^2+\nu_2^{-1}S_{n+1}^{1/2}\left\|\nabla u_2^{n+1}\right\|_{\Omega_2}\right)\|\nabla\eta_2^{n+1}\|_{\Omega_2}^2.
\end{aligned}\tag{5.39}$$

Combining (5.38) and (5.39) gives the global estimate

$$\begin{aligned}
&\frac{1}{2\Delta t}\left(\|\boldsymbol{\phi}^{n+1}\|^2-\|\boldsymbol{\phi}^n\|^2+\|\boldsymbol{\phi}^{n+1}-\boldsymbol{\phi}^n\|^2\right)+\frac{7\nu_1}{8}\|\nabla\phi_1^{n+1}\|_{\Omega_1}^2+\frac{7\nu_2}{8}\|\nabla\phi_2^{n+1}\|_{\Omega_2}^2\\
&\leq C\tilde{\nu}^3\left(1+\|\nabla\mathbf{u}(t^{n+1})\|^4+\kappa^4M^{n+1}\right)\left\|\boldsymbol{\phi}^{n+1}\right\|^2\\
&+C\tilde{\nu}\left(\left\|\frac{\boldsymbol{\eta}^{n+1}-\boldsymbol{\eta}^n}{\Delta t}\right\|_{V'}^2+\|R_1^{n+1}\|_{V_1'}^2+\|R_2^{n+1}\|_{V_2'}^2+\|\mathbf{p}(t^{n+1})-\mathbf{q}^{n+1}\|^2\right)\\
&+\frac{\nu_1}{8}\left(\|\nabla\phi_1^n\|_{\Omega_1}^2+\left\|\nabla\phi_1^{n-1}\right\|_{\Omega_1}^2\right)+\frac{\nu_2}{8}\left(\|\nabla\phi_2^n\|_{\Omega_2}^2+\left\|\nabla\phi_2^{n-1}\right\|_{\Omega_2}^2\right)\\
&+C\kappa^2L^{n+1}P^{n+1}+C\kappa^4M^{n+1}\tilde{\nu}^3\left(\|\boldsymbol{\phi}^n\|^2+\left\|\boldsymbol{\phi}^{n-1}\right\|^2\right)\\
&+C\left(\hat{\nu}+\tilde{\nu}\|\nabla\mathbf{u}(t^{n+1})\|^2+\tilde{\nu}S_{n+1}^{1/2}\left\|\nabla\mathbf{u}^{n+1}\right\|\right)\|\nabla\boldsymbol{\eta}^{n+1}\|^2.
\end{aligned}\tag{5.40}$$

Rearranging terms gives

$$\begin{aligned}
&\frac{1}{2\Delta t}\left(\|\boldsymbol{\phi}^{n+1}\|^2-\|\boldsymbol{\phi}^n\|^2+\|\boldsymbol{\phi}^{n+1}-\boldsymbol{\phi}^n\|^2\right)+\frac{\nu_1}{2}\left\|\nabla\phi_1^{n+1}\right\|_{\Omega_1}^2+\frac{\nu_2}{2}\left\|\nabla\phi_2^{n+1}\right\|_{\Omega_2}^2\\
&+\frac{\nu_1}{4}\left(\left\|\nabla\phi_1^{n+1}\right\|_{\Omega_1}^2-\|\nabla\phi_1^n\|_{\Omega_1}^2\right)+\frac{\nu_1}{8}\left(\|\nabla\phi_1^n\|_{\Omega_1}^2-\left\|\nabla\phi_1^{n-1}\right\|_{\Omega_1}^2\right)\\
&+\frac{\nu_2}{4}\left(\left\|\nabla\phi_2^{n+1}\right\|_{\Omega_2}^2-\|\nabla\phi_2^n\|_{\Omega_2}^2\right)+\frac{\nu_2}{8}\left(\|\nabla\phi_2^n\|_{\Omega_2}^2-\left\|\nabla\phi_2^{n-1}\right\|_{\Omega_2}^2\right)\\
&\leq C\,A^{n+1}+C\,B^{n+1}+C\tilde{\nu}^3\left(1+\|\nabla\mathbf{u}(t^{n+1})\|^4+\kappa^4M^{n+1}\right)\left\|\boldsymbol{\phi}^{n+1}\right\|^2\\
&+C\kappa^2L^{n+1}P^{n+1}+C\kappa^4M^{n+1}\tilde{\nu}^3\left(\|\boldsymbol{\phi}^n\|^2+\left\|\boldsymbol{\phi}^{n-1}\right\|^2\right)
\end{aligned}\tag{5.41}$$

where A^{n+1} and B^{n+1} are defined by

$$\begin{aligned} A^{n+1} &= \tilde{\nu}\left(\left\|\frac{\boldsymbol{\eta}^{n+1}-\boldsymbol{\eta}^{n}}{\Delta t}\right\|_{V'}^{2} + \|R_1^{n+1}\|_{V_1'}^2 + \|R_2^{n+1}\|_{V_2'}^2 + \|\mathbf{p}(t^{n+1}) - \mathbf{q}^{n+1}\|^2\right) \\ B^{n+1} &= \left(\hat{\nu} + \tilde{\nu}\|\nabla \mathbf{u}(t^{n+1})\|^2 + \tilde{\nu} S_{n+1}^{1/2}\left\|\nabla \mathbf{u}^{n+1}\right\|\right)\|\nabla \boldsymbol{\eta}^{n+1}\|^2. \end{aligned} \tag{5.42}$$

Summing over $n = 1, 2, \ldots, p-1$, multiplying through by $2\Delta t$, and rearranging gives a global error estimate at time t^p:

$$\begin{aligned} &\|\boldsymbol{\phi}^p\|^2 + \sum_{n=1}^{p-1}\left\|\boldsymbol{\phi}^{n+1}-\boldsymbol{\phi}^n\right\|^2 + \Delta t\left(\nu_1\sum_{n=1}^{p-1}\left\|\nabla\phi_1^{n+1}\right\|_{\Omega_1}^2 + \nu_2\sum_{n=1}^{p-1}\left\|\nabla\phi_2^{n+1}\right\|_{\Omega_2}^2\right) \\ &\quad + \frac{\Delta t\,\nu_1}{4}\left(2\left\|\nabla\phi_1^p\right\|_{\Omega_1}^2 + \left\|\nabla\phi_1^{p-1}\right\|_{\Omega_1}^2\right) + \frac{\Delta t\,\nu_2}{4}\left(2\left\|\nabla\phi_2^p\right\|_{\Omega_2}^2 + \left\|\nabla\phi_2^{p-1}\right\|_{\Omega_2}^2\right) \\ &\le \left(1 + C\Delta t\,\tilde{\nu}^3\kappa^4(M^2+M^3)\right)\left\|\boldsymbol{\phi}^1\right\|^2 + C\Delta t\,\tilde{\nu}^3\kappa^4 M^2\left\|\boldsymbol{\phi}^0\right\|^2 \\ &\quad + \frac{\Delta t\,\nu_1}{2}\left(\left\|\nabla\phi_1^1\right\|_{\Omega_1}^2 + \frac{1}{2}\left\|\nabla\phi_1^0\right\|_{\Omega_1}^2\right) + \frac{\Delta t\,\nu_2}{2}\left(\left\|\nabla\phi_2^1\right\|_{\Omega_2}^2 + \frac{1}{2}\left\|\nabla\phi_2^0\right\|_{\Omega_2}^2\right) \\ &\quad + C\,\Delta t\sum_{n=1}^{p-1}\left(A^{n+1} + B^{n+1} + \kappa^2 L^{n+1}P^{n+1}\right) + C\Delta t\sum_{n=1}^{p-1} D^{n+1}\left\|\boldsymbol{\phi}^{n+1}\right\|^2 \end{aligned} \tag{5.43}$$

where D^{n+1} is defined by

$$D^{n+1} = \tilde{\nu}^3\left(1 + \kappa^4 E^{n+1} + \left\|\nabla\mathbf{u}(t^{n+1})\right\|^4\right), \tag{5.44}$$

with

$$E^{n+1} = \begin{cases} M^{n+3} + M^{n+2} + M^{n+1} & \text{if } 1 \le n \le p-3 \\ M^{n+2} + M^{n+1} & \text{if } n = p-2 \\ M^{n+1} & \text{if } n = p-1 \end{cases}. \tag{5.45}$$

To use the discrete Gronwall's inequality (see [45]), note that for $j = 1, 2, \ldots, N$, write (5.43) as

$$\begin{aligned} &a^{j+1} + \sum_{n=1}^{j} b^{n+1} + \Delta t\sum_{n=1}^{j} c^{n+1} \\ &\qquad \le J + C\Delta t\sum_{n=1}^{j} D^{n+1}a^{n+1} + C\,\Delta t\,\sum_{n=1}^{j}\left(A^{n+1} + B^{n+1} + \kappa^2 L^{n+1}P^{n+1}\right) \end{aligned} \tag{5.46}$$

where

$$a^{j+1} = \left\|\boldsymbol{\phi}^{j+1}\right\|^2, \quad b^{j+1} = \left\|\boldsymbol{\phi}^{j+1} - \boldsymbol{\phi}^{j}\right\|^2, \quad c^{j+1} = \nu_1 \left\|\nabla\phi_1^{j+1}\right\|_{\Omega_1}^2 + \nu_2 \left\|\nabla\phi_2^{j+1}\right\|_{\Omega_2}^2,$$

and

$$\begin{aligned} J = &\left(1 + C\Delta t\,\tilde{\nu}^3\kappa^4(M^2 + M^3)\right)\left\|\boldsymbol{\phi}^1\right\|^2 + C\Delta t\,\tilde{\nu}^3\kappa^4 M^2\left\|\boldsymbol{\phi}^0\right\|^2 \\ &+ \frac{\Delta t\,\nu_1}{2}\left(\left\|\nabla\phi_1^1\right\|_{\Omega_1}^2 + \frac{1}{2}\left\|\nabla\phi_1^0\right\|_{\Omega_1}^2\right) + \frac{\Delta t\,\nu_2}{2}\left(\left\|\nabla\phi_2^1\right\|_{\Omega_2}^2 + \frac{1}{2}\left\|\nabla\phi_2^0\right\|_{\Omega_2}^2\right). \end{aligned}$$

Applying Gronwall's inequality, (5.46) gives

$$\begin{aligned} &a^{j+1} + \sum_{n=1}^{j} b^{n+1} + \Delta t \sum_{n=1}^{j} c^{n+1} \\ &\qquad \leq \exp\left(C\Delta t \sum_{n=1}^{j} \sigma^{n+1}\right)\left\{J + C\Delta t \sum_{n=1}^{j}\left(A^{n+1} + B^{n+1} + \kappa^2 L^{n+1} P^{n+1}\right)\right\} \end{aligned} \tag{5.47}$$

where

$$\sigma^{n+1} = \frac{D^{n+1}}{1 - \Delta t\, D^{n+1}}. \tag{5.48}$$

It remains to bound the individual terms on the right-hand side of (5.47). The terms in J are bounded using the triangle inequality. The terms in A^{n+1} are bounded in the usual way (see the proof of Theorem 4.1 of [18], for example). In B^{n+1}, the summed factor $\|\nabla\mathbf{u}^{n+1}\|$ is bounded using the stability estimate (5.21) and the $\|\nabla\mathbf{u}(t^{n+1})\|$ term is bounded by a standard a priori estimate on the solution to the continuous problem. The terms in L^{n+1} and M^{n+1} are bounded by a standard a priori estimate on $\|\mathbf{u}(t^{n+1})\|$ or using S^n for the discrete solutions, (the bound (5.13), and the stability estimate (5.21)). The terms in P^{n+1} are bounded the same way. The estimate (5.27) is derived through the application of the triangle inequality to the left hand side of (5.47). □

Corollary 5.3.1 (Convergence rate for MINI-element)**.** *Let* $(\mathbf{u}, \mathbf{p})$ *be a solution of* (5.1)-(5.6) *satisfying the assumptions of Lemma 5.3.1 and Theorem 5.3.2, approximated using the MINI-element on a mesh of maximum element width* h *by Algorithm 5.2.1. Assume the velocity data* $\mathbf{u}^0, \mathbf{u}^1$ *satisfies*

$$\|\mathbf{u}(t^0) - \mathbf{u}^0\|_X + \|\mathbf{u}(t^1) - \mathbf{u}^1\|_X \leq C_1\, h,$$

for a generic constant C_1 *independent of* $\Delta t, h$*. Then there exists* $C > 0$ *independent of* $h, \Delta t$ *such that the discrete velocity satisfies the optimal error estimate*

$$\begin{aligned}\Delta t \left(\nu_1 \sum_{k=1}^{n} \left\| \nabla (u_1(t^{k+1}) - u_1^{k+1}) \right\|_{\Omega_1}^2 + \nu_2 \sum_{k=1}^{n} \left\| \nabla (u_2(t^{k+1}) - u_2^{k+1}) \right\|_{\Omega_2}^2 \right) \\ \leq C\,(h^2 + \Delta t^2).\end{aligned}$$

Proof. This follows by using standard interpolation error estimates for the MINI-element, e.g. [11, 45], in the right hand side of the error bound (5.27). □

5.4 NUMERICAL EXPERIMENTS

In this section numerical experiments are presented that support the theory described in the previous sections. In addition to the GA scheme previously described, the following algorithms will be compared:

Algorithm 5.4.1 (Fully Implicit Scheme)**.** *Let* $\Delta t > 0$, $\mathbf{f} \in V'$*. For each* $M \in \mathbb{N}, M \leq \frac{T}{\Delta t}$*, given* $\mathbf{u}^n \in V_h$*,* $n = 0, 1, 2, \cdots, M-1$*, find* $\mathbf{u}^{n+1} \in V_{1,h}$ *satisfying*

$$\begin{aligned}\left(\frac{\mathbf{u}^{n+1} - \mathbf{u}^n}{\Delta t}, \mathbf{v} \right) + \boldsymbol{\nu} \left(\nabla \mathbf{u}^{n+1}, \mathbf{v} \right) + \sum_{i=1,2} c_i(u_i^{n+1}; u_i^{n+1}, v_i) \\ + \int_I \kappa |[\mathbf{u}^n]| [\mathbf{u}^{n+1}] [\mathbf{v}] = (\mathbf{f}(t^{n+1}), \mathbf{v})\,.\end{aligned} \tag{5.49}$$

Algorithm 5.4.2 (First-order IMEX Scheme)**.** *Let* $\Delta t > 0$, $\mathbf{f} \in V'$. *For each* $M \in \mathbb{N}, M \leq \frac{T}{\Delta t}$, *given* $\mathbf{u}^n \in V_h$, $n = 0, 1, 2, \cdots, M-1$, *find* $u_1^{n+1} \in V_{1,h}$ *satisfying*

$$\begin{aligned}\left(\frac{u_1^{n+1}-u_1^n}{\Delta t}, v_1\right)_{\Omega_1} &+ \nu_1 \left(\nabla u_1^{n+1}, \nabla v_1\right)_{\Omega_1} + c_1(u_1^{n+1}; u_1^{n+1}, v_1) \\ &+ \kappa \int_I |[\mathbf{u}^n]| u_1^{n+1} \cdot v_1 \, ds - \kappa \int_I |[\mathbf{u}^n]| u_2^n \cdot v_1 \, ds \\ &= \left(f_1(t^{n+1}), v_1\right)_{\Omega_1}, \ \forall v_1 \in V_{1,h}.\end{aligned} \tag{5.50}$$

and $u_2^{n+1} \in V_{2,h}$ *satisfying*

$$\begin{aligned}\left(\frac{u_2^{n+1}-u_2^n}{\Delta t}, v_2\right)_{\Omega_2} &+ \nu_2 \left(\nabla u_2^{n+1}, \nabla v_2\right)_{\Omega_2} + c_2(u_2^{n+1}; u_2^{n+1}, v_2) \\ &+ \kappa \int_I |[\mathbf{u}^n]| u_2^{n+1} \cdot v_2 \, ds - \kappa \int_I |[\mathbf{u}^n]| u_1^n \cdot v_2 \, ds \\ &= \left(f_2(t^{n+1}), v_2\right)_{\Omega_2}, \ \forall v_2 \in V_{2,h}.\end{aligned} \tag{5.51}$$

5.4.1 Problem 1: Analytic Solution

Assume $\Omega_1 = [0,1] \times [0,1]$ and $\Omega_2 = [0,1] \times [-1,0]$, so I is the portion of the x-axis from 0 to 1. Then $\mathbf{n}_1 = [0, \ -1]^T$ and $\mathbf{n}_2 = [0, \ 1]^T$. For a, ν_1, ν_2, and κ all arbitrary positive constants, the right hand side function $\mathbf{f}_1$ is chosen to ensure that

$$\begin{aligned} u_{1,1}(t,x,y) &= ax^2(1-x)^2(1-y)e^{-t}, \\ u_{1,2}(t,x,y) &= axy(-2+y+6x-3xy-4x^2+2x^2y)e^{-t}, \\ p_1(t,x,y) &= e^{-t}\cos(\pi x)\sin(\pi y). \end{aligned}$$

One may verify that the above velocity field is divergence-free and that $u_{1,2}$ is zero on I. The function $\mathbf{f}_2$ is chosen to ensure that 1) $u_{2,1}$ satisfies the interface condition, 2) $u_{2,2}$ is zero on I, 3) u_2 is a divergence-free velocity field, and 4) $p_2 = p_1$.

The spatial discretization is accomplished using the conforming P_1+bubble/P_1 element pair. All computations were performed using the software package FreeFem++, [35]. Computational results comparing the performance of the two methods are listed for two test problems:

- Test Problem 1: $a = \nu_1 = \nu_2 = \kappa = 1$, $T = 1$.

Table 15: Velocity errors for computed approximations, test problem 1

		Implicit			
Δt	h	$Err(u_1)$	rate	$Err(u_2)$	rate
1/2	0.1846	0.047742		0.099814	
1/4	0.1005	0.029857	0.70	0.055870	0.83
1/8	0.0555	0.014682	1.07	0.032177	0.87
1/16	0.0256	0.007305	0.96	0.015745	1.00
1/32	0.0131	0.003866	0.95	0.008037	0.94
		IMEX			
Δt	h	$Err(u_1)$	rate	$Err(u_2)$	rate
1/2	0.1846	0.047966		0.099804	
1/4	0.1005	0.029955	0.70	0.055862	0.83
1/8	0.0555	0.014732	1.07	0.032171	0.87
1/16	0.0256	0.007329	0.96	0.015740	1.00
1/32	0.0131	0.003877	0.95	0.008032	0.94
		GA			
Δt	h	$Err(u_1)$	rate	$Err(u_2)$	rate
1/2	0.1846	0.048166		0.099803	
1/4	0.1005	0.030032	0.71	0.055861	0.83
1/8	0.0555	0.014769	1.07	0.032169	0.87
1/16	0.0256	0.007347	0.96	0.015738	1.00
1/32	0.0131	0.003884	0.95	0.008031	0.94

- Test Problem 2: $a = 1, \nu_1 = 10, \nu_2 = 0.1, \kappa = 1000$, $T = 1$.

Tables 15 and 16 give the velocity errors produced by each of the methods. The pressure errors are listed in Tables 17 and 18. A compact notation is used to denote the various errors. Letting $u_i(t), p_i(t)$ denote the NSE solution in $\Omega_i, i = 1, 2$, approximated at $t = t^n$ by u_i^n, p_i^n respectively, the errors are

$$\mathrm{Err}(u_i) = \left(\Delta t \sum_{n=0}^{N} \|u_i(t^n) - u_i^n\|^2_{H^1(\Omega_i)} \right)^{1/2}$$
$$\mathrm{Err}(p_i) = \left(\Delta t \sum_{n=0}^{N} \|p_i(t^n) - p_i^n\|^2_{L^2(\Omega_i)} \right)^{1/2}.$$

The results of problem 1 show almost identical behavior for the velocity fields with each method and the expected convergence rate is observed. The results of test problem 2 show different behavior in the two subdomains. The IMEX method generates a more accurate approximation of the velocity field in Ω_2, whereas the GA method exhibits superior performance in Ω_1. This result is due to the different decoupling strategies and may demonstrate

Table 16: Velocity errors for computed approximations, test problem 2

		Implicit			
Δt	h	$Err(u_1)$	rate	$Err(u_2)$	rate
1/2	0.1846	0.047899		1.521740	
1/4	0.1005	0.028168	0.81	0.946804	0.72
1/8	0.0555	0.015763	0.82	0.546786	0.83
1/16	0.0256	0.008541	0.93	0.222828	1.23
1/32	0.0131	0.003780	1.15	0.127603	0.81
		IMEX			
Δt	h	$Err(u_1)$	rate	$Err(u_2)$	rate
1/2	0.1846	0.051014		1.519762	
1/4	0.1005	0.031509	0.72	0.827436	0.87
1/8	0.0555	0.015783	1.04	0.450806	0.96
1/16	0.0256	0.030379	-0.90	0.252060	0.81
1/32	0.0131	0.033161	-0.13	0.145956	0.76
		GA			
Δt	h	$Err(u_1)$	rate	$Err(u_2)$	rate
1/2	0.1846	0.051497		1.519950	
1/4	0.1005	0.031836	0.72	0.828039	0.87
1/8	0.0555	0.016204	1.02	0.460119	0.93
1/16	0.0256	0.009117	0.79	0.261543	0.79
1/32	0.0131	0.008301	0.14	0.175407	0.56

the advantage using geometric averaging in coupling terms to help control error propagation through superior stabilization of the computations over the IMEX method. In general it should be expected the consistency error using the GA method will be higher than for IMEX, as seen in Ω_2. However, stability of the IMEX method is inferior to that of the GA method (see Section 5.4.2 below) so using geometric averaging offers an attractive alternative for problems requiring larger time steps or longer time calculations.

Test problem 1 exhibits important behavior in that the pressure is not optimally approximated by the fully implicit method for the chosen range of discretization values. A variety of tests were performed using different parameter choices and it was observed that the pressure errors will concentrate where the derivatives of the vector field are largest. For example, the parameter choices for test problem 1 yield pressure errors largest in the bottom right corner of Ω_2. Increasing κ to 1000 and keeping all other parameters the same, the size of the derivatives of the vector field decrease in Ω_2, and optimal approximation of the pressure was then observed. In all cases studied, convergence rates of the discrete velocity solution generated using the implicit method approached the optimal rate $O(h)$.

Table 17: Pressure errors for computed approximations, test problem 1

		Implicit			
Δt	h	$Err(p_1)$	rate	$Err(p_2)$	rate
1/2	0.1846	0.041421		0.050367	
1/4	0.1005	0.009949	2.13	0.023795	1.07
1/8	0.0555	0.005559	0.88	0.017088	0.52
1/16	0.0256	0.001744	1.59	0.016536	0.05
1/32	0.0131	0.000676	1.41	0.016740	-0.02
		IMEX			
Δt	h	$Err(p_1)$	rate	$Err(p_2)$	rate
1/2	0.1846	0.042344		0.050039	
1/4	0.1005	0.010738	2.05	0.023449	1.08
1/8	0.0555	0.005878	0.91	0.016835	0.52
1/16	0.0256	0.001972	1.50	0.016402	0.04
1/32	0.0131	0.000803	1.34	0.016673	-0.02
		GA			
Δt	h	$Err(p_1)$	rate	$Err(p_2)$	rate
1/2	0.1846	0.043042		0.049930	
1/4	0.1005	0.011267	2.00	0.023341	1.08
1/8	0.0555	0.006087	0.93	0.016759	0.52
1/16	0.0256	0.002112	1.45	0.016364	0.03
1/32	0.0131	0.000880	1.30	0.016655	-0.02

Table 18: Pressure errors for computed approximations, test problem 2

		Implicit			
Δt	h	$Err(p_1)$	rate	$Err(p_2)$	rate
1/2	0.1846	0.391527		0.226876	
1/4	0.1005	0.155362	1.41	0.069922	1.79
1/8	0.0555	0.052053	1.55	0.028199	1.38
1/16	0.0256	0.021054	1.38	0.010724	1.33
1/32	0.0131	0.006389	1.68	0.004256	1.34
		IMEX			
Δt	h	$Err(p_1)$	rate	$Err(p_2)$	rate
1/2	0.1846	0.495810		0.219627	
1/4	0.1005	0.176246	1.54	0.084434	1.36
1/8	0.0555	0.098930	0.87	0.029426	1.67
1/16	0.0256	0.401356	-1.92	0.017330	0.74
1/32	0.0131	0.462211	-0.21	0.020890	-0.26
		GA			
Δt	h	$Err(p_1)$	rate	$Err(p_2)$	rate
1/2	0.1846	0.509778		0.219870	
1/4	0.1005	0.189283	1.48	0.084701	1.36
1/8	0.0555	0.108590	0.84	0.034592	1.42
1/16	0.0256	0.076997	0.47	0.024680	0.47
1/32	0.0131	0.096480	-0.34	0.034266	-0.46

The convergence of the pressure solution is not fully understood and is an important open problem. There are a number of possible reasons this behavior is observed. Here is a list of some ideas to investigate this issue:

1. Check boundedness and convergence of the discrete time derivative
2. Use a higher order approximation of the discrete time derivative (e.g. BDF-2)
3. Check stability of the pressure analytically
4. There may be issues related to the linear solver
5. Using uniform nested meshes may clarify the behavior of the pressure error

5.4.2 Stability of Decoupled Methods

Lemma 5.3.1 predicts energetic stability of the GA method regardless of the choice of problem parameters or discretization parameters. A similar result for the IMEX method is not known. Computational evidence shows that a general unconditional energetic stability result for the IMEX partitioned method without geometric averaging is not possible. Some time step restriction for stability is required depending on the problem parameters. To show this, the above test is repeated choosing

$$\nu_1 = 0.005\,,\ \nu_2 = 0.1\,,\ a = 100\,,\ \text{and}\ \kappa = 100$$

and the size of the discrete solutions generated by both the IMEX and GA methods are listed in Table 19 using the norm

$$\|\mathbf{u}^n\| = \left(\Delta t \sum_{n=0}^{N} \|u_1^n\|^2_{H^1(\Omega_1)} + \|u_2^n\|^2_{H^1(\Omega_2)} \right)^{1/2}.$$

The convective term was linearized for both methods in the standard way:

$$c_i(u_i^{n+1}, u_i^{n+1}, v_i) \to c_i(u_i^n, u_i^{n+1}, v_i)$$

which does not affect stability. For the fully (nonlinearly) implicit convective term the nonlinear solve would fail before obtaining relevant results. Note that for the partitioned algorithms, linearizing the convective term in turn linearizes the entire calculation. As a result, any energetic blow up may be attributed to the method of decoupling and not to errors accruing in nonlinear solution substeps.

Table 19: Stability of the decoupled methods.

Δt	h	$\|\mathbf{u}^n\|$-Implicit	$\|\mathbf{u}^n\|$-GA	$\|\mathbf{u}^n\|$-IMEX
1/4	0.1846	3.2596E+1	4.2461E+1	1.7896E+2
1/8	0.1005	3.4840E+1	5.9751E+1	1.8844E+3
1/16	0.0555	3.5981E+1	4.1034E+1	2.1835E+7
1/32	0.0256	3.6556E+1	3.7801E+1	3.1742E+10
1/64	0.0131	3.6845E+1	3.8387E+1	7.4102E+16

5.4.3 Problem 2: Model Ocean-Atmosphere Problem

The GA partitioned method is used to approximate the solution to a coupled fluid system representative of atmosphere-ocean systems, motivated by previous studies (see [7, 12]). The subdomains are $\Omega_1 = [0, 10] \times [0, 1]$ and $\Omega_2 = [0, 10] \times [-1, 0]$. The system (5.1)-(5.5) is solved subject to zero Dirichlet boundary conditions on Γ_2, an inflow profile $u_1(x = 0, y) = \langle (1 + y)/2, 0 \rangle$ for the left boundary of Ω_1, and do-nothing boundary conditions on the remainder of Γ_1. The viscous and frictional parameters are $\nu_1 = 1/200$, $\nu_2 = 1/2000$ and $\kappa = 2.45E - 3$. The initial profile is $u_1(x, y, t = 0) = u_1(0, y)$ in Ω_1 and $u_2(x, y, t = 0) = 0$ in Ω_2. Zero forcing is chosen, $\mathbf{f}_1 = \mathbf{f}_2 = 0$. At final time $T = 1$ the GA approximation is plotted in Figure 7 using time step size $\Delta t = 1/384$ and mesh size $h = 1/96$, showing the velocity field in Ω_1 and streamlines in Ω_2. The drag of the fluid in Ω_1 on the fluid in Ω_2 causes a global recirculation in Ω_2, while the laminar flow in Ω_1 is preserved over time. This agrees qualitatively with results presented in the above mentioned reports. A reference solution was generated using the implicit, coupled method choosing $\Delta t = 1/1536$ and $h = 1/96$. The approximation using the GA method is compared to this reference solution, in lieu of the true solution. The resulting "errors" are listed in Table 20 using the norms defined above. A driven cavity is represented in Ω_2, so fluid stresses will be high in the corners of Ω_2 along the interface. This may affect the pressure results, similar to observations in Section 5.4.1. Also likely are errors resulting from resolution of the boundary layer near I and the characteristic fluid overturn. These features may make this problem interesting as a benchmark for comparing coupled fluid codes.

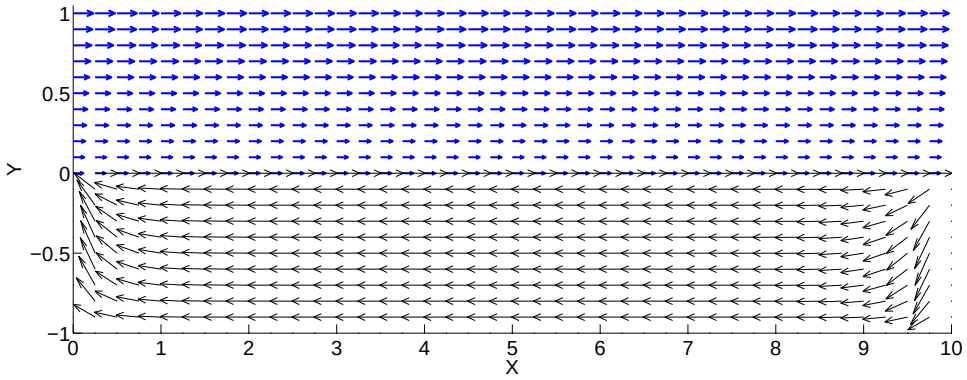

Figure 7: Coupled fluid solution at time $T = 1$, normalized in Ω_2.

5.5 CONCLUSIONS

For nonlinear interface conditions, stability of partitioned methods depends critically on their precise treatment. We have shown that, perhaps surprisingly, geometric averaging yields an unconditionally stable partitioned method while the most natural treatment is unstable. The kinetic energy and energy dissipation predicted by the model has been proven to deviate from values obtained using a fully implicit discretization by an amount proportional (asymptotically) to the time step size. Convergence as time and spatial discretization parameters go to zero was proven.

Table 20: Errors for computed GA approximations

Δt	h	$Err(u_1)$	rate	$Err(u_2)$	rate	$Err(p_1)$	rate	$Err(p_2)$	rate
1/24	1/6	0.214113		0.326636		2.5013E-4		2.4633E-4	
1/48	1/12	0.130309	0.72	0.284095	0.20	1.1210E-4	1.16	1.7364E-4	0.50
1/96	1/24	0.071209	0.87	0.202704	0.49	6.5128E-5	0.78	7.1259E-5	1.29
1/192	1/48	0.036975	0.95	0.116452	0.80	3.1784E-5	1.04	1.7880E-5	1.99

6.0 INDEPENDENT TIME STEPPING FOR THE ATMOSPHERE AND OCEAN SUBPROBLEMS

6.1 INTRODUCTION

In this chapter a new time stepping algorithm is introduced for the same model of two coupled fluids presented in Chapter 5. Some desirable properties for the algorithm studied are determined by the following considerations.

- Atmosphere-ocean solves are decoupled at each time step, recoupling by flux passing between steps.
- Efficiency mandates independent time stepping (and meshing) for the atmosphere and ocean subproblems due to different time and space scales.
- Long time calculations are needed to understand global climate phenomena.

This chapter proposes a full discretization of the coupled fluid problem that is subsequently shown to have the following properties.

1. The momentum equations for the two fluids may be solved in parallel.
2. A different time step size may be used for each fluid.
3. Stability is maintained for any size time step.
4. A balanced, two-way flux passing is implemented using mixed boundary conditions and semi-implicit time stepping.

A full numerical analysis for the proposed method is provided. To demonstrate the efficiency of the method a numerical test is performed which exemplifies some of the key dynamic properties of the atmosphere-ocean system. It is observed that for this numerical test the time step size for the fluid representing the ocean may be taken at least 16 times

larger than for the other fluid with the dominant spatial errors remaining locally supported on a small region around a part of the interface. As a result, average velocity is calculated and it is observed that the error introduced in this measurement is much smaller than the H^1 error.

6.1.1 The Model Problem and Related Properties

The main details of the model in Chapter 5 are reviewed here for convenience. Let the domain $\Omega \subset \mathbb{R}^d$ for $d = 2, 3$ consist of two subdomains Ω_1 and Ω_2 with outward unit normal vectors $\hat{n}_1$ and $\hat{n}_2$, respectively. The subdomains are coupled across an interface $I = \partial\Omega_1 \cap \partial\Omega_2$ (example in Figure 2). Let $\hat{\tau}$ be any tangent vector on I.

The problem is: *given* $\nu_i > 0, f_i : [0,T] \to H^1(\Omega_i), u_i(0) \in H^1(\Omega_i)$ *and* $\kappa \in \mathbb{R}$, *find (for* $i = 1, 2$*)* $u_i : \Omega_i \times (0,T) \to \mathbb{R}^d$ *and* $p_i : \Omega_i \times (0,T) \to \mathbb{R}$ *satisfying for* $i, j = 1, 2$ *and* $i \neq j$

$$
\begin{aligned}
u_{i,t} + u_i \cdot \nabla u_i - \nu_i \Delta u_i + \nabla p_i &= f_i, \text{ and } \nabla \cdot u_i = 0 \text{ in } \Omega_i, && (6.1)\\
-\nu_i \hat{n}_i \cdot \nabla u_i \cdot \hat{\tau} &= \kappa |u_i - u_j| (u_i - u_j) \cdot \hat{\tau} \text{ and } u_i \cdot \hat{n}_i = 0 \text{ on } I, && (6.2)\\
u_i(x,0) &= u_i^0(x), \quad \text{in } \Omega_i, && (6.3)\\
u_i &= 0, \quad \text{on } \Gamma_i = \partial\Omega_i \setminus I. && (6.4)
\end{aligned}
$$

The nonlinear coupling conditions (6.2) are the central focus. The corresponding weak problem is derived using the following function spaces. Let

$$
\begin{aligned}
X_i &:= \{v_i \in H^1(\Omega_i)^d : v_i = 0 \text{ on } \Gamma_i = \partial\Omega_i \setminus I \,, v_i \cdot \hat{n}_i = 0 \text{ on } I\}\\
Q_i &:= \left\{ q_i \in L^2(\Omega_i) : \int_{\Omega_i} q_i \, d\Omega_i = 0 \right\}.
\end{aligned}
$$

For $u_i \in X_i$ we denote $\mathbf{u} = (u_1, u_2)$ and $X := \{\mathbf{v} = (v_1, v_2) : v_i \in X_i,\ i = 1, 2\}$. Similarly, for $q_i \in Q_i$ we denote $\mathbf{q} = (q_1, q_2)$ and $Q := \{\mathbf{q} = (q_1, q_2) : q_i \in Q_i,\ i = 1, 2\}$. The subdomain variational formulation for (6.1)-(6.4) is obtained by multiplying where appropriate by v_i

and q_i, integrating and applying the divergence theorem. The problem is to find (for $i, j = 1, 2, i \neq j$) $u_i : [0, T] \to X_i$ and $p_i : [0, T] \to Q_i$ satisfying

$$\begin{aligned}(u_{i,t}, v_i)_{\Omega_i} + (\nu_i \nabla u_i, \nabla v_i)_{\Omega_i} + (u_i \cdot \nabla u_i, v_i)_{\Omega_i} - (p_i, \nabla \cdot v_i)_{\Omega_i} \\ + \int_I \kappa |u_i - u_j|(u_i - u_j) \cdot v_i ds = (f_i, v_i)_{\Omega_i}, \ \forall\, v_i \in X_i \\ (\nabla \cdot u_i, q_i)_{\Omega_i} = 0\,, \ \forall q_i \in Q_i.\end{aligned} \tag{6.5}$$

Let $[\cdot]$ denote the jump of the indicated quantity across the interface I , $(\cdot, \cdot)$ the $L^2(\Omega_1 \cup \Omega_2)$ inner product and $\nu = \nu_i$ and $f = f_i$ in Ω_i. The coupled or monolithic problem for (6.1)-(6.4) is found by summing (6.5) over $i, j = 1, 2$ and $i \neq j$ and is to find $\mathbf{u} : [0, T] \to X$ and $\mathbf{p} : [0, T] \to Q$ satisfying

$$\begin{aligned}(\mathbf{u}_t, \mathbf{v}) + (\nu \nabla \mathbf{u}, \nabla \mathbf{v}) + (\mathbf{u} \cdot \nabla \mathbf{u}, \mathbf{v}) - (\mathbf{p}, \nabla \cdot \mathbf{v}) \\ + \int_I \kappa\, |[\mathbf{u}]|\, [\mathbf{u}] \cdot [\mathbf{v}] ds = (f, \mathbf{v}), \forall v \in X, \\ (\nabla \cdot \mathbf{u}, \mathbf{q}) = 0\,, \ \forall \mathbf{q} \in Q.\end{aligned} \tag{6.6}$$

6.1.2 Climate Model Strategies

Computations for the global climate require resolution of a large range of spatial and temporal scales for the atmosphere and ocean velocity fields. In the atmosphere the dominant eddies are between 500-10,000 km over time scales up to 1 year, [52]. In the ocean it is desirable to resolve eddies on the order of 10 - 10,000 km, [52], over time scales exceeding 1000 years [8, 28]. (See also [70] for more climate details). A climate code must employ insightful strategies to control the spatial degrees of freedom, the total number of time steps and perform calculations as efficiently as possible with limited computational power.

Efficient codes take advantage of our understanding of some climate dynamics. An example is the rigid-lid model of the atmosphere-ocean interface. The horizontal length scale is large and the result is relatively thin layers in the atmosphere and ocean along the interface. It is well known that fluxes of heat, momentum and other quantities are essentially constant across what are called the Prandtl layers, [70]. One goal of climate models is to conserve fluxes across the Prandtl layers, but for efficiency the point-wise velocities in the layers and

motion of the interface are not resolved with the rigid-lid model. The boundary condition (6.2) represents the flux of momentum across the Prandtl layers by relating the viscous drag between them to the change in velocity in the normal direction with a proportionality constant κ, [47, 70].

A natural parallel implementation is then to decouple the equations for the atmosphere and ocean components across the constant flux layers. One method is partitioned time stepping, whereby explicit updating of fluxes or interface data is used to decouple the equations numerically. Further efficiency comes from different meshing and time stepping for the decoupled subproblems. These are commonly implemented in full scale climate models, e.g. [21, 22, 27]. In the ocean more spatial degrees of freedom are needed to resolve eddies around 10-50 km than for the atmosphere where eddies below 500 km do not have as large an effect on flow statistics, [17, 67]. However, more time steps are desirable for the atmosphere to resolve time scales below an hour [52] compared to days for the ocean [70]. It is sometimes desirable to take large time steps (years) for tests which include a "spin-up" phase where the system is first run to equilibrium, requiring resolution of thousands of years due to the slow overturn of the deep ocean, [8, 28].

Current climate models are limited in the size of time step which can be taken before losing stability. Efforts have been made to relieve time step restrictions using semi-implicit time stepping, [17, 44, 62, 67], for the subproblems. To the authors knowledge no such schemes have been developed for the coupled atmosphere-ocean problem satisfying the two-way interaction condition (6.2). This chapter introduces such a scheme which allows arbitrarily large time steps while retaining stability. This is accomplished through a special partitioned time stepping scheme which balances the two-way passing of momentum flux with a semi-implicit rule for (6.2). Different size time steps are allowed for the decoupled subproblems, say Δt on Ω_1 and Δs on Ω_2, with any integer ratio $m = \Delta s/\Delta t$ between them.

Section 6.2 of this chapter introduces notational conventions and the partitioned algorithm. Preliminary lemmas useful for the numerical analysis are also provided. A full stability and convergence analysis is performed in Section 6.3. Then in Section 6.4 a computational test is performed with dynamic characteristics typical of the atmosphere-ocean system. The fluid in Ω_1 requires resolving smaller time scales with less spatial degrees of

freedom than in Ω_2. The proposed algorithm is implemented and it is shown that a time step ratio at least $m = 16$ and speed up in computational time of 13 is possible for this problem. Also, increasing the time step ratio from $m = 2$ to $m = 16$ results in a factor of 3.7 increase in error in the H^1 norm by the final time step, a sublinear growth in error with m. Also, average velocity is computed. It is observed that the relative increase in error of this measurement with the time step ratio is an order of magnitude smaller than the H^1 spatial error. This is consistent with the goal of climate modeling to reproduce statistics of flows with better accuracy than is attainable for the point-wise values of the constituent variables.

6.2 METHOD DESCRIPTION, NOTATION AND PRELIMINARIES

This section presents the numerical schemes for (6.1)-(6.4), and provides the necessary definitions and lemmas for the stability and convergence analysis. Notation follows Chapter 5 though we review a few specifics here for clarity. Let the domain $\Omega \subset \mathbb{R}^d$ $(d = 2, 3)$ have convex, polygonal subdomains Ω_i for $i = 1, 2$ with $\partial\Omega_1 \cap \partial\Omega_2 = \Omega_1 \cap \Omega_2 = I$. Let Γ_i denote the portion of $\partial\Omega_i$ that is not on I, i.e. $\Gamma_i = \partial\Omega_i \setminus I$. For $i = 1, 2$, let $X_i = \{v \in H^1(\Omega_i) \mid v|_{\Gamma_i} = g_i\}$, let $(\cdot,\cdot)_{\Omega_i}$ denote the standard L^2 inner product on Ω_i, and let $(\cdot,\cdot)_{X_i}$ denote the standard H^1 inner product on Ω_i. Define $X = X_1 \times X_2$ and $L^2(\Omega) = L^2(\Omega_1) \times L^2(\Omega_2)$ for $\mathbf{u}, \mathbf{v} \in X$ with $\mathbf{u} = [u_1, u_2]^T$ and $\mathbf{v} = [v_1, v_2]^T$, define the L^2 inner product

$$(\mathbf{u}, \mathbf{v}) = \sum_{i=1,2} \int_{\Omega_i} u_i v_i \, dx \,,$$

and H^1 inner product

$$(\mathbf{u}, \mathbf{v})_X = \sum_{i=1,2} \left(\int_{\Omega_i} u_i v_i \, dx + \int_{\Omega_i} \nabla u_i \cdot \nabla v_i \, dx \right) ,$$

and the induced norms $\|\mathbf{v}\| = (\mathbf{v}, \mathbf{v})^{1/2}$ and $\|\mathbf{v}\|_X = (\mathbf{v}, \mathbf{v})_X{}^{1/2}$, respectively. For functions $u_i \in X_i$ we further denote the L^2 norm and H^1 semi-norm by $\|u_i\|_{L^2(\Omega_i)} = \|u_i\|_{\Omega_i}$ and $|u_i|_{H^1(\Omega_i)} = |u_i|_{\Omega_i}$, respectively. The case where $g_i = 0, i = 1, 2$ will be considered here, and can be easily extended to the case of nonhomogeneous Dirichlet conditions on $\partial\Omega_i \setminus I$.

For functions $u, v, w \in X_i, i = 1, 2$ we define

$$c_i(u; v, w) = \frac{1}{2}(u \cdot \nabla v, w)_{\Omega_i} - \frac{1}{2}(u \cdot \nabla w, v)_{\Omega_i} \tag{6.7}$$

The following bounds are used in the analysis, where $u, v, w \in H^1(\Omega_i), i = 1, 2$ and $C > 0$ is a fixed constant.

$$\begin{aligned} c_i(u; v, w) &\leq C \|u\|_{\Omega_i}^{1/2} \|\nabla u\|_{\Omega_i}^{1/2} \|\nabla v\|_{\Omega_i} \|\nabla w\|_{\Omega_i} && (6.8) \\ \int_I u|[v]| \cdot w \, ds &\leq C \|u\|_{L^3(I)} \|[v]\|_{L^3(I)} \|w\|_{L^3(I)} && (6.9) \\ \|u\|_{L^3(I)} &\leq C \|u\|_{\Omega_i}^{1/4} \|\nabla u\|_{\Omega_i}^{3/4} && (6.10) \end{aligned}$$

To maintain a compact notation, we denote by $\|\cdot\|_I$ the norm on $L^3(I)$. The numerical analysis will be greatly simplified by repeated application of the following lemma, which will be used to bound errors occuring in the subsequent algorithm due to the method of time discretization. The lemma was proved in Chapter 5.

Lemma 6.2.1. *Let $i, j \in \{1, 2\}$ and $\{\alpha_1, \alpha_2, \beta_1, \beta_2\}$ arbitrary positive real numbers. For functions $u_i \in X_i$, $v_j \in X_j$, $\mathbf{w} \in X$ the following bounds hold.*

$$\begin{aligned} \kappa \int_I |u_i||[\mathbf{w}]||v_j| \, ds &\leq C \frac{\kappa^2}{4} \|u_i\|_I^2 \|[\mathbf{w}]\|_I^2 + \frac{\alpha_j^3}{\nu_j^3} \|v_j\|_{\Omega_j}^2 + \frac{\nu_j}{2\alpha_j} \|\nabla v_j\|_{\Omega_j}^2 && (6.11) \\ \kappa \int_I |u_i||[\mathbf{w}]||v_j| \, ds &\leq C \frac{\kappa^4 \alpha_i^3}{\nu_i^3} \|[\mathbf{w}]\|_I^4 \|u_i\|_{\Omega_i}^2 + \frac{\nu_i}{4\alpha_i} \|\nabla u_i\|_{\Omega_i}^2 \\ &+ C \frac{\kappa^4 \beta_j^3}{\nu_j^3} \|[\mathbf{w}]\|_I^4 \|v_j\|_{\Omega_j}^2 + \frac{\nu_j}{4\beta_j} \|\nabla v_j\|_{\Omega_j}^2 && (6.12) \\ \kappa \int_I |u_i||[\mathbf{w}]||v_j| \, ds &\leq C\kappa^4 \|u_i\|_I^4 \left\{ \frac{\alpha_1^3}{\nu_1^3} \|w_1\|_{\Omega_1}^2 + \frac{\alpha_2^3}{\nu_2^3} \|w_2\|_{\Omega_2}^2 + \frac{2\beta_j^3}{\nu_j^3} \|v_j\|_{\Omega_j}^2 \right\} \\ &+ \frac{1}{4} \left\{ \frac{\nu_1}{\alpha_1} \|\nabla w_1\|_{\Omega_1}^2 + \frac{\nu_2}{\alpha_2} \|\nabla w_2\|_{\Omega_2}^2 + \frac{2\nu_j}{\beta_j} \|\nabla v_j\|_{\Omega_j}^2 \right\} && (6.13) \end{aligned}$$

The following identity valid for vector w^{j+1}, w^j is used in the stability proof and later for convergence.

$$(w^{j+1} - w^j) \cdot w^{j+1} = \frac{1}{2} \left(|w^{j+1}|^2 + |w^{j+1} - w^j|^2 - |w^j|^2 \right). \tag{6.14}$$

6.2.1 Discretization of the Weak Problem

Choose a uniform distribution of discrete time levels

$$\mathcal{P} = \{t^0 = 0, t^1, t^2, \ldots, t^N = T\},$$

where $t^n = n\Delta t, n = 0, 1, \ldots, N$ for $\Delta t = \frac{t_f}{N}$. Denote by

$$\mathcal{S} = \{t^{n_0}, t^{n_1}, \ldots, t^{n_M}\} \subset \mathcal{P}$$

a subset satisfying $t^{n_k} = km\Delta t$ such that $m \in \mathbb{N}$ is fixed and $Mm = N$. The time step size on Ω_2 is given a separate notation hereafter, $\Delta s = m\Delta t$. For $t^k \in [0, T]$, $(\mathbf{u}^k, \mathbf{p}^k)$ will denote the discrete approximation to $(\mathbf{u}(t^k), \mathbf{p}(t^k))$.

The polygonal subdomains Ω_1 and Ω_2 are covered by simplex meshes τ_1^h and τ_2^h. The mesh size h is the largest diameter of a simplex in either τ_1^h or τ_2^h. Finite element spaces X_i^h for velocity and Q_i^h for pressure relative to the meshes τ_i^h, $i = 1, 2$, are assumed to satisfy the LBB^h condition. Discretely divergence free velocities will be sought in the test space

$$V_i^h = \left\{ v \in X_i^h : \int_{\Omega_i} q \, \nabla \cdot v \, d\Omega_i = 0, \ \forall q \in Q_i^h \right\}, \ i = 1, 2.$$

Also, the following optimal approximation properties are assumed for $i = 1, 2$ and some $r \in \mathbb{N}$:

$$\inf_{v \in V_i^h} \|u - v\|_{L^2(\Omega_i)} \leq Ch^{r+1} |u|_{H^{r+1}(\Omega_i)}$$

$$\inf_{v \in V_i^h} \|u - v\|_{H^1(\Omega_i)} \leq Ch^{r} |u|_{H^{r+1}(\Omega_i)}$$

$$\inf_{q \in Q_i^h} \|u - v\|_{L^2(\Omega_i)} \leq Ch^{r+1} |u|_{H^{r+1}(\Omega_i)}.$$

The approximations $u_1^{n+1} \in V_{1,h}$ for $n = n_1, n_1 + 1, \ldots, N - 1$ and $u_2^{n_{k+1}} \in V_{2,h}$ for $k = 1, \ldots, M - 1$ are calculated using Algorithm 6.2.1. In practice only the data at times t^0 and t^{n_1} would need to be provided. However, the statement of the algorithm and presentation of stability and convergence results is made more concise assuming the data u_1^n, $n = 0, 1, \ldots, n_1$ and $u_2^{n_k}$ for $k = 0, 1$ to be given. One important feature of Algorithm 6.2.1 is that u_1^{n+1} can be calculated for $n = n_k, n_k + 1, \ldots, n_{k+1} - 1$ in parallel with $u_2^{n_{k+1}}$.

Algorithm 6.2.1 (Partitioned Scheme)**.** *Let* $\mathbf{f} \in L^2(\Omega)$. *Given* $u_2^{n_k}$, $u_2^{n_{k-1}} \in V_{2,h}$ *and* $u_1^j \in V_{1,h}$ *for* $j = n_{k-1}, n_{k-1}+1, \ldots, n_k$ *do the following.*

- *Set* $S^k = \frac{1}{m}\sum_{n=n_{k-1}}^{n_k-1} u_1^{n+1}$.
- *Find* $u_1^{n+1} \in V_{1,h}$ *for* $n = n_k, n_k+1, \ldots, n_{k+1}-1$ *satisfying*

$$\begin{aligned}\left(\frac{u_1^{n+1}-u_1^n}{\Delta t}, v_1\right)_{\Omega_1} &+ \nu_1\left(\nabla u_1^{n+1}, \nabla v_1\right)_{\Omega_1} + c_1(u_1^{n+1}; u_1^{n+1}, v_1) \\ &+ \kappa\int_I |[\mathbf{u}^{n_k}]| u_1^{n+1}\cdot v_1\, ds - \kappa\int_I |[\mathbf{u}^{n_k}]|^{1/2}|[\mathbf{u}^{n_{k-1}}]|^{1/2} u_2^{n_k}\cdot v_1\, ds \\ &= \left(f_1(t^{n+1}), v_1\right)_{\Omega_1},\ \forall v_1 \in V_{1,h}.\end{aligned} \tag{6.15}$$

- *Find* $u_2^{n_{k+1}} \in V_{2,h}$ *satisfying*

$$\begin{aligned}\left(\frac{u_2^{n_{k+1}}-u_2^{n_k}}{m\Delta t}, v_2\right)_{\Omega_2} &+ \nu_2\left(\nabla u_2^{n_{k+1}}, \nabla v_2\right)_{\Omega_2} + c_2(u_2^{n_{k+1}}; u_2^{n_{k+1}}, v_2) \\ &+ \kappa\int_I |[\mathbf{u}^{n_k}]| u_2^{n_{k+1}}\cdot v_2\, ds - \kappa\int_I |[\mathbf{u}^{n_k}]|^{1/2}|[\mathbf{u}^{n_{k-1}}]|^{1/2} S^k\cdot v_2\, ds \\ &= \left(f_2(t^{n_{k+1}}), v_2\right)_{\Omega_2},\ \forall v_2 \in V_{2,h}.\end{aligned} \tag{6.16}$$

- *Set* $k = k+1$ *and repeat until* $k = M$.

6.3 NUMERICAL ANALYSIS

Lemma 6.3.1. *(Partitioned Stability) Let* $u_1^j \in X_{1,h}$ *satisfy (6.15) for each* $j \in \{0, \cdots, n_p\}$, *and* $u_2^{n_k} \in X_{2,h}$ *satisfy (6.16) for each* $k \in \{0, 1, 2, \cdots, p \le M\}$. *Then Algorithm 6.2.1 is*

unconditionally stable, and at time step n_p satisfies:

$$\begin{aligned}
&\|\mathbf{u}^{n_p}\|^2 + \sum_{k=1}^{p-1} \|u_2^{n_{k+1}} - u_2^{n_k}\|_{\Omega_2}^2 + \sum_{n=n_1}^{n_p-1} \|u_1^{n+1} - u_1^n\|_{\Omega_1}^2 \\
&+ \nu_1 \, \Delta t \sum_{n=n_1}^{n_p-1} \|\nabla u_1^{n+1}\|_{\Omega_1}^2 + m \, \Delta t \, \nu_2 \sum_{k=1}^{p-1} \|\nabla u_2^{n_{k+1}}\|_{\Omega_2}^2 \\
&+ m \, \kappa \Delta t \int_I |u_2^{n_p}|^2 |[\mathbf{u}^{n_{p-1}}]| \, ds + \kappa \Delta t \sum_{n_{p-1}}^{n_p-1} \int_I |u_1^{n+1}|^2 |[\mathbf{u}^{n_{p-1}}]| \, ds \qquad (6.17) \\
&\leq \frac{\Delta t}{\nu_1} \sum_{n=n_k}^{n_{k+1}-1} \|f_1(t^{n+1})\|_{X_1'}^2 + \frac{m \Delta t}{\nu_2} \|f_2(t^{n_{k+1}})\|_{X_2'}^2 + \|\mathbf{u}^{n_1}\|^2 \\
&+ m \, \kappa \Delta t \int_I |u_2^{n_1}|^2 |[\mathbf{u}^0]| \, ds + \kappa \Delta t \sum_{n=0}^{n_1-1} \int_I |u_1^{n+1}|^2 |[\mathbf{u}^0]| \, ds.
\end{aligned}$$

Proof. Choose $v_1 = u_1^{n+1}$ in (6.15). After summation over $n = n_k, n_k + 1, \ldots, n_{k+1} - 1$ one obtains

$$\begin{aligned}
&\sum_{n=n_k}^{n_{k+1}-1} \left(\frac{u_1^{n+1} - u_1^n}{\Delta t}, u_1^{n+1} \right)_{\Omega_1} + \nu_1 \sum_{n=n_k}^{n_{k+1}-1} \|\nabla u_1^{n+1}\|_{\Omega_1}^2 \\
&\quad + \sum_{n=n_k}^{n_{k+1}-1} \left\{ \kappa \int_I |u_1^{n+1}|^2 |[\mathbf{u}^{n_k}]| \, ds - \kappa \int_I u_2^{n_k} \cdot u_1^{n+1} |[\mathbf{u}^{n_k}]|^{1/2} |[\mathbf{u}^{n_{k-1}}]|^{1/2} \, ds \right\} \qquad (6.18) \\
&\qquad = \sum_{n=n_k}^{n_{k+1}-1} \left(f_1(t^{n+1}), u_1^{n+1} \right)_{\Omega_1}.
\end{aligned}$$

Choose $v_2 = u_2^{n_{k+1}}$ in (6.16). Multiply through (6.16) by m and substitute in for S^k to obtain:

$$\begin{aligned}
&\frac{1}{\Delta t} \left(u_2^{n_{k+1}} - u_2^{n_k}, u_2^{n_{k+1}} \right)_{\Omega_2} + m \, \nu_2 \|\nabla u_2^{n_{k+1}}\|_{\Omega_2}^2 + m \, \kappa \int_I |u_2^{n_{k+1}}|^2 |[\mathbf{u}^{n_k}]| \, ds \\
&\quad - \sum_{n=n_{k-1}}^{n_k-1} \kappa \int_I u_1^{n+1} \cdot u_2^{n_{k+1}} |[\mathbf{u}^{n_k}]|^{1/2} |[\mathbf{u}^{n_{k-1}}]|^{1/2} \, ds = m \left(f_2(t^{N_{n+1}}), u_2^{n_{k+1}} \right)_{\Omega_2}.
\end{aligned} \qquad (6.19)$$

Substitute using (6.14) for the first terms on the left hand side of (6.18)-(6.19). Combining results, it follows

$$\begin{aligned}
&\frac{1}{2\Delta t}\Big\{\|\mathbf{u}^{n_{k+1}}\|^2 - \|\mathbf{u}^{n_k}\|^2 + \|u_2^{n_{k+1}} - u_2^{n_k}\|_{\Omega_2}^2 + \sum_{n=n_k}^{n_{k+1}-1} \|u_1^{n+1} - u_1^n\|_{\Omega_1}^2\Big\} \\
&\quad + \nu_1 \sum_{n=n_k}^{n_{k+1}-1} \|\nabla u_1^{n+1}\|_{\Omega_1}^2 + m\,\nu_2 \|\nabla u_2^{n_{k+1}}\|_{\Omega_2}^2 + \sum_{n=n_k}^{n_{k+1}-1} \kappa \int_I |u_1^{n+1}|^2 |[\mathbf{u}^{n_k}]|\, ds \\
&\quad + m\,\kappa \int_I |u_2^{n_{k+1}}|^2 |[\mathbf{u}^{n_k}]|\, ds - \sum_{n=n_k}^{n_{k+1}-1} \kappa \int_I u_2^{n_k} \cdot u_1^{n+1} |[\mathbf{u}^{n_k}]|^{1/2} |[\mathbf{u}^{n_{k-1}}]|^{1/2}\, ds \\
&\quad - \sum_{n=n_{k-1}}^{n_k-1} \kappa \int_I u_1^{n+1} \cdot u_2^{n_{k+1}} |[\mathbf{u}^{n_k}]|^{1/2} |[\mathbf{u}^{n_{k-1}}]|^{1/2}\, ds \\
&\quad = \sum_{n=n_k}^{n_{k+1}-1} \left(f_1(t^{n+1}), u_1^{n+1}\right)_{\Omega_1} + m \left(f_2(t^{N_{n+1}}), u_2^{n_{k+1}}\right)_{\Omega_2}.
\end{aligned} \tag{6.20}$$

Estimates are now shown for the interface integrals in (6.20) which will illustrate the stability of the method. In particular, the positive interface terms control the terms being subtracted, which can be seen by first bounding the size of the latter terms.

$$\begin{aligned}
&\sum_{n=n_k}^{n_{k+1}-1} \kappa \int_I u_2^{n_k} \cdot u_1^{n+1} |[\mathbf{u}^{n_k}]|^{1/2} |[\mathbf{u}^{n_{k-1}}]|^{1/2}\, ds \\
&\qquad \le \sum_{n=n_k}^{n_{k+1}-1} \frac{\kappa}{2} \int_I |u_1^{n+1}|^2 |[\mathbf{u}^{n_k}]|\, ds + m\,\frac{\kappa}{2} \int_I |u_2^{n_k}|^2 |[\mathbf{u}^{n_{k-1}}]|\, ds
\end{aligned} \tag{6.21}$$

$$\begin{aligned}
&\sum_{n=n_{k-1}}^{n_k-1} \kappa \int_I u_1^{n+1} \cdot u_2^{n_{k+1}} |[\mathbf{u}^{n_k}]|^{1/2} |[\mathbf{u}^{n_{k-1}}]|^{1/2}\, ds \\
&\le \sum_{n=n_{k-1}}^{n_k-1} \frac{\kappa}{2} \int_I |u_1^{n+1}|^2 |[\mathbf{u}^{n_{k-1}}]|\, ds + \frac{m\kappa}{2} \int_I |u_2^{n_{k+1}}|^2 |[\mathbf{u}^{n_k}]|\, ds
\end{aligned} \tag{6.22}$$

Bound the right hand side of (6.20) by:

$$\sum_{n=n_k}^{n_{k+1}-1} \left(f_1(t^{n+1}), u_1^{n+1}\right)_{\Omega_1} + m\left(f_2(t^{n_{k+1}}), u_2^{n_{k+1}}\right)$$
$$\leq \frac{1}{2\nu_1} \sum_{n=n_k}^{n_{k+1}-1} \|f_1(t^{n+1})\|_{X_1'}^2 + \frac{m}{2\nu_2}\|f_2(t^{n_{k+1}})\|_{X_2'}^2 \tag{6.23}$$
$$+ \frac{\nu_1}{2} \sum_{n=n_k}^{n_{k+1}-1} \|\nabla u_1^{n+1}\|_{\Omega_1}^2 + \frac{m\,\nu_2}{2}\|u_2^{n_{k+1}}\|_{\Omega_2}^2.$$

Insert the results (6.21)-(6.23) into (6.20). After some basic algebra,

$$\frac{1}{2\Delta t}\left\{\|\mathbf{u}^{n_{k+1}}\|^2 - \|\mathbf{u}^{n_k}\|^2 + \|u_2^{n_{k+1}} - u_2^{n_k}\|_{\Omega_2}^2 + \sum_{n=n_k}^{n_{k+1}-1} \|u_1^{n+1} - u_1^n\|_{\Omega_1}^2\right\}$$
$$+ \frac{\nu_1}{2} \sum_{n=n_k}^{n_{k+1}-1} \|\nabla u_1^{n+1}\|_{\Omega_1}^2 + \frac{m\,\nu_2}{2}\|\nabla u_2^{n_{k+1}}\|_{\Omega_2}^2$$
$$+ \frac{m\,\kappa}{2}\int_I |u_2^{n_{k+1}}|^2 |[\mathbf{u}^{n_k}]|\, ds - \frac{m\,\kappa}{2}\int_I |u_2^{n_k}|^2 |[\mathbf{u}^{n_{k-1}}]|\, ds$$
$$+ \sum_{n=n_k}^{n_{k+1}-1} \frac{\kappa}{2}\int_I |u_1^{n+1}|^2 |[\mathbf{u}^{n_k}]|\, ds - \sum_{n=n_{k-1}}^{n_k-1} \frac{\kappa}{2}\int_I |u_1^{n+1}|^2 |[\mathbf{u}^{n_{k-1}}]|\, ds$$
$$\leq \frac{1}{2\nu_1} \sum_{n=n_k}^{n_{k+1}-1} \|f_1(t^{n+1})\|_{X_1'}^2 + \frac{m}{2\nu_2}\|f_2(t^{n_{k+1}})\|_{X_2'}^2.$$

Next multiply through by $2\Delta t$ and sum over $k = 1, 2, \ldots, (p-1) \leq (M-1)$. Rearranging terms yields the final result. □

The structure of the interface integrals in Algorithm 6.2.1 and different time steps used in the subdomains results in a technical convergence proof with numerous terms in the error estimates. The strategy is to first decompose the error $u_i(t^j) - u_i^j$ into $\eta_i^j + \phi_i^j$ such that $\eta_i^j = u_i(t^j) - \tilde{u}_i^j$ and $\phi_i^j = \tilde{u}_i^j - u_i^j$ with $\tilde{u}_i^j \in X_i^h$ arbitrary. Then preliminary error estimates are developed separately for ϕ_1^j in Lemma 6.3.2 and for ϕ_2^j in Lemma 6.3.3. Theorem 6.3.4 then combines these results and explains a non-standard application of the discrete Gronwall inequality in developing the final estimates.

Lemma 6.3.2. *Let $u_2^{n_{k+1}} \in X_{2,h}$ satisfy (6.16) for each $k \in \{1, 2, \cdots, p \leq M-1\}$ and $u_1^{j+1} \in X_{1,h}$ satisfy (6.15) for each $j \in \{n_1, n_1+1, \cdots, q \leq N-1\}$, $n_p < q$. Assume a sufficiently regular solution $(\mathbf{u}, \mathbf{p})$ to (6.6). Then there exists a constant $C > 0$ depending only on Ω, $\mathbf{u}$, $\mathbf{p}$, $\mathbf{f}$ such that*

$$
\begin{aligned}
&\frac{1}{2\Delta t}\left(\|\phi_1^{n+1}\|_{\Omega_1}^2 - \|\phi_1^n\|_{\Omega_1}^2 + \|\phi_1^{n+1} - \phi_1^n\|_{\Omega_1}^2\right) + \frac{7\nu_1}{8}\|\nabla\phi_1^{n+1}\|_{\Omega_1}^2 \\
&\leq C\left\{ {\nu_1}^{-1}\|\frac{\eta_1^{n+1} - \eta_1^n}{\Delta t}\|_{X_1'}^2 + \nu_1^{-1}\|p_1(t^{n+1}) - q_1\|_{\Omega_1}^2 + \nu_1^{-1}\|R_1^{n+1}\|_{X_1'}^2 \right. \\
&+ \left(\nu_1 + (1+\nu_1^{-1})\|\nabla u_1(t^{n+1})\|_{\Omega_1}\right)\|\nabla\eta_1^{n+1}\|_{\Omega_1}^2 + \kappa^2 L_k^{n+1} P_k^{n+1} \\
&+ \left(1 + \nu_1^{-1} + \nu_1^{-3} + \nu_1^{-1}\|\nabla u_1(t^{n+1})\|_{\Omega_1}^2 + \nu_1^{-3}\|\nabla u_1(t^{n+1})\|_{\Omega_1}^4\right)\|\phi_1^{n+1}\|_{\Omega_1}^2 \\
&\left. + \kappa^4 J_k^{n+1}\left(\nu_1^{-3}\|\phi_1^{n+1}\|_{\Omega_1}^2 + m\sum_{i=1,2}(1+\nu_i^{-3})\left\{\|\phi_i^{n_k}\|_{\Omega_i}^2 + \|\phi_i^{n_{k-1}}\|_{\Omega_i}^2\right\}\right)\right\} \\
&+ \frac{\nu_1}{8m}\|\nabla\phi_1^{n_k}\|_{\Omega_1}^2 + \frac{\nu_2}{8}\|\nabla\phi_2^{n_k}\|_{\Omega_2}^2 + \frac{\nu_1}{8m}\|\nabla\phi_1^{n_{k-1}}\|_{\Omega_1}^2 + \frac{\nu_2}{8}\|\nabla\phi_2^{n_{k-1}}\|_{\Omega_2}^2.
\end{aligned}
\tag{6.24}
$$

where J_k^{n+1} and L_k^{n+1} are defined for $n_k \leq n < n_{k+1}$, $k = 1, 2, \ldots, M-1$ by:

$$
\begin{aligned}
J_k^{n+1} &= \left\|u_1(t^{n+1})\right\|_I^4 + \left\|u_2(t^{n+1})\right\|_I^4 + \|u_1^{n_k}\|_I^4 + \|u_2^{n_k}\|_I^4 + \left\|u_1^{n_{k+1}}\right\|_I^4 + \left\|u_2^{n_{k+1}}\right\|_I^4, \\
L_k^{n+1} &= \left\|u_1(t^{n+1})\right\|_I^2 + \left\|u_2(t^{n+1})\right\|_I^2 + \|u_1^{n_k}\|_I^2 + \|u_2^{n_k}\|_I^2 + \left\|u_1^{n_{k+1}}\right\|_I^2 + \left\|u_2^{n_{k+1}}\right\|_I^2,
\end{aligned}
$$

P_k^{n+1} is defined for $n_k \leq n < n_{k+1}$, $k = 1, 2, \ldots, M-1$ by:

$$
\begin{aligned}
P_k^{n+1} = &\left\|u_1(t^{n+1}) - u_1(t^{n_k})\right\|_I^2 + \left\|u_2(t^{n+1}) - u_2(t^{n_k})\right\|_I^2 \\
&+ \left\|u_1(t^{n+1}) - u_1(t^{n_{k-1}})\right\|_I^2 + \left\|u_2(t^{n+1}) - u_2(t^{n_{k-1}})\right\|_I^2 \\
&+ \|\eta_1^{n_k}\|_I^2 + \|\eta_2^{n_k}\|_I^2 + \left\|\eta_1^{n_{k-1}}\right\|_I^2 + \left\|\eta_2^{n_{k-1}}\right\|_I^2 + \left\|\eta_1^{n+1}\right\|_I^2,
\end{aligned}
$$

and R_1^{n+1} is defined for $n = n_1, n_1+1, \ldots, N-1$ by:

$$
R_1^{n+1} = \frac{u_1(t^{n+1}) - u_1(t^n)}{\Delta t} - \frac{\partial u_1(t^{n+1})}{\partial t}.
$$

Proof. Take the variational formulation for the true solution $u_1(t^{n+1})$ on Ω_1 and subtract (6.15),

$$\begin{aligned}
&\frac{1}{\Delta t}\left((u_1(t^{n+1})-u_1^{n+1})-(u_1(t^n)-u_1^n),v_1\right)_{\Omega_1}+\nu_1\left(\nabla(u_1(t^{n+1})-u_1^{n+1}),\nabla v_1\right)_{\Omega_1}\\
&\quad+c_1\left(u_1(t^{n+1});u_1(t^{n+1}),v_1\right)-c_1\left(u_1^{n+1};u_1^{n+1},v_1\right)-\left(p_1(t^{n+1})-q_1,\nabla\cdot v_1\right)_{\Omega_1}\\
&\quad+\kappa\int_I u_1(t^{n+1})|[\mathbf{u}(t^{n+1})]|\cdot v_1\,ds-\kappa\int_I u_1^{n+1}|[\mathbf{u}^{n_k}]|\cdot v_1\,ds\\
&\quad+\kappa\int_I u_2^{n_k}|[\mathbf{u}^{n_k}]|^{1/2}|[\mathbf{u}^{n_{k-1}}]|^{1/2}\cdot v_1\,ds-\kappa\int_I u_2(t^{n+1})|[\mathbf{u}(t^{n+1})]|\cdot v_1\,ds\\
&\quad=\left(\frac{u_1(t^{n+1})-u_1(t^n)}{\Delta t}-\frac{\partial u_1(t^{n+1})}{\partial t},v_1\right)_{\Omega_1},\ \forall v_1\in V_{1,h}\,,\ \forall q_1\in Q_{1,h}.
\end{aligned}$$

Errors are decomposed using the equation

$$u_i(t^j)-u_i^j=(u_i(t^j)-\tilde{u_i}^j)+(\tilde{u_i}^j-u_i^j)=\eta_i^j+\phi_i^j$$

as previously described. Choosing $v_1=\phi_1^{n+1}$ the above error equation is rewritten as

$$\begin{aligned}
&\frac{1}{\Delta t}\left(\eta_1^{n+1}-\eta_1^n,\phi_1^{n+1}\right)_{\Omega_1}+\frac{1}{\Delta t}\left(\phi_1^{n+1}-\phi_1^n,\phi_1^{n+1}\right)_{\Omega_1}+\nu_1\left(\nabla\eta_1^{n+1},\nabla\phi_1^{n+1}\right)_{\Omega_1}+\nu_1\|\nabla\phi_1^{n+1}\|_{\Omega_1}^2\\
&\quad+c_1\left(u_1(t^{n+1});u_1(t^{n+1}),\phi_1^{n+1}\right)-c_1\left(u_1^{n+1};u_1^{n+1},\phi_1^{n+1}\right)-\left(p_1(t^{n+1})-q_1,\nabla\cdot v_1\right)_{\Omega_1}\\
&\quad+\kappa\int_I u_1(t^{n+1})|[\mathbf{u}(t^{n+1})]|\cdot\phi_1^{n+1}\,ds-\kappa\int_I u_1^{n+1}|[\mathbf{u}^{n_k}]|\cdot\phi_1^{n+1}\,ds\\
&\quad+\kappa\int_I u_2^{n_k}|[\mathbf{u}^{n_k}]|^{1/2}|[\mathbf{u}^{n_{k-1}}]|^{1/2}\cdot\phi_1^{n+1}\,ds-\kappa\int_I u_2(t^{n+1})|[\mathbf{u}(t^{n+1})]|\cdot\phi_1^{n+1}\,ds\\
&\quad=\left(R_1^{n+1},\phi_1^{n+1}\right)_{\Omega_1},
\end{aligned}$$

The goal is to bound ϕ_1^{n+1}, hence we move many terms to the right hand side. The identity (6.14) is then applied on the left hand side:

$$\begin{aligned}
&\frac{1}{2\Delta t}\left(\|\phi_1^{n+1}\|_{\Omega_1}^2 - \|\phi_1^{n}\|_{\Omega_1}^2 + \|\phi_1^{n+1}-\phi_1^{n}\|_{\Omega_1}^2\right) + \nu_1\|\nabla\phi_1^{n+1}\|_{\Omega_1}^2 \\
&\quad + \left\{\kappa\int_I u_1(t^{n+1})|[\mathbf{u}(t^{n+1})]|\cdot\phi_1^{n+1}\,ds - \kappa\int_I u_1^{n+1}|[\mathbf{u}^{n_k}]|\cdot\phi_1^{n+1}\,ds\right\} \\
&\quad + \left\{\kappa\int_I u_2^{n_k}|[\mathbf{u}^{n_k}]|^{1/2}|[\mathbf{u}^{n_{k-1}}]|^{1/2}\cdot\phi_1^{n+1}\,ds - \kappa\int_I u_2(t^{n+1})|[\mathbf{u}(t^{n+1})]|\cdot\phi_1^{n+1}\,ds\right\} \\
&\quad = -\frac{1}{\Delta t}\left(\eta_1^{n+1}-\eta_1^{n},\phi_1^{n+1}\right)_{\Omega_1} - \nu_1\left(\nabla\eta_1^{n+1},\nabla\phi_1^{n+1}\right)_{\Omega_1} + \left(p_1(t^{n+1})-q_1,\nabla\cdot\phi_1^{n+1}\right)_{\Omega_1} \\
&\quad - c_1\left(u_1(t^{n+1});u_1(t^{n+1}),\phi_1^{n+1}\right) + c_1\left(u_1^{n+1};u_1^{n+1},\phi_1^{n+1}\right) + \left(R_1^{n+1},\phi_1^{n+1}\right)_{\Omega_1}.
\end{aligned} \tag{6.25}$$

Bounds for the non-interface terms follow as in the standard NSE case, (see e.g. [45]). The interface terms require special treatment. First, note by adding and subtracting terms in sequence one may derive the following expression.

$$\begin{aligned}
\kappa\int_I u_1(t^{n+1})|[\mathbf{u}(t^{n+1})]|\cdot\phi_1^{n+1}\,ds - \kappa\int_I u_1^{n+1}|[\mathbf{u}^{n_k}]|\cdot\phi_1^{n+1}\,ds& \\
= \kappa\int_I u_1(t^{n+1})\left(|[\mathbf{u}(t^{n+1})]| - |[\mathbf{u}(t^{n_k})]|\right)\cdot\phi_1^{n+1}\,ds& \\
+ \kappa\int_I u_1(t^{n+1})\left(|[\mathbf{u}(t^{n_k})]| - |[\tilde{\mathbf{u}}^{n_k}]|\right)\cdot\phi_1^{n+1}\,ds& \\
+ \kappa\int_I u_1(t^{n+1})\left(|[\tilde{\mathbf{u}}^{n_k}]| - |[\mathbf{u}^{n_k}]|\right)\cdot\phi_1^{n+1}\,ds& \\
+ \kappa\int_I \eta_1^{n+1}|[\mathbf{u}^{n_k}]|\cdot\phi_1^{n+1}\,ds + \kappa\int_I |\phi_1^{n+1}|^2|[\mathbf{u}^{n_k}]|\,ds.&
\end{aligned} \tag{6.26}$$

The splitting used for the remaining pair of interface integrals is more complicated due to the product $|[\mathbf{u}^{n_k}]|^{1/2}|[\mathbf{u}^{n_{k-1}}]|^{1/2}$. The key is to recognize an error of $O(\Delta t)$ is committed in replacing the product $|[\mathbf{u}(t^{n_k})]|^{1/2}|[\mathbf{u}(t^{n_{k-1}})]|^{1/2}$ with the average $\frac{1}{2}(|[\mathbf{u}(t^{n_k})]|+|[\mathbf{u}(t^{n_{k-1}})]|)$.

We proceed as follows.

$$
\begin{aligned}
&\kappa \int_I u_2^{n_k} |[\mathbf{u}^{n_k}]|^{1/2} |[\mathbf{u}^{n_{k-1}}]|^{1/2} \cdot \phi_1^{n+1}\, ds - \kappa \int_I u_2(t^{n+1}) |[\mathbf{u}(t^{n+1})]| \cdot \phi_1^{n+1}\, ds \\
&= \kappa \int_I u_2^{n_k} \left\{ |[\mathbf{u}^{n_k}]|^{1/2} |[\mathbf{u}^{n_{k-1}}]|^{1/2} - \frac{1}{2}(|[\mathbf{u}^{n_k}]| + |[\mathbf{u}^{n_{k-1}}]|) \right\} \cdot \phi_1^{n+1}\, ds \\
&+ \frac{1}{2}\kappa \int_I u_2^{n_k} \left\{ (|[\mathbf{u}^{n_k}]| + |[\mathbf{u}^{n_{k-1}}]|) - (|[\tilde{\mathbf{u}}^{n_k}]| + |[\tilde{\mathbf{u}}^{n_{k-1}}]|) \right\} \cdot \phi_1^{n+1}\, ds \\
&+ \frac{1}{2}\kappa \int_I u_2^{n_k} \left\{ (|[\tilde{\mathbf{u}}^{n_k}]| + |[\tilde{\mathbf{u}}^{n_{k-1}}]|) - (|[\mathbf{u}(t^{n_k})]| + |[\mathbf{u}(t^{n_{k-1}})]|) \right\} \cdot \phi_1^{n+1}\, ds \\
&+ \kappa \int_I u_2^{n_k} \left\{ \frac{1}{2}(|[\mathbf{u}(t^{n_k})]| + |[\mathbf{u}(t^{n_{k-1}})]|) - |[\mathbf{u}(t^{n+1})]| \right\} \cdot \phi_1^{n+1}\, ds \\
&- \kappa \int_I \phi_2^{n_k} |[\mathbf{u}(t^{n+1})]| \cdot \phi_1^{n+1}\, ds - \kappa \int_I \eta_2^{n_k} |[\mathbf{u}(t^{n+1})]| \cdot \phi_1^{n+1}\, ds \\
&+ \kappa \int_I (u_2(t^{n_k}) - u_2(t^{n+1})) |[\mathbf{u}(t^{n+1})]| \cdot \phi_1^{n+1}\, ds
\end{aligned}
\tag{6.27}
$$

Using (6.26) - (6.27), substitution for the interface integrals in (6.25) is performed. The last term of (6.26) is positive and may be kept on the left hand side of (6.25), but all other interface terms are now moved to the right hand side, and bounded. Applying the reverse triangle inequality and the equality $[a] - [b] = [a - b]$ for $a, b \in X$, we first note

$$
\begin{aligned}
\big| |[\mathbf{u}(t^j)]| - |[\tilde{\mathbf{u}}^j]| \big| &\leq |[\boldsymbol{\eta}^j]| \\
\big| |[\tilde{\mathbf{u}}^j]| - |[\mathbf{u}^j]| \big| &\leq |[\boldsymbol{\phi}^j]|
\end{aligned}
$$

and thus one may derive the following error inequality:

$$
\begin{aligned}
&\frac{1}{2\Delta t} \left(\|\phi_1^{n+1}\|_{\Omega_1}^2 - \|\phi_1^n\|_{\Omega_1}^2 + \|\phi_1^{n+1} - \phi_1^n\|_{\Omega_1}^2 \right) + \nu_1 \|\nabla \phi_1^{n+1}\|_{\Omega_1}^2 + \kappa \int_I |\phi_1^{n+1}|^2 |[\mathbf{u}^{n_k}]|\, ds \\
&\leq -\frac{1}{\Delta t} \left(\eta_1^{n+1} - \eta_1^n, \phi_1^{n+1} \right)_{\Omega_1} - \nu_1 \left(\nabla \eta_1^{n+1}, \nabla \phi_1^{n+1} \right)_{\Omega_1} + \left(p_1(t^{n+1}) - q_1, \nabla \cdot \phi_1^{n+1} \right)_{\Omega_1} \\
&- c_1 \left(u_1(t^{n+1}); u_1(t^{n+1}), \phi_1^{n+1} \right) + c_1 \left(u_1^{n+1}; u_1^{n+1}, \phi_1^{n+1} \right) + \left(R_1^{n+1}, \phi_1^{n+1} \right)_{\Omega_1} \\
&+ I1 + I2 + I3 + I4.
\end{aligned}
\tag{6.28}
$$

The Ij-terms denote the following interface integrals, which will be subsequently bounded.

$$
\begin{aligned}
I1 &= \kappa \int_I |u_1(t^{n+1})|||[\mathbf{u}(t^{n+1}) - \mathbf{u}(t^{n_k})]|||\phi_1^{n+1}|\, ds + \kappa \int_I |u_1(t^{n+1})|||[\boldsymbol{\eta}^{n_k}]|||\phi_1^{n+1}|\, ds \\
&+ \kappa \int_I |u_2(t^{n_k}) - u_2(t^{n+1})|||[\mathbf{u}(t^{n+1})]|||\phi_1^{n+1}|\, ds + \kappa \int_I |\eta_1^{n+1}|||[\mathbf{u}^{n_k}]|||\phi_1^{n+1}|\, ds \\
&+ \frac{1}{2}\kappa \int_I |u_2^{n_k}|(|[\boldsymbol{\eta}^{n_k}]| + |[\boldsymbol{\eta}^{n_{k-1}}]|)|\phi_1^{n+1}|\, ds + \kappa \int_I |\eta_2^{n_k}|||[\mathbf{u}(t^{n+1})]|||\phi_1^{n+1}|\, ds \\
I2 &= \frac{1}{2}\kappa \int_I |u_2^{n_k}|(|[\boldsymbol{\phi}^{n_k}]| + |[\boldsymbol{\phi}^{n_{k-1}}]|)|\phi_1^{n+1}|\, ds + \kappa \int_I |u_1(t^{n+1})|||[\boldsymbol{\phi}^{n_k}]||\phi_1^{n+1}|\, ds \\
&+ \kappa \int_I |\phi_2^{n_k}|||[\mathbf{u}(t^{n+1})]|||\phi_1^{n+1}|\, ds \\
I3 &= \kappa \int_I |u_2^{n_k}| \left| \frac{1}{2}(|[\mathbf{u}(t^{n_k})]| + |[\mathbf{u}(t^{n_{k-1}})]|) - |[\mathbf{u}(t^{n+1})]| \right| |\phi_1^{n+1}|\, ds \\
I4 &= \kappa \int_I |u_2^{n_k}| \left| |[\mathbf{u}^{n_k}]|^{1/2}|[\mathbf{u}^{n_{k-1}}]|^{1/2} - \frac{1}{2}(|[\mathbf{u}^{n_k}]| + |[\mathbf{u}^{n_{k-1}}]|) \right| |\phi_1^{n+1}|\, ds
\end{aligned}
$$

The error terms on the right hand side appearing before the Ij-terms are commonly encountered in the numerical analysis of computational fluid algorithms and are treated analogously. In the term $I1$, each piece is bounded using (6.11) with $\alpha_1 = 192$. Then the first two terms of $I2$ are bounded using (6.13) with $\alpha_1 = 16\,m$, $\alpha_2 = 32$, $\beta_1 = 96$ and the last term using (6.12) with $\alpha_2 = 8$ and $\beta_1 = 96$.

Some basic inequalities can be used to simplify $I3, I4$ and derive corresponding error estimates. We apply the reverse triangle inequality here for $I3$.

$$
\begin{aligned}
&\left| \frac{1}{2}(|[\mathbf{u}(t^{n_k})]| + |[\mathbf{u}(t^{n_{k-1}})]|) - |[\mathbf{u}(t^{n+1})]| \right| \\
&\leq \frac{1}{2} \left| |[\mathbf{u}(t^{n_k})]| - |[\mathbf{u}(t^{n+1})]| \right| + \frac{1}{2} \left| |[\mathbf{u}(t^{n_{k-1}})]| - |[\mathbf{u}(t^{n+1})]| \right| \\
&\leq \frac{1}{2} \left| [\mathbf{u}(t^{n_k}) - \mathbf{u}(t^{n+1})] \right| + \frac{1}{2} \left| [\mathbf{u}(t^{n_{k-1}}) - \mathbf{u}(t^{n+1})] \right|.
\end{aligned} \tag{6.29}
$$

$I4$ is bounded by first noting

$$
\begin{aligned}
\left| |[\mathbf{u}^{n_k}]|^{1/2}|[\mathbf{u}^{n_{k-1}}]|^{1/2} - \frac{1}{2}(|[\mathbf{u}^{n_k}]| + |[\mathbf{u}^{n_{k-1}}]|) \right| &= \frac{1}{2} \left| |[\mathbf{u}^{n_k}]|^{1/2} - |[\mathbf{u}^{n_{k-1}}]|^{1/2} \right|^2 \\
&\leq \frac{1}{2} \left| |[\mathbf{u}^{n_k}]|^{1/2} - |[\mathbf{u}^{n_{k-1}}]|^{1/2} \right| \left| |[\mathbf{u}^{n_k}]|^{1/2} + |[\mathbf{u}^{n_{k-1}}]|^{1/2} \right| \\
&= \frac{1}{2} \left| |[\mathbf{u}^{n_k}]| - |[\mathbf{u}^{n_{k-1}}]| \right| \leq \frac{1}{2} \left| [\mathbf{u}^{n_k} - \mathbf{u}^{n_{k-1}}] \right|.
\end{aligned}
$$

Add and subtract $\mathbf{u}(t^{n_k}) - \mathbf{u}(t^{n_{k-1}})$,

$$\begin{aligned}
&\left| |[\mathbf{u}^{n_k}]|^{1/2} |[\mathbf{u}^{n_{k-1}}]|^{1/2} - \frac{1}{2}(|[\mathbf{u}^{n_k}]| + |[\mathbf{u}^{n_{k-1}}]|) \right| \\
&\leq \frac{1}{2} \left| [(\mathbf{u}^{n_k} - \mathbf{u}(t^{n_k})) + (\mathbf{u}(t^{n_{k-1}}) - \mathbf{u}^{n_{k-1}})] \right| + \frac{1}{2} \left| [\mathbf{u}(t^{n_k}) - \mathbf{u}(t^{n_{k-1}})] \right| \\
&\leq \frac{1}{2} \Big\{ |[\boldsymbol{\phi}^{n_k}]| + |[\boldsymbol{\phi}^{n_{k-1}}]| + |[\boldsymbol{\eta}^{n_k}]| + |[\boldsymbol{\eta}^{n_{k-1}}]| + |[\mathbf{u}(t^{n_k}) - \mathbf{u}(t^{n_{k-1}})]| \Big\}.
\end{aligned} \tag{6.30}$$

The results (6.29) - (6.30) are combined with (6.9)-(6.10), Young's inequality and Lemma 6.2.1 is applied as described above for $I1, I2$. Then (6.24) follows from (6.28).

□

Lemma 6.3.3. *Given the assumptions of Lemma 6.3.2 there exists a constant $C > 0$ depending only on Ω, $\mathbf{u}$, $\mathbf{p}$, $\mathbf{f}$ such that*

$$\begin{aligned}
&\frac{1}{2\Delta t} \left(\|\phi_2^{n_{k+1}}\|_{\Omega_2}^2 - \|\phi_2^{n_k}\|_{\Omega_2}^2 + \|\phi_2^{n_{k+1}} - \phi_2^{n_k}\|_{\Omega_2}^2 \right) + m\,\nu_2 \|\nabla \phi_2^{n_{k+1}}\|_{\Omega_2}^2 \\
&\quad \leq C \Bigg\{ \nu_2^{-1} \| \frac{\eta_2^{n_{k+1}} - \eta_2^{n_k}}{\Delta t} \|_{X_2'}^2 + m\nu_2^{-1} \|p_2(t^{n_{k+1}}) - q_2\|_{\Omega_2}^2 \\
&\quad + m \left(\nu_2 + (1 + \nu_2^{-1}) \|\nabla u_2(t^{n_{k+1}})\|_{\Omega_2} \right) \|\nabla \eta_2^{n_{k+1}}\|_{\Omega_2}^2 \\
&\quad + \kappa^2 \sum_{n=n_{k-1}}^{n_k - 1} \Big(L_k^{n+1} Q_k^{n+1} + \kappa^2 J_k^{n+1} \Big(\nu_1^{-3} \|\phi_1^{n+1}\|_{\Omega_1}^2 + \nu_2^{-3} \|\phi_2^{n_{k+1}}\|_{\Omega_2}^2 \\
&\qquad + m \sum_{i=1,2} (1 + \nu_i^{-3}) \left\{ \|\phi_i^{n_k}\|_{\Omega_i}^2 + \|\phi_i^{n_{k-1}}\|_{\Omega_i}^2 \right\} \Big) \Big) + m\nu_2^{-1} \|R_2^{n_{k+1}}\|_{X_2'}^2 \\
&\quad + m \left(1 + \nu_2^{-1} + \nu_2^{-3} + \nu_2^{-1} \|\nabla u_2(t^{n_{k+1}})\|_{\Omega_2}^2 + \nu_2^{-3} \|\nabla u_2(t^{n_{k+1}})\|_{\Omega_2}^4 \right) \|\phi_2^{n_{k+1}}\|_{\Omega_2}^2 \Bigg\} \\
&\quad + \frac{\nu_1}{8} \sum_{j=n_{k-1}}^{n_k - 1} \|\nabla \phi_1^{j+1}\|_{\Omega_1}^2 + \frac{\nu_1}{8} \|\nabla \phi_1^{n_k}\|_{\Omega_1}^2 + \frac{m\,\nu_2}{8} \|\nabla \phi_2^{n_k}\|_{\Omega_2}^2 + \frac{m\,\nu_2}{8} \|\nabla \phi_2^{n_{k+1}}\|_{\Omega_2}^2 \\
&\quad + \frac{\nu_1}{8} \|\nabla \phi_1^{n_{k-1}}\|_{\Omega_1}^2 + \frac{m\,\nu_2}{8} \|\nabla \phi_2^{n_{k-1}}\|_{\Omega_2}^2
\end{aligned} \tag{6.31}$$

where Q_k^{n+1} is defined for $n_k \leq n < n_{k+1}$, $k = 1, 2, \ldots, M-1$ by:

$$\begin{aligned}
Q_k^{n+1} = &\left\| u_1(t^{n+1}) - u_1(t^{n_k}) \right\|_I^2 + \|u_2(t^{n_{k+1}}) - u_2(t^{n_k})\|_I^2 \\
&+ \left\| u_1(t^{n+1}) - u_1(t^{n_{k-1}}) \right\|_I^2 + \left\| u_2(t^{n+1}) - u_2(t^{n_{k-1}}) \right\|_I^2 \\
&+ \left\| \eta_1^{n+1} \right\|_I^2 + \|\boldsymbol{\eta}^{n_{k+1}}\|_I^2 + \|\boldsymbol{\eta}^{n_k}\|_I^2 + \|\boldsymbol{\eta}^{n_{k-1}}\|_I^2
\end{aligned}$$

and $R_2^{n_{k+1}}$ *is defined for* $k = 1, 2, \ldots, M-1$ *by:*

$$R_2^{n_{k+1}} = \frac{u_2(t^{n_{k+1}}) - u_2(t^{n_k})}{\Delta s} - \frac{\partial u_2(t^{n_{k+1}})}{\partial t}.$$

Proof. Subtracting (6.16) from the variational formulation for the true NSE on Ω_2,

$$\begin{aligned}
&\frac{1}{m\Delta t}\left((u_2(t^{n_{k+1}}) - u_2^{n_{k+1}}) - (u_2(t^{n_k}) - u_2^{n_k}), v_2\right)_{\Omega_2} + \nu_2\left(\nabla(u_2(t^{n_{k+1}}) - u_2^{n_{k+1}}), \nabla v_2\right)_{\Omega_2} \\
&\quad + c_2\left(u_2(t^{n_{k+1}}); u_2(t^{n_{k+1}}), v_2\right) - c_2\left(u_2^{n_{k+1}}; u_2^{n_{k+1}}, v_2\right) - \left(p_2(t^{n_{k+1}}) - q_2, \nabla\cdot v_2\right)_{\Omega_2} \\
&\quad + \kappa\int_I u_2(t^{n_{k+1}})|[\mathbf{u}(t^{n_{k+1}})]|\cdot v_2\, ds - \kappa\int_I u_2^{n_{k+1}}|[\mathbf{u}^{n_k}]|\cdot v_2\, ds \\
&\quad + \kappa\int_I |[\mathbf{u}^{n_k}]|^{1/2}|[\mathbf{u}^{n_{k-1}}]|^{1/2} S^k\cdot v_2\, ds - \kappa\int_I u_1(t^{n_{k+1}})|[\mathbf{u}(t^{n_{k+1}})]|\cdot v_2\, ds \\
&\quad = \left(\frac{u_2(t^{n_{k+1}}) - u_2(t^{n_k})}{m\Delta t} - \frac{\partial u_2(t^{n_{k+1}})}{\partial t}, v_2\right)_{\Omega_2},\ \forall v_2\in V_{2,h}\,,\ \forall q_2\in Q_{2,h}.
\end{aligned}$$

The analysis proceeds as for the above case for Ω_1, splitting the error and moving terms around, so after multiplying through by m we get

$$\begin{aligned}
&\frac{1}{2\Delta t}\left(\|\phi_2^{n_{k+1}}\|_{\Omega_2}^2 - \|\phi_2^{n_k}\|_{\Omega_2}^2 + \|\phi_2^{n_{k+1}} - \phi_2^{n_k}\|_{\Omega_2}^2\right) + m\,\nu_2\|\nabla\phi_2^{n_{k+1}}\|_{\Omega_2}^2 \\
&+ m\,\kappa\int_I u_2(t^{n_{k+1}})|[\mathbf{u}(t^{n_{k+1}})]|\cdot\phi_2^{n_{k+1}}\, ds - m\,\kappa\int_I u_2^{n_{k+1}}|[\mathbf{u}^{n_k}]|\cdot\phi_2^{n_{k+1}}\, ds \\
&+ m\,\kappa\int_I |[\mathbf{u}^{n_k}]|^{1/2}|[\mathbf{u}^{n_{k-1}}]|^{1/2} S^k\cdot\phi_2^{n_{k+1}}\, ds - m\,\kappa\int_I u_1(t^{n_{k+1}})|[\mathbf{u}(t^{n_{k+1}})]|\cdot\phi_2^{n_{k+1}}\, ds \\
&= -\frac{1}{\Delta t}\left(\eta_2^{n_{k+1}} - \eta_2^{n_k}, \phi_2^{n_{k+1}}\right)_{\Omega_2} - m\,\nu_2\left(\nabla\eta_2^{n_{k+1}}, \nabla\phi_2^{n_{k+1}}\right)_{\Omega_2} + m\left(p_2(t^{n_{k+1}}) - q_2, \nabla\cdot v_2\right)_{\Omega_2} \\
&- m\,c_2\left(u_2(t^{n_{k+1}}); u_2(t^{n_{k+1}}), \phi_2^{n_{k+1}}\right) + m\,c_2\left(u_2^{n_{k+1}}; u_2^{n_{k+1}}, \phi_2^{n_{k+1}}\right) + m\left(R_2^{n_{k+1}}, \phi_2^{n_{k+1}}\right)_{\Omega_2}.
\end{aligned} \tag{6.32}$$

We will substitute in for the first pair of interface integrals on the left hand side using this equality:

$$
\begin{aligned}
m\kappa \int_I u_2(t^{n_{k+1}})|[\mathbf{u}(t^{n_{k+1}})]| \cdot \phi_2^{n_{k+1}}\, ds - m\kappa \int_I u_2^{n_{k+1}}|[\mathbf{u}^{n_k}]| \cdot \phi_2^{n_{k+1}}\, ds \\
&= m\kappa \int_I u_2(t^{n_{k+1}}) \left(|[\mathbf{u}(t^{n_{k+1}})]| - |[\mathbf{u}(t^{n_k})]|\right) \cdot \phi_2^{n_{k+1}}\, ds \\
&+ m\kappa \int_I u_2(t^{n_{k+1}}) \left(|[\mathbf{u}(t^{n_k})]| - |[\tilde{\mathbf{u}}^{n_k}]|\right) \cdot \phi_2^{n_{k+1}}\, ds \\
&+ m\kappa \int_I u_2(t^{n_{k+1}}) \left(|[\tilde{\mathbf{u}}^{n_k}]| - |[\mathbf{u}^{n_k}]|\right) \cdot \phi_2^{n_{k+1}}\, ds \\
&+ m\kappa \int_I \eta_2^{n_{k+1}}|[\mathbf{u}^{n_k}]| \cdot \phi_2^{n_{k+1}}\, ds + m\kappa \int_I |\phi_2^{n_{k+1}}|^2|[\mathbf{u}^{n_k}]|\, ds.
\end{aligned} \tag{6.33}
$$

The main difference between estimating (6.32) and the derivation of (6.24) lies in the remaining interface terms. Note that after substituting in for S^k,

$$
\begin{aligned}
&m\,\kappa \int_I |[\mathbf{u}^{n_k}]|^{1/2}|[\mathbf{u}^{n_{k-1}}]|^{1/2} S^k \cdot \phi_2^{n_{k+1}}\, ds - m\,\kappa \int_I u_1(t^{n_{k+1}})|[\mathbf{u}(t^{n_{k+1}})]| \cdot \phi_2^{n_{k+1}}\, ds \\
&= \sum_{n=n_{k-1}}^{n_k-1} \left\{ \kappa \int_I u_1^{n+1} \cdot \phi_2^{n_{k+1}} |[\mathbf{u}^{n_k}]|^{1/2}|[\mathbf{u}^{n_{k-1}}]|^{1/2}\, ds - \kappa \int_I u_1(t^{n_{k+1}}) \cdot \phi_2^{n_{k+1}}|[\mathbf{u}(t^{n_{k+1}})]|\, ds \right\}
\end{aligned} \tag{6.34}
$$

The terms are split analogously to (6.27):

$$
\begin{aligned}
&\kappa \int_I |[\mathbf{u}^{n_k}]|^{1/2}|[\mathbf{u}^{n_{k-1}}]|^{1/2} u_1^{n+1} \cdot \phi_2^{n_{k+1}}\, ds - \kappa \int_I |[\mathbf{u}(t^{n_{k+1}})]| u_1(t^{n_{k+1}}) \cdot \phi_2^{n_{k+1}}\, ds \\
&= \kappa \int_I \left\{ |[\mathbf{u}^{n_k}]|^{1/2}|[\mathbf{u}^{n_{k-1}}]|^{1/2} - \frac{1}{2}(|[\mathbf{u}^{n_k}]| + |[\mathbf{u}^{n_{k-1}}]|) \right\} u_1^{n+1} \cdot \phi_2^{n_{k+1}}\, ds \\
&+ \frac{1}{2}\kappa \int_I \left\{ (|[\mathbf{u}^{n_k}]| + |[\mathbf{u}^{n_{k-1}}]|) - (|[\tilde{\mathbf{u}}^{n_k}]| + |[\tilde{\mathbf{u}}^{n_{k-1}}]|) \right\} u_1^{n+1} \cdot \phi_2^{n_{k+1}}\, ds \\
&+ \frac{1}{2}\kappa \int_I \left\{ (|[\tilde{\mathbf{u}}^{n_k}]| + |[\tilde{\mathbf{u}}^{n_{k-1}}]|) - (|[\mathbf{u}(t^{n_k})]| + |[\mathbf{u}(t^{n_{k-1}})]|) \right\} u_1^{n+1} \cdot \phi_2^{n_{k+1}}\, ds \\
&+ \kappa \int_I \left\{ \frac{1}{2}(|[\mathbf{u}(t^{n_k})]| + |[\mathbf{u}(t^{n_{k-1}})]|) - |[\mathbf{u}(t^{n_{k+1}})]| \right\} u_1^{n+1} \cdot \phi_2^{n_{k+1}}\, ds \\
&- \kappa \int_I |[\mathbf{u}(t^{n_{k+1}})]| \phi_1^{n+1} \cdot \phi_2^{n_{k+1}}\, ds - \kappa \int_I |[\mathbf{u}(t^{n_{k+1}})]| \eta_1^{n+1} \cdot \phi_2^{n_{k+1}}\, ds \\
&+ \kappa \int_I |[\mathbf{u}(t^{n_{k+1}})]| (u_1(t^{n+1}) - u_1(t^{n_{k+1}})) \cdot \phi_2^{n_{k+1}}\, ds.
\end{aligned} \tag{6.35}
$$

The equalities (6.33)-(6.35) are combined and used to substitute for the interface terms in (6.32). Then move all the interface terms to the right hand side and bound them using (6.8) - (6.10) with Young's inequality and Lemma 6.2.1 as in Lemma 6.3.2. In this way, one can derive (6.31).

□

Theorem 6.3.4 (Convergence of Algorithm 6.2.1)**.** *Assume a sufficiently regular solution* $(\mathbf{u}, \mathbf{p})$ *to* (6.1)*, approximated at the initial time steps* $t^0, t^1, t^2, \ldots, t^{n_1}$ *in* Ω_1 *by* u_1^j*,* $j = 0, 1, \ldots n_1$ *and at times* t^0, t^{n_1} *in* Ω_2 *by* u_2^0*,* $u_2^{n_1}$*. Let these approximations satisfy*

$$\begin{aligned} \|u_1(t^j) - u_1^j\|^2_{H^1(\Omega_1)} &\leq C_0 \left(\Delta t^2 + h^{2r}\right), \ j = 0, 1, \ldots, n_1 \\ \|u_2(t^{n_k}) - u_2^{n_k}\|^2_{H^1(\Omega_2)} &\leq C_0 \left(\Delta s^2 + h^{2r}\right), \ k = 0, 1 \end{aligned} \tag{6.36}$$

for a fixed number $C_0 > 0$*. Then there exists a constant* $C > 0$ *depending only on* Ω*,* $\mathbf{u}$*,* $\mathbf{p}$*,* $\mathbf{f}$*,* C_0*, the initial data at times* t^j *for* $j = 0, 1, \ldots, n_1$ *and the final time* t_f *such that if*

$$C\Delta t \left\{2 + \nu_1^{-1} + \nu_2^{-1} + (\nu_1^{-3} + \nu_2^{-3})(1 + m^2 + m\kappa^4)\right\} < 1, \tag{6.37}$$

then for $n_k \leq q < n_{k+1}$ *with* $k = 1, 2, \ldots, M-1$*, Algorithm 6.2.1 satisfies:*

$$\begin{aligned} &\|u_1(t^{q+1}) - u_1^{q+1}\|^2_{\Omega_1} + \|u_2(t^{n_{p+1}}) - u_2^{n_{p+1}}\|^2_{\Omega_2} \\ &+ \frac{\nu_1}{4}\Delta t \sum_{j=n_1}^{q} \|\nabla(u_1(t^{j+1}) - u_1^{j+1})\|^2_{\Omega_1} + \frac{1}{2} m\, \nu_2 \Delta t \sum_{k=1}^{p} \|\nabla(u_2(t^{n_{k+1}}) - u_2^{n_{k+1}})\|^2_{\Omega_2} \\ &= \mathcal{O}\Big(\Delta s^2 \left\{1 + \kappa^2 + (\nu_1/m^3 + \nu_2)\Delta s \right. \\ &\qquad + \Delta s\, \kappa^4(1 + \nu_1^{-3})/m^2 + m(\Delta s + \kappa^4)(1 + \nu_2^{-3})\} \\ &\quad + h^{2r} \left\{m + \nu_1 + m\nu_2 + \nu_1^{-1} + m\nu_2^{-1} + \Delta s\, \kappa^4(1 + \nu_1^{-3})h^2 \right. \\ &\qquad \left. \left. + h^2 m(\Delta s + \kappa^4)(1 + \nu_2^{-3}) + h^2\kappa^2\right\}\Big). \end{aligned} \tag{6.38}$$

Proof. . Let $1 \le p < M$ be an integer. Sum (6.24) over $n = n_1, n_1+1, \ldots, q$ for any integer q such that $n_p \le q < n_{p+1}$. Then sum (6.31) over $k = 1, 2, \ldots, p$, add the two resulting inequalities and multiply through by $2\Delta t$, yielding

$$
\begin{aligned}
&\|\phi_1^{q+1}\|_{\Omega_1}^2 + \|\phi_2^{n_{p+1}}\|_{\Omega_2}^2 + 2\Delta t \sum_{n=n_1}^{q} \|\phi_1^{n+1} - \phi_1^n\|_{\Omega_1}^2 + 2\Delta t \sum_{k=1}^{p} \|\phi_2^{n_{k+1}} - \phi_2^{n_k}\|_{\Omega_2}^2 \\
&+ \frac{7\nu_1}{4}\Delta t \sum_{n=n_1}^{q} \|\nabla\phi_1^{n+1}\|_{\Omega_1}^2 + 2m\,\nu_2 \Delta t \sum_{k=1}^{p} \|\nabla\phi_2^{n_{k+1}}\|_{\Omega_2}^2 \\
&\le C \Bigg\{ \Delta t \sum_{n=n_1}^{q} W_1^{n+1} + \Delta t \sum_{k=1}^{p} W_2^{n_{k+1}} + \Delta t \kappa^2 \sum_{k=1}^{p-1} \sum_{n=n_k}^{n_{k+1}-1} \left\{ L_k^{n+1} P_k^{n+1} + L_{k+1}^{n+1} Q_{k+1}^{n+1} \right\} \\
&+ \Delta t \kappa^2 \sum_{n=n_p}^{q} L_k^{n+1} P_k^{n+1} + H \\
&+ \Delta t \sum_{k=1}^{p-1} \sum_{n=n_k}^{n_{k+1}-1} c_{k+1}^{n+1} \|\phi_1^{n+1}\|_{\Omega_1}^2 + \Delta t \sum_{n=n_p}^{q} c_{p+1}^{n+1} \|\phi_1^{n+1}\|_{\Omega_1}^2 + \Delta t \sum_{k=2}^{p+1} d_k^{n+1} \|\phi_2^{n_k}\|_{\Omega_2}^2 \Bigg\} \\
&+ \nu_1 \Delta t \sum_{k=2}^{p} \|\nabla\phi_1^{n_k}\|_{\Omega_1}^2 + \frac{\nu_1 \Delta t}{2} \sum_{n=n_1}^{n_p-1} \|\nabla\phi_1^{n+1}\|_{\Omega_1}^2 + \frac{3m\nu_2\Delta t}{2} \sum_{k=1}^{p} \|\nabla\phi_2^{n_{k+1}}\|_{\Omega_1}^2
\end{aligned}
\tag{6.39}
$$

with additional notation defined by

$$
\begin{aligned}
\mu_1^{n+1} &= 1 + \nu_1^{-1} + \nu_1^{-3} + \nu_1^{-1} \|\nabla u_1(t^{n+1})\|_{\Omega_1}^2 + \nu_1^{-3} \|\nabla u_1(t^{n+1})\|_{\Omega_1}^4 \\
\mu_2^{n_{k+1}} &= 1 + \nu_2^{-1} + \nu_2^{-3} + \nu_2^{-1} \|\nabla u_2(t^{n_{k+1}})\|_{\Omega_2}^2 + \nu_2^{-3} \|\nabla u_2(t^{n_{k+1}})\|_{\Omega_2}^4 \\
c_{k+1}^{n+1} &= \mu_1^{n+1} + \kappa^4 (J_k^{n+1} + J_{k+1}^{n+1})(1 + \nu_1^{-3}) + m^2 (1 + \nu_1^{-3}) \\
&\quad + m\kappa^4 (1 + \nu_1^{-3}) \left(\sum_{j=n_{k-1}}^{n_k - 1} J_k^{j+1} + \sum_{j=n_k}^{n_{k+1}-1} J_{k+1}^{j+1} \right) \\
d_k^{n+1} &= \mu_2^{n_k} + m\kappa^4 (1 + \nu_2^{-3}) \left(\sum_{j=n_{k-2}}^{n_{k-1}-1} J_{k-1}^{j+1} + \sum_{j=n_{k-1}}^{n_k - 1} J_k^{j+1} + \sum_{j=n_k}^{n_{k+1}-1} J_{k+1}^{j+1} \right)
\end{aligned}
$$

$$
\begin{aligned}
\lambda_1^{n+1} &= \nu_1 + (1+\nu_1^{-1})\|\nabla u_1(t^{n+1})\|_{\Omega_1} \\
\lambda_2^{n_{k+1}} &= \nu_2 + (1+\nu_2^{-1})\|\nabla u_2(t^{n_{k+1}})\|_{\Omega_2} \\
W_1^{n+1} &= \nu_1^{-1}\|\frac{\eta_1^{n+1}-\eta_1^n}{\Delta t}\|_{X_1'}^2 + \lambda_1^{n+1}\|\nabla\eta_1^{n+1}\|_{\Omega_1}^2 \\
&\quad + \nu_1^{-1}\|R_1^{n+1}\|_{X_1'}^2 + \nu_1^{-1}\|p_1(t^{n+1}) - q_1\|_{\Omega_1}^2 \\
W_2^{n_{k+1}} &= \nu_2^{-1}\|\frac{\eta_2^{n_{k+1}}-\eta_1^{n_k}}{\Delta t}\|_{X_2'}^2 + m\lambda_2^{n_{k+1}}\|\nabla\eta_2^{n_{k+1}}\|_{\Omega_2}^2 \\
&\quad + m\nu_2^{-1}\|R_2^{n_{k+1}}\|_{X_2'}^2 + m\nu_2^{-1}\|p_2(t^{n_{k+1}}) - q_2\|_{\Omega_2}^2
\end{aligned}
$$

and with the additional notation H defined by

$$
\begin{aligned}
H &= \|\boldsymbol{\phi}^{n_1}\|^2 + \Delta t\nu_1\left(\|\nabla\phi_1^0\|_{\Omega_1}^2 + \|\nabla\phi_1^{n_1}\|_{\Omega_1}^2\right) + \frac{3}{2}m\Delta t\nu_2\left(\|\nabla\phi_2^0\|_{\Omega_2}^2 + \|\nabla\phi_2^{n_1}\|_{\Omega_2}^2\right) \\
&\quad + \Delta t\kappa^4 m(1+\nu_1^{-3})J_1^1\|\phi_1^0\|_{\Omega_1}^2 + \Delta t(1+\nu_2^{-3})\left(m^2 + m\kappa^4\sum_{j=0}^{n_1-1}J_1^{j+1}\right)\|\phi_2^0\|_{\Omega_2}^2 \\
&\quad + \Delta t(1+\nu_2^{-3})\left(2m^2 + m\kappa^4\Big(\sum_{j=0}^{n_1-1}J_1^{j+1} + \sum_{n_1}^{n_2-1}J_2^{j+1}\Big)\right)\|\phi_2^{n_1}\|_{\Omega_2}^2 \\
&\quad + \Delta t\kappa^2\sum_{n=0}^{n_1-1}L_1^{n+1}Q_1^{n+1}.
\end{aligned}
$$

Insert the upper bound

$$
\nu_1\Delta t\sum_{k=2}^{p}\|\nabla\phi_1^{n_k}\|_{\Omega_1}^2 + \frac{\nu_1\Delta t}{2}\sum_{n=n_1}^{n_p-1}\|\nabla\phi_1^{n+1}\|_{\Omega_1}^2 \le \frac{3\nu_1\Delta t}{2}\sum_{n=n_1}^{q}\|\nabla\phi_1^{n+1}\|_{\Omega_1}^2
$$

into (6.39) and subsume the last line of (6.39),

$$
\begin{aligned}
&\|\phi_1^{q+1}\|_{\Omega_1}^2 + \|\phi_2^{n_{p+1}}\|_{\Omega_2}^2 + 2\Delta t \sum_{n=n_1}^{q} \|\phi_1^{n+1} - \phi_1^n\|_{\Omega_1}^2 + 2\Delta t \sum_{k=1}^{p} \|\phi_2^{n_{k+1}} - \phi_2^{n_k}\|_{\Omega_2}^2 \\
&+ \frac{\nu_1}{4}\Delta t \sum_{n=n_1}^{q} \|\nabla\phi_1^{n+1}\|_{\Omega_1}^2 + \frac{1}{2} m\,\nu_2 \Delta t \sum_{k=1}^{p} \|\nabla\phi_2^{n_{k+1}}\|_{\Omega_2}^2 \\
&\leq C \left\{ \Delta t \sum_{n=n_1}^{q} W_1^{n+1} + \Delta t \sum_{k=1}^{p} W_2^{n_{k+1}} + \Delta t \kappa^2 \sum_{k=1}^{p-1} \sum_{n=n_k}^{n_{k+1}-1} \left\{ L_k^{n+1} P_k^{n+1} + L_{k+1}^{n+1} Q_{k+1}^{n+1} \right\} \right. \\
&+ \Delta t \kappa^2 \sum_{n=n_p}^{q} L_k^{n+1} P_k^{n+1} + H \\
&\left. + \Delta t \sum_{k=1}^{p-1} \sum_{n=n_k}^{n_{k+1}-1} c_{k+1}^{n+1} \|\phi_1^{n+1}\|_{\Omega_1}^2 + \Delta t \sum_{n=n_p}^{q} c_{p+1}^{n+1} \|\phi_1^{n+1}\|_{\Omega_1}^2 + \Delta t \sum_{k=2}^{p+1} d_k^{n+1} \|\phi_2^{n_k}\|_{\Omega_2}^2 \right\}.
\end{aligned}
\tag{6.40}
$$

Appling Gronwall's inequality requires the inequality to be in the necessary form. Begin with the following definitions. If $n_k \leq n < n_{k+1}$ for a given $k = 1, 2, \ldots, p$,

$$
\begin{aligned}
a^{n+1} &= \|\phi_1^{n+1}\|_{\Omega_1}^2 + \|\phi_2^{n_{k+1}}\|_{\Omega_2}^2 \\
b^{n+1} &= c_{k+1}^{n+1} + d_k^{n+1} \\
e^{n+1} &= W_1^{n+1} + W_2^{n_{k+1}} + \kappa^2 \left\{ L_k^{n+1} P_k^{n+1} + L_{k+1}^{n+1} Q_{k+1}^{n+1} \right\}.
\end{aligned}
$$

The usage of Gronwall's inequality follows from noting that by addition of some nonnegative terms on the right hand side of (6.40), it follows

$$
\begin{aligned}
&a^{q+1} + 2\Delta t \sum_{n=n_1}^{q} \|\phi_1^{n+1} - \phi_1^n\|_{\Omega_1}^2 + 2\Delta t \sum_{k=1}^{p} \|\phi_2^{n_{k+1}} - \phi_2^{n_k}\|_{\Omega_2}^2 \\
&+ \frac{\nu_1}{4}\Delta t \sum_{n=n_1}^{q} \|\nabla\phi_1^{n+1}\|_{\Omega_1}^2 + \frac{1}{2} m\,\nu_2 \Delta t \sum_{k=1}^{p} \|\nabla\phi_2^{n_{k+1}}\|_{\Omega_2}^2 \\
&\leq C \left\{ \Delta t \sum_{n=n_1}^{q} e^{n+1} + \Delta t \sum_{n=n_1}^{q} a^{n+1} b^{n+1} + H \right\}.
\end{aligned}
\tag{6.41}
$$

It is easily verified that

$$
\Delta t \sum_{n=n_1}^{N-1} b^{n+1} < \infty.
$$

Applying Gronwall's inequality and inserting the expression for a^{q+1},

$$\begin{aligned}
&\|\phi_1^{q+1}\|_{\Omega_1}^2 + \|\phi_2^{n_{p+1}}\|_{\Omega_2}^2 + 2\Delta t \sum_{n=n_1}^{q} \|\phi_1^{n+1} - \phi_1^n\|_{\Omega_1}^2 + 2\Delta t \sum_{k=1}^{p} \|\phi_2^{n_{k+1}} - \phi_2^{n_k}\|_{\Omega_2}^2 \\
&+ \frac{\nu_1}{4}\Delta t \sum_{n=n_1}^{q} \|\nabla\phi_1^{n+1}\|_{\Omega_1}^2 + \frac{1}{2} m\,\nu_2 \Delta t \sum_{k=1}^{p} \|\nabla\phi_2^{n_{k+1}}\|_{\Omega_2}^2 \qquad (6.42) \\
&\leq C\,\exp\left(\Delta t \sum_{n=n_1}^{q} \sigma^{n+1}\right)\left\{\Delta t \sum_{n=n_1}^{q} e^{n+1} + H\right\}.
\end{aligned}$$

where $\sigma^{n+1} = \frac{b^{n+1}}{1-\Delta t\, b^{n+1}}$. The time step restriction required to use Gronwall's inequality is determined by substituting in for c_{k+1}^{n+1} and d_k^{n+1}, from which (6.37) follows. Applying the error inequalities (6.36) and standard interpolation error estimates,

$$\begin{aligned}
H = \mathcal{O}\Big(&\Delta s^2\left\{1 + \kappa^2 + (\nu_1/m^3 + \nu_2)\Delta s + \Delta s\,\kappa^4(1+\nu_1^{-3})/m^2 + m(\Delta s + \kappa^4)(1+\nu_2^{-3})\right\} \\
&+h^{2r}\left\{h^2 + (\nu_1/m + \nu_2)\Delta s + \Delta s\,\kappa^4(1+\nu_1^{-3})h^2 + h^2 m(\Delta s + \kappa^4)(1+\nu_2^{-3}) + h^2\kappa^2\right\}\Big).
\end{aligned}$$

The final result is derived in the usual way by applying the triangle inequality and taking the infimum over $\mathbf{v} \in X_h$ and $\mathbf{q} \in Q_h$, e.g. [45]. Then apply interpolation error estimates for spatial errors and Taylor's theorem for errors in time. □

6.4 NUMERICAL EXPERIMENTS

An example of the utility of Algorithm 6.2.1 is provided here for a numerical test case with properties similar to some important atmosphere-ocean dynamics. The subdomains are $\Omega_1 = [0, 10] \times [0, 1]$ and $\Omega_2 = [0, 10] \times [-1, 0]$. Some Dirichlet boundary conditions are prescribed on $\Gamma_1 = \partial\Omega_1 \cap \{x = 0\}$ and $\Gamma_2 = \partial\Omega_2 \setminus I$,

$$\begin{aligned}
&u_1(x = 0, y, t) = 5.0\,(1.5 + 0.5\cos(2\pi\, t + \pi))(1 + y)\langle 1, 0\rangle \text{ on } \Gamma_1 \times [0, 1], \\
&\text{and } u_2(x, y, t) = 0 \text{ on } \Gamma_2 \times [0, 1].
\end{aligned}$$

"Do nothing" boundary conditions are imposed on $\partial\Omega_1 \setminus (I \cup \Gamma_1)$. The body forcing is taken to be $\mathbf{f} = 0$. The kinematic viscosities are $\nu_1 = 0.1$ and $\nu_2 = 0.01$. We consider a characteristic velocity $U = 10.0$ and length $L = 10.0$. The large scale Reynolds numbers are thus $Re_1 = 1000$ and $Re_2 = 10000$. The interface parameter is $\kappa = 0.05$.

The finite element spaces used are Taylor-Hood elements (globally continuous, piecewise polynomials of degree 2 for velocity and degree 1 for pressure). The computations were performed with the freely available finite element package FreeFEM++. The machine used was running Ubuntu Linux with an Intel Xeon quad-core processor and 32 Gb RAM. The computations for Ω_1 and Ω_2 were performed in parallel with implementation of OpenMPI on 2 cores. A static, unstructured mesh was generated using the automatic 2-D Delaunay-Voronoi algorithm. This mesh is shown in Figure 8. The velocity space in Ω_1 consisted of 11,210 degrees of freedom and 126,336 degrees of freedom in Ω_2.

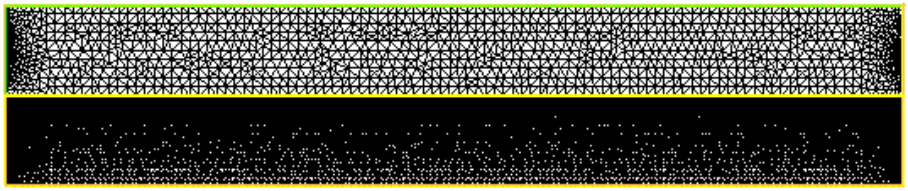

Figure 8: The meshes for Ω_1 and Ω_2.

Initial conditions are generated by first running an auxiliary computation where the boundary condition on Γ_1 is replaced with a static boundary condition, $u_1(x = 0, y) = 5.0\,(1 + y)\langle 1, 0\rangle$, corresponding to setting $t = 0$ in (6.4). Computations were then performed starting from zero initial data, $\mathbf{u} = 0$, with time step size $\Delta t = 0.005$ and a backward-Euler (implicit and coupled) algorithm. The coupling was linearized by extrapolation, estimating

$$|u_1(t^{n+1}) - u_2(t^{n+1})| \approx |u_1^n - u_2^n|.$$

This algorithm is known to be unconditionally stable from work in the previous chapters. Instead of running for some chosen number of time steps, a tolerance on the discrete time derivative was used as a stopping criterion:

$$\left\| \frac{u_1^{n+1} - u_1^n}{\Delta t} \right\|^2_{H^1(\Omega_1)} + \left\| \frac{u_2^{n+1} - u_2^n}{\Delta t} \right\|^2_{H^1(\Omega_2)} < 10^{-2}.$$

Initial conditions for the numerical test were then set to this discrete solution, $\mathbf{u}^0 \leftarrow \mathbf{u}^{n+1}$.

The small scale of time fluctuations for this problem is due to the boundary condition on Γ_1. The time step size $\Delta t = 1280^{-1}$ was determined to sufficiently resolve the necessary time scales (without losing major flow features). The solution to Algorithm 6.2.1 was calculated using time step ratios of $m = 1, 2, 4, 8, 16, 32$ with a total of 640 time steps for the solution on Ω_1. The magnitude of velocity is plotted on Ω_1 (Figure 9) and on Ω_2 (Figure 10) at the final time for $m = 1$. All plots and tables below are for the final time step.

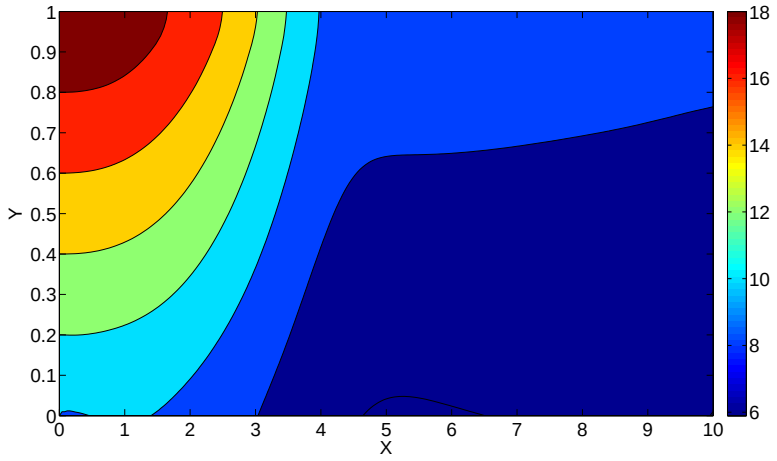

Figure 9: The magnitude of velocity on Ω_1, $m = 1$.

Denote by $\mathbf{u}(m)$ the solution using Algorithm 6.2.1 with time step ratio m at the final time. The relative difference between solutions in each subdomain using time step ratio 1 versus $m = 2, 4, 8, 16, 32$ was calculated as

$$D_i u(m) = \|u_i(m) - u_i(1)\|_{H^1(\Omega_i)} / \|u_i(1)\|_{H^1(\Omega_i)}, \ i = 1, 2.$$

In Ω_1 the relative change in average horizontal velocity, denoted $E_1\overline{u_1}(m)$, and average vertical velocity, denoted $E_2\overline{u_1}(m)$, were calculated for $m = 2, 4, 8, 16, 32$. These quantities are defined using the horizontal velocities $u_{1,1}(m)$ and vertical velocities $u_{1,2}(m)$ by

$$E_1\overline{u_1}(m) = \left| \int_{\Omega_1} (u_{1,1}(m) - u_{1,1}(1))\, d\Omega_1 \div \int_{\Omega_1} u_{1,1}(1)\, d\Omega_1 \right|,$$
$$E_2\overline{u_1}(m) = \left| \int_{\Omega_1} (u_{1,2}(m) - u_{1,2}(1))\, d\Omega_1 \div \int_{\Omega_1} u_{1,2}(1)\, d\Omega_1 \right|.$$

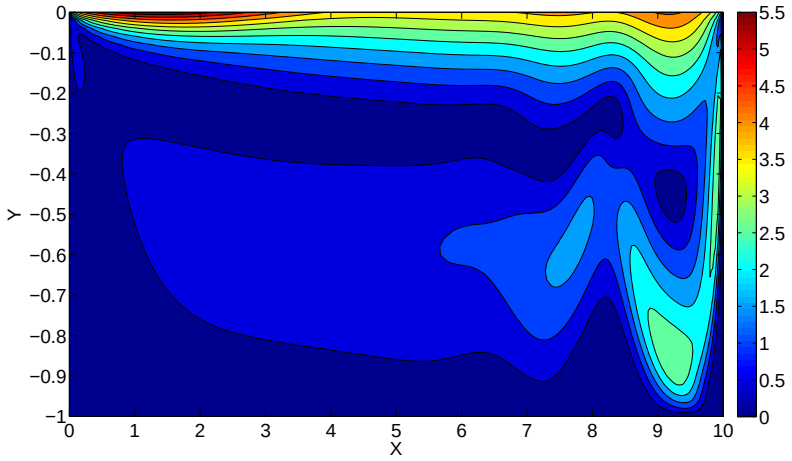

Figure 10: The magnitude of velocity on Ω_2, $m = 1$.

The total run time for the code in each case is presented in Table 21, along with the values of $D_i(m)$ and $E_i(m)$.

Table 21: Approximation run times and difference against case $m = 1$.

m	Run time (sec)	speed up	$D_1(m)$	$D_2(m)$	$E_1\overline{u_1}(m)$	$E_2\overline{u_1}(m)$
1	19087	—	—	—	—	—
2	9785	1.95	0.0212	0.0779	7.6026E-4	2.2953E-07
4	5276	3.62	0.0416	0.1511	1.4114E-3	3.9034E-07
8	2832	6.74	0.0608	0.2158	1.9595E-3	5.1578E-07
16	1445	13.21	0.0784	0.2705	2.4191E-3	6.1867E-07
32	1174	16.26	0.0945	0.3147	2.7994E-3	7.0621E-07

There is some relative solve time for the linear system corresponding to Ω_2 versus that of Ω_1. Once the ratio m exceeds this value, the speed up will no longer increase much as m increases (for a fixed mesh). Table 21 shows that this value is in excess of 13. The values $D_i(m)$ can be interpreted as the relative loss in accuracy by increasing the time step ratio. These values should decrease with Δt. For the chosen value of Δt the data shows that increasing the ratio m from 2 to 16 results in an increase in error by a factor of ≈ 3.70 on Ω_1 and ≈ 3.47 on Ω_2. The growth in error with m for this problem is sublinear up to the limit of efficiency.

The relative difference in average horizontal and vertical velocities on Ω_1 are an order of

magnitude smaller than the differences $D_i(m)$, demonstrating how localized errors may not adversely effect statistics of the flow as much as the point-wise values of the variables. In this case the errors are mainly localized near the interface. This is visualized in Figures 11 - 12, which show the magnitude of the difference in velocities with $m = 1$ and $m = 16$ on Ω_1 and Ω_2, respectively.

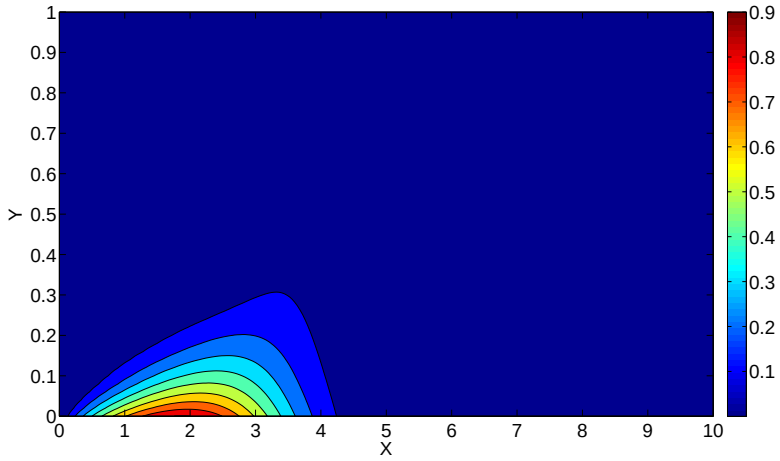

Figure 11: The magnitude of difference in velocity on Ω_1, $m = 1$ versus $m = 16$.

6.5 CONCLUSIONS

A full discretization of the coupled system of fluids was proposed allowing different size time steps for the decoupled subcalculations and proved to be stable for any size time step. The algorithm was proved to be first order accurate in time with optimal approximation of spatial derivatives in $L^2(\Omega)$ in terms of the mesh parameter. This result may require a time step restriction, not dependent on the mesh size. The stability and convergence results hold for any ratio of time steps in the two subdomains. Numerical testing showed a speed up of approximately 16 was possible for a certain example problem. Also, increasing the time step ratio from 2 to 16 resulted in an estimated factor of 3.70 increase in error in the velocity in $H^1(\Omega_1)$ and a factor of 3.47 for $H^1(\Omega_2)$. This is a sublinear growth in error with the time

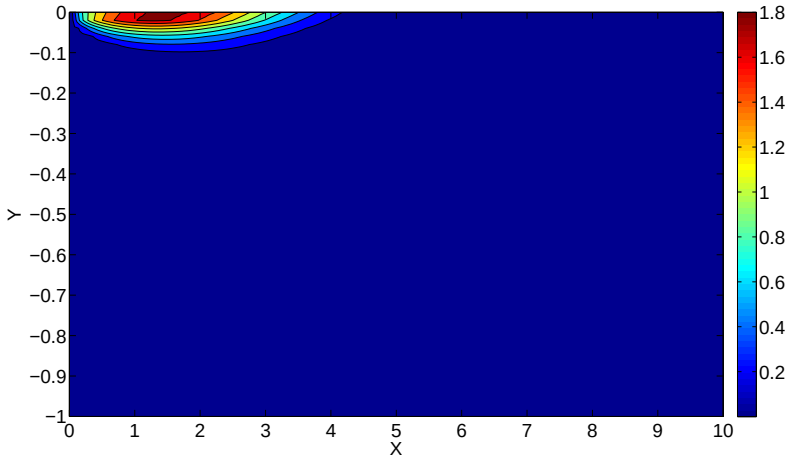

Figure 12: The magnitude of difference in velocity on Ω_2, $m = 1$ versus $m = 16$.

step ratio. The accuracy of the average velocity was found to be effected to a lesser degree by increasing m, with relative change one order of magnitude smaller than for the error in the sense of H^1.

7.0 UNCERTAINTY QUANTIFICATION FOR A TWO DOMAIN NATURAL CONVECTION PROBLEM

7.1 INTRODUCTION

This chapter investigates uncertainty in numerical algorithms for a model of two coupled fluids with natural heat convection. Thus the equations (and the domain, explained below) will differ from the previous chapters. The model is motivated by the dynamic core of climate codes in which the atmosphere and ocean equations are coupled across their common interface, e.g. [21, 22, 27]. The ocean surface is represented as a rigid lid. Numerical models for climate research are based on uncoupled atmosphere and ocean solves with flux passing across the interface at each time step. Understanding the reliability of climate models and methods is critical. Uncertainty occurs from modeling parameters, data inputs and many other sources. The paper studies what effect partitioned methods have on growth, generation and distribution of uncertainty.

Three methods are studied for the coupled natural convection model:

1. a monolithic method (coupled across the interface),
2. a partitioned method (numerically decoupled),
3. and a common further simplification in which the momentum flux is determined by wind velocity independent of ocean surface currents.

The chapter provides

- a full stability analysis of the monolithic and partitioned method,
- a comprehensive numerical study of uncertainty in these same methods
- and a comparison of uncertainty in average surface temperature for all three methods.

In conclusion, it is shown

- methods 1 and 2 are stable for any time step size,
- the variance values in velocity grow to be on the order of the expected values,
- method 1 generates standard deviations in temperature up to 57 Kelvin,
- method 2 generates standard deviations in temperature up to 21 Kelvin,
- variance concentrates at the interface and propagates into the bulk fluid,
- the differences in expected values of average surface temperature between the three methods are initially greater than the variance values,
- method 1 has the smallest uncertainty in average surface temperature and
- method 3 has the largest uncertainty in average surface temperature.

7.1.1 The Continuum Model

Climate models have often used a rigid-lid approximation of the atmosphere-ocean interface, [46, 70]. Nonlinear boundary conditions are used to conserve fluxes across the Prandtl (constant flux) layers. Since it is computationally prohibitive to resolve these layers and the interface directly, this offers an alternative. The variables are interpreted as averaged values or values at the edge of the layer where there is a transition to bulk domain behavior. A thorough presentation of physical boundary conditions at the interface is provided in [55].

To reduce the problem to a simpler form that still retains the essential difficulty of the atmosphere-ocean coupling, let the domain $\Omega \subset \mathbb{R}^d$ for $d = 2, 3$ consist of two subdomains Ω_1 and Ω_2. Denote outward unit normal vectors by $\hat{n}_1$ and $\hat{n}_2$, respectively. The subdomains are coupled across an interface $I = \partial\Omega_1 \cap \partial\Omega_2$. Take Γ_2 to be the upper boundary and Γ_3 the lower boundary as in Figure 13. Let τ be any tangent vector on I, so $\tau \cdot \hat{n}_i = 0$. The problem is: *given* $Q_i : [0, t_f] \to H^1(\Omega_i)$, $u_i^0 \in H^1(\Omega_i)^2$ *and* $T_i^0 \in H^1(\Omega_i)$, *find (for* $i = 1, 2$*)*

$u_i : \overline{\Omega}_i \times [0, t_f] \to \mathbb{R}^d$ *and* $T_i,\ p_i : \overline{\Omega}_i \times [0, t_f] \to \mathbb{R}$ *satisfying*

$$
\begin{aligned}
u_{i,t} + u_i \cdot \nabla u_i - \nu_i \Delta u_i + \nabla p_i &= G(1 - \beta_i(T_i - \overline{T_i})), \quad \text{in } \Omega_i, && (7.1)\\
T_{i,t} + u_i \cdot \nabla T_i - \alpha_i \Delta T_i &= Q_i(t), \quad \text{in } \Omega_i, && (7.2)\\
-\nu_i \hat{n}_i \cdot \nabla u_i \cdot \hat{\tau} &= \kappa |(u_i - u_j)|(u_i - u_j) \cdot \hat{\tau}, && (7.3)\\
-\alpha_i \hat{n}_i \cdot \nabla T_i &= (-1)^{i+1} C_{sol} + C_{ir}(T_i - T_j) && (7.4)\\
&\quad + \mu |u_i - u_j|(T_i - T_j),\\
\text{on} \quad I &\quad , \text{for } i, j = 1, 2\ ,\ i \neq j\ ,\\
u_i \cdot \hat{n}_i &= 0 \ \text{ on } I,\ i = 1, 2 && (7.5)\\
\nabla \cdot u_i &= 0\ , \text{in}\, \Omega_i && (7.6)\\
u_i(x, 0) &= u_i^0(x), \text{ and } T_i(x, 0) = T_i^0(x) \quad \text{in } \Omega_i, && (7.7)
\end{aligned}
$$

for $t \in (0, t_f]$. On the external boundaries the following static conditions are applied. In the lateral direction the solution is periodic and

$$
\begin{aligned}
-\alpha_1 \hat{n}_1 \cdot \nabla T_1 = C_{atm}|T_1|T_1 \text{ and } -\nu_1 \hat{n}_1 \cdot \nabla u_1 \cdot \hat{\tau}_1 = u_1 \cdot \hat{n}_1 &= 0, \quad \text{on } \Gamma_2 && (7.8)\\
-\alpha_2 \hat{n}_2 \cdot \nabla T_2 = 0\ ,\ u_2 &= 0, \quad \text{on } \Gamma_3. && (7.9)
\end{aligned}
$$

The problem (7.1)-(7.9) is chosen to exemplify the key elements of the temperature and velocity equations in the atmosphere-ocean system proposed and analyzed by Lions, Temam and Wang, [47, 48, 49]. The velocity field in Ω_i is u_i, pressure is p_i and temperature is T_i, with average value

$$\overline{T}_i = \frac{1}{|\Omega_i|} \int_{\Omega_i} T_i \, d\Omega_i.$$

The kinematic viscocities and thermal diffusivities are denoted by ν_i and α_i, respectively. Gravitational acceleration is denoted by $G = \langle 0, -g \rangle$ for $d = 2$ or $G = \langle 0, 0, -g \rangle$ for $d = 3$, $g \approx 9.81 \frac{m}{s^2}$. The heat source in Ω_i is $Q_i(t)$. The parameters in the interface conditions are all positive constants. C_{sol} relates to solar energy heating the Prandtl layers of the atmosphere and ocean. C_{ir} determines longwave (infrared) radiation, and μ is a coefficient of sensible heat transfer due to convection.

The parameter C_{atm} controls heat loss through Γ_2 by radiative transfer. This boundary condition is derived by simplifying the more physical radiative condition

$$-\alpha_1 \hat{n}_1 \cdot \nabla T_1 = C^*_{atm} \sigma T_1^4$$

where $\sigma = 5.7 \times 10^{-8}\ Wm^{-2}K^{-4}$ is the Stefan-Boltzmann constant, and $C^*_{atm} > 0$ is a proportionality constant. Using a reference temperature T_{ref},

$$C^*_{atm} \sigma T_1^4 \approx C^*_{atm} \sigma T_{ref}^2 T_1^2 = C^*_{atm} \sigma T_{ref}^2 |T_1| T_1.$$

The last equality is justified since $T_i > 0\,,\ i = 1, 2$, is measured in Kelvin. Then choose $C_{atm} = C^*_{atm} \sigma T_{ref}^2$ to obtain (7.8).

The interface coupling (7.4) and the Boussinesq forcing for the momentum equation are derived by asymptotic approximations with respect to temperature, [47, 38]. The accuracy of these approximations decreases as the temperature value grows apart from the reference temperature. Global heating may be balanced by cooling through Γ_2 to control the difference between the calculated temperature and the reference temperature without the added analytical problems (for $d = 3$, see Theorem 7.2.3) of a fourth-order nonlinear boundary term. Climate simulations must balance incoming solar energy with reflected and radiated outgoing energy, [70]. Alternatively, the temperature boundary condition on Γ_2 facilitates a global energy balance by a judicious choice of C_{atm}.

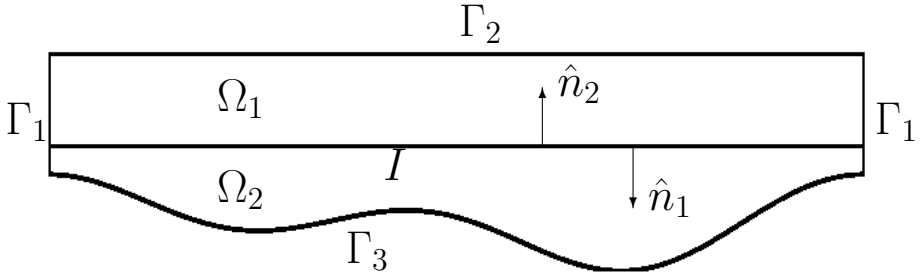

Figure 13: The subdomains, coupled across an interface I.

7.1.2 The Monolithic Weak Formulation

Denote the coordinates of $x \in \mathbb{R}^d$ by x_j and let $\hat{e}_j$ be the unit vectors in the direction of the coordinate axes for $1 \le j \le d$. Solutions are sought with periodicity in the coordinates with $j < d$ and period L. Let $\Gamma_1 = \partial\Omega \setminus (\Gamma_2 \cup \Gamma_3)$. For the subdomains ($i = 1, 2$) consider the function spaces

$$X_1^* := \Big\{ v_1 = \sum_{j=1}^{d} v_{1,j}(x)\hat{e}_j \in C^\infty(\overline{\Omega_1})^d : \; v_1(x_j + L) = v_1(x_j),\ 1 \le j < d, \\ \text{and } v_{1,d} = 0 \text{ on } \Gamma_2 \text{ and } I \Big\}$$

$$X_2^* := \Big\{ v_2 = \sum_{j=1}^{d} v_{2,j}(x)\hat{e}_j \in C^\infty(\overline{\Omega_2})^d : \; v_2(x_j + L) = v_2(x_j), \text{ if } x \in \Gamma_1, \\ 1 \le j < d,\ v_{2,d} = 0 \text{ on } I, v_2 = 0 \text{ on } \Gamma_3 \Big\}$$

$$P_i^* := \Big\{ q_i \in C^\infty(\overline{\Omega_i}) : \int_{\Omega_i} q_i \, d\Omega_i = 0 \,,\ q_i(x_j + L) = q_i(x_j) \,,\ 1 \le j < d,\ x \in \Gamma_1 \Big\}$$

$$\Theta_i^* := \Big\{ \theta_i \in C^\infty(\overline{\Omega_i}) : \; \theta_i(x_j + L) = \theta_i(x_j) \,,\ 1 \le j < d,\ x \in \Gamma_1 \Big\}.$$

Then the weak function spaces sought are defined through appropriate closure operations for $i = 1, 2$:

$$X_i := \text{closure of } \; X_i^* \text{ in } H^1(\Omega_i)^d$$

$$P_i := \text{closure of } \; P_i^* \text{ in } L^2(\Omega_i)$$

$$\Theta_i := \text{closure of } \; \Theta_i^* \text{ in } H^1(\Omega_i).$$

For $u_i \in X_i$ we denote $\mathbf{u} = (u_1, u_2)$ and $X := \{\mathbf{v} = (v_1, v_2) : v_i \in X_i,\ i = 1, 2\}$. Similarly, for $q_i \in P_i$ we denote $\mathbf{q} = (q_1, q_2)$ and $P := \{\mathbf{q} = (q_1, q_2) : q_i \in P_i,\ i = 1, 2\}$, and for $\theta_i \in \Theta_i$ we denote $\boldsymbol{\theta} = (\theta_1, \theta_2)$ and $\Theta := \{\boldsymbol{\theta} = (\theta_1, \theta_2) : \theta_i \in \Theta_i,\ i = 1, 2\}$.

The subdomain variational formulation for (7.1)-(7.9) is obtained by multiplying (7.1) by v_i, (7.6) by q_i, (7.2) by θ_i, integrating and applying the divergence theorem. That is, to find (for $i, j = 1, 2, i \ne j$) $u_i : (0, t_f] \to X_i$ and $p_i : (0, t_f] \to Q_i$ satisfying

$$(u_{i,t}, v_i)_{\Omega_i} + (\nu_i \nabla u_i, \nabla v_i)_{\Omega_i} + (u_i \cdot \nabla u_i, v_i)_{\Omega_i} - (p_i, \nabla \cdot v_i)_{\Omega_i} \\ + \int_I \kappa |u_i - u_j|(u_i - u_j) \cdot v_i ds = (G(1 - \beta_i(T_i - \overline{T_i})), v_i)_{\Omega_i}, \; \forall\, v_i \in X_i \qquad (7.10)$$

$$\text{and } (\nabla \cdot u_i, q_i)_{\Omega_i} = 0 \,, \; \forall q_i \in P_i$$

and $T_i : (0, t_f] \to \Theta_i$ satisfying

$$
\begin{aligned}
&(T_{i,t}, \theta_i)_{\Omega_i} + (\alpha_i \nabla T_i, \nabla \theta_i)_{\Omega_i} + (u_i \cdot \nabla T_i, \theta_i)_{\Omega_i} \\
&+ (2-i) \int_{\Gamma_2} C_{atm} |T_1| T_1 \theta_1 \, ds + \int_I (-1)^{i+1} C_{sol} \theta_i \, ds \\
&+ \int_I \{ C_{ir}(T_i - T_j) + \mu |u_i - u_j| (T_i - T_j) \} \, \theta_i ds = (Q_i, \theta_i)_{\Omega_i}, \ \forall \, \theta_i \in \Theta_i.
\end{aligned}
\tag{7.11}
$$

Let $[\cdot]$ denote the jump of the indicated quantity across the interface I , $(\cdot, \cdot)$ the $L^2(\Omega_1 \cup \Omega_2)$ inner product with $\nu = \nu_i$, $\alpha = \alpha_i$, $\beta = \beta_i$, $\hat{n} = \hat{n}_i$ and $Q = Q_i$ in Ω_i. The natural coupled or monolithic variational formulation for (7.1)-(7.9) is found by summing (7.10) and (7.11) over $i, j = 1, 2$ and $i \neq j$. That is, to find $\mathbf{u} : (0, t_f] \to X$, $\mathbf{p} : (0, t_f] \to P$ and $\mathbf{T} : (0, t_f] \to \Theta$ satisfying

$$
\begin{aligned}
&(\mathbf{u}_t, \mathbf{v}) + (\nu \nabla \mathbf{u}, \nabla \mathbf{v}) + (\mathbf{u} \cdot \nabla \mathbf{u}, \mathbf{v}) - (\mathbf{p}, \nabla \cdot \mathbf{v}) \\
&+ \int_I \kappa \, |[\mathbf{u}]| \, [\mathbf{u}] \cdot [\mathbf{v}] ds = (G(1 - \beta(\mathbf{T} - \overline{\mathbf{T}})), \mathbf{v}), \forall \mathbf{v} \in X, \\
&(\mathbf{T}_t, \boldsymbol{\theta}) + (\alpha \nabla \mathbf{T}, \nabla \boldsymbol{\theta}) + (\mathbf{u} \cdot \nabla \mathbf{T}, \boldsymbol{\theta}) + \int_{\Gamma_2} C_{atm} |T_1| T_1 \theta_1 \, ds \\
&+ \int_I \{ C_{sol} + C_{ir}[\mathbf{T}] + \mu \, |[\mathbf{u}]| \, [\mathbf{T}] \} \, [\boldsymbol{\theta}] ds = (Q, \boldsymbol{\theta}), \forall \boldsymbol{\theta} \in \Theta, \\
&\text{and } (\nabla \cdot \mathbf{u}, \mathbf{q}) = 0 \, , \, \forall \mathbf{q} \in P.
\end{aligned}
\tag{7.12}
$$

Energetic stability of solutions to the monolithic problem follows by choosing $\mathbf{v} = \mathbf{u}$, $\mathbf{q} = \mathbf{p}$ and $\boldsymbol{\theta} = \mathbf{T}$ in (7.12). An important feature of this problem is that the two-way coupling of the equations across I allows energy transfer between subdomains in both directions. This is made clear by deriving the energy equations for a single subdomain, say Ω_1, using (7.10) - (7.11). One sees that the energy of the solution on Ω_1 depends directly on the interface data of the solution on Ω_2 (and vice versa). As a result, numerically decoupling the equations and maintaining stability becomes nontrivial, particularly in light of the nonlinearity of the coupling.

7.1.3 Uncertainty Quantification

Uncertainty Quantification (UQ) is the process of determining the effect of input uncertainties on output quantities of interest. Although originally developed for engineering applications [34], UQ can also give important measures of confidence and sensitivity in numerical predictions for the natural sciences. More specifically, these techniques are currently being applied to climate models, given their significance in recent years, e.g. [20, 56, 58, 60, 63, 64, 65]. Although UQ is still an emerging field, many now classify uncertainties into two types: *aleatory* uncertainty from natural randomness in measured quantities, and *epistemic* uncertainty from lack of knowledge in the physical process, [30].

Aleatory uncertainty can be modeled with random variables or processes as one or more model inputs, and exponentially increases the size of the deterministic problem. Many techniques have recently been developed to efficiently propagate these uncertainties such as stochastic finite elements [34, 26, 6], which requires modification to a deterministic model. Stochastic collocation [71, 5, 33] is another promising approach, which uses existing deterministic models in a black-box fashion similar to, but more efficiently than, Monte Carlo simulation. Conversely, epistemic uncertainty, by its very nature, is not easy to quantify with a probabilistic framework. Model reduction techniques can be one source of this kind of uncertainty. For the sake of more efficient computations, over-simplifications are sometimes committed that sacrifice physical fidelity. The paper [37] discusses how the use of UQ in increasingly accurate models can provide an indirect estimate of (and thereby, hope to reduce) this type of uncertainty.

In this work we introduce a two-dimensional, uniformly distributed, random parameter space for κ and μ appearing in the nonlinear coupling terms in (7.3) and (7.4). UQ is performed via the stochastic collocation method on a tensor product grid with Clenshaw-Curtis quadrature [30]. Expectation and variance are calculated for full pressure, temperature, and velocity fields, as well as the average surface temperature as a quantity of interest.

Predicting trends in average near-surface air temperature or sea-surface temperature is one important goal of climate modeling. Long time studies of global surface temperature, [13], may be used as a benchmark for climate models, [70]. Recently there have been

steadily increasing efforts to quantify the uncertainty of average near surface or sea surface temperature to aid in understanding global warming and related adaptation strategies, [20, 56, 58, 60, 63, 64, 65].

The remainder of this chapter is organized as follows. Section 7.2 introduces notational conventions, defines two full discretizations using finite elements in space and semi-implicit time stepping, then presents preliminary results useful in the analysis of the deterministic model. One numerical method decouples the velocity and temperature calculations but retains coupling across the interface. The other method will decouple the calculations across I as well. The latter is a new, special purpose semi-implicit method, (see e.g. [4, 23, 40] for others.) Unconditional stability of both algorithms is proved in Section 7.3. In practice the interface parameters may be calculated time step by time step in a way that conserves the desired flux quantities, or may be prescribed from some observed data. Either way some inherent uncertainty exists in their values. UQ computations are performed in Section 7.4.

The latter part of Section 7.4 investigates uncertainty in average surface temperature. An additional algorithm is included that approximates the interface boundary conditions (7.3) and (7.4) based on an assumption sometimes used in coupled climate models, [70]. Separately, our numerical experiments quantify the aleatory uncertainty created by the unknown interface parameters in each model, showing the rate at which variance increases in time. Together, the comparison of these tests gives evidence of the epistemic uncertainty caused by the use of the decoupling and the relative accuracy to the continuum model.

The following observations are made. There is a significant difference in the expected values of velocity, temperature and average surface temperature among the numerical methods when using coarse time steps. Variance in the velocity and temperature fields propagates from the interface into the bulk of the fluids. The velocity variance values grow to be on the order of the expected values. The temperature field variance values grow until a standard deviation in excess of ≈ 20 Kelvin is observed with all models. Epistemic uncertainty initially outweighs aleatory uncertainty for coarse time steps, though both grow with time. In measuring average surface temperature, the monolithic method exhibits the smallest variance of the three methods studied. The extra aforementioned modeling assumption causes an increase in variance measuring average surface temperature.

7.2 METHOD DESCRIPTION, NOTATION AND PRELIMINARIES

This section presents the numerical schemes and provides the necessary definitions and lemmas for the stability analysis. For $D \subset \Omega$, the Sobolev space $H^k(D) = W^{k,2}(D)$ is equipped with the usual norm $\|\cdot\|_{H^k(D)}$, and semi-norm $|\cdot|_{H^k(D)}$, for $1 \leq k < \infty$, e.g. Adams [1]. The L^2 norm is denoted by $\|\cdot\|_D$. For functions $v(x,t)$ defined for almost every $t \in (0,t_f)$ on a function space $V(D)$, we define the norms $(1 \leq p \leq \infty)$

$$\|v\|_{L^\infty(0,t_f;V)} = \operatorname*{ess\,sup}_{0<t<t_f} \|v(\cdot,t)\|_V \quad \text{and} \quad \|v\|_{L^p(0,t_f;V)} = \left(\int_0^{t_f} \|v\|_V^p dt\right)^{1/p}.$$

The dual space of the Banach space V is denoted V'.

The interface coupling parameters κ and μ of the continuum model are considered as independent, uniformly distributed random variables $\kappa \sim \text{Unif}[a,b]$ and $\mu \sim \text{Unif}[c,d]$. The midpoints of these intervals are the means $E(\kappa) = \kappa_0$ and $E(\mu) = \mu_0$ and the widths of these intervals are chosen to add 10% noise. The probability density functions corresponding to the random variables are ρ_κ and ρ_μ.

Definition 7.2.1. *Given a stochastic function $f = f(\kappa,\mu)$, $E(f)$ denotes the expected value of f, defined by*

$$E(f) = \int_a^b \int_c^d f(z_1,z_2)\rho_\kappa(z_1)\rho_\mu(z_2)\,dz_1\,dz_2\,,$$

$V(f)$ denotes the variance, defined by

$$V(f) = E(f^2) - E(f)^2$$

and the standard deviation $\sigma(f)$ is defined by

$$\sigma(f) = \sqrt{V(f)}.$$

The following quantities are used in the computations (Section 7.4). The Prandtl value determines the relative sizes of momentum and thermal boundary layers.

Definition 7.2.2. *The Prandtl value of the fluid on Ω_i for $i = 1,2$ is defined by*

$$Pr_i = \frac{\nu_i}{\alpha_i}.$$

The average surface temperature is defined to be the average of the temperature of the fluid in Ω_1 over the interface I. The average surface temperature is denoted by $AST : [0, t_f] \to \mathbb{R}^+$.

Definition 7.2.3. *Let $T_1(x,t)$ be the temperature solution for Ω_1. Then the average surface temperature is defined by*

$$AST(t) = \frac{1}{|I|} \int_I T_1(x,t)\, ds.$$

Let the domain $\Omega \subset \mathbb{R}^d$ have polygonal subdomains Ω_i for $i = 1, 2$ with $\partial\Omega_1 \cap \partial\Omega_2 = \Omega_1 \cap \Omega_2 = I$. The boundaries $\partial\Omega_i$, $i = 1, 2$, are assumed to be Lipschitz continuous. Further boundary labels are defined as in Figure 13, specifically choosing $I \subset \{x_d = 0\}$, $\Gamma_2 \subset \partial\Omega_1$ to be the boundary in the direction $\hat{e}_d$, $\Gamma_3 \subset \partial\Omega_2$ to be the boundary in the direction $-\hat{e}_d$, and $\Gamma_1 = (\partial\Omega_1 \setminus (I \cup \Gamma_2)) \cup (\partial\Omega_2 \setminus (I \cup \Gamma_3))$. For $i = 1, 2$, let $(\cdot,\cdot)_{\Omega_i}$ denote the standard L^2 inner product on Ω_i, and let $(\cdot,\cdot)_{X_i}$ denote the standard H^1 inner product on Ω_i. Define $L^2(\Omega) = L^2(\Omega_1) \times L^2(\Omega_2)$. For $\mathbf{u}, \mathbf{v} \in X$ with $\mathbf{u} = [u_1, u_2]^{tr}$ and $\mathbf{v} = [v_1, v_2]^{tr}$, define the L^2 inner product

$$(\mathbf{u}, \mathbf{v}) = \sum_{i=1,2} \int_{\Omega_i} u_i \cdot v_i \, dx \,,$$

and H^1 inner product

$$(\mathbf{u}, \mathbf{v})_X = \sum_{i=1,2} \left(\int_{\Omega_i} u_i \cdot v_i \, dx + \int_{\Omega_i} \nabla u_i : \nabla v_i \, dx \right) ,$$

and the induced norms $\|\mathbf{v}\| = (\mathbf{v}, \mathbf{v})^{1/2}$ and $\|\mathbf{v}\|_X = (\mathbf{v}, \mathbf{v})_X{}^{1/2}$, respectively. It is understood, using the same notation, that the corresponding inner products on P and Θ are analogous, using scalar valued functions.

For functions $u_i \in X_i$ and $v_i, w_i \in X_i$ (or $v_i, w_i \in \Theta_i, i = 1, 2$) the explicitly skew-symmetrized nonlinear form on Ω_i is defined by

$$c_i(u_i; v_i, w_i) = \frac{1}{2}(u_i \cdot \nabla v_i, w_i)_{\Omega_i} - \frac{1}{2}(u_i \cdot \nabla w_i, v_i)_{\Omega_i}, \tag{7.13}$$

and to maintain a compact notation, we define

$$c(\mathbf{u}; \mathbf{v}, \mathbf{w}) = \sum_{i=1,2} c_i(u_i; v_i, w_i). \tag{7.14}$$

Lemma 7.2.1. *Let $u \in X_i$ with $\nabla \cdot u = 0$ and $v, w \in X_i$ (or Θ_i), $i = 1, 2$. Then*

$$c_i(u; v, w) = (u \cdot \nabla v, w)_{\Omega_i} . \tag{7.15}$$

Proof. Integrating by parts,

$$\begin{aligned}(u \cdot \nabla v, w)_{\Omega_i} &= \int_{\partial\Omega_i} (u \cdot \hat{n}_i)(v \cdot w)\, d\sigma - (\nabla \cdot u, v \cdot w)_{\Omega_i} - (u \cdot \nabla w, v)_{\Omega_i} \\ &= \int_{\partial\Omega_i} (u \cdot \hat{n}_i)(v \cdot w)\, d\sigma - (u \cdot \nabla w, v)_{\Omega_i} .\end{aligned}$$

Recalling that $u \cdot \hat{n}_i = 0$ on Γ_2, Γ_3 and I, the boundary integral reduces to

$$\int_{\partial\Omega_i} (u \cdot \hat{n}_i)(v \cdot w)\, d\sigma = \int_{\Gamma_1 \cap \partial\Omega_i} (u \cdot \hat{n}_i)(v \cdot w)\, d\sigma = 0,$$

by periodicity. Therefore,

$$(u \cdot \nabla v, w)_{\Omega_i} = - (u \cdot \nabla w, v)_{\Omega_i}$$

and the result follows. □

The following results are used to show well-posedness for weak solutions in $\mathbb{R}^2$ and in the stability analysis for the discrete algorithms.

Lemma 7.2.2. *Let $u \in H^1(\Omega_i)$ for $i = 1, 2$. Then there exists $C = C(\Omega_1, \Omega_2) > 0$, a finite constant such that*

$$\|u\|_{L^2(\partial\Omega_i)} \leq C \|u\|_{\Omega_i}^{1/2} \|u\|_{H^1(\Omega_i)}^{1/2} \tag{7.16}$$

and for $\Omega_i \subset \mathbb{R}^2$, $i = 1, 2$,

$$\|u\|_{L^4(\Omega_i)} \leq C \|u\|_{\Omega_i}^{1/2} \|u\|_{H^1(\Omega_i)}^{1/2}. \tag{7.17}$$

Proof. See e.g. Galdi [32] for these standard results. □

The identity below is useful in handling boundary integrals. Given real numbers a, b, c, d:

$$ab - cd = \frac{1}{2}(a - c)(b + d) + \frac{1}{2}(a + c)(b - d). \tag{7.18}$$

The polarization identity for vectors w^{j+1} and w^j is used in the stability proofs:

$$(w^{j+1} - w^j) \cdot w^{j+1} = \frac{1}{2}\left(|w^{j+1}|^2 + |w^{j+1} - w^j|^2 - |w^j|^2\right). \tag{7.19}$$

A brief justification of existence is provided here for $d = 2, 3$ with a complete proof of uniqueness if $d = 2$.

Theorem 7.2.3. *The weak problem* (7.12) *admits a weak solution* $(\mathbf{u}, \mathbf{p}, \mathbf{T})$ *satisfying*

$$\begin{aligned} &\mathbf{u} \in L^\infty(0, t_f; L^2(\Omega)) \cap L^2(0, t_f; X) \\ &\mathbf{p} \in L^2(0, t_f; P) \\ &\mathbf{T} \in L^\infty(0, t_f; L^2(\Omega)) \cap L^2(0, t_f; \Theta). \end{aligned} \tag{7.20}$$

If $d = 2$ this solution is unique.

Proof. Existence follows from applying the classical Galerkin procedure to discretize (7.12) in space, e.g. [66]. Existence and uniform boundedness of a family of discrete solutions is found and compactness is applied to recover the weak solution. This procedure differs from well-known results only in checking recovery of the boundary terms, and the regularity (7.20) is checked from the energy inequalities in the standard way.

If $\Omega \subset \mathbb{R}^2$ recovery of boundary terms is clear, as $H^{1/2}(\partial\Omega_i)$ is compactly embedded in $L^p(\partial\Omega_i)$ for $1 \leq p < \infty$. Existence will hold as well in $\mathbb{R}^3$ since this embedding is still compact for $1 \leq p < 4$, e.g. [1]. As an example, assuming a uniformly bounded family of

discrete solutions $(\mathbf{u}^m, \mathbf{T}^m)$, $m \in \mathbb{N}$,

$$
\begin{aligned}
&\left| \int_I |[\mathbf{u}^m]|[\mathbf{T}^m][\boldsymbol{\theta}]\, ds - \int_I |[\mathbf{u}]|[\mathbf{T}][\boldsymbol{\theta}]\, ds \right| \\
&\leq \int_I \big| |[\mathbf{u}^m]| - |[\mathbf{u}]| \big|\, |[\mathbf{T}^m]||[\boldsymbol{\theta}]|\, ds + \int_I |[\mathbf{T}^m] - [\mathbf{T}]|\, |[\mathbf{u}]||[\boldsymbol{\theta}]|\, ds \\
&\leq \int_I |[\mathbf{u}^m - \mathbf{u}]|\, |[\mathbf{T}^m]||[\boldsymbol{\theta}]|\, ds + \int_I |[\mathbf{T}^m - \mathbf{T}]|\, |[\mathbf{u}]||[\boldsymbol{\theta}]|\, ds \\
&\leq \left\{ \|u_1^m - u_1\|_{L^3(I)} + \|u_2^m - u_2\|_{L^3(I)} \right\} \|[\mathbf{T}^m]\|_{L^3(I)} \|[\boldsymbol{\theta}]\|_{L^3(I)} \\
&+ \left\{ \|T_1^m - T_1\|_{L^3(I)} + \|T_2^m - T_2\|_{L^3(I)} \right\} \|[\mathbf{u}]\|_{L^3(I)} \|[\boldsymbol{\theta}]\|_{L^3(I)} \\
&\leq C \sum_{i=1,2} \left\{ \|u_i^m - u_i\|_{L^3(\partial\Omega_i)} + \|T_i^m - T_i\|_{L^3(\partial\Omega_i)} \right\}.
\end{aligned}
$$

The constant $C > 0$ is independent of the index m and convergence is strong in $L^3(\partial\Omega_i)$, $i = 1, 2$, by compactness. The remaining boundary terms are treated similarly. Note that if $d = 3$, these arguments would fail for a boundary condition on Γ_2 of the form

$$
-\alpha_1 \nabla T_1 \cdot \hat{n}_1 = C\, T_1^4.
$$

Furthermore, integrals of $T_1^4 \theta_1$ on Γ_2 for $\theta_1 \in H^1(\Omega_1)$ would not even be bounded in general, requiring a different choice of function space, hence the choice of the quadratic approximation (7.8) used herein for this boundary condition.

To prove uniqueness when $d = 2$, assume two solutions $(\mathbf{u}^1, \mathbf{p}^1, \mathbf{T}^1)$ and $(\mathbf{u}^2, \mathbf{p}^2, \mathbf{T}^2)$. Define the differences

$$
\mathbf{u}^1 - \mathbf{u}^2 = \mathbf{e}_u\,, \;\; \mathbf{p}^1 - \mathbf{p}^2 = \mathbf{e}_p \,\text{and}\, \mathbf{T}^1 - \mathbf{T}^2 = \mathbf{e}_T.
$$

Write the variational problem (7.12) with each set of solutions separately, then subtract and choose test functions $\mathbf{v} = \mathbf{e}_u$, $\mathbf{q} = \mathbf{e}_p$ and $\boldsymbol{\theta} = \mathbf{e}_T$. The pressure difference drops out and the result may be written as

$$
\begin{aligned}
&\frac{1}{2}\frac{d}{dt}\|\mathbf{e}_u\|^2 + \|\nu^{1/2}\nabla \mathbf{e}_u\|^2 + (\mathbf{e}_u \cdot \nabla \mathbf{u}^1, \mathbf{e}_u) + (\mathbf{u}^2 \cdot \nabla \mathbf{e}_u, \mathbf{e}_u) \\
&+ \int_I \kappa \left\{ \big|[\mathbf{u}^1]\big|\, [\mathbf{u}^1] - \big|[\mathbf{u}^2]\big|\, [\mathbf{u}^2] \right\} \cdot [\mathbf{e}_u] ds = -(\beta G(\mathbf{e}_T - \overline{\mathbf{e}_T}), \mathbf{e}_u)
\end{aligned}
\tag{7.21}
$$

and

$$\begin{aligned}
&\frac{1}{2}\frac{d}{dt}\|\mathbf{e}_T\|^2 + \|\alpha^{1/2}\nabla\mathbf{e}_T\|^2 + (\mathbf{e}_u\cdot\nabla\mathbf{T}^1,\mathbf{e}_T) + (\mathbf{u}^2\cdot\nabla\mathbf{e}_T,\mathbf{e}_T)\\
&+\int_{\Gamma_2} C_{atm}\left\{|T_1^1|T_1^1 - |T_1^2|T_1^2\right\}(\mathbf{e}_T)_1\,ds + \int_I C_{ir}|[\mathbf{e}_T]|^2\,ds\\
&+\mu\int_I\left\{\left|[\mathbf{u}^1]\right|[\mathbf{T}^1] - \left|[\mathbf{u}^2]\right|[\mathbf{T}^2]\right\}[\mathbf{e}_T]\,ds = 0.
\end{aligned} \tag{7.22}$$

Two of the convective terms are zero by skew-symmetry. The nonlinear interface integrals are rewritten using (7.18). Insert these results in (7.21)- (7.22). Then rearrange terms and bound above:

$$\begin{aligned}
&\frac{1}{2}\frac{d}{dt}\|\mathbf{e}_u\|^2 + \|\nu^{1/2}\nabla\mathbf{e}_u\|^2 + \int_I\frac{\kappa}{2}\left\{\left|[\mathbf{u}^1]\right| + \left|[\mathbf{u}^2]\right|\right\}|[\mathbf{e}_u]|^2 ds\\
&\le |(\beta G(\mathbf{e}_T - \overline{\mathbf{e}_T}),\mathbf{e}_u)| + |(\mathbf{e}_u\cdot\nabla\mathbf{u}^1,\mathbf{e}_u)|\\
&+\int_I\frac{\kappa}{2}\left||[\mathbf{u}^1]| - |[\mathbf{u}^2]|\right|\left|[\mathbf{u}^1] + [\mathbf{u}^2]\right||[\mathbf{e}_u]|\,ds
\end{aligned}$$

and

$$\begin{aligned}
&\frac{1}{2}\frac{d}{dt}\|\mathbf{e}_T\|^2 + \|\alpha^{1/2}\nabla\mathbf{e}_T\|^2 + \int_I C_{ir}|[\mathbf{e}_T]|^2\,ds\\
&+\int_{\Gamma_2}\frac{C_{atm}}{2}\left\{|T_1^1| + |T_1^2|\right\}|(\mathbf{e}_T)_1|^2\,ds + \frac{\mu}{2}\int_I\left\{\left|[\mathbf{u}^1]\right| + \left|[\mathbf{u}^2]\right|\right\}|[\mathbf{e}_T]|^2\,ds\\
&\le \left|(\mathbf{e}_u\cdot\nabla\mathbf{T}^1,\mathbf{e}_T)\right| + \int_{\Gamma_2}\frac{C_{atm}}{2}\left||T_1^1| - |T_1^2|\right|\left|T_1^1 + T_1^2\right||(\mathbf{e}_T)_1|\,ds\\
&+\frac{\mu}{2}\int_I\left||[\mathbf{u}^1]| - |[\mathbf{u}^2]|\right|\left|[\mathbf{T}^1] + [\mathbf{T}^2]\right||[\mathbf{e}_T]|\,ds.
\end{aligned}$$

The interface integral terms on the right hand side are bounded precisely by the analogous nonnegative terms on the left hand side. To reveal this apply the reverse triangle inequality and triangle inequality,

$$\begin{aligned}
&\frac{1}{2}\frac{d}{dt}\|\mathbf{e}_u\|^2 + \|\nu^{1/2}\nabla\mathbf{e}_u\|^2 + \int_I\frac{\kappa}{2}\left\{\left|[\mathbf{u}^1]\right| + \left|[\mathbf{u}^2]\right|\right\}|[\mathbf{e}_u]|^2 ds\\
&\le |(\beta G(\mathbf{e}_T - \overline{\mathbf{e}_T}),\mathbf{e}_u)| + |(\mathbf{e}_u\cdot\nabla\mathbf{u}^1,\mathbf{e}_u)|\\
&+\int_I\frac{\kappa}{2}\left\{\left|[\mathbf{u}^1]\right| + \left|[\mathbf{u}^2]\right|\right\}|[\mathbf{e}_u]|^2 ds\,,
\end{aligned}$$

and

$$\begin{aligned}
&\frac{1}{2}\frac{d}{dt}\|\mathbf{e}_T\|^2 + \|\alpha^{1/2}\nabla\mathbf{e}_T\|^2 + \int_I C_{ir}|[\mathbf{e}_T]|^2\,ds \\
&+ \int_{\Gamma_2}\frac{C_{atm}}{2}\left\{|T_1^1| + |T_1^2|\right\}|(\mathbf{e}_T)_1|^2\,ds + \frac{\mu}{2}\int_I\left\{\left|[\mathbf{u}^1]\right| + \left|[\mathbf{u}^2]\right|\right\}|[\mathbf{e}_T]|^2\,ds \\
&\leq \left|(\mathbf{e}_u\cdot\nabla\mathbf{T}^1,\mathbf{e}_T)\right| + \int_{\Gamma_2}\frac{C_{atm}}{2}\left\{|T_1^1| + |T_1^2|\right\}|(\mathbf{e}_T)_1|^2\,ds \\
&+ \frac{\mu}{2}\int_I\left\{\left|[\mathbf{u}^1]\right| + \left|[\mathbf{u}^2]\right|\right\}|[\mathbf{e}_T]|^2\,ds.
\end{aligned}$$

Subtract the interface integral terms appearing on the right hand side from both sides of the inequalities and add the inequalities,

$$\begin{aligned}
&\frac{1}{2}\frac{d}{dt}\left\{\|\mathbf{e}_u\|^2 + \|\mathbf{e}_T\|^2\right\} \\
&+ \|\nu^{1/2}\nabla\mathbf{e}_u\|^2 + \|\alpha^{1/2}\nabla\mathbf{e}_T\|^2 + \int_I C_{ir}|[\mathbf{e}_T]|^2\,ds \\
&\leq |(\beta G(\mathbf{e}_T - \overline{\mathbf{e}_T}),\mathbf{e}_u)| + |(\mathbf{e}_u\cdot\nabla\mathbf{u}^1,\mathbf{e}_u)| + \left|(\mathbf{e}_u\cdot\nabla\mathbf{T}^1,\mathbf{e}_T)\right|.
\end{aligned} \tag{7.23}$$

Define $\beta^* = \max\{\beta_1,\beta_2\}$. Bound the first term on the right hand side using Hölder's inequality:

$$\begin{aligned}
&|(\beta G(\mathbf{e}_T - \overline{\mathbf{e}_T}),\mathbf{e}_u)| \\
&\leq \beta^* g\sum_{i=1,2}\left|\int_{\Omega_i}(e_T)_i(e_u)_{i,d}\,d\Omega_i\right| + \beta^* g\sum_{i=1,2}\left|\int_{\Omega_i}\left(\frac{1}{|\Omega_i|}\int_{\Omega_i}(e_T)_i\,d\Omega_i\right)(e_u)_{i,d}\,d\Omega_i\right| \\
&\leq 2\beta^* g\sum_{i=1,2}\|(e_T)_i\|_{\Omega_i}\|(e_u)_{i,d}\|_{\Omega_i}.
\end{aligned}$$

Applying Young's inequality,

$$\begin{aligned}
&|(\beta G\mathbf{e}_T - \overline{\mathbf{e}_T},\mathbf{e}_u)| \leq \beta^* g\sum_{i=1,2}\left\{\|(e_T)_i\|_{\Omega_i}^2 + \|(e_u)_{i,d}\|_{\Omega_i}^2\right\} \\
&\leq \beta^* g\left\{\|\mathbf{e}_T\|^2 + \|\mathbf{e}_u\|^2\right\}.
\end{aligned} \tag{7.24}$$

The next term on the right hand side of (7.23) is bounded also using Hölder's and Young's inequalities, with (7.17),

$$\begin{aligned}
&|(\mathbf{e}_u\cdot\nabla\mathbf{u}^1,\mathbf{e}_u)| \leq \|\mathbf{e}_u\|_{L^4(\Omega)}^2\|\nabla\mathbf{u}^1\| \\
&\leq C\|\mathbf{e}_u\|\|\mathbf{e}_u\|_X\|\nabla\mathbf{u}^1\| \leq C(\nu_1,\nu_2)\|\nabla\mathbf{u}^1\|^2\|\mathbf{e}_u\|^2 + \frac{1}{2}\|\nu^{1/2}\nabla\mathbf{e}_u\|^2.
\end{aligned}$$

The remaining term on the right hand side of (7.23) is bounded analogously. Inserting these results and (7.24) into (7.23),

$$\begin{aligned}
&\frac{1}{2}\frac{d}{dt}\left\{\|\mathbf{e}_u\|^2 + \|\mathbf{e}_T\|^2\right\} \\
&+ \|\nu^{1/2}\nabla\mathbf{e}_u\|^2 + \|\alpha^{1/2}\nabla\mathbf{e}_T\|^2 + \int_I C_{ir}|[\mathbf{e}_T]|^2\,ds \\
&\leq C(\nu,\alpha,\beta,g)\left\{1 + \|\nabla\mathbf{u}^1\|^2 + \|\nabla\mathbf{T}^1\|^2\right\}\left\{\|\mathbf{e}_u\|^2 + \|\mathbf{e}_T\|^2\right\} \\
&+ \frac{1}{2}\|\nu^{1/2}\nabla\mathbf{e}_u\|^2 + \frac{1}{2}\|\alpha^{1/2}\nabla\mathbf{e}_T\|^2.
\end{aligned}$$

Some algebraic simplification results in the following form of the inequality:

$$\begin{aligned}
&\frac{d}{dt}\left\{\|\mathbf{e}_u\|^2 + \|\mathbf{e}_T\|^2\right\} + \|\nu^{1/2}\nabla\mathbf{e}_u\|^2 + \|\alpha^{1/2}\nabla\mathbf{e}_T\|^2 + 2\int_I C_{ir}|[\mathbf{e}_T]|^2\,ds \\
&\leq G(t)\left\{\|\mathbf{e}_u\|^2 + \|\mathbf{e}_T\|^2\right\},\ G(t) = C(\nu,\alpha,\beta,g)\left\{1 + \|\nabla\mathbf{u}^1\|^2 + \|\nabla\mathbf{T}^1\|^2\right\},\ \forall t\in[0,T].
\end{aligned}$$

Since $G(t)\in L^1(0,T)$, we may integrate in time and Gronwall's inequality may be applied to yield

$$\begin{aligned}
&\left\{\|\mathbf{e}_u(t)\|^2 + \|\mathbf{e}_T(t)\|^2\right\} \\
&+ \int_0^t \left\{\|\nu^{1/2}\nabla\mathbf{e}_u(\tau)\|^2 + \|\alpha^{1/2}\nabla\mathbf{e}_T(\tau)\|^2 + 2\int_I C_{ir}|[\mathbf{e}_T(\tau)]|^2\,ds\right\} d\tau \\
&\leq \exp\left(\int_0^t G(\tau)\,d\tau\right)\left\{\|\mathbf{e}_u(0)\|^2 + \|\mathbf{e}_T(0)\|^2\right\}.
\end{aligned}$$

Since the two solutions share initial conditions, $\mathbf{e}_u(0) = 0$ and $\mathbf{e}_T(0) = 0$, hence

$$\begin{aligned}
&\left\{\|\mathbf{e}_u(t)\|^2 + \|\mathbf{e}_T(t)\|^2\right\} \\
&+ \int_0^t \left\{\|\nu^{1/2}\nabla\mathbf{e}_u(\tau)\|^2 + \|\alpha^{1/2}\nabla\mathbf{e}_T(\tau)\|^2 + 2\int_I C_{ir}|[\mathbf{e}_T(\tau)]|^2\,ds\right\} d\tau \leq 0,
\end{aligned}$$

which implies $\mathbf{e}_u(t) = 0$ and $\mathbf{e}_T(t) = 0$ for $t\in[0,T]$. Inserting these results in the weak monolithic formulation,

$$((e_p)_i, \nabla\cdot v_i)_{\Omega_i} = 0\,,\ \forall v_i\in X_i\,,\ i = 1,2\,,$$

and $\mathbf{e}_p$ has mean value zero. Then $\mathbf{e}_p = 0$ follows in the standard way, e.g. [32]. □

7.2.1 Numerical Methods

Spatial discretization is by continuous finite elements. Let τ_i^h denote a simplex mesh on Ω_i for $i = 1, 2$, with maximum element diameter h. The finite element spaces used herein are denoted for $i = 1, 2$ by

$$X_{i,h} \subset X_i \ , \ P_{i,h} \subset P_i \ , \ \Theta_{i,h} \subset \Theta_i$$
$$V_{i,h} := \{v \in X_{i,h} : (\nabla \cdot v, q)_{\Omega_i} = 0, \forall q \in P_{i,h}\}.$$

Notation for use in monolithic formulations is analogous to the definitions of X, P, Θ:

$$X_h = X_{1,h} \times X_{2,h} \ , \ P_h = P_{1,h} \times P_{2,h}$$
$$V_h = V_{1,h} \times V_{2,h} \ , \ \Theta_h = \Theta_{1,h} \times \Theta_{2,h}$$

It is assumed the following LBB^h condition will hold for the chosen finite element spaces:

$$\inf_{q \in P_{i,h}} \sup_{v \in V_{i,h}} \frac{(\nabla \cdot v, q)_{\Omega_i}}{\|q\|_{\Omega_i} \|\nabla v\|_{\Omega_i}} \geq \beta > 0 \, , \, \forall h > 0 \, , \, i = 1, 2.$$

For $t^n \in [0, t_f]$, $(\mathbf{u}^n, \mathbf{T}^n)$ will denote the discrete approximation to $(\mathbf{u}(t^n), \mathbf{T}(t^n))$, where the discrete times t^n are calculated from the uniform time step size $\Delta t = t_f/N$ by $t^n = n\Delta t$, $n = 0, 1, \ldots, N$. Then the approximations $(u_i^n, T_i^n) \in V_{i,h} \times \Theta_{i,h}$ for $i = 1, 2$ and $n = 2, 3, \ldots, N$ are calculated from either Algorithm 7.2.1 or Algorithm 7.2.2. It should be noted that Algorithm 7.2.2 requires values at two initial time steps, $\mathbf{u}^0$, $\mathbf{u}^1$ and $\mathbf{T}^1$. In both methods, the L^2-projection of the initial data into the finite element space is used for the discrete initial data $\mathbf{u}^0$ and $\mathbf{T}^0$.

The first method employs a backward-Euler time discretization with extrapolation to decouple momentum and heat calculations. Coupling across the interface is maintained between the velocity subdomain variables, and also for temperature. The method is of a monolithic variety and referred to hereafter as the "two-way monolithic" (TWM) method.

Algorithm 7.2.1 (TWM Scheme). *Let* $\Delta t > 0$, $Q \in \Theta'$. *Given* $\mathbf{u}^n \in V_h$ *and* $\mathbf{T}^n \in \Theta_h$, $n \in \{1, 2, \cdots, N-1\}$, *find* $\mathbf{u}^{n+1} \in V_h$ *satisfying*

$$\begin{aligned} &\frac{1}{\Delta t}(\mathbf{u}^{n+1} - \mathbf{u}^n, \mathbf{v}) + (\nu \nabla \mathbf{u}^{n+1}, \nabla \mathbf{v}) + c\left(\mathbf{u}^{n+1}; \mathbf{u}^{n+1}, \mathbf{v}\right) \\ &+ \kappa \int_I |[\mathbf{u}^n]|[\mathbf{u}^{n+1}] \cdot [\mathbf{v}]\, ds = (G(1 - \beta(\mathbf{T}^n - \overline{\mathbf{T}^n})), \mathbf{v}), \ \forall \mathbf{v} \in V_h. \end{aligned} \tag{7.25}$$

and $\mathbf{T}^{n+1} \in \Theta_h$ *satisfying*

$$\begin{aligned} &\frac{1}{\Delta t}(\mathbf{T}^{n+1} - \mathbf{T}^n, \boldsymbol{\theta}) + (\alpha \nabla \mathbf{T}^{n+1}, \nabla \boldsymbol{\theta}) + c(\mathbf{u}^n; \mathbf{T}^{n+1}, \boldsymbol{\theta}) + \int_{\Gamma_2} C_{atm} |T_1^n| T_1^{n+1} \theta_1 \, ds \\ &+ \int_I \left\{ C_{sol} + C_{ir}[\mathbf{T}^{n+1}] + \mu \left| [\mathbf{u}^n] \right| [\mathbf{T}^{n+1}] \right\} [\boldsymbol{\theta}] ds = (Q(t^{n+1}), \boldsymbol{\theta}), \forall \boldsymbol{\theta} \in \Theta_h. \end{aligned} \tag{7.26}$$

Algorithm 7.2.2 (TWP-GA Scheme). *Let* $\Delta t > 0$, $Q \in \Theta'$. *Given* $\mathbf{u}^{n-1}, \mathbf{u}^n \in V_h$ *and* $\mathbf{T}^n \in \Theta_h$, $n \in \{1, 2, \cdots, N-1\}$, *find* $u_i^{n+1} \in V_{i,h}$ *satisfying*

$$\begin{aligned} &\frac{1}{\Delta t}\left(u_i^{n+1} - u_i^n, v_i\right)_{\Omega_i} + \nu_i \left(\nabla u_i^{n+1}, \nabla v_i\right)_{\Omega_i} + c_i\left(u_i^{n+1}; u_i^{n+1}, v_i\right) \\ &+ \kappa \int_I |[\mathbf{u}^n]| u_i^{n+1} \cdot v_i \, ds - \kappa \int_I |[\mathbf{u}^n]|^{1/2} |[\mathbf{u}^{n-1}]|^{1/2} u_j^n \cdot v_i \, ds \\ &= \left(G(1 - \beta_i(T_i^n - \overline{T_i^n})), v_i\right)_{\Omega_i}, \ \forall v_i \in V_{i,h}, \, i = 1, 2 \,, \, i \neq j. \end{aligned} \tag{7.27}$$

and $T_i^{n+1} \in \Theta_{i,h}$ *satisfying*

$$\begin{aligned} &\frac{1}{\Delta t}\left(T_i^{n+1} - T_i^n, \theta_i\right)_{\Omega_i} + \alpha_i \left(\nabla T_i^{n+1}, \nabla \theta_i\right)_{\Omega_i} + c_i(u_i^n; T_i^{n+1}, \theta_i) \\ &+ (2 - i) \int_{\Gamma_2} C_{atm} |T_1^n| T_1^{n+1} \theta_1 \, ds \\ &+ \int_I \left\{ C_{sol}(-1)^{i+1} + C_{ir} T_i^{n+1} + \mu \left| [\mathbf{u}^n] \right| T_i^{n+1} \right\} \theta_i \, ds \\ &- \int_I \left\{ C_{ir} T_j{}^n + \mu \left| [\mathbf{u}^n] \right|^{1/2} \left| [\mathbf{u}^{n-1}] \right|^{1/2} T_j^n \right\} \theta_i \, ds \\ &= \left(Q_i(t^{n+1}), \theta_i\right)_{\Omega_i}, \forall \theta_i \in \Theta_{i,h}, \, i = 1, 2 \,, \, i \neq j. \end{aligned} \tag{7.28}$$

The use of the geometric average $|[\mathbf{u}^n]|^{1/2}|[\mathbf{u}^{n-1}]|^{1/2}$ in the coupling terms has been shown to have a stabilizing effect for (7.27), [19]. Hence Algorithm 7.2.2 is referred to as the "two-way partitioned method with geometric averaging", or *TWP-GA method*. The approach used to decouple in the linear terms has been studied in [18] for the Navier-Stokes equations.

7.3 NUMERICAL ANALYSIS

Theorem 7.3.1. *(TWM Method Stability) Let* $\mathbf{u}^j \in V_h$ *satisfy (7.25) and* $\mathbf{T}^j \in \Theta_h$ *satisfy (7.26) for each* $j \in \{0, 1, 2, \cdots, n-1, n\}$. *Then the solution of Algorithm 7.2.1 satisfies the following energy equalities at time step* $n+1$*:*

$$\begin{aligned}\left\|\mathbf{T}^{n+1}\right\|^2 + \sum_{j=0}^{n}\left\|\mathbf{T}^{j+1}-\mathbf{T}^{j}\right\|^2 + 2\Delta t\sum_{j=0}^{n}\left\|\alpha^{1/2}\nabla\mathbf{T}^{j+1}\right\|^2 \\ + 2\Delta t\sum_{j=0}^{n}\int_{\Gamma_2} C_{atm}|T_1^j||T_1^{j+1}|^2\,ds + 2\Delta t\sum_{j=0}^{n}\int_I \left\{C_{ir}+\mu\left|[\mathbf{u}^j]\right|\right\}|[\mathbf{T}^{j+1}]|^2\,ds \\ = \left\|\mathbf{T}^0\right\|^2 + 2\Delta t\sum_{j=0}^{n}\left\{(Q(t^{j+1}),\mathbf{T}^{j+1}) - \int_I C_{sol}[\mathbf{T}^{j+1}]\,ds\right\}. \quad (7.29)\end{aligned}$$

and

$$\begin{aligned}\left\|\mathbf{u}^{n+1}\right\|^2 + \sum_{j=0}^{n}\left\|\mathbf{u}^{j+1}-\mathbf{u}^{j}\right\|^2 + 2\Delta t\sum_{j=0}^{n}\left\|\nu^{1/2}\nabla\mathbf{u}^{j+1}\right\|^2 \\ + 2\kappa\,\Delta t\sum_{j=0}^{n}\int_I |[\mathbf{u}^j]||[\mathbf{u}^{j+1}]|^2\,ds = \left\|\mathbf{u}^0\right\|^2 + 2\Delta t\sum_{j=0}^{n}\left(G(1-\beta(\mathbf{T}^j-\overline{\mathbf{T}^j})),\mathbf{u}^{j+1}\right). \quad (7.30)\end{aligned}$$

Furthermore, the algorithm is unconditionally stable, satisfying:

$$\begin{aligned}\left\|\mathbf{T}^{n+1}\right\|^2 + \Delta t\sum_{j=0}^{n}\left\|\alpha^{1/2}\nabla\mathbf{T}^{j+1}\right\|^2 \le A\,e^{t_f}, \\ A = \left\|\mathbf{T}^0\right\|^2 + \Delta t\sum_{j=0}^{N}(1+2\Delta t)\left\|Q(t^{j+1})\right\|^2 + t_f\,|I|\frac{C_{sol}^2}{C_{ir}}, \quad (7.31)\end{aligned}$$

and

$$\begin{aligned}\left\|\mathbf{u}^{n+1}\right\|^2 + \Delta t\sum_{j=0}^{n}\left\|\nu^{1/2}\nabla\mathbf{u}^{j+1}\right\|^2 \\ \le \left\|\mathbf{u}^0\right\|^2 + 2g^2\,t_f\,Ae^{t_f}\,C(\Omega,\beta)\max\{\nu_1^{-1},\nu_2^{-1}\}. \quad (7.32)\end{aligned}$$

Proof. Choosing $\boldsymbol{\theta} = \mathbf{T}^{j+1}$ in (7.26), apply (7.19) to obtain

$$\frac{1}{2\Delta t}\left\{\left\|\mathbf{T}^{j+1}\right\|^2 + \left\|\mathbf{T}^{j+1} - \mathbf{T}^j\right\|^2 - \left\|\mathbf{T}^j\right\|^2\right\} + \left\|\alpha^{1/2}\nabla\mathbf{T}^{j+1}\right\|^2 + \int_{\Gamma_2} C_{atm}|T_1^j||T_1^{j+1}|^2\,ds + \int_I \left\{C_{ir} + \mu\left|[\mathbf{u}^j]\right|\right\}|[\mathbf{T}^{j+1}]|^2\,ds = (Q(t^{j+1}), \mathbf{T}^{j+1}) - \int_I C_{sol}[\mathbf{T}^{j+1}]\,ds. \quad (7.33)$$

Multiply through by $2\Delta t$ and sum over $j = 0, 1, \ldots, n$ to derive (7.29). To derive a bound, instead subtract and add back $\mathbf{T}^j$,

$$\begin{aligned}(Q(t^{j+1}), \mathbf{T}^{j+1}) &= (Q(t^{j+1}), \mathbf{T}^{j+1} - \mathbf{T}^j) + (Q(t^{j+1}), \mathbf{T}^j)\\ &\le \left\|Q(t^{j+1})\right\|\left\|\mathbf{T}^{j+1} - \mathbf{T}^j\right\| + \left\|Q(t^{j+1})\right\|\left\|\mathbf{T}^j\right\|\\ &\le \Delta t\,\left\|Q(t^{j+1})\right\|^2 + \frac{1}{4\Delta t}\left\|\mathbf{T}^{j+1} - \mathbf{T}^j\right\|^2 + \frac{1}{2}\left\{\left\|Q(t^{j+1})\right\|^2 + \left\|\mathbf{T}^j\right\|^2\right\}.\end{aligned}$$

Also, bound the right hand side interface integral as follows:

$$\begin{aligned}\int_I C_{sol}[\mathbf{T}^{j+1}]\,ds &\le \int_I \frac{C_{sol}^2}{2\left\{C_{ir} + \mu\left|[\mathbf{u}^j]\right|\right\}}\,ds + \frac{1}{2}\int_I \left\{C_{ir} + \mu\left|[\mathbf{u}^j]\right|\right\}|[\mathbf{T}^{j+1}]|^2\,ds\\ &\le \frac{|I|\,C_{sol}^2}{2C_{ir}} + \frac{1}{2}\int_I \left\{C_{ir} + \mu\left|[\mathbf{u}^j]\right|\right\}|[\mathbf{T}^{j+1}]|^2\,ds.\end{aligned}$$

Inserting these results in (7.33) and rearranging terms,

$$\frac{1}{2\Delta t}\left\{\left\|\mathbf{T}^{j+1}\right\|^2 + \frac{1}{2}\left\|\mathbf{T}^{j+1} - \mathbf{T}^j\right\|^2 - \left\|\mathbf{T}^j\right\|^2\right\} + \left\|\alpha^{1/2}\nabla\mathbf{T}^{j+1}\right\|^2 + \int_{\Gamma_2} C_{atm}|T_1^j||T_1^{j+1}|^2\,ds + \frac{1}{2}\int_I \left\{C_{ir} + \mu\left|[\mathbf{u}^j]\right|\right\}|[\mathbf{T}^{j+1}]|^2\,ds \le \Delta t\,\left\|Q(t^{j+1})\right\|^2 + \frac{1}{2}\left\{\left\|Q(t^{j+1})\right\|^2 + \left\|\mathbf{T}^j\right\|^2\right\} + \frac{|I|\,C_{sol}^2}{2C_{ir}}. \quad (7.34)$$

Multiply through (7.34) by $2\Delta t$ and sum over $j = 0, 1, \ldots, n$,

$$\begin{aligned}&\left\|\mathbf{T}^{n+1}\right\|^2 + \Delta t\sum_{j=0}^{n}\left\{\frac{1}{2}\left\|\mathbf{T}^{j+1} - \mathbf{T}^j\right\|^2 + \left\|\alpha^{1/2}\nabla\mathbf{T}^{j+1}\right\|^2\right\}\\ &\quad + 2\Delta t\sum_{j=0}^{n}\int_{\Gamma_2} C_{atm}|T_1^j||T_1^{j+1}|^2\,ds + \Delta t\sum_{j=0}^{n}\int_I \left\{C_{ir} + \mu\left|[\mathbf{u}^j]\right|\right\}|[\mathbf{T}^{j+1}]|^2\,ds\\ &\quad \le \left\|\mathbf{T}^0\right\|^2 + \Delta t\sum_{j=0}^{n}\left\{(1 + 2\Delta t)\,\left\|Q(t^{j+1})\right\|^2 + \left\|\mathbf{T}^j\right\|^2\right\} + (n+1)\Delta t\,\frac{|I|\,C_{sol}^2}{C_{ir}}. \quad (7.35)\end{aligned}$$

Apply the discrete Gronwall inequality and (7.31) follows. The bound on the temperature is used in turn to bound the velocity solution. Choosing $\mathbf{v} = \mathbf{u}^{j+1}$ in (7.25) and applying (7.19),

$$\begin{aligned} &\frac{1}{2\Delta t}\left\{\left\|\mathbf{u}^{j+1}\right\|^2 + \left\|\mathbf{u}^{j+1}-\mathbf{u}^{j}\right\|^2 - \left\|\mathbf{u}^{j}\right\|^2\right\} + \left\|\nu^{1/2}\nabla\mathbf{u}^{j+1}\right\|^2 \\ &+ \kappa\int_I |[\mathbf{u}^j]||[\mathbf{u}^{j+1}]|^2\,ds = (G(1-\beta(\mathbf{T}^j - \overline{\mathbf{T}^j})), \mathbf{u}^{j+1}). \end{aligned} \tag{7.36}$$

Multiply through by $2\Delta t$ and sum over $j = 0, 1, \ldots, n$ to derive (7.30). To derive a bound, instead note that the right hand side of (7.36) can be expressed as

$$(G(1-\beta(\mathbf{T}^j - \overline{\mathbf{T}^j})), \mathbf{u}^{j+1}) = -g\sum_{i=1,2}\int_{\Omega_i}(1-\beta_i(T_i^j - \overline{T_i^j}))u_{i,d}^{j+1}\,d\Omega_i.$$

The boundary conditions on Γ_2 and Γ_3 for $u_{i,d}^{j+1}$, $i = 1, 2$ allow for usage of the Poincaré-Friedrich's inequality, hence

$$\begin{aligned} &(G(1-\beta(\mathbf{T}^j - \overline{\mathbf{T}^j})), \mathbf{u}^{j+1}) \leq g\sum_{i=1,2}\left\|1-\beta_i(T_i^j - \overline{T_i^j})\right\|_{\Omega_i}\left\|u_{i,d}^{j+1}\right\|_{\Omega_i} \\ &\leq g\sum_{i=1,2}\left\|1-\beta_i(T_i^j - \overline{T_i^j})\right\|_{\Omega_i} C_{PF}\left\|\nabla u_{i,d}^{j+1}\right\|_{\Omega_i} \\ &\leq \sum_{i=1,2}\frac{g^2\,C_{PF}^2}{2\nu_i}\left\|1-\beta_i(T_i^j - \overline{T_i^j})\right\|_{\Omega_i}^2 + \frac{\nu_i}{2}\left\|\nabla u_i^{j+1}\right\|_{\Omega_i}^2 \\ &\leq \sum_{i=1,2}\frac{g^2}{\nu_i}C(\Omega_i,\beta_i)\left\|T_i^j\right\|_{\Omega_i}^2 + \frac{\nu_i}{2}\left\|\nabla u_i^{j+1}\right\|_{\Omega_i}^2 \\ &\leq g^2\,\max\{\nu_1^{-1},\nu_2^{-1}\}C(\Omega_1,\Omega_2,\beta_1,\beta_2)\left\|\mathbf{T}^j\right\|^2 + \sum_{i=1,2}\frac{\nu_i}{2}\left\|\nabla u_i^{j+1}\right\|_{\Omega_i}^2. \end{aligned}$$

Insert this result into (7.36), so that rearranging terms yields

$$\begin{aligned} &\frac{1}{2\Delta t}\left\{\left\|\mathbf{u}^{j+1}\right\|^2 + \left\|\mathbf{u}^{j+1}-\mathbf{u}^{j}\right\|^2 - \left\|\mathbf{u}^{j}\right\|^2\right\} + \frac{1}{2}\left\|\nu^{1/2}\nabla\mathbf{u}^{j+1}\right\|^2 \\ &+ \kappa\int_I |[\mathbf{u}^j]||[\mathbf{u}^{j+1}]|^2\,ds \leq g^2\,\max\{\nu_1^{-1},\nu_2^{-1}\}C(\Omega_1,\Omega_2,\beta_1,\beta_2)\left\|\mathbf{T}^j\right\|^2, \end{aligned}$$

and (7.32) then follows by inserting the temperature bound (7.31), multiplying through by $2\Delta t$ and summing over $j = 0, 1, \ldots, n$. □

Theorem 7.3.2. *(TWP-GA Method Stability) Let $u_i^j \in V_{i,h}$ satisfy (7.27) and $T_i^j \in \Theta_{i,h}$ satisfy (7.28) for $i = 1, 2$ and each $j \in \{0, 1, 2, \cdots, n-1, n\}$. Then the solution of Algorithm 7.2.2 satisfies the following energy equalities at time step $n+1$:*

$$\begin{aligned}
&\left\|\mathbf{T}^{n+1}\right\|^2 + \sum_{j=1}^{n} \left\|\mathbf{T}^{j+1} - \mathbf{T}^{j}\right\|^2 + 2\Delta t \sum_{j=1}^{n} \left\|\alpha^{1/2}\nabla \mathbf{T}^{j+1}\right\|^2 + \Delta t \sum_{j=1}^{n} \Lambda^{j+1} \\
&\quad + \Delta t \int_I \{C_{ir} + \mu\,|[\mathbf{u}^n]|\}\,|\mathbf{T}^{n+1}|^2\,ds = \left\|\mathbf{T}^{1}\right\|^2 + \Delta t \int_I \left\{C_{ir} + \mu\left|[\mathbf{u}^0]\right|\right\}|\mathbf{T}^{1}|^2\,ds \\
&\qquad\qquad + 2\Delta t \sum_{j=1}^{n} \left\{(Q(t^{j+1}), \mathbf{T}^{j+1}) - \int_I C_{sol}[\mathbf{T}^{j+1}]\,ds\right\}, \quad (7.37)
\end{aligned}$$

$$\begin{aligned}
&\textit{with } \Lambda^{j+1} = 2\int_{\Gamma_2} C_{atm}|T_1^j||T_1^{j+1}|^2\,ds + \int_I \frac{C_{ir}}{2}\left\{|T_1^{j+1} - T_2^j|^2 + |T_2^{j+1} - T_1^j|^2\right\} ds \\
&+ \int_I \mu\left||[\mathbf{u}^j]|^{1/2}T_1^{j+1} - |[\mathbf{u}^{j-1}]|^{1/2}T_2^j\right|^2 ds + \int_I \mu\left||[\mathbf{u}^j]|^{1/2}T_2^{j+1} - |[\mathbf{u}^{j-1}]|^{1/2}T_1^j\right|^2 ds,
\end{aligned}$$

and the velocity fields satisfy

$$\begin{aligned}
&\left\|\mathbf{u}^{n+1}\right\|^2 + \sum_{j=1}^{n} \left\|\mathbf{u}^{j+1} - \mathbf{u}^{j}\right\|^2 + 2\Delta t \sum_{j=1}^{n} \left\|\nu^{1/2}\nabla \mathbf{u}^{j+1}\right\|^2 \\
&\qquad + \kappa\,\Delta t \int_I |[\mathbf{u}^n]||\mathbf{u}^{n+1}|^2\,ds + \kappa\,\Delta t \sum_{j=1}^{n} \Psi^{j+1} \\
&\quad = \left\|\mathbf{u}^{0}\right\|^2 + 2\Delta t \sum_{j=1}^{n} \left(G(1 - \beta(\mathbf{T}^j - \overline{\mathbf{T}^j})), \mathbf{u}^{j+1}\right) + \kappa\,\Delta t \int_I |[\mathbf{u}^0]||\mathbf{u}^1|^2\,ds, \quad (7.38)
\end{aligned}$$

$$\textit{with } \Psi^{j+1} = \int_I \left||[\mathbf{u}^j]|^{1/2}u_1^{j+1} - |[\mathbf{u}^{j-1}]|^{1/2}u_2^j\right|^2 + \left||[\mathbf{u}^j]|^{1/2}u_2^{j+1} - |[\mathbf{u}^{j-1}]|^{1/2}u_1^j\right|^2 ds.$$

Furthermore, the algorithm is unconditionally stable, satisfying:

$$\begin{aligned}
&\left\|\mathbf{T}^{n+1}\right\|^2 + \Delta t \sum_{j=1}^{n} \left\|\alpha^{1/2}\nabla \mathbf{T}^{j+1}\right\|^2 \le F\,e^{\gamma t_f}, \\
&F = \left\|\mathbf{T}^{1}\right\|^2 + \Delta t(1 + 2\Delta t)\sum_{j=1}^{N} \left\|Q(t^{j+1})\right\|^2 + t_f \frac{|I|C_{sol}^2 C}{2}\left\{\frac{1}{\alpha_1} + \frac{1}{\alpha_2}\right\} \quad (7.39) \\
&+ t_f|I|\frac{4C_{sol}^2}{C_{ir}} + \Delta t \int_I \{C_{ir} + \mu\left|[\mathbf{u}^0]\right|\}|\mathbf{T}^1|^2\,ds \textit{ and } \gamma = 1 + 2\max\{\alpha_1, \alpha_2\},
\end{aligned}$$

and

$$\begin{aligned}
&\left\|\mathbf{u}^{n+1}\right\|^2 + \Delta t \sum_{j=1}^{n} \left\|\nu^{1/2}\nabla \mathbf{u}^{j+1}\right\|^2 \le G, \\
&G = \left\|\mathbf{u}^{1}\right\|^2 + \kappa\,\Delta t \int_I |[\mathbf{u}^0]||[\mathbf{u}^1]|^2\,ds + 2g^2\,t_f\,F e^{\gamma t_f}\,C(\Omega, \beta)\max\{\nu_1^{-1}, \nu_2^{-1}\}. \quad (7.40)
\end{aligned}$$

Proof. . Let $j \in \{1, 2, \ldots, N-1\}$ and consider (7.28) with $n = j$. Setting $\theta_i = T_i^{j+1}$ in (7.28), summing over $i = 1, 2$ and applying (7.19) yields

$$\begin{aligned}
&\frac{1}{2\Delta t}\left\{\left\|\mathbf{T}^{j+1}\right\|^2 - \left\|\mathbf{T}^{j}\right\|^2 + \left\|\mathbf{T}^{j+1} - \mathbf{T}^{j}\right\|^2\right\} + \left\|\alpha^{1/2}\nabla\mathbf{T}^{j+1}\right\|^2 \\
&+ \int_{\Gamma_2} C_{atm}|T_1^j||T_1^{j+1}|^2\,ds + \int_I C_{sol}[\mathbf{T}^{j+1}]\,ds \\
&+ \int_I C_{ir}\{T_1{}^{j+1} - T_2^j\}T_1^{j+1}\,ds + \int_I C_{ir}\{T_2{}^{j+1} - T_1^j\}T_2^{j+1}\,ds \\
&+ \int_I \mu\{\left|[\mathbf{u}^j]\right| T_1^{j+1} - \left|[\mathbf{u}^j]\right|^{1/2}\left|[\mathbf{u}^{j-1}]\right|^{1/2} T_2^j\}T_1^{j+1}\,ds \\
&+ \int_I \mu\{\left|[\mathbf{u}^j]\right| T_2^{j+1} - \left|[\mathbf{u}^j]\right|^{1/2}\left|[\mathbf{u}^{j-1}]\right|^{1/2} T_1^j\}T_2^{j+1}\,ds = (Q(t^{j+1}), \mathbf{T}^{j+1})
\end{aligned} \tag{7.41}$$

Applying the polarization identity again,

$$\begin{aligned}
&\int_I C_{ir}\{T_1{}^{j+1} - T_2^j\}T_1^{j+1}\,ds + \int_I C_{ir}\{T_2{}^{j+1} - T_1^j\}T_2^{j+1}\,ds \\
&= \frac{1}{2}\int_I C_{ir}\{|T_1{}^{j+1}|^2 - |T_2^j|^2 + |T_1{}^{j+1} - T_2{}^j|^2\}\,ds \\
&+ \frac{1}{2}\int_I C_{ir}\{|T_2{}^{j+1}|^2 - |T_1^j|^2 + |T_2{}^{j+1} - T_1{}^j|^2\}\,ds \\
&= \frac{1}{2}\int_I C_{ir}\{|\mathbf{T}^{j+1}|^2 - |\mathbf{T}^j|^2 + |T_1{}^{j+1} - T_2{}^j|^2 + |T_2{}^{j+1} - T_1{}^j|^2\}\,ds.
\end{aligned} \tag{7.42}$$

Bounding the third line of (7.41) requires one more application of (7.19) with $w^{j+1} = |[\mathbf{u}^j]|^{1/2} T_1^{j+1}$ and $w^j = |[\mathbf{u}^{j-1}]|^{1/2} T_2^j$. It follows

$$\begin{aligned}
&\int_I \mu\{\left|[\mathbf{u}^j]\right| T_1^{j+1} - \left|[\mathbf{u}^j]\right|^{1/2}\left|[\mathbf{u}^{j-1}]\right|^{1/2} T_2^j\}T_1^{j+1}\,ds \\
&= \frac{1}{2}\int_I \mu\{\left|[\mathbf{u}^j]\right| |T_1^{j+1}|^2 - \left|[\mathbf{u}^{j-1}]\right| |T_2^j|^2\}\,ds \\
&+ \frac{1}{2}\int_I \mu\left||[\mathbf{u}^j]|^{1/2} T_1^{j+1} - |[\mathbf{u}^{j-1}]|^{1/2} T_2^j\right|^2\,ds.
\end{aligned} \tag{7.43}$$

A bound analogous to (7.43) is used for the fourth line of (7.41). Combining these results with (7.42), inserting in (7.41) and rearranging terms,

$$\begin{aligned}
&\frac{1}{2\Delta t}\left\{\left\|\mathbf{T}^{j+1}\right\|^2 - \left\|\mathbf{T}^{j}\right\|^2 + \left\|\mathbf{T}^{j+1} - \mathbf{T}^{j}\right\|^2\right\} + \left\|\alpha^{1/2}\nabla\mathbf{T}^{j+1}\right\|^2 \\
&+ \frac{1}{2}\int_I \mu\{\left|[\mathbf{u}^j]\right| |\mathbf{T}^{j+1}|^2 - \left|[\mathbf{u}^{j-1}]\right| |\mathbf{T}^j|^2\}\,ds + \frac{1}{2}\Lambda^{j+1} \\
&+ \frac{1}{4}\int_I C_{ir}\{|T_1^{j+1} - T_2^j|^2 - |T_2^{j+1} - T_1^j|^2\}\,ds \\
&+ \frac{1}{2}\int_I C_{ir}\{|\mathbf{T}^{j+1}|^2 - |\mathbf{T}^j|^2\}\,ds = (Q(t^{j+1}), \mathbf{T}^{j+1}) - \int_I C_{sol}[\mathbf{T}^{j+1}]\,ds,
\end{aligned} \tag{7.44}$$

with Λ^{j+1} as defined in the theorem statement. Multiply through by $2\Delta t$, sum over $j = 1, 2, \ldots, n$ and rearrange terms to achieve (7.37). To derive a bound for the temperature, instead bound the term $(Q(t^{j+1}), \mathbf{T}^{j+1})$ as in the proof of Theorem 7.3.1. Then only one term remains to be bounded,

$$\begin{aligned}
&-\int_I C_{sol}[\mathbf{T}^{j+1}]\,ds = -C_{sol}\int_I T_1^{j+1} - T_2^j + T_2^j - T_1^j + T_1^j - T_2^{j+1}\,ds \\
&\leq C_{sol}\int_I |T_1^{j+1} - T_2^j|\,ds + C_{sol}\int_I |T_2^j - T_1^j|\,ds + C_{sol}\int_I |T_1^j - T_2^{j+1}|\,ds \\
&\leq \int_I \frac{2C_{sol}^2}{C_{ir}}\,ds + \frac{C_{ir}}{4}\int_I |T_1^{j+1} - T_2^j|^2\,ds \\
&+ C_{sol}\int_I |T_2^j - T_1^j|\,ds + \frac{C_{ir}}{4}\int_I |T_2^{j+1} - T_1^j|^2\,ds.
\end{aligned} \tag{7.45}$$

Applying the triangle inequality followed by Young's inequality and (7.16),

$$\begin{aligned}
&C_{sol}\int_I |T_2^j - T_1^j|\,ds \leq \frac{|I|C_{sol}^2}{2}\left\{\frac{1}{\epsilon_1} + \frac{1}{\epsilon_2}\right\} + \frac{\epsilon_1}{2}\int_I |T_1^j|^2\,ds + \frac{\epsilon_2}{2}\int_I |T_2^j|^2\,ds \\
&\leq \frac{|I|C_{sol}^2}{2}\left\{\frac{1}{\epsilon_1} + \frac{1}{\epsilon_2}\right\} + \frac{C\epsilon_1}{2}\left\|T_1^j\right\|_{\Omega_1}\left\|T_1^j\right\|_{H^1(\Omega_1)} + \frac{C\epsilon_2}{2}\left\|T_2^j\right\|_{\Omega_2}\left\|T_2^j\right\|_{H^1(\Omega_2)} \\
&\leq \frac{|I|C_{sol}^2}{2}\left\{\frac{1}{\epsilon_1} + \frac{1}{\epsilon_2}\right\} + \frac{C\epsilon_1}{2}\left\|T_1^j\right\|_{\Omega_1}^2 + \frac{C\epsilon_1}{4}\left\|\nabla T_1^j\right\|_{\Omega_1}^2 + \frac{C\epsilon_2}{2}\left\|T_2^j\right\|_{\Omega_2}^2 + \frac{C\epsilon_2}{4}\left\|\nabla T_2^j\right\|_{\Omega_2}^2.
\end{aligned}$$

Choose $\epsilon_i = 2\alpha_i/C$, $i = 1, 2$ and insert this result in (7.45), from which (7.44) may subsequently be bounded by

$$\begin{aligned}
&\frac{1}{2\Delta t}\left\{\left\|\mathbf{T}^{j+1}\right\|^2 - \left\|\mathbf{T}^j\right\|^2 + \frac{1}{2}\left\|\mathbf{T}^{j+1} - \mathbf{T}^j\right\|^2\right\} + \frac{1}{2}\left\|\alpha^{1/2}\nabla\mathbf{T}^{j+1}\right\|^2 \\
&+ \frac{1}{2}\int_I \mu\{\left|[\mathbf{u}^j]\right|\,|\mathbf{T}^{j+1}|^2 - \left|[\mathbf{u}^{j-1}]\right|\,|\mathbf{T}^j|^2\}\,ds + \frac{1}{2}\Lambda^{j+1} \\
&+ \frac{1}{2}\int_I C_{ir}\{|\mathbf{T}^{j+1}|^2 - |\mathbf{T}^j|^2\}\,ds \leq \Delta t\,\left\|Q(t^{j+1})\right\|^2 + \frac{1}{2}\left\{\left\|Q(t^{j+1})\right\|^2 + \left\|\mathbf{T}^j\right\|^2\right\} \\
&+ \frac{|I|C_{sol}^2 C}{4}\left\{\frac{1}{\alpha_1} + \frac{1}{\alpha_2}\right\} + \alpha_1\left\|T_1^j\right\|_{\Omega_1}^2 + \alpha_2\left\|T_2^j\right\|_{\Omega_2}^2 + |I|\frac{2C_{sol}^2}{C_{ir}}.
\end{aligned}$$

Using $\gamma = 1 + 2\max\{\alpha_1, \alpha_2\}$, the discrete Gronwall inequality is applied after multiplication by $2\Delta t$. Then rearranging terms yields the desired result, (7.39). Deriving the bound for

the velocity is somewhat simpler. Choose $v_1 = u_1^{j+1}$ and $v_2 = u_2^{j+1}$ in (7.27), so that adding the resulting equations and proceeding as with previous arguments,

$$\begin{aligned}\frac{1}{2\Delta t}\left(\left\|\mathbf{u}^{j+1}\right\|^2 - \left\|\mathbf{u}^{j}\right\|^2 + \left\|\mathbf{u}^{j+1} - \mathbf{u}^{j}\right\|^2\right) + \left\|\nu^{1/2}\nabla\mathbf{u}^{j+1}\right\|^2 \\ + \kappa\int_I \left|u_1^{j+1}\right|^2 \left|[\mathbf{u}^j]\right| \, ds + \kappa\int_I \left|u_2^{j+1}\right|^2 \left|[\mathbf{u}^j]\right| \, ds \\ - \kappa\int_I u_2^j \cdot u_1^{j+1} \left|[\mathbf{u}^j]\right|^{1/2} \left|[\mathbf{u}^{j-1}]\right|^{1/2} \, ds - \kappa\int_I u_1^j \cdot u_2^{j+1} \left|[\mathbf{u}^j]\right|^{1/2} \left|[\mathbf{u}^{j-1}]\right|^{1/2} \, ds \\ = \left(G(1-\beta(\mathbf{T}^j - \overline{\mathbf{T}^j})), \mathbf{u}^{j+1}\right). \quad (7.46)\end{aligned}$$

The right hand side of (7.46) is bounded analogously to the monolithic case, the only difference being the bound on the temperature. Only application of (7.19) is needed to deal with the interface terms. Apply (7.19) once with $w^{j+1} = u_1^{j+1}|[\mathbf{u}^j]|^{1/2}$ and $w^j = u_2^j|[\mathbf{u}^{j-1}]|^{1/2}$, and again with $w^{j+1} = u_2^{j+1}|[\mathbf{u}^j]|^{1/2}$ and $w^j = u_1^j|[\mathbf{u}^{j-1}]|^{1/2}$, yielding

$$\begin{aligned}\frac{1}{2\Delta t}\left(\left\|\mathbf{u}^{j+1}\right\|^2 - \left\|\mathbf{u}^{j}\right\|^2 + \left\|\mathbf{u}^{j+1} - \mathbf{u}^{j}\right\|^2\right) + \left\|\nu^{1/2}\nabla\mathbf{u}^{j+1}\right\|^2 \\ + \frac{\kappa}{2}\int_I \left|\mathbf{u}^{j+1}\right|^2 \left|[\mathbf{u}^j]\right| \, ds - \frac{\kappa}{2}\int_I \left|\mathbf{u}^{j}\right|^2 \left|[\mathbf{u}^{j-1}]\right| \, ds + \frac{\kappa}{2}\Psi^{j+1} \\ \leq g^2 \max\{\nu_1^{-1}, \nu_2^{-1}\} C(\Omega_1, \Omega_2, \beta_1, \beta_2) \left\|\mathbf{T}^j\right\|^2 + \sum_{i=1,2} \frac{\nu_i}{2} \left\|\nabla u_i^{j+1}\right\|_{\Omega_i}^2, \quad (7.47)\end{aligned}$$

where Ψ^{j+1} defined in the theorem statement. Subsume the velocity gradient terms on the right hand side. The desired result follows by applying the temperature bound (7.39), multiplying through by $2\Delta t$ and summing over $j = 1, 2, \ldots, n$, then rearranging terms. □

7.4 NUMERICAL EXPERIMENTS

Computational tests were performed for a domain $\Omega \subset \mathbb{R}^2$ as described in Section 7.2 and by Figure 13. Specifically, we chose $I = [0, 10] \times \{0\}$, $\Gamma_2 = [0, 10] \times \{1\}$ and the bottom border of Ω_2, Γ_3, is the curve

$$y(x) = 0.3\cos(\frac{\pi x}{5} - s) - 0.83 + 0.3\cos(1 - s + \frac{2\pi x}{5})$$

which for some s is at least a C^1 bottom boundary when extended periodically in x, where $s \approx 0.68012709$.

The numerical algorithms TWM and TMP-GA were implemented using the freely available finite element solver package FreeFem++, [35]. A uniformly distributed noise of 10% was assumed in the stochastic parameters κ, μ. Expected values were calculated using a 25 point tensor-grid quadrature rule (Clenshaw-Curtis) for 2 stochastic dimensions, exact for integrands that are products of any two polynomials each having degree less than 5.

Prandtl values were chosen in Ω_1 as air at standard temperature and pressure and in Ω_2 as water. Kinematic viscosities were chosen larger than for air and water to save computational expense. The choice of κ_0 is from [12, 19] and $\mu_0 > \kappa_0$ to emphasize the role of sensible heat transfer. Motivation for the remaining parameter choices is explained in [47, 70]. The problem parameter values are:

- Kinematic viscosities: $\nu_1 = 0.05$ and $\nu_2 = 0.005$
- Interface coupling for velocity (mean): $\kappa_0 = 0.00245$
- Interface coupling for temperature (mean): $\mu_0 = 0.1$
- Interface solar constant: $C_{sol} = 0.75$
- Interface longwave radiation constant: $C_{ir} = (2.23398 \times 10^{-7}) \times 293.15^3$
- Radiative constant on Γ_2: $C_{atm} = 7.016 \times 10^{-6}$
- Gravitational constant $G = \langle 0, -9.81 \rangle (m/s^2)$
- Coefficients of thermal expansion: $\beta_1 = 0.00343$ and $\beta_2 = 2.07 \times 10^{-4}$
- Prandtl numbers: $Pr_1 = 0.713$ and $Pr_2 = 7.0$
- Heat dissipation constants: $\alpha_i = \nu_i / Pr_i$, $i = 1, 2$

The heating source was set to zero in Ω_2, $Q_2(t) = 0$, and in Ω_1 is

$$Q_1(x, y, t) = \max\{342.0\,(2\cos(2\pi\,(x - 10t)/20)^2 - 1), 0\}.$$

Computations were performed using non-dimensionalized equations based upon reference values of temperature, velocity and length:

- $T_0 = 293.15$ Kelvin
- $U = 1.0$ meters/second

- $L = 100.0$ meters

and the initial velocities were set to zero. The temperature profiles in Ω_1 and Ω_2 were initially set to

$$T_1^0(x, y) = 1.0 - 0.02\, y$$

$$\text{and} \quad T_2^0(x, y) = 283.15\,(1.0 + 10.0\, y/273.15)/293.15.$$

Additionally, algorithm TWP-GA requires the data for the first time step $t = \Delta t$. This data was provided by substituting in the results at $t = \Delta t$ from the algorithm TWM. A time step size of $\Delta t = 1/50$ was used to solve on the interval $t \in [0, 20]$. Spatial discretization was performed using MINI velocity-pressure finite elements and globally continuous, piecewise linear polynomial elements for temperature. The spatial degrees of freedom used to approximate the velocity u_i, pressure p_i and temperature T_i on Ω_i for $i = 1, 2$ are shown in Table 22.

The automated Delaunay-Voronoi algorithm was used to generate the unstructured mesh used. In Figure 14 a coarse mesh is shown as an example. The mesh is more refined in the upper right and left hand corners of Ω_2 and along I since flow features were expected to be smallest in these regions.

Table 22: Degrees of freedom for discrete solutions.

	u_1	p_1	T_1	u_2	p_2	T_2
DOF's	30958	5310	5310	26098	4513	4513

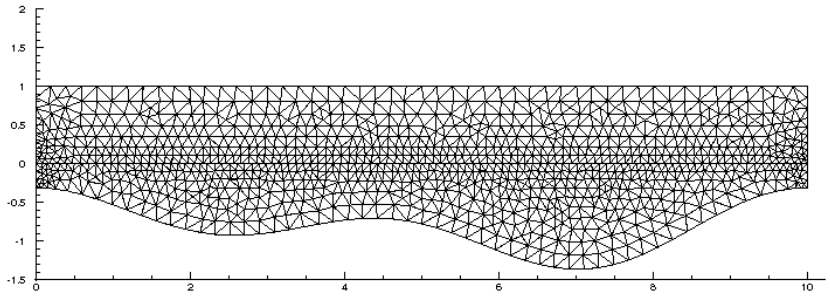

Figure 14: A coarse mesh placed across Ω_1 and Ω_2.

7.4.1 Solution Behavior and Epistemic Uncertainty

The heating function $Q_1(x, y, t)$ was chosen to heat the fluid in Ω_1 locally on a region with small support in the x-direction, but moving from left to right over time, repeating the motion periodically. We intend to loosely represent the heating of the sun moving over the surface of the ocean and induce the associated wind patterns (for this 2D, single-layer model) by allowing heat to dissipate radiatively through the upper atmosphere. The result is convective currents in Ω_1, which through surface friction and heat exchange on the interface subsequently induce currents in Ω_2. This behavior is shown using streamlines in Figure 15 for the TWM algorithm at time $t_f = 20$. A different result is seen in Figure 16 for the TWP-GA method. In particular the two velocity fields do not share the same rotational structures.

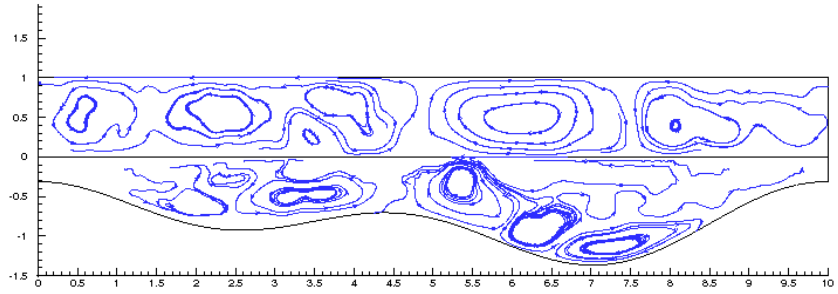

Figure 15: Streamlines for expectation of velocity: TWM method.

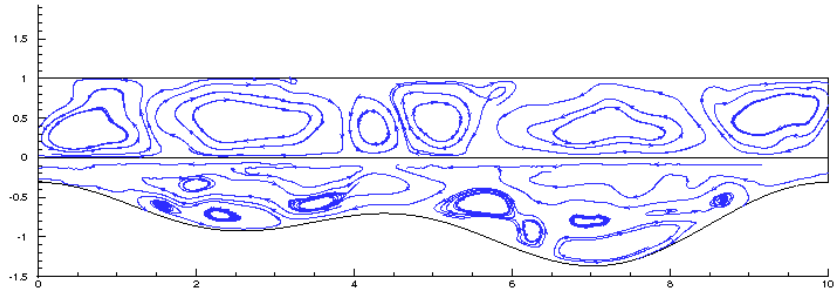

Figure 16: Streamlines for expectation of velocity: TWP-GA method.

Figure 17 shows the temperature expectation field for the TWM algorithm at the final time. Comparing with the TWP-GA algorithm temperature expectation in Figure 18 it

is clear the TWM algorithm predicts higher average temperatures in Ω_1, and it has been verified directly that a higher average temperature is predicted in Ω_2 as well. A close study of the plots indicates this is due to a higher concentration of heat near I in Ω_2 for the TWM algorithm. The TWP-GA algorithm appears to dissipate heat energy more than the TWM algorithm. This could be related to a different initial transient response. We return to this point in Section 7.4.3.

The differences in velocity and temperature expectation values using the two algorithms are not surprising as the time step size and mesh size are both somewhat coarse. The epistemic uncertainty in the velocity and temperature fields is significant, using the difference in expected values between the numerical models as a measure. It is also interesting for long time calculations to ascertain the level of aleatory uncertainty. Thus we focus next on the variance calculations.

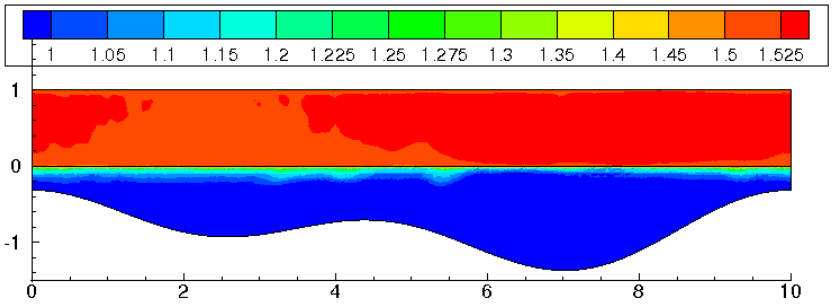

Figure 17: Expectation of temperature: TWM method.

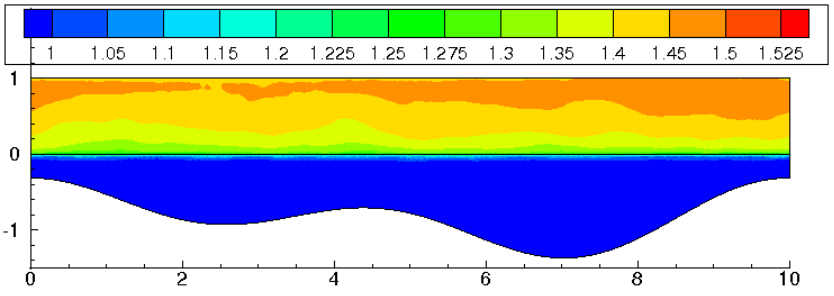

Figure 18: Expectation of temperature: TWP-GA method.

7.4.2 Characterizing Aleatory Uncertainty

The magnitude of variance in the velocity fields for both algorithms is on the order of the magnitude of the expected values of the velocities by the final time $t_f = 20$, as shown in Figures 19 - 20. The variance is largest in Ω_1 which is consistent with the size of the velocities being larger in Ω_1 than in Ω_2. Also, the largest variance values occur near the interface for both algorithms. While the velocity variance values are similar for both algorithms, the TWP-GA code yields the largest variance in velocity over a nontrivial region.

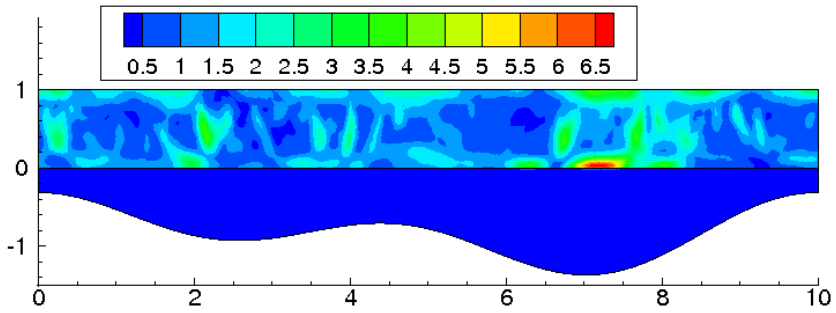

Figure 19: Magnitude of variance of velocity: TWM method.

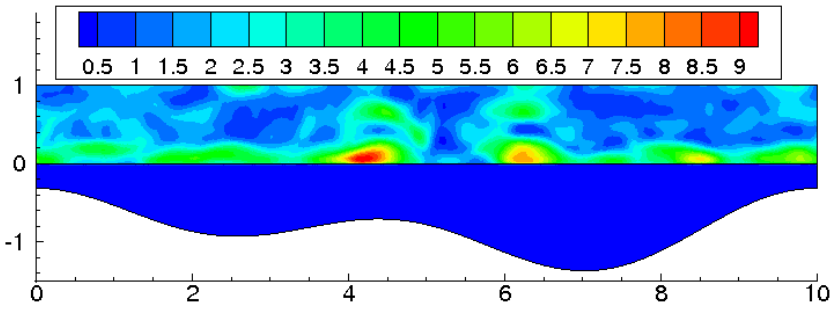

Figure 20: Magnitude of variance of velocity: TWP-GA method.

In Figure 21 the variance is seen to be as large as 0.038, which corresponds to a standard deviation of roughly $\sigma \approx 0.1949$. This is in the dimensionless system, so rescaling yields an equivalent standard deviation of roughly 57 Kelvin. Perhaps surprisingly, the TWP-GA code (Figure 22) does not achieve as high of a variance in the point-wise temperature field, with a maximum around 0.0052, translating to an equivalent standard deviation of roughly

21 Kelvin. The temperature variance values in the bulk fluid are much smaller than occur near the interface in both cases.

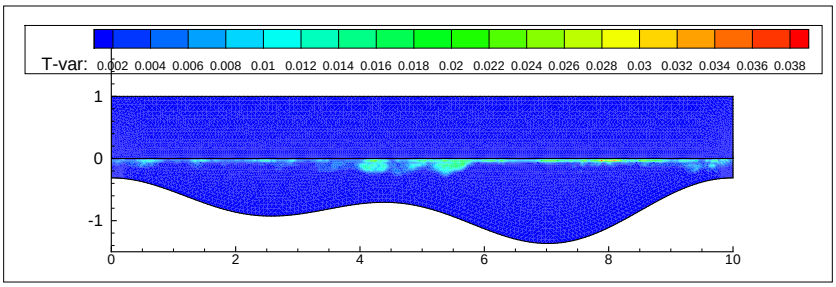

Figure 21: Variance of temperature: TWM method.

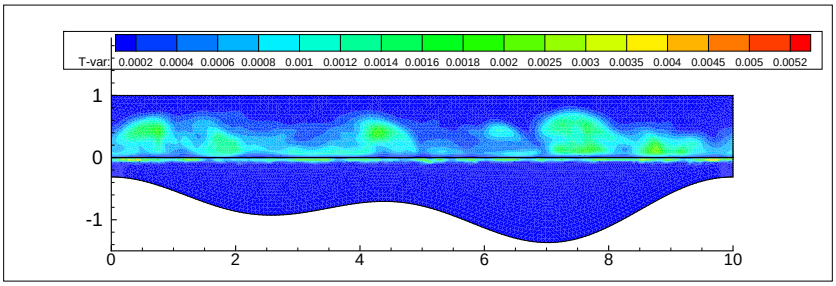

Figure 22: Variance of temperature: TWP-GA method.

Solving the monolithic climate problem is not generally considered practical as evidenced by a variety of current climate models, [21, 22, 27]. The relevant issue is then whether the variance predicted is catastrophically large using a model decoupled across the fluid-fluid interface like TWP-GA. The TWM algorithm is considered as a benchmark problem. In the current investigation the velocity variance in the TWP-GA model does not appear to be even an order of magnitude larger than for the TWM model, while the maximum temperature variance for the TWP-GA model is smaller than for the TWM model. As the variance in the velocity is only large in certain localized regions of the global domain, we expect statistical data such as average temperature to have a much better variance behavior.

7.4.3 Predicting Statistical Data: Average Surface Temperature

Reliability of average surface temperature (AST, see Definition 7.2.3) calculations is important in climate research [13, 20, 56, 58, 60, 63, 64, 65, 70]. The TWP-GA method has only been compared against the monolithic TWM algorithm. Both are based upon approximating the solution to a two-way coupled continuum model. We add a third algorithm for comparison in calculating AST, motivated by an approximation sometimes made in climate models to decouple the momentum equation calculations for the atmosphere and ocean, [70]. The idea is to assume the velocity of the ocean near the interface is on average much smaller than the atmospheric currents near I, hence in the coupling conditions one may neglect the ocean velocity in the jump: $[\mathbf{u}] = u_1 - u_2 \approx u_1$. This is equivalent to simply setting $u_2 = 0$ only in the interface integrals of the monolithic weak problem (7.10)-(7.11). Thus the third algorithm is defined by setting the corresponding terms to zero in algorithm TWP-GA.

The resulting algorithm is classified herein as a "one-way" coupled model because the interfacial boundary condition for velocity on Ω_1 is independent of the velocity on Ω_2, though it is not strictly speaking a one way model. The velocity boundary condition becomes

$$-\nu_1 \hat{n}_1 \cdot \nabla u_1 \cdot \hat{\tau}_1 = \kappa |u_1 \cdot \hat{\tau}_1| u_1 \cdot \hat{\tau}_1 = \nu_2 \hat{n}_2 \cdot \nabla u_2 \cdot \hat{\tau}_2,$$

and we set $u_2 = 0$ in the temperature boundary condition as well. The transfer of quantities like momentum flux and heat flux across I may still be modeled conservatively using such a continuum model. However, such an approximation still changes the way information is shared between subdomains sufficiently to justify inquiring as to the effects on model uncertainty. This method will be referred to as the "one-way partitioned method with geometric averaging", or *OWP-GA* method.

The expected value of the average surface temperature and variance were calculated with each algorithm at every time step, using the same problem and parameter choices described in the beginning of Section 7.4. Figure 23 shows the values of $E(AST)$ at each time step with each method. A rapid fluctuation was observed in $E(AST(t))$ near $t = 0$ that is not well approximated with the given time step size. This is likely due to some incompatability of the initial conditions with respect to the continuum model. There is also a significant difference in the average temperature at the final time predicted by the three models.

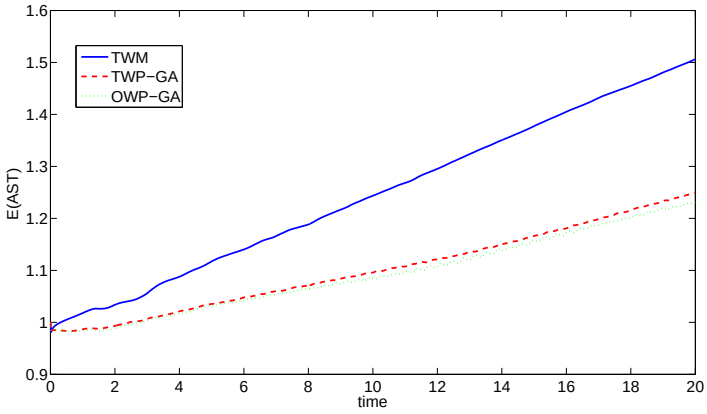

Figure 23: Expectation of AST.

Taking smaller time steps a closer agreement is seen between all three models, and the initial fluctuation in $E(AST(t))$ near $t = 0$ is better represented. This was observed by decreasing the time step size to $\Delta t = 0.001$ and rerunning the algorithms over the time interval $t \in [0, 1]$. Figure 24 shows the results for each algorithm using $\Delta t = 1/50$ (left) and $\Delta t = 1/1000$ (right). The values of $E(AST)$ are in much closer agreement among the three methods using the smaller time step. Figure 25 shows the same plot, but on the smaller interval $t \in [0, 0.1]$ to make clear the improvement in approximating $E(AST)$ with all of the methods at these time steps.

The differences between the expected values of AST among the three methods is larger than the size of variances in AST. Thus a question remains of whether variance in this statistic ever grows fast enough under the conditions studied here to outweigh the differences in the expected value $E(AST)$. We choose not to pursue an answer in this thesis due to the prohibitive computational expense of using sufficiently many time steps to investigate the issue. However, the differences between the two decoupled models TWP-GA and OWP-GA are not so big as comparing against the TWM model, as seen below. This is interesting since in climate applications the TWM model is not considered computationally attractive due to the expense of solving the monolithic problem. Then given a choice between the TWP-GA and OWP-GA models, the TWP-GA model seems attractive due to a smaller

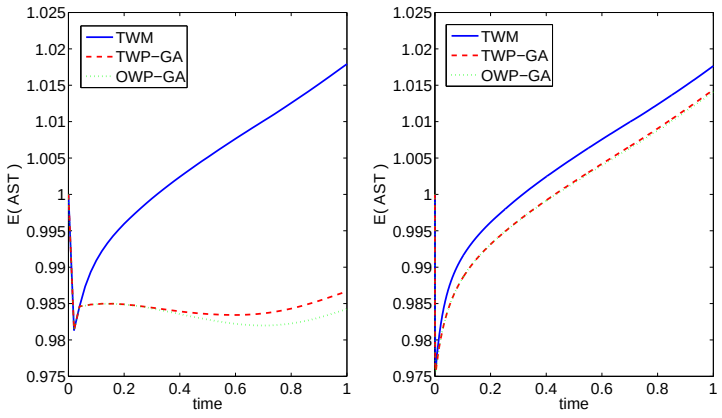

Figure 24: E(AST) using $\Delta t = 1/50$ (left) and $\Delta t = 1/1000$ (right) for $t \in [0, 1]$.

aleatory uncertainty.

The standard deviation in $AST(t)$ was calculated and the expected value of AST is plotted in Figure 26 for each method as a solid line. Dotted lines show the result of adding or subtracting one standard deviation at each time step. Significant differences in variance were only observed close to the final time and hence the plots are for $19 \leq t \leq 20$. The TWM algorithm produces significantly smaller variances than the partitioned models, yielding a standard deviation of $\sigma(t = 20) \approx 1.7951 \times 10^{-3}$ at the final time. The TWP-GA algorithm generated a larger value $\sigma(20) \approx 5.9488 \times 10^{-3}$, and the OWP-GA algorithm yet a higher value $\sigma(20) \approx 1.7289 \times 10^{-2}$. Rescaling these numbers corresponds to standard deviations of $0.5262\,K$, $1.7439\,K$ and $5.0684\,K$, respectively.

Note that by the final time the aleatory uncertainty in AST for the decoupled models has grown large enough that one can no longer distinguish between the results using the TWP-GA or OWP-GA methods if taking one standard deviation into consideration. Ideally, the expected values of AST calculated with each method would be in close agreement, in the present case requiring smaller discretization parameter choices. If the discretization were fine enough to accomplish this, the same behavior in growth of uncertainty may still persist, so that the TWP-GA model would supply an advantage over the OWP-GA model.

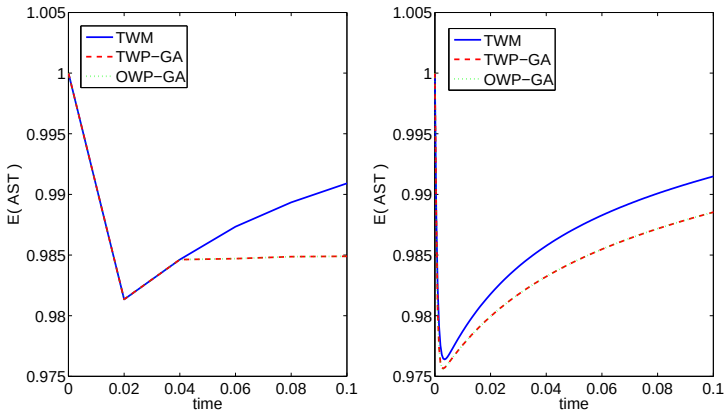

Figure 25: E(AST) using $\Delta t = 1/50$ (left) and $\Delta t = 1/1000$ (right) for $t \in [0, 0.1]$.

7.5 CONCLUSIONS

Unconditional stability has been demonstrated for the monolithic TWM algorithm with heat equations decoupled from the momentum equations and for the proposed partitioned algorithm (TWP-GA) that further decouples the calculations across the fluid-fluid interface for efficiency in parallel implementation. The TWP-GA model offers a potential advantage over the OWP-GA one-way coupled model due to a smaller uncertainty in measuring average surface temperature. As the computations evolve in time there is initially a higher epistemic uncertainty versus aleatory uncertainty using coarse time steps.

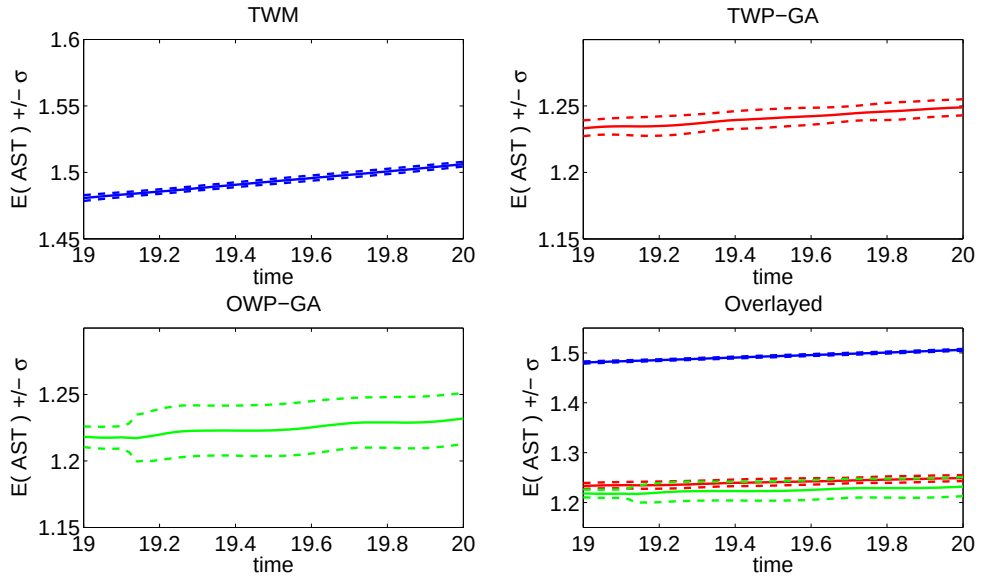

Figure 26: E(AST) (solid line) and adding or subtracting σ (dotted lines).

8.0 CONCLUDING REMARKS AND FUTURE WORK

The case of linear coupling is now fairly well understood. It has been shown that unconditionally stable, decoupled and convergent algorithms exist in this case. The time accuracy can be improved with deferred correction to arbitrary order. Interestingly, explicit treatment of the coupling terms proved to be an inferior approach to the alternative semi-implicit partitioning. Clearly such explicit methods cannot be used for nonlinear coupling either. In Chapters 2 - 3 computational evidence was provided which strongly supports these conclusions.

Extending partitioned time stepping techniques for nonlinear coupling is challenging. It is possible to do so and retain unconditional stability. However, a time step restriction is needed for accuracy in each case studied except when adding artificial dissipation, which appears to be too dissipative in practice. The time step restriction does not depend on the mesh size as in current climate models. This remains true for the algorithm in Chapter 6 which also allows different size time steps to be taken for the decoupled subproblems. It has been shown that large time steps may be possible for the ocean in practice with this strategy as errors due to the larger time step size may be localized near the interface and not effect statistical measurements. As demonstrated in Chapter 7, the ideas can be extended to include heat transport and likely the full atmosphere-ocean system.

In studying reliability of computations based on the knowledge of coupling parameters, it was shown that variance values using coupled versus decoupled algorithms are similar in the point-wise velocity and temperature fields. The variance is concentrated at the interface and propagates into the bulk fluid. Measuring average surface temperature, the coupled algorithm proved to have the smallest variance and predicts a higher temperature. Partitioned methods introduce numerical dissipation through decoupling. However, the two-way coupling studied in this thesis proved to generate a smaller variance in average surface tem-

perature compared with the one-way coupling investigated.

Some questions regarding climate modeling follow from the work:

1. Is it necessary to use nonlinear coupling in application?
2. Concerning efficiency, is the limitation on mesh size for climate codes due to a CFL condition, memory usage or linear solvers? (If the former, the methods studied here become even more attractive).
3. Is decoupling the atmosphere and ocean calculations really beneficial, considering time step restrictions and increased uncertainty?
4. Is there a better strategy allowing *some* of the equations to remain coupled?

8.0.1 Future Work

The following research projects would help develop further computational capabilities for atmosphere-ocean interaction:

1. Develop algorithms with higher order time accuracy for nonlinear coupling, still allowing large time steps. Methods with time step restrictions should be considered, focusing on using larger time steps than are currently possible in climate models.
2. Using different time step sizes for the decoupled subproblems, the data on the subdomains are not solved for at all the same times. So how may interpolation or extrapolation be used in the algorithm to improve representation of this data when passed across the interface? Can the accuracy be improved in this way? Exploring these issues could be done by first making adaptations to existing codes for the academic tests in this thesis to see if there is any improvement over reported results.
3. The work herein suggests that partitioned methods and fully implicit methods may predict significantly different flow statistics, which would be difficult to study for climate models due to the expense of implicit methods (and probably programmer effort). A further investigation of the simplified model in Chapter 7 using smaller time step and mesh sizes could help determine if variance in statistical measurements due to uncertainty in the coupling parameters will outweigh the differences in expected values using semi-implicit versus implicit coupling.

4. It should be checked that the numerical methods in this thesis are adaptable to equations with more realistic physics. One example is coupled fluids where one is compressible (the atmosphere) and is modelled using the so-called "σ coordinate system" that uses pressure as the vertical coordinate. In this way the continuity equation reduces to look like a divergence free condition. Alternatively, there are the shallow water equations.
5. The numerical algorithms herein should be incorporated with the types of schemes used in real climate codes. An example is using spectral elements, finite differences or finite volumes.
6. Treatment of other fluxes should be considered, most notably water.
7. Some work has been done in climate models to relax the rigid lid hypothesis, in which case the numericals methods in this work may need to be adapted accordingly.
8. The numerical methods of this thesis should be adapted to include a model for interaction of molecular viscocity with the spatial mesh, i.e. subgrid modelling.
9. The convergence of the pressure solution is not fully understood in Chapter 5 and is an important open problem. There are a number of possible reasons this behavior is observed. Here is a list of some ideas to investigate this issue:

- Check boundedness and convergence of the discrete time derivative
- Use a higher order approximation of the discrete time derivative (e.g. BDF-2)
- Check stability of the pressure analytically
- There may be issues related to the linear solver
- Using uniform nested meshes may clarify the behavior of the pressure error

BIBLIOGRAPHY

[1] R.A. Adams and J.J.F. Fournier, *Sobolev Spaces*, vol. 140 of Pure and Applied Mathematics, Academic Press, 2003.

[2] M. Anitescu, W. Layton and F. Pahlevani, Implicit for local effects and explicit for nonlocal is unconditionally stable, ETNA 18, 2004, 174-187.

[3] Uri M. Ascher and Linda R. Petzold, Computer Methods for Ordinary Differential Equations and Differential-Algebraic Equations, SIAM, Philadelphia, 1998.

[4] U. M. Ascher, S. J. Ruuth and B. T. R. Wetton, Implicit-explicit methods for time-dependent partial differential equations, SIAM J. Num. Anal. 32(3), 1995.

[5] I. Babuška, F. Nobile and R. Tempone, A stochastic collocation method for elliptic partial differential equations with random input data, SIAM Jour. Num. Analysis, vol. 45, no. 3, pp. 1005-1034, 2007.

[6] I. Babuška, F. Nobile and G. E. Zouraris, Galerkin finite element approximations of stochastic elliptic partial differential equations, SIAM Jour. Num. Analysis, vol. 42, no. 2, pp. 800-825, 2004.

[7] C. Bernardi, T. Chacon-Rebello, R. Lewandowski, F. Murat, A model of two coupled turbulent fluids, Part II: Numerical approximations by spectral discretization, SIAM Jour. Num. Analysis, Vol. 40, No. 6, pp. 2368-2394, 2003.

[8] E. Bernsen, H. A. Dijkstra and F. W. Wubs, A method to reduce the spin-up time of ocean models, Ocean Modelling, Vol. 20, 2008, pp. 380-392.

[9] H. Blum, S. Lisky and R. Rannacher, A Domain Splitting Algorithm for Parabolic Problems, Computing 49, 11-23, 1992.

[10] K. Böhmer, P. W. Hemker, H. J. Stetter, The defect correction approach, in: K. Böhmer, H. J. Stetter (Eds.),*Defect Correction Methods. Theory and Applications*, Springer Verlag, 1984, pp. 1–32.

[11] S.C. Brenner and L.R. Scott, *The Mathematical Theory of Finite Element Methods*, Springer-Verlag, 2002.

[12] D. Bresch and J. Koko, Operator-Splitting and Lagrange Multiplier Domain Decomposition Methods for Numerical Simulation of Two Coupled Navier-Stokes Fluids, Int. J. Appl. Math. Comput. Sci., Vol. 16, No. 4, 2006, pp. 419-429.

[13] P. Brohan, J. J. Kennedy, I. Harris, S. F. B. Tett and P. D. Jones, Uncertainty estimates in regional and global observed temperature changes: A new data set from 1850, J. Geophys. Res., vol. 111, no. D12106, 2006, pp. 419-429.

[14] E. Burman, Miguel A. Fernández, Stabilization of explicit coupling in fluid-structure interaction involving fluid incompressibility, INRIA Research Rept. RR-6455, Feb. 2008.

[15] E. Burman, P. Hansbo, Interior penalty stabilized Lagrange multiplier for the finite element solution of elliptic interface problems, to appear in IMA Journal of Numerical Analysis. 2007

[16] P. Causin, J.-F. Gerbeau and F. Nobile, Added-mass effect in the design of partitioned algorithms for fluid-structure problems, INRIA Rept. 5084, 2004.

[17] D. Caya and R. Laprise, A Semi-Implicit Semi-Lagrangian Regional Climate Model: The Canadian RCM, Monthly Weather Review, Vol. 127, 1999, pp. 341-362.

[18] J. Connors, J. Howell and W. Layton, Partitioned timestepping for a parabolic two domain problem, SIAM Jour. Num. Analysis, vol. 47, no. 5, 2009, pp. 3526-3549.

[19] J. Connors, J. Howell and W. Layton, Decoupled time stepping methods for fluid-fluid interaction, SIAM Jour. Num. Analysis, 2009.

[20] M. Collins, B. B. B. Booth, G. R. Harris, J. M. Murphy, D. M. H. Sexton and M. J. Webb, Towards quantifying uncertainty in transient climate change, Climate Dynamics, vol. 27, 2006, pp. 127-147.

[21] M. Collins, S. F. B. Tett and C. Cooper, The internal climate variability of HadCM3, a version of the Hadley Centre coupled model without flux adjustments, Climate Dynamics, vol. 17, no. 1, 2001, pp. 61-81.

[22] W. D. Collins, C. M. Bitz, M. L. Blackmon, G. B. Bonan, C. S. Bretherton, J. A. Carton, P. Chang, S. C. Doney, J. J. Hack, T. B. Henderson, J. T. Kiehl, W. G. Large, D. S. McKenna, B. D. Santer and R. D. Smith, The Community Climate System Model Version 3 (CCSM3), Journal of Climate, vol. 19, no. 11, 2006, pp. 2122-2143.

[23] G.T. Cooper and A. Sayfy, Additive Runge-Kutta methods for stiff ordinary differential equations, Mathematics of Computation, Vol. 40, No. 161, pp. 207-218.

[24] G. G. Dahlquist, A special stability problem for linear multistep methods, BIT Numerical Mathematics, 3 (1), 1963.

[25] C. N. Dawson and Q. Du, A Finite Element Domain Decomposition Method for Parabolic Equations, Fourth International Symposium on Domain Decomposition Methods for PDEs, edited by R. Glowinski et al, pp255-263, SIAM, Philadelphia, 1991.

[26] M. K. Deb, I. M. Babuška and J. T. Oden, Solution of stochastic partial differential equations using Galerkin finite element techniques, Computer Methods in Applied Mechanics and Engineering, vol. 190, no. 48, pp. 6359-6372, 2001.

[27] Delworth et al., GFDL's CM2 Global Coupled Climate Models. Part I: Formulation and Simulation Characteristics, Journal of Climate, vol. 19, no. 5, pp. 643-674, 2006.

[28] H. A. Dijkstra, H. Oksuzoglu, F. W. Wubs and E. F. F. Botta, A fully implicit model of the three-dimensional thermohaline ocean circulation, Journal of Computational Physics, Vol. 173, pp. 685-715, 2001.

[29] A. Dutt, L. Greengard, V. Rokhlin, Spectral Deferred Correction Methods for Ordinary Differential Equations, BIT 40 (2), 2000, pp241-266.

[30] M. S. Eldred and J. Burkardt, Comparison of non-intrusive polynomial chaos and stochastic collocation methods for uncertainty quantification, AIAA (2009-0976), 2009.

[31] R. Frank, W. Ueberhuber, Iterated Defect Correction for the Efficient Solution of Stiff Systems of Ordinary Differential Equations, BIT 17, 1977, pp146-159.

[32] G. P. Galdi, An Introduction to the Mathematical Theory of the Navier-Stokes Equations, Springer Tracts in Natural Philosophy, Volume I, Springer-Verlag, New York, 1994.

[33] B. Ganis, H. Klie, M. F. Wheeler, T. Wildey, I. Yotov and D. Zhang, Stochastic collocation and mixed finite elements for flow in porous media, Computer Methods in Applied Mechanics and Engineering, vol. 197, no. 43-44, 3547-3559, 2008.

[34] R. G. Ghanem and P. D. Spanos, Stochastic Finite Elements: A Spectral Approach, Springer-Verlag, New York, 1991.

[35] F. Hecht, A. LeHyaric and O. Pironneau. Freefem++ version 2.24-1, 2008. `http://www.freefem.org/ff++`.

[36] J. G. Heywood and R. Rannacher, Finite-elements approximation of the nonstationary Navier-Stokes problem part IV: Error analysis for second-order discretization. SIAM J. Numer. Anal. 1990, vol. 27(2), pp. 353-384.

[37] G. Iaccarino and P. Constantine, Large Eddy Simulations of Flow Around a Cylinder with Uncertain Wall Heating, 47th AIAA Aerospace Sciences Meeting Including the New Horizons Forum and Aerospace Exposition(Disc 1), 2009, American Institute of Aeronautics and Astronautics, 1801 Alexander Bell Drive, Suite 500, Reston, VA, 20191-4344, USA.

[38] F. P. Incropera, D. P. DeWitt, T. L. Bergman and A. S. Lavine, Introduction to Heat Transfer, 5th edition, John Wiley and Sons, USA, 2007.

[39] H. Johnston and J.-G. Liu, Accurate, stable and efficient Navier-Stokes solvers based on explicit treatment of the pressure term, J. Comput. Phys. 199 (2004), 221–259.

[40] C.A. Kennedy and M. H. Carpenter, Additive Runge-Kutta schemes for convection-diffusion-reaction equations, Applied Numerical Math., Vol. 44, pp. 139-181, 2003.

[41] J. T. Kiehl and P. R. Gent, The community climate system model version 2, Journal of Climate (17), 2004, pp. 3666-3682.

[42] A. Labovschii, A Defect Correction Method for the Evolutionary Convection Diffusion Problem with Increased Time Accuracy, submitted to Computational Methods in Applied Mathematics, 2007.

[43] A. Labovschii, A Defect Correction Method for the Time-Dependent Navier-Stokes Equations, (to appear in Numerical Methods for Partial Differential Equations) 2007.

[44] P. H. Lauritzen, A stability analysis of finite-volume advection schemes permitting long time steps, Monthly Weather Review, vol. 135, 2007, pp. 2658-2673.

[45] W. J. Layton, *Introduction to the Numerical Analysis of Incompressible, Viscous Flows*, SIAM Comp. Sci. and Engr. 6, 2008.

[46] R. Lewandowski, *Analyse Mathématique et Océanographic*, collection RMA, Masson, 1997.

[47] J. -L. Lions, R. Temam and S. Wang, Models for the coupled atmosphere and ocean (CAO I), Computational Mechanics Advances 1, 1993, pp. 1-54.

[48] J. -L. Lions, R. Temam and S. Wang, Numerical analysis of the coupled atmosphere-ocean models (CAO II), Computational Mechanics Advances 1, 1993, pp. 55-119.

[49] J. -L. Lions, R. Temam and S. Wang, Mathematical theory for the coupled atmosphere-ocean models (CAO III), J. Math. Pures. Appl. (74), 1995, pp. 105-163.

[50] Manabe, S. and Bryan, K., Climate calculations with a combined ocean-atmosphere model, Jour. Atmos. Sci., Vol. 26, pp. 786-789, 1969.

[51] Marotzke, J., Giering, R., Zhang, K. Q., Stammer, D., Hill, C. and Lee, T., Construction of the adjoint MIT ocean general circulation model and application to Atlantic heat transport variability, Jour. Geophysical Res. (104), 1999.

[52] K. McGuffie and A. Henderson-Sellers, A climate modelling primer, Second edition, John Wiley and Sons, England, 1997.

[53] M. L. Minion, *Spectral Deferred Corrections and Projection Methods*, proceedings for Workshop for Innovative Time Integrators for PDEs, 2003.

[54] M. L. Minion, *Semi-Implicit Spectral Deferred Correction Methods for Ordinary Differential Equations*, Comm. Math. Sci. 1 (2003), 471–500.

[55] P. Müller, The equations of oceanic motions, Cambridge University Press, Cambridge, UK, 2006.

[56] J. M. Murphy, D. M. H. Sexton, D. N. Barnett, G. S. Jones, M. J. Webb, M. Collins and D. A. Stainforth, Quantification of modelling uncertainties in a large ensemble of climate change simulations, Nature, vol. 430, 2004, pp. 768-772.

[57] L. Perko, Differential Equations and Dynamical Systems, third edition, Springer, New York, 2001.

[58] J. Rougier, D. M. H. Sexton, J. M. Murphy and D. Stainforth, Quantifying Uncertainty in Projections of Regional Climate Change: A Bayesian Approach to the Analysis of Multimodel Ensembles, Journal of Climate, vol. 22, 2009, pp. 3540-3557.

[59] Gary L. Russell, James R. Miller and David Rind, A coupled atmosphere-ocean model for transient climate change studies, Atmosphere-ocean 33 (4), 1995, pp. 683-730.

[60] K. Sargsyan, C. Safta, B. Debusschere and H. Najm, Uncertainty Quantification in the Presence of Limited Climate Model Data with Discontinuities, International Conference on Data Mining Workshops, vol. 0, 2009, pp. 241-247, IEEE Computer Society, Los Alamitos, CA, USA.

[61] H. Schlichting and K. Gersten, Boundary Layer Theory, Springer-Verlag Berlin Heidelberg, Germany, 2000.

[62] A. St-Cyr and S. J. Thomas, Nonlinear operator integration factor splitting for the shallow water equations, Applied Numerical Mathematics, Vol. 52, No. 4, 2005, pp. 429-448.

[63] D. A. Stainforth, T. Aina, T. Christensen, M. Collins, N. Faull, D. J. Frame, J. A. Kettleborough, S. Knight, A. Martin, J. M. Murphy, C. Piani, D. Sexton, L. A. Smith, R. A. Spicer, A. J. Thorpe and M. R. Allen, Uncertainty in predictions of the climate response to rising levels of greenhouse gases, Nature, vol. 433, 2005, pp. 403-406.

[64] P. A. Stott and J. A. Kettleborough, Origins and estimates of uncertainty in predictions of twenty-first century temperature rise, Nature, vol. 416, 2002, pp. 723-726.

[65] C. Tebaldi, R. L. Smith, D. Nychka and L. O. Mearns, Quantifying Uncertainty in Projections of Regional Climate Change: A Bayesian Approach to the Analysis of Multimodel Ensembles, Journal of Climate, vol. 18, 2005, 1524-1540.

[66] R. Temam, Navier-Stokes Equations, 2001, AMS Chelsea, Providence, Rhode Island.

[67] S. J. Thomas and R. D. Loft, The NCAR Spectral Element Climate Dynamical Core: Semi-Implicit Eulerian Formulation, SIAM Jour. Sci. Comp., Vol. 25, pp. 307-322, 2005.

[68] L. N. Trefethen, Is Gauss quadrature better than Clenshaw-Curtis?, SIAM Review, vol. 50, pp. 67-87, 2008.

[69] A. Quarteroni and A. Valli, *Numerical Approximation of Partial Differential Equations*. Springer, 1994.

[70] W. M. Washington and C. L. Parkinson, An introduction to three-dimensional climate modeling, second edition, University Science Books, California, 2005.

[71] D. Xiu and J. S. Hesthaven, High-order collocation methods for differential equations with random inputs, SIAM Journal on Scientific Computing, vol. 27, pp. 1118, 2005.